Impacts of land use/land cover and climate variability on the hydrological cycle with a specific focus on evapotranspiration

By

Amirhossein Shadmehri Toosi
Ph.D.

Thesis Submitted to Flinders University for the degree of
Doctor of Philosophy

College of Science and Engineering
March-2025

TABLE OF CONTENTS

ABSTRACT

Water systems and biophysical environments undergo multiple complex interactions at both spatial and temporal scales. Over recent years, our understanding of hydrological processes and the conceptual details have remarkably increased. Much of the knowledge on these subjects results from applying remote sensing techniques and in situ observational information, which has significantly augmented data availability and coincidently increased computing capabilities. However, modelling hydrological processes on a large scale presents challenges, particularly in the context of climate change and Land Use-Land Cover (LULC) changes. The efficacy of current hydrologic models under conditions of change remains uncertain. To effectively integrate land cover dynamics and deepen our understanding of their impacts, assessing how LULC is represented in existing models and identifying any shortcomings is essential. These models consist of various components, each tailored to simulate specific elements of water partitioning within the hydrological cycle. Moreover, it is necessary to evaluate whether the variability in current LULC data is substantial enough to justify its inclusion in modelling efforts and how this variability might influence other processes like Actual Evapotranspiration (AET). Therefore, this study deals with these important subjects in three phases. First, in a comprehensive review, we discuss the hydrological processes affected by LULC and how conceptual models capture physical hydrologic processes and conceptualise LULC. This review highlights the existing gaps in LULC modelling and identifies avenues for improvement. Emphasis is placed on selecting the best model based on expected outcomes and improving LULC data. Finally, it highlights the need for a standardised LULC classification system for uniform modelling and comparison.

In the second phase of the investigation, we conduct a detailed analysis of year-on-year land cover changes within the Murray Darling Basin (MDB), leveraging the most accurate and contemporary datasets available. This endeavour aims to explain the significance of these land cover dynamics, pinpointing spatial and temporal patterns and emerging trends within MDB, which holds paramount economic and ecological value in Australia. The results indicate significant increases in natural bare surfaces and decrease in water bodies, with shifts in agricultural land use driven by water recovery initiatives and infrastructure developments. The drivers of LULC changes are influenced by climate variability, natural disasters, and water management practices, demonstrating varied impacts across different regions within the basin.

Subsequently, the third phase analyses the CMRSET and MODIS AET datasets over MDB. The study examines the temporal patterns and differences in AET across various land cover types, along with the existence of notable AET variation among the major land cover categories within the MDB. The research aims to determine if AET, on a broad scale, is affected by variations in rainfall or changes in

land cover. The study reveals a reasonable alignment between the datasets in overall AET patterns, but significant variations in magnitude were observed. Basin-scale water balance assessments indicate that MODIS considerably underestimates AET. Rainfall is identified as the primary driver of AET variability across different land covers in most catchments.

This thesis points out areas that need improvement and the challenges we face because of limited and not always accurate data. It contributes to improved decision-making, formulating effective policy options, and predicting the likely unforeseen impacts for sustainable land and water management. Furthermore, the study highlights the need for regional studies given diverse hydrological characteristics and the significant influence of regional climate, terrain, and land cover changes on the hydrological process.

DECLARATION

I certify that this thesis:

1. does not incorporate without acknowledgment any material previously submitted for a degree or diploma in any university

2. and the research within will not be submitted for any other future degree or diploma without the permission of Flinders University; and

3. to the best of my knowledge and belief, does not contain any material previously published or written by another person except where due reference is made in the text.

Signed: Amirhossein Shadmehri Toosi

Date: 12-Aug-2024

ACKNOWLEDGEMENTS

Getting my PhD has been an incredible journey full of challenges and opportunities, and I couldn't have done it without the support of some amazing people.

I want to start with my Family. It has been a long three years, and I simply wouldn't be here without your sacrifices and belief in me. Your encouragement has truly been my anchor and kept me going.

I want to thank my supervisors and advisors, Okke Batelan, Margaret Shanafield, and Huade Guan, for their support and guidance. Your support has been key to my research and academic development, and I'm so grateful for it.

I also want to extend my gratitude to my thesis committee members, Howard Fallowfield, Sally Thompson, and Vinod Kumar. Your insights, constructive feedback, and encouragement have been crucial in sharpening my research and scholarly work.

I want to give a big thanks to Flinders University and the National Centre of Groundwater Research and Training (NCGRT) for providing a great academic environment and the resources I needed to do my research. I'm grateful for the financial support from The Flinders International Postgraduate Research Scholarship (FIPRS). It made all the difference in funding my studies and research activities.

Shoutout to my friends and colleagues—Shahab Doulabian, Warren Falcon, Shervin Shokri, Morteza Shokri, Ehsan Kamali Maskooni and Sina Alaghmand. You have been fantastic friends, constantly motivating me and serving as my emotional pillars.

Lastly, I want to thank my colleagues at WSP, especially Justin Weaver, Tom Castley, and Scott Gallacher, for their steady support and understanding during my PhD studies. Your help in providing opportunities for my engagement, collaboration, and professional growth has been invaluable.

LIST OF FIGURES

LIST OF TABLES

LIST OF ABBREVIATIONS

Abbreviation	Definition	Abbreviation	Definition
AET	Actual Evapotranspiration	IPO	Interdecadal Pacific Oscillation
AGCD	Australian Gridded Climate Data	LAI	Leaf Area Index
ALUM	Australian Land Use and Management	LCCS	Land Cover Classification System
ANN	Artificial Neural Network	LE	Latent heat flux
AS	Artificial Surfaces	LULC	land use and Land cover
AWS	Amazon Web Services	MDB	Murray Darling Basin
CLC	Corine Land Cover	MDBA	Murray Darling Basin Authority
CN	Curve Number	ML	Machine Learning
CTV	Cultivated Terrestrial Vegetation	NAV	Natural Aquatic Vegetation
DEA	Digital Earth Australia	NCGRT	National Centre for Groundwater Research and Training
DEM	Digital Elevation Model	NCI	National Computational Infrastructure
DL	Deep Learning	NS	Natural Bare Surface
EC	Eddy Covariance	NTV	Natural Terrestrial Vegetation
ENSO	El Niño-Southern Oscillation	PET	Potential Evapotranspiration
EO	Earth Observation	PLE	Potential Latent Heat Flux
ET	Evapotranspiration	PRMS	Precipitation-Runoff Modeling System
FAO	Food and Agriculture Organization	SDL	Sustainable Diversion Limits
GA	Genetic Algorithms	TWS	Terrestrial Water Storage
GIS	Geographic Information System	USGS	United States Geological Survey
GL	Gigaliters	VIC	Variable Infiltration Capacity
GLC	Global Land Cover		
IGBP	International Geosphere-Biosphere Programme		

CHAPTER 1

INTRODUCTION AND BACKGROUND

1.1 Introduction

Land Use-Land Cover (LULC) change is a global issue with numerous physical, ecological, and socio-economic consequences (Teklay et al., 2019; Zeng et al., 2020). It is important for its impact on processes ranging from local water supply to water balance and carbon cycling on the global scale (Dile et al., 2018; Li et al., 2018). Further, it has been shown that the hydrologic cycle can be adversely affected by LULC change more than climate change (Aghsaei et al., 2020). Therefore, knowledge of how LULC impacts the hydrologic cycle is needed to optimise natural resources management (Cartwright et al., 2017; Sun et al., 2017).

Along with LULC change, climate change has significantly impacted our environment in recent decades. This trend is exacerbated by ever-increasing greenhouse gas emissions, resulting in a rise in global air temperature, a significant increase in evapotranspiration, and shifting rainfall patterns (Pour et al., 2020). The increased temperature is associated with increased air capacity to hold water vapour, resulting in more frequent and intense rainfall events (Al-Ghussain, 2019; Letz et al., 2021). It is expected to be accompanied by a decrease in the frequency of medium and low-intensity events or an overall drop in rainfall frequency (Ghasemi Tousi et al., 2021; Owor et al., 2009).

Changes in LULC and rainfall patterns can significantly impact Actual Evapotranspiration (AET). However, the hydrological partitioning response to these changes will depend heavily on climate, land cover, soil type, and other land features (Luo et al., 2020; Peng et al., 2021). Traditionally, vegetation and water storage interaction are poorly conceptualised and represented in most hydrological models. Despite major advances in our understanding of hydrologically relevant vegetation processes and properties, we lack integration of these features in hydrological models (Sun et al., 2017). Hydrological models simplify the process by a hypothesis or set of hypotheses relevant to the model objective, making simulation possible at large-scale studies where experimental methods are difficult to apply (Liu et al., 2019).

Understanding land cover dynamics and the significance of year-to-year changes is critical in gaining insights into the potential hydrological consequences that may follow these changes. By analysing these changes, we can identify the impacts that they may have on the water cycle, including changes to runoff, infiltration, and evapotranspiration. Despite the availability of airborne and satellite remote sensing techniques for monitoring land surface parameters and processes, the dynamics of LULC are still not well incorporated into hydrological models or undermined by their simplistic assumptions (e.g., stationarity). Even in more recent dynamic modelling practices, land use is typically allowed to vary over time but held constant for processes related to land use for months or years. Thus, better integration of the LULC dynamics in hydrological modelling is needed to accurately represent the interactions between land use, climate, and hydrology (Castillo et al., 2014). Understanding the role

of LULC in hydrological processes is crucial, as these processes are intricate and interdependent. Identifying gaps in current hydrological modelling practice and necessary future developments requires thoroughly comprehending LULC's impact.

1.2 Research gaps

Despite the significant progress in understanding the effects of LULC changes on hydrological processes, research gaps still need to be addressed. One such gap is the lack of a systematic synthesis of how LULC is characterised and incorporated into hydrological modelling frameworks. While LULC has been utilised in hydrological models for decades, existing reviews often focus on specific hydrological processes or limited geographical contexts. There is no comprehensive overview that evaluates the overarching methodologies, integration approaches, and uncertainties associated with LULC characterisation in hydrological models. Addressing this gap would provide a clearer understanding of the state of LULC characterisation and inform future modelling improvements.

Another research gap relates to the year-to-year dynamics of land cover, particularly at catchment scales. Despite the growing recognition of the importance of analysing land cover dynamics at the catchment scale, there is still a significant research gap regarding the lack of consensus on reliable data sources and the need to test their accuracy. No single data source can capture all the relevant information, and different data sources have varying degrees of accuracy, coverage, resolution and temporal frequency. Furthermore, there is a lack of consensus on the effects of land cover changes on AET at large scales. While some studies have shown that AET change is derived from land cover change, others have reported that the impact of climatic factors is more important (Feng et al., 2020; Wei et al., 2021).

1.3 Research questions

The emergence of remote sensing technologies has dramatically improved our capability to monitor LULC changes dynamically, enabling a more detailed assessment of their impacts on hydrological processes amidst climate change. This technological progress prompts a crucial inquiry: Given these advancements, how significant are the dynamics of land cover changes, and what potential do they hold for improving LULC representation in hydrological models? Such improvements are vital for a deeper comprehension of the influence of LULC dynamics on various hydrological processes. In this study, we conduct a thorough exploration of these research questions, structured across three comprehensive chapters, each dedicated to a detailed examination of distinct aspects of this topic:

Chapter 2:

- Which hydrological processes are influenced by LULC changes, and what limitations exist within current modelling methodologies that could be enhanced for better accuracy?
- Can current modelling practices accurately capture LULC and its impact on hydrological processes?

Chapter 3:

- How significant are land cover dynamics on a yearly time scale in the Murray-Darling Basin (MDB)?
- What are the spatial and temporal patterns and trends in land cover changes over three decades in the MDB?
- What are the main drivers of land cover change within different catchments in MDB?

Chapter 4:

- How significant are AET dynamics on a yearly time scale in MDB catchments?
- Is AET variation dominated by precipitation or land cover?
- Are there any significant differences in average AET among different land cover types over MDB catchments?

1.4 Research hypothesis

Chapter 2 Hypotheses:

- Hydrological processes are significantly influenced by LULC, with current models showing limitations in accurately capturing these dynamics.
- Enhancements in the modeling process have the potential to improve accuracy.

Chapter 3 Hypotheses:

- Yearly land cover dynamics are significant in the MDB over 31 years (1990-2020).
- The MDB has experienced significant land cover changes over the last three decades, driven by natural and anthropogenic factors.

Chapter 4 Hypotheses:

- Yearly AET dynamics are significant in MDB catchments, with impacts on water availability and hydrological processes over 20 years (2001-2020).
- AET variation across MDB catchments is influenced by both precipitation and land cover changes, with the relative impact of these factors varying by location.

- There is a significant difference between average AET over different land cover types and catchments in the MDB.

1.5 Research objectives

This research is dedicated to understanding the complex relationships between LULC and hydrological processes, critically evaluating the existing knowledge base while pinpointing gaps in the research. A key element of this investigation is determining whether LULC experiences significant annual variations or exhibits a degree of stability over time. This initial exploration is crucial for appreciating the potential benefits of integrating LULC data with high spatial and temporal resolution into hydrological models. Among hydrological processes, AET emerged as a key process for detailed examination, given its essential role in the water cycle and its responsiveness to land cover modifications. The Murray Darling Basin was chosen as the focal area for this investigation, reflecting its importance as an agricultural and ecological zone in Australia, characterised by intricate water resource management issues and the notable impact of land cover changes on its hydrological dynamics. The research will unfold in three phases, with specific research questions guiding each chapter as follows:

Chapter 2

To evaluate the theory and assumptions that underlie the considerations of LULC in current hydrological models. This involves reviewing how LULC is integrated into hydrological models and identifying gaps in current practices.

Chapter 3

To investigate three decades of land cover changes in the MDB to understand the yearly dynamics of land cover types and identify spatial and temporal patterns and trends.

Chapter 4

To investigate two decades (2001-2020) of AET dynamics in the MDB to understand how AET responds to land cover changes and how these responses vary across different catchments.

1.6 Significance of Research

The LULC changes are important for their impact on processes ranging from local water supply to water balance and carbon cycling on the global scale (Cohn et al., 2019; Lawrence & Vandecar, 2015). Understanding the effects of LULC changes (e.g., deforestation) on the dynamics of hydrological variables, mainly AET, would significantly improve the comprehension of vast

hydrological consequences followed by these changes (Liu et al., 2019). Dramatic land cover change has been recorded over Australia in the past decades, with significant impacts on hydrologic characteristics of basins such as streamflow, recharge rate, temperature, and precipitation (Grafton et al., 2020; Liu et al., 2019). Particularly the MDB is vulnerable for LULC change at it is highly dependent on the available water resources for agricultural, industrial, and domestic purposes (Baumgartner et al., 2020; Pollino et al., 2021).

The MDB, located in southeastern Australia, is one of the most significant river systems in the country, providing water for agriculture, industry, and urban centers. In 2020 ABC NEWS reported that from 2012 to 2019 more than 2 trillion liters of water have gone missing from the largest and most precious river system — the Murray-Darling Basin (NEWS, 2020). MDB is experiencing increasingly severe water scarcity due to a combination of factors, including changes in land cover and climate, leading to more significant variability in temperature and rainfall (Grafton, 2019; Wheeler, 2022; Wheeler et al., 2020). Understanding the hydrological responses to these changes would help locate vulnerable areas, prevent water losses, increase long-term terrestrial ecosystem sustainability, and have better interannual water allocation planning due to changing land cover and precipitation patterns (Cheng & Yu, 2019; Cohn et al., 2019; Lawrence & Vandecar, 2015). In this regard, validating AET products and evaluating their dynamic and water balance analysis is crucial to maintain sustainable water exploitation and allocation (Mohamed & Gonçalvès, 2021; Tangdamrongsub et al., 2021). Understanding the water balance in the Murray Darling Basin is crucial for effective water management, particularly in the face of climate change and land cover change.

1.7 Scope and limitations

This study aims to provide insights into the dynamic interaction between land cover changes and AET. The study investigates the impact of climate and LULC changes on hydrological processes, specifically the trend and dynamics of AET across different land cover types over MDB. The study's limitations include the reliability of data, which could affect the accuracy of the analysis. Moreover, the study may not cover all the factors that affect hydrological processes, and it may not be possible to capture all the complexities involved in the dynamic interaction between rainfall, AET, and land cover changes. This study can provide insights into the subject and guide future research in MDB.

1.8 Organization of the thesis

The thesis will be structured into three chapters, each of which will be dedicated to specific objectives related to the research topic.

The first chapter critically evaluates the current state of LULC conceptualisation in hydrological models at the catchment scale. This evaluation includes an overview of LULC processes,

conceptualisation, theory, and assumptions and a review of how LULC has been integrated into hydrological models and the hydrological processes affected by LULC. This chapter aims to provide a comprehensive understanding of the status of LULC in hydrological modelling, which can help researchers select suitable models for their study objectives and spatiotemporal scales and pave the way for future model developments.

The second chapter of the thesis focuses on analysing LULC trends and variability over the Murray Darling Basin and its catchments using the latest DEA Land cover dataset. This analysis provides valuable insights into the dynamic nature of land cover at different spatial and temporal scales, which can inform water resource management decisions.

The third chapter investigates the relationship between land cover change, rainfall variability, and AET dynamics in the MDB. This analysis focuses on the interaction between land cover dynamics, rainfall variability, and AET from a data-driven perspective, as they are the most important elements in the water balance. The results of this investigation provide a better understanding of the impact of land cover changes on water resources in the basin, which can guide policy decisions aimed at improving water sustainability.

1.9 References

Aghsaei, H., Mobarghaee Dinan, N., Moridi, A., Asadolahi, Z., Delavar, M., Fohrer, N., & Wagner, P. D. (2020). Effects of dynamic land use/land cover change on water resources and sediment yield in the Anzali wetland catchment, Gilan, Iran. Science of the Total Environment, 712, 136449. https://doi.org/10.1016/j.scitotenv.2019.136449

Al-Ghussain, L. (2019). Global warming: review on driving forces and mitigation. Environmental Progress and Sustainable Energy, 38(1), 13–21. https://doi.org/10.1002/ep.13041

Baumgartner, L. J., Gell, P., Thiem, J. D., Finlayson, C., & Ning, N. (2020). Ten complementary measures to assist with environmental watering programs in the Murray–Darling river system, Australia. River Research and Applications, 36(4), 645–655. https://doi.org/10.1002/rra.3438

Cartwright, I., Cendón, D., Currell, M., & Meredith, K. (2017). A review of radioactive isotopes and other residence time tracers in understanding groundwater recharge: Possibilities, challenges, and limitations. Journal of Hydrology, 555, 797–811. https://doi.org/10.1016/j.jhydrol.2017.10.053

Castillo, C. R., Güneralp, I., & Güneralp, B. (2014). Influence of changes in developed land and precipitation on hydrology of a coastal Texas watershed. Applied Geography, 47, 154–167. https://doi.org/10.1016/j.apgeog.2013.12.009

Cheng, Z., & Yu, B. (2019). Effect of land clearing and climate variability on streamflow for two large basins in Central Queensland, Australia. Journal of Hydrology, 578, 124041. https://doi.org/10.1016/j.jhydrol.2019.124041

Cohn, A. S., Bhattarai, N., Campolo, J., Crompton, O., Dralle, D., Duncan, J., & Thompson, S. (2019). Forest loss in Brazil increases maximum temperatures within 50 km. Environmental Research Letters, 14(8), 084047. https://doi.org/10.1088/1748-9326/ab31fb

Dile, Y. T., Tekleab, S., Kaba, E. A., Gebrehiwot, S. G., Worqlul, A. W., Bayabil, H. K., Yimam, Y. T., Tilahun, S. A., Daggupati, P., Karlberg, L., & Srinivasan, R. (2018). Advances in water resources research in the Upper Blue Nile basin and the way forward: A review. Journal of Hydrology, 560, 407–423. https://doi.org/10.1016/j.jhydrol.2018.03.042

Dile, Y. T., Tekleab, S., Kaba, E. A., Gebrehiwot, S. G., Worqlul, A. W., Bayabil, H. K., Yimam, Y. T., Tilahun, S. A., Daggupati, P., Karlberg, L., & Srinivasan, R. (2018). Advances in water resources research in the Upper Blue Nile basin and the way forward: A review. Journal of Hydrology, 560, 407–423. https://doi.org/10.1016/j.jhydrol.2018.03.042

Ghasemi Tousi, E., O'Brien, W., Doulabian, S., & Shadmehri Toosi, A. (2021). Climate changes impact on stormwater infrastructure design in Tucson Arizona. Sustainable Cities and Society, 72, 103014. https://doi.org/10.1016/j.scs.2021.103014

Grafton, Q., Colloff, M., Marshall, V., & Williams, J. (2020). Confronting a'post-truth water world'in the Murray-Darling Basin, Australia.

Grafton, R. Q. (2019). Policy review of water reform in the Murray–Darling Basin, Australia: the "do's" and "do'nots." Australian Journal of Agricultural and Resource Economics, 63(1), 116–141. https://doi.org/10.1111/1467-8489.12288

Lawrence, D., & Vandecar, K. (2015). Effects of tropical deforestation on climate and agriculture. Nature Climate Change, 5(1), 27–36. https://doi.org/10.1038/nclimate2430

Letz, O., Siebner, H., Avrahamov, N., Egozi, R., Eshel, G., & Dahan, O. (2021). The impact of geomorphology on groundwater recharge in a semi-arid mountainous area. Journal of Hydrology, 603, 127029. https://doi.org/10.1016/j.jhydrol.2021.127029

Li, Y., Piao, S., Li, L. Z. X., Chen, A., Wang, X., Ciais, P., Huang, L., Lian, X., Peng, S., Zeng, Z., Wang, K., & Zhou, L. (2018). Divergent hydrological response to large-scale afforestation and vegetation greening in China. Science Advances, 4(5). https://doi.org/10.1126/sciadv.aar4182

Liu, N., Harper, R. J., Smettem, K. R. J., Dell, B., & Liu, S. (2019). Responses of streamflow to vegetation and climate change in southwestern Australia. Journal of Hydrology, 572, 761–770. https://doi.org/10.1016/j.jhydrol.2019.03.005

Luo, Y., Yang, Y., Yang, D., & Zhang, S. (2020). Quantifying the impact of vegetation changes on global terrestrial runoff using the Budyko framework. Journal of Hydrology, 590, 125389. https://doi.org/10.1016/j.jhydrol.2020.125389

Mohamed, A., & Gonçalvès, J. (2021). Hydro-geophysical monitoring of the North Western Sahara Aquifer System's groundwater resources using gravity data. Journal of African Earth Sciences, 178, 104188. https://doi.org/10.1016/j.jafrearsci.2021.104188
Mohamed, A., & Gonçalvès, J. (2021). Hydro-geophysical monitoring of the North Western Sahara Aquifer System's groundwater resources using gravity data. Journal of African Earth Sciences, 178, 104188. https://doi.org/10.1016/j.jafrearsci.2021.104188
NEWS, A. (2020). The mystery of the Murray-Darling's vanishing flows. https://www.abc.net.au/news/2020-09-03/the-mystery-of-the-murray-darlings-vanishing-flows/12612166 (accessed 1 March 2023).

Owor, M., Taylor, R. G., Tindimugaya, C., & Mwesigwa, D. (2009). Rainfall intensity and groundwater recharge: Empirical evidence from the Upper Nile Basin. Environmental Research Letters, 4(3), 035009. https://doi.org/10.1088/1748-9326/4/3/035009

Peng, Q., Wang, R., Jiang, Y., Li, C., & Guo, W. (2021). The change of hydrological variables and its effects on vegetation in Central Asia. Theoretical and Applied Climatology, 146(1–2), 741–753. https://doi.org/10.1007/s00704-021-03730-w

Pollino, C. A., Hart, B. T., Nolan, M., Byron, N., & Marsh, R. (2021). Rural and regional communities of the Murray–Darling Basin. In Murray-Darling Basin, Australia (pp. 21–46). Elsevier. https://doi.org/10.1016/B978-0-12-818152-2.00002-4

Pour, S. H., Wahab, A. K. A., Shahid, S., Asaduzzaman, M., & Dewan, A. (2020). Low impact development techniques to mitigate the impacts of climate-change-induced urban floods: Current trends, issues and challenges. Sustainable Cities and Society, 62, 102373. https://doi.org/10.1016/j.scs.2020.102373

Sun, L., Yang, L., Hao, L., Fang, D., Jin, K., & Huang, X. (2017). Hydrological effects of vegetation cover degradation and environmental implications in a semiarid temperate Steppe, China. Sustainability (Switzerland), 9(2), 281. https://doi.org/10.3390/su9020281

Tangdamrongsub, N., Jasinski, M. F., & Shellito, P. J. (2021). Development and evaluation of 0.05g terrestrial water storage estimates using Community Atmosphere Biosphere Land Exchange (CABLE) land surface model and assimilation of GRACE data. Hydrology and Earth System Sciences, 25(7), 4185–4208. https://doi.org/10.5194/hess-25-4185-2021

Teklay, A., Dile, Y. T., Setegn, S. G., Demissie, S. S., & Asfaw, D. H. (2019). Evaluation of static and dynamic land use data for watershed hydrologic process simulation: A case study in Gummara watershed, Ethiopia. Catena, 172, 65–75. https://doi.org/10.1016/j.catena.2018.08.013

Wheeler, S. A. (2022). Debunking Murray-Darling Basin water trade myths. Australian Journal of Agricultural and Resource Economics, 66(4), 797–821. https://doi.org/10.1111/1467-8489.12490

Wheeler, S. A., Xu, Y., & Zuo, A. (2020). Modelling the climate, water and socio-economic drivers of farmer exit in the Murray-Darling Basin. Climatic Change, 158(3–4), 551–574. https://doi.org/10.1007/s10584-019-02601-8

Zeng, Y., Yang, X., Fang, N., & Shi, Z. (2020). Large-scale afforestation significantly increases permanent surface water in China's vegetation restoration regions. Agricultural and Forest Meteorology, 290, 108001. https://doi.org/10.1016/j.agrformet.2020.108001

CHAPTER 2

LAND USE-LAND COVER AND HYDROLOGICAL MODELLING: A REVIEW

Highlights

High-resolution, consistent Land use-land cover (LULC) data is often unavailable.

LULC changes introduce significant uncertainty in model parameters.

Accurate modelling of interception remains a challenge in hydrological models.

LULC changes violate the assumption of hydrological stationarity.

Dynamic LULC complicates calibration but enhances model validity.

Land use-land cover and hydrological modelling: A review

A. Shadmehri Toosi[1,2*], O. Batelaan[1,2], M. Shanafield[1,2], H. Guan[1,2]

College of Science and Engineering, Flinders University, GPO Box 2100, Adelaide, SA 5001, Australia
National Centre for Groundwater Research and Training, Flinders University, GPO Box 2100, Adelaide, SA 5001, Australia

*Corresponding author

Email: amirh.shadmehr@flinders.edu.au

2.1 Abstract

Given the extent of recent land use-land cover changes and the consequences for hydrological effects, it is important to capture the role that land use-land cover plays in hydrological model conceptualisation. This need is amplified under a changing climate, as the hydrological sensitivity of catchments to climate change can vary depending on the land use-land cover. Despite the availability of airborne and satellite remote sensing techniques for monitoring land surface parameters over large scales and frequently in time, the spatiotemporal characteristics of land use are still not well integrated into hydrological models. By analysing the conceptualisations of land use-land cover related hydrological processes within models, this paper reviews the progress in and current state of modelling approaches and discusses future research needs and directions.

Keywords: Hydrological modelling, land use, land cover, conceptualisation

2.2 Introduction

The extent and nature of different land cover types and how people utilise the landscape are documented by land use and land cover (LULC) data. Land cover refers to the physical materials on the earth's surface, such as vegetation, water bodies, and artificial structures, which can be identified through satellite and aerial imagery analysis (Green et al., 1994). On the other hand, land use denotes how these land covers are utilised by humans, a less directly observable dimension from remote sensing techniques (Green et al., 1994). Despite their differences, land use and land cover are often analysed as LULC changes, reflecting their intertwined roles in shaping environmental outcomes. LULC change has significant implications for hydrological processes, among other physical, ecological, and socioeconomic dimensions (Li et al., 2018a; Teklay et al., 2019; Zeng et al., 2020). For example, constructing a dam can have important local to regional impacts on water balances, or deforestation can impact carbon cycling (Dile et al., 2018; Li et al., 2018b). Understanding the effects of LULC change on the hydrological processes is needed to optimise natural resources management (Scanlon et al., 2005). Documenting the spatial patterns and determining the magnitude of LULC change effects is essential for understanding and managing hydrological systems (Cheng & Yu, 2019). Moreover, the global impact of LULC change on hydrological processes may surpass the impact of climate change or could be amplified by it (Aghsaei et al., 2020). Therefore, a better understanding of LULC's role in hydrological processes is vital to employing adaptive measures to minimise the inevitable adverse effects of change in LULC (Cartwright et al., 2017; Sun et al., 2017).

Many different types of hydrological models that incorporate LULC have been used to simulate the implications of LULC change (Dwarakish et al., 2015; Dey & Mishra, 2017). The four primary processes affected by LULC are radiation energy partitioning, water interception dynamics, on-ground water partitioning, and subsurface processes. Hydrological models represent these processes with different detail and complexity levels and allow simulations at various spatial and temporal scales. Although a simplified integration of LULC provides valuable insights into the functioning of hydrological systems, the underlying assumptions and simplifications used for simulating hydrological processes may introduce inaccuracies in the results (Beven, 2018; Beven, 2019a). Yet, there are challenges to realistically incorporate each of these processes.

Traditionally, most hydrological models represent a highly simplified version of the interaction between vegetation and water. Despite major advances in our understanding of hydrologically relevant vegetation processes and properties in recent years, we lack integration of these features in hydrological models (Sun et al., 2017). Furthermore, even with the advancements in airborne and satellite remote sensing techniques for monitoring land surface parameters, the temporal dynamics of LULC have not been fully integrated into models. While current data availability permits LULC variations over time, models often assume constant land use for extended periods, spanning months

or even years. To accurately capture the interactions between LULC, climate, and hydrology, tighter temporal integration of LULC dynamics and hydrological processes is required (Castillo et al., 2014). Although there are many reviews of the state of the art of hydrological modelling, an overall picture of the current status of LULC characterisation in the processes used in hydrological models does not exist (Sood & Smakhtin, 2015; Noszczyk, 2019; Moges et al., 2020; Van Stan II & Friesen, 2020).

Therefore, in this work, we start with four key processes influenced by LULC and a brief overview of the physical mechanisms affected by LULC. Further, we review how these processes are typically represented within hydrological models and discuss the associated challenges and limitations. With this foundation established, we guide the reader through a discussion on the current LULC data sources and their limitations. We emphasise the importance of selecting an appropriate model to investigate LULC impacts and enhancing the LULC representation within the model process to better align with study objectives. Finally, we delve into current model evaluation and calibration techniques and discuss ways to refine them. Readers are encouraged to refer to the supplementary material for the overview of the main hydrological model types and their respective strengths and limitations. We believe this work helps better evaluate the current gaps in hydrological modelling practice and the needed future developments, and it promotes best practices in modelling LULC impacts.

2.3 Review of main hydrological processes affected by LULC

2.3.1 Radiation energy partitioning and surface energy balance

2.3.1.1 Physical mechanisms

LULC influences solar radiation partitioning through alterations in surface albedo, landscape thermal properties, and vegetation cover dynamics. This impact extends to sensible and latent heat fluxes, plant growth, wind patterns, and snowmelt (Zhang et al., 2010). Variations in vegetation can shift surface radiative properties and contribute to greenhouse gas emissions, notably from activities such as deforestation. Consequently, energy partitioning is influenced by local conditions including vegetation type and density. Specific ecosystem features such as soil type, water availability, and biodiversity, along with daylight hours and altitude, further influence this energy partitioning (Hammerle et al., 2007; Zhang et al., 2010). Such shifts can impact local climate and surface energy balance, underscoring the significant influence of LULC on radiation balance (Duveiller et al., 2018).

Radiation splits into direct (solar) and diffuse (reflection and emittance) forms, as shown in Figure 2.1. Atmospheric transmissivity, governed by cloud cover and pollution, dictates the fraction of solar radiation reaching the Earth. The discrepancy between incoming and outgoing radiation, termed net radiation, is vital for evaporation, snowmelt, and soil heat flux.

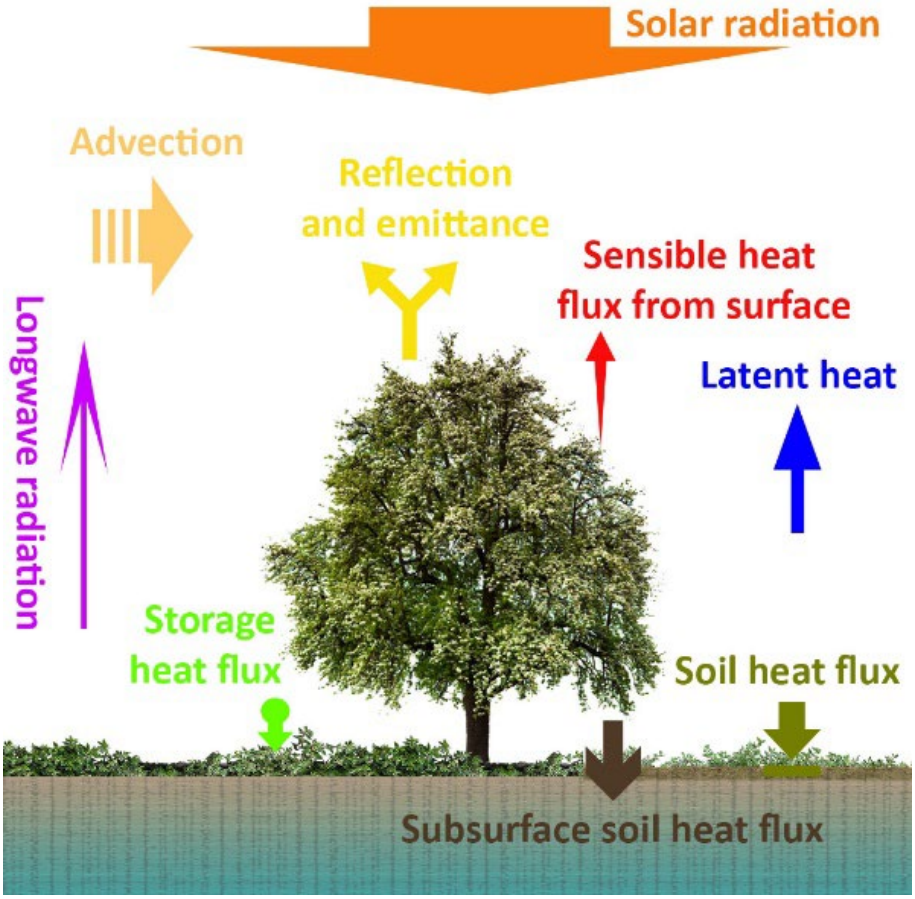

Figure 2.1: Schematic picture of surface energy partitioning by vegetation

2.3.1.2 Modelling approaches

The global water budget is intrinsically linked to the global energy budget due to its impact on processes like evapotranspiration, snowmelt, and soil heat dynamics (Wang et al., 2018). When water changes of phase (solid, liquid, and gas), energy is absorbed or released, thus affecting the energy budget (Healy et al., 2007). Incoming solar radiation is the fundamental energy driving the processes of photosynthesis, evaporation, heating of the soil, and energy storage in vegetation (Gu et al., 2005). Evaporation is the phenomenon by which water is converted from its liquid into its vapour phase, regardless of whether it resides in the soil, on the surface (including plants) or in vegetation. A simple energy budget for the Earth is (Sellers, 1969):

$$R_n = G + LE + H \qquad \text{Eq. 1}$$

Where R_n is net radiation, the sum of incoming solar and longwave radiation minus reflected solar and emitted longwave radiation; G is the surface heat flux, i.e., the energy used to warm soil or water in the case of a surface-water body; LE is the latent heat flux, i.e., the energy used to evaporate water; and H is the sensible heat flux, or the energy used to warm air (Healy et al., 2007). Equation 1 states that available energy at the Earth's surface goes to heating the surface, warming the air, and

evaporating water (Figure 2.1). Latent heat flux is the product of latent heat of vaporisation (λ) and evapotranspiration rate (*ET*); i.e., $LE = \lambda ET$. Evapotranspiration directly links the energy and the water budget because it appears in both.

In hydrological models, radiation energy partitioning and surface energy balance are pivotal in shaping processes such as evapotranspiration, soil moisture dynamics, snowmelt, and vegetation growth. These processes, in turn, have a significant impact on water temperature and surface runoff. Thus, vegetation dynamics inevitably affect or provide feedback to surface energy partitioning and water budget (Forzieri et al., 2020; Lan et al., 2021). The following subsections will focus on evapotranspiration and snow processes, as these are critical elements of energy partitioning.

2.3.1.2.1 Evapotranspiration

Evapotranspiration, in conditions without snow, refers to the collective water vapour from direct evaporation from the soil's surface layer, transpiration from both the roots and canopy of vegetation, and the evaporation of precipitation captured by the plant canopy (Singh, 2017). Hydrological models typically handle evapotranspiration by either accepting it as input or calculating it as an output parameter. These models may treat evaporation in several ways: as a constant, as a set of monthly average values, as a user-defined time series of values on different temporal scales (monthly/seasonal), or compute them based on climatological variables like temperatures, wind, and sunshine hours (Bormann et al., 1996; Li et al., 2009; Zhang et al., 2016; Singh, 2017; Chia et al., 2020).

There are two groups of evapotranspiration estimation methods in hydrological models: one first estimates separately open water evaporation, soil evaporation and vegetation transpiration and then integrates them to calculate actual evapotranspiration. The other one first estimates potential evapotranspiration and then converts it into actual evapotranspiration, applying a soil moisture extraction function. Zhao et al. (2013) called the first classification gathering methods and the second integrated converting methods. Integrated converting methods are typically applied in lumped conceptual, system, and distributed models. Conversely, physically based hydrological models often employ classification gathering methods for estimating basin evapotranspiration; for more details, refer to Zhao et al. (2013).

The ratio of the actual over the potential evapotranspiration changes with water availability in the soil. Hydrological models commonly utilise soil moisture extraction functions to depict the relationship between actual and potential evapotranspiration. Based on the function employed, it can be associated with the soil type and the Leaf Area Index (LAI). The LAI is intricately linked to the growth stage of the vegetation (Ritchie, 1972; Mintz & Walker, 1993).

The potential evapotranspiration estimation methods can be divided into energy-based, temperature-based and mass transfer-based methods, depending on their mechanisms. Consequently, they vary strongly in data needs. Widely used methods are Hargreaves (Hargreaves & Samani, 1985), Priestley-Taylor (Priestley & Taylor, 1972), and Penman-Monteith (Monteith, 1965).

The Penman-Monteith method requires air temperature, relative humidity, solar radiation, and wind speed. The Priestley-Taylor method requires solar radiation, air temperature and relative humidity. The Hargreaves method requires air temperature only. Independent “ground truth” data is preferably used as a benchmark to assess the performance of these models. Eddy Covariance (EC) systems are widely regarded as the premier method for continuous evaporation measurement (Wang & Dickinson, 2012) and are used worldwide, e.g., FLUXNET (Baldocchi et al., 2001).

2.3.1.2.2 Snow process

The most common snow modelling approaches are based on either conceptual (temperature-based models) or physically based models (energy balance-based models) (Singh, 2017; Liu & Ren, 2019). Bucket-type snow models are typically based on a temperature-index approach, assuming a direct relationship between temperature and snow accumulation and melt. Most of these models aggregate data spatially into areas with similar hydrological responses, known as Hydrological Response Units (HRUs), which facilitates faster computational times and reduces the amount of input data required. HRUs are defined through a detailed hydrological systems analysis using Geographic Information System (GIS) techniques (Flügel, 1995). This analysis incorporates key physiographic basin properties, including topography, soils, geology, rainfall patterns, and land use (Freudiger et al., 2017). By integrating these diverse factors, GIS helps ensure that each HRU accurately reflects the unique hydrological characteristics of its area, facilitating more precise and effective hydrological modelling.

Extended temperature-index approaches that include spatially distributed solar radiation are frequently used in hybrid methods, reducing the computational effort (Hock, 1999). The inclusion of solar radiation is particularly relevant for high elevations, often glacierised areas, where temperatures seldom rise above freezing. This adaptation enhances model accuracy by accounting for the significant role of solar radiation in melting processes under consistently cold conditions (Pellicciotti et al., 2014; Gabbi et al., 2017).

More complex models are evolving from uniform snow cover models to more complex ones, allowing non-uniform cover due to topography, drifting, shading, and land cover. These models are generally highly complex, distributed, physically based, and very detailed, with a high spatial and temporal resolution. All energy fluxes are considered in these models (Lundberg & Halldin, 2001). Still, their

use is thus constrained by data availability and computational time, rendering them most suitable for small catchments or plot scales and limited durations, such as a few winter seasons or specific events only (Lundberg & Halldin, 2001).

2.3.1.3 Challenges

Differences between evaporation models and observations stem from both conceptual limitations in the models and flaws in measurement techniques (Coenders-Gerrits et al., 2020). In his 2004 article, Savenije criticises the term ‘evapotranspiration’, deeming it outdated due to its oversimplified grouping of diverse evaporative processes such as evaporation from intercepted water, transpiration from plants, soil evaporation, and open-water evaporation. He notes that these processes vary significantly in their temporal dynamics, physical properties, climatic interactions, and isotopic compositions, advocating for a more nuanced approach in hydrological studies (Savenije, 2004).

In this context, the complexity of accurately modelling evaporation becomes evident when considering the role of atmospheric composition in influencing radiative fluxes, as highlighted by Dhara (2020). These fluxes significantly affect the earth’s surface heating, which impacts evaporation rates. Similarly, Yin et al. (2019) emphasised the critical role of evaporative cooling on the earth’s surface, which modulates radiation conversion into sensible heat, affecting temperature readings and further complicating evaporation modelling. These insights emphasise the complex interplay between atmospheric conditions and evaporation, reinforcing the need for sophisticated modelling approaches that can accurately reflect these dynamics.

In most existing studies, water budget and surface energy partitioning were generally examined in isolation regarding vegetation greening (Lan et al., 2021). However, these elements should not be analysed in isolation due to their close interdependencies with LAI-related biophysical processes (Pitman, 2003; Bagley et al., 2017; Zeng et al., 2017). The continuous rise in LAI, a result of vegetation greening, impacts surface albedo, thereby influencing the net terrestrial radiation (Rn) that is crucial for driving both latent and sensible heat fluxes (Kala et al., 2014). This, in turn, modifies the surface energy partitioning (Kleidon, 2019; Forzieri et al., 2020). Therefore, a detailed examination of how surface energy partitioning and water budgets respond to vegetation dynamics amid widespread greening is essential (Kala et al., 2014; Ma et al., 2017).

Though the Penman-Monteith method is the standard for modelling potential evapotranspiration, its detailed process might not align with other models’ accuracies, especially concerning soil moisture extraction functions (Neitsch et al., 2011). Some soil moisture extraction methods consider factors like root suction and canopy density, yet they often fail to account for spatial and temporal variations in surface characteristics. This oversight can lead to significant errors when calculating average daily soil moisture values (Baier & Robertson, 1966). Moreover, using the Penman-Monteith equation with

mean daily climatic parameters can result in substantial inaccuracies. Such errors are due to diurnal variations in wind speed, humidity, and net radiation, which are conditions not captured by daily averages, leading to potential discrepancies in evapotranspiration estimates. (Neitsch et al., 2011). Hence, we need further research on how to select appropriate potential evapotranspiration equations and soil moisture extraction functions for different hydrological models to reduce their uncertainty.

Operational hydrology simplifies snow interception, even though snow storage, both in mass and duration, typically exceeds that for rain, making it a critical model component. The evaporation of snow intercepted by forest canopies remains a poorly understood element of the winter water-balance equation (Lundberg & Halldin, 2001). Ignoring it in hydrological models can alter the timing and volume of simulated snowmelt and affect the catchment water balance (Freudiger et al., 2017). In catchment-scale hydrological modelling, simulating separately the snow cover accumulation inside and beneath the canopy has rarely been applied so far, so more effort is needed in modelling snow processes (Gouttevin et al., 2015; Förster et al., 2018).

The effects of the forest canopy on snow accumulation and snowmelt processes need to be considered in simulations of the hydrological response of catchments with a significant fraction of the forested area. Despite the well-established accuracy of process-based, energy-budget snowmelt models, there is a propensity towards using temperature-index or degree-day snowmelt relationships in hydrological models to simulate snowpack processes (Walter et al., 2005). However, the critical temperature of these methods is not constant across basins; it varies with topography and elevation (Walter et al., 2005; Liu & Ren, 2019). Models must also consider variations in canopy albedo due to its significant impact on snow interception (Lundberg & Halldin, 2001). Oddly, many models employ energy balance approaches, like the Penman equation, for estimating potential evapotranspiration. Thus, it is inconsistent that these models do not employ the same energy balance approaches for modelling snowmelt (Walter et al., 2005).

The dynamics of precipitation characteristics, including type, duration, spatial distribution, and intensity, can significantly impact evaporation. Additionally, the interaction between precipitation and interception effects on sublimation and condensation poses challenges for accurate modelling (Svoma, 2016; Gutmann, 2020). Sublimation from canopies in winter, although less in volume than summer evaporation, plays a more significant role than evaporation in modelling winter hydrological processes, and measurements are scarce (Frank et al., 2019). Energy budgets have challenges explaining snow interception losses, as they need to account for melting, evaporation, and sublimation (Molotch et al., 2007; Allen et al., 2020). Incorrect snowmelt modelling affects not only the day on which the melt event was predicted inaccurately but also the day of the actual melt event, resulting in multiple periods of incorrect streamflow simulation (Zeinivand & De Smedt, 2008). Hence, accurate spatial distribution of snow depth is vital for precise runoff calculations (Liu & Ren, 2019).

2.3.2 Water interception dynamics

2.3.2.1 Physical mechanisms

Interception refers to the portion of rainfall captured by the Earth's surface (e.g., vegetation). Part of this intercepted water evaporates back into the atmosphere (Muzylo et al., 2009; Meili et al., 2021). LULC, rainfall patterns, and evaporative demand influence the rate, capacity, and loss of interception (Van Meter et al., 2016; Zhou, 2022). While built-up areas experience interception, its significance is more pronounced in vegetated regions. With their vast surface area, trees, shrubs and litter capture a large volume of rainwater, shielding the soil from direct impact (Figure 2.2). This conserves soil integrity and curtails erosion while modulating water flow to streams, thereby reducing flooding potential (Gerrits & Savenije, 2011).

Canopy water storage varies based on intrinsic factors like vegetation density and plant morphology and extrinsic factors like storm conditions (intensity and duration) and temperature (Van Stan II & Friesen, 2020). These factors differ across plant species, leading to diverse canopy storage capacities (Klamerus-Iwan et al., 2020). Similarly, these factors influence a canopy's ability to store snow. Snow storage in canopies surpasses rain and has been observed to cover a significantly broader spectrum and seasonal variation depending on storm and climate conditions (Lundberg & Halldin, 2001; Storck et al., 2002; Förster et al., 2018). Several extrinsic factors impact the response and capacity of the canopy reservoir, like hydrometeorological (storm) conditions that control crystal form, internal bonding of snow and adhesion of snow to vegetation (Satterlund & Haupt, 1967; Schmidt & Pomeroy, 1990; Klamerus-Iwan et al., 2020). As a large proportion of intercepted water evaporates from the canopy, also the understorey and litter layer can significantly affect subsequent hydrological processes (Gerrits & Savenije, 2011; Van Der Ent et al., 2014; Porada et al., 2018).

The ground layer's characteristics vary by region and ecology, ranging from short vegetation to decomposing organic materials or bare soil (Gerrits & Savenije, 2011). These variations significantly influence local water processes, including precipitation interception and evaporation (Gerrits & Savenije, 2011). The litter layer, often lacking deep-rooted vegetation, primarily experiences water movement through gravity and evaporation, with minimal transpiration (Klamerus-Iwan et al., 2020). This layer serves as a transitional zone, impacting water storage through variations in litter composition and its seasonal dynamics (Gerrits & Savenije, 2011; Van Stan et al., 2017; Klamerus-Iwan et al., 2020). Hence, conceptualising water storage at the land surface is challenging due to the litter layer but also due to the variability in precipitation type and intensity (Gerrits et al., 2007; Gerrits et al., 2010; Klamerus-Iwan et al., 2020). Although forest floor evaporation seems to overlap with soil evaporation, the distinction is that soil evaporation pertains to the water in the root zone (Groen & Savenije, 2006).

In forest ecosystems, microclimates significantly influence hydrological processes. Wind plays a role in understory evaporation but has limited impact on litter storage due to vegetation's wind-reducing effects (Singh, 2017). The forest floor experiences less evaporation than the overstory due to lower radiation, yet intermittent storms can heighten evaporation, affecting litter storage and throughfall (Gerrits et al., 2009; Gerrits & Savenije, 2011). Additionally, snow dynamics under the canopy are complex. Canopies can alter ground snow processes, causing non-uniform snow patterns and influencing melt timing (Förster et al., 2018). Snow interception by dense canopies and subsequent sublimation or melt of intercepted snow can reduce sub-canopy snow accumulation by up to 60% (Hardy et al., 1997). Factors like shading and reduced wind contribute to delayed melting, while increased tree-emitted radiation accelerates it (Sicart et al., 2004; Essery et al., 2008; Pomeroy et al., 2009; Strasser et al., 2011; Lundquist et al., 2013).

The primary factors influencing snow processes are canopy density and specific geographical attributes such as elevation, slope, and weather conditions (Pomeroy et al., 2002; Jost et al., 2007; Strasser et al., 2011). In contrast to the influence of phenology and morphology on the movement of liquid water, the discharge of intercepted snow is predominantly determined by hydrometeorological factors rather than the specific characteristics of individual trees. However, these relationships have not been extensively researched (Satterlund & Haupt, 1970; Schmidt & Gluns, 1991; Gouttevin et al., 2015). These nuanced interactions underscore the complex interdependencies within forest hydrology, shaped by the delicate balance of microclimatic factors and vegetative structures.

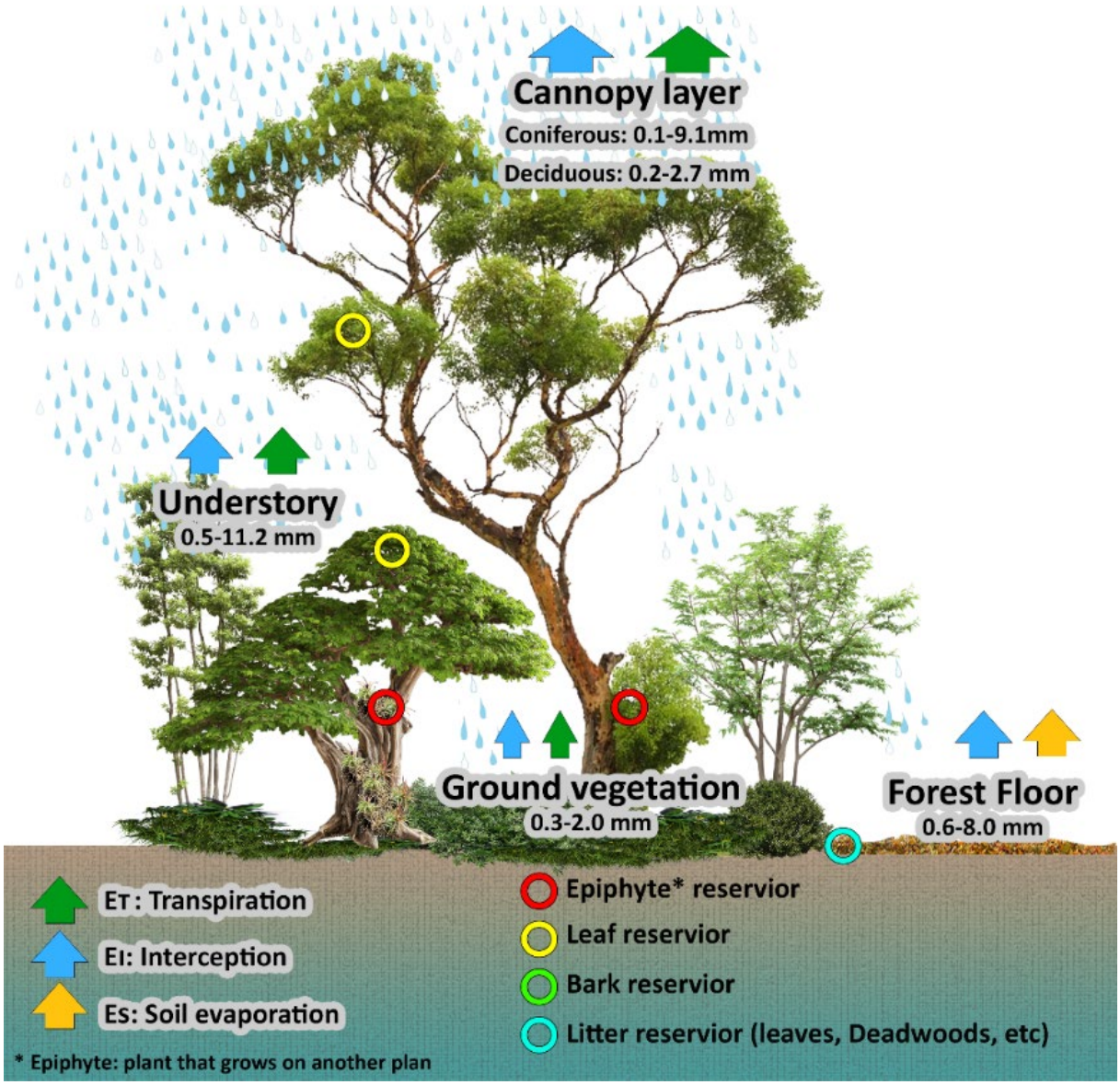

Figure 2.2: Schematic representation of the multi-layer reservoirs within vegetated ecosystems, highlighting the water storage and movement dynamics (Reservoir capacities are based on Klamerus-Iwan et al. (2020)).

2.3.2.2 Modelling approaches

In large-scale modelling, the concept of interception predominantly pertains to vegetated areas. Considering that the proportion of urban areas is typically minimal in comparison to other LULC categories, it is widely accepted that, over extended periods like a year, rainwater intercepted by ground surfaces and building roofs tends to evaporate fully (Daba & You, 2020; Zhou, 2022). Therefore, the runoff coefficient determines solely the rainwater interception evaporation on sealed ground and pavement (Zhou, 2022).

Numerous models have been developed for simulating interception, especially in forested contexts. These models can be adapted to account for interception on the forest floor or any other surface

(Gerrits & Savenije, 2011). The modelling of this interception incorporates diverse approaches, each characterised by its unique methodology (Muzylo et al., 2009). The Gash Analytical Model (Gash, 1979) is a prominent example among models frequently utilised in hydrological studies, known for its grounding in observed data and statistical correlations. This model, and others like it, employs parameters such as total precipitation, canopy evaporation, throughfall, and storage capacity. While the strength of the Gash Analytical Model lies in its simplicity and robust empirical basis, this simplicity may also limit its comprehensive applicability in capturing all aspects of hydrological processes (Gash, 1979). It is important to note that this limitation is not unique to the Gash Analytical Model but is a characteristic shared by similar models in the field.

Conceptual models usually deal with redistributing rainfall volume using a mass balance equation. For example, the Rutter model uses a bucket-type approach to divide rainfall into intercepted and throughfall components based on canopy storage capacity (Gash & Morton, 1978). Stochastic models in this category may use Markov Chains to represent the probabilistic nature of rainfall (De Groen, 2002). Conceptual models provide a more structured representation compared to empirical models, dividing the canopy into different layers and using parameters like total precipitation, storage capacity, and evaporation rate to estimate interception, storage, and evaporation processes (Muzylo et al., 2009).

Physical models are the most detailed, often employing differential equations to simulate water flow over leaves, infiltration, and evaporation. (Muzylo et al., 2009; Paniconi & Putti, 2015). These models may be three-dimensional and incorporate variables such as wind speed, temperature, relative humidity, LAI, and storage capacity. These parameters are crucial for accurately modelling the complex behaviours involved in water interception by vegetation, including how water is captured, stored, and eventually evaporated or absorbed by the plant (Herwitz & Slye, 1995; Bussière et al., 2002; Muzylo et al., 2009).

2.3.2.3 Challenges

Operational hydrology often oversimplifies the interception process, potentially leading to evaporation underestimation in hydrological models (Lindström et al., 1994; Lundberg & Halldin, 2001; Mueller et al., 2013; Liu et al., 2016). Modelling interception is challenging due to the complexities of landscapes. While short vegetation is frequently reasonably modelled, forests are multi-layered and have varying water interception rates across layers, which presents modelling challenges (Breuer et al., 2003; Gerrits & Savenije, 2011). Comparing different forest evapotranspiration models with Eddy Covariance (EC) data has shown the highest discrepancy, indicating that forest systems are likely not yet modelled correctly (Ershadi et al., 2014; Ha et al., 2015).

In vegetated areas, the mechanisms of water interception are often modelled and simplified as the dynamic processes of filling and emptying static water storage compartments. Most models conceptualise the storage and redistribution of precipitation water on vegetation as a uniform-sized reservoir, or, more recently, the LAI is used by models to compute the maximum storage at any time in the land cover/crop growth cycle. However, accurately measuring and quantifying LAI is challenging due to sensor spectral and spatial resolution limitations and the variability in vegetation structure and density (Luo et al., 2020; Xu et al., 2020; Chen et al., 2023; Li et al., 2023).

Numerous hydrological models directly correlate canopy storage with the LAI, adjusted by a daily phenological multiplier specific to different plant functional types (Gerten et al., 2004; Murray, 2014; Klamerus-Iwan et al., 2020). The storage capacities indicated by these models are generally low (0.2–2 mm) compared to field measurements (1–16 mm), likely due to the limitation of LAI in encompassing the diverse other storage components present within vegetated ecosystems (Gerrits & Savenije, 2011; Van Stan II & Pypker, 2015; Porada et al., 2018; Klamerus-Iwan et al., 2020). Vegetated ecosystems possess interconnected reservoirs with different capacities and operational timescales. Components such as tree crowns, trunks, understory and litter are often overlooked in models, although their storage capacities can be significant (Klamerus-Iwan et al., 2020).

In multilayer systems (e.g., forested systems), multiple storages' filling and spilling characteristics induce temporal shifts (Gerrits et al., 2010). Moreover, the potential evaporation below the canopy is typically lower than that above the canopy. Coupled with the generally larger storage capacity of the forest floor, this leads to residence times for forest floor interception ranging from several hours to days. In contrast, water intercepted by the canopy typically has a residence time of less than an hour (Levia et al., 2011; Wang-Erlandsson et al., 2014; Li et al., 2017; Coenders-Gerrits et al., 2020).

In fact, modelling the sequence in the understorey and forest floor storage and the uncertainty in potential evaporation are the major challenges in modelling the forested setting (Coenders-Gerrits et al., 2020). In addition, there is high seasonal variation and complexity in vegetated systems. For example, using LAI methods, the wintertime interception is close to zero for deciduous trees; however, the forest floor can still have significant water content that can be evaporated (Gerrits et al., 2010; Gerrits & Savenije, 2011; Van Stan et al., 2017). Furthermore, if the growing season's length is not considered in the model, apparently, the vegetation transpired more efficiently than would be expected from air temperature alone (Blöschl & Montanari, 2010). The amount of actual evapotranspiration contributed by intercepted rainfall can be significant, especially in forests where, in some instances, evaporation of intercepted rainfall is greater than transpiration (Neitsch et al., 2011).

It is commonly assumed that interception in leafless deciduous vegetation is low due to rapid unloading under dry snow conditions. However, this may contrast with conifers, where denser intercepted snow can lead to significant snow storage. This discrepancy can result in models overestimating the amount of water entering the unsaturated zone. Consequently, transpiration rates may be inaccurately high, either in reality or as a result of calibration (Van den Hoof et al., 2013). However, this suggests that the model is fundamentally flawed, carrying significant implications for research involving, for instance, climate and/or change modelling (Coenders-Gerrits et al., 2020). To accurately depict snow processes in forested areas, it is essential to adopt a comprehensive approach that simulates both the snow melt rate and the timing of meltwater release (Whitaker & Sugiyama, 2005; Zheng et al., 2016; Förster et al., 2018). The potential benefits of incorporating intercepted snow evaporation into models have been highlighted in recent studies, suggesting a possible route to refining their accuracy (Lundberg & Halldin, 2001).

2.3.3 Water partitioning between runoff and infiltration

2.3.3.1 Physical mechanisms

Upon reaching the ground, precipitation partitions into runoff and infiltration. Both processes are influenced by LULC following precipitation or melting events. Vegetation and litter layers protect soil from raindrop splashes by intercepting precipitation, preventing surface sealing and crusting of soil, extending the time of soil infiltration, and enhancing sediment deposition by increasing soil surface roughness (Li et al., 2014). Additionally, factors like terrain, slope, geology, rainfall characteristics and climate play crucial roles in determining runoff and infiltration, with variations often linked to LULC (Bhark & Small, 2003; Wu et al., 2021).

Human activities associated with different LULC patterns significantly influence on-ground water partitioning. For instance, agricultural practices such as tillage can modify infiltration patterns, either retaining or directing water (Hangen et al., 2002). In urban areas, impermeable surfaces like roads increase runoff and reduce infiltration (Shuster et al., 2005). Urban storm sewers can also amplify streamflow, potentially leading to flooding (Shadmehri Toosi et al., 2019). Infrastructure developments, such as dams, play a role in altering outflow and the volume of water downstream (Schmutz & Moog, 2018).

Moreover, changes in LULC, such as deforestation or the expansion of agriculture, expose soil to erosion. This erodes the nutrient-rich topsoil and diminishes its infiltration and retention capacities (Belay & Mengistu, 2021; Alem, 2022; Prashanth et al., 2023). As erosion continues, it degrades the soil, forming surface crusts that further impede infiltration. The eroded particles accumulate in depressions and streams, elevating runoff levels. This process can lead to the formation of gullies or rills, which act as fast channels for water, reducing the time available for infiltration. Without the

protective cover of vegetation, the health of soil biota, essential for maintaining soil quality, deteriorates. Overall, these LULC-induced alterations result in increased runoff.

2.3.3.2 Modelling approaches

Hydrological models employ diverse techniques to partition rainfall into runoff and infiltration (Sitterson et al., 2018). Empirical models are best suited for ungauged watersheds where runoff is the primary output of interest due to their simplicity, quick computational turnaround, and cost efficiency (Dawson & Wilby, 2001; Pechlivanidis et al., 2011). A typical example is the Curve Number (CN) method, developed by the USDA (Mishra & Singh, 2003). It provides a runoff estimate predicated on soil attributes and overarching LULC (Kokkonen et al., 2001; Devia et al., 2015; Sitterson et al., 2018). Another example is the Rational Method, which is used to estimate peak flow rates based on runoff coefficient, rainfall intensity, and drainage area. While the Rational Method incorporates a runoff coefficient, it does not have the same level of detail or methodology as the CN method (Rossi, 1994). Models, such as Horton's equation designed for infiltration assessment, indirectly aid in runoff estimation. In its original form, Horton's equation does not explicitly include LULC like the CN method. However, the parameters of Horton's equation can be adjusted based on LULC and other factors in practical modelling applications (Horton, 1940). The limitations of empirical models include their dependence on field observations, which are sometimes unavailable (Morbidelli et al., 2018).

Conceptual models like HSPF, TOPMODEL, HBV, Stanford, and ABCD are on the other end of the spectrum, offering a simplified representation of physical hydrological processes (Crawford & Linsley, 1966; Bergström, 1976; Beven & Kirkby, 1979; Thomas Jr, 1981; Bicknell et al., 1997). Conceptual models view a catchment as interconnected storage units with flow movements defined by mathematical functions (Jehanzaib et al., 2022). A significant limitation is that their parameters are not directly derived from catchments, necessitating calibration (Madsen, 2000). In the HSPF model, different LULC types are represented through land segments, each with its distinct set of parameters tailored to the hydrological response of that specific LULC (Bicknell et al., 1997). TOPMODEL integrates LULC by influencing the topographic wetness index with different land covers, affecting parameters like evapotranspiration rates (Beven et al., 2021). The HBV model adopts a distributed approach, where different LULC types are represented by unique response units, each characterised by its hydrological parameters (Bergström & Forsman, 1973). The Stanford Watershed Model employs land use coefficients to adjust hydrological parameters in accordance with the specific LULC type (Crawford & Linsley, 1966). Lastly, the ABCD hydrological model simulates the rainfall-runoff process in a catchment using four parameters: A, B, C, and D (Thomas Jr, 1981). The model can account for the effects of LULC changes on hydrology by adjusting the values of these parameters according to the characteristics of different LULC types.

Physical (process-based) models employ differential equations to simulate catchment behaviour over space and time, as highlighted in the review by Devia et al. (2015). These models intricately describe mass and momentum balances for individual grid cells or sub-catchments and incorporate boundary conditions to account for interconnectivity (Todini, 1988). A key aspect of these models is their approach to modelling infiltration and runoff processes. Infiltration is typically modelled by considering the soil's capacity to absorb water, which is influenced by soil texture, structure, and moisture content. This can involve the use of equations like the Richards equation to simulate the movement of moisture through unsaturated soils. On the other hand, runoff is modelled based on the excess water that cannot infiltrate, often using approaches like the kinematic wave model or the diffusion wave model to represent overland flow dynamics (Orlandini & Rosso, 1996; Singh, 1997; Kim et al., 2012). While these models do not require extensive meteorological and hydrological data for calibration, they do necessitate a detailed assessment of watershed physical characteristics, including soil profiles and topographical features, as emphasised by (Devia et al., 2015). This detailed characterisation is crucial for accurately capturing the complex interactions between infiltration, soil moisture dynamics, and surface runoff in varied catchment conditions.

Notable physical models include MIKE-SHE, KINEROS, VIC, and PRMS (Abbott et al., 1986; Todini, 1988). These modelling approaches are grounded in different mathematical and physical laws (Sitterson et al., 2018). The MIKE-SHE model, known for its comprehensive approach, integrates LULC by determining evapotranspiration, runoff coefficients, and infiltration rates, allowing for a spatial representation of different land covers (Refsgaard & Storm, 1995). KINEROS, an event-oriented model, emphasises the role of LULC in overland flow generation and infiltration, representing different land covers as distinct polygons or grid cells (Goodrich et al., 2012). The Variable Infiltration Capacity (VIC) model, designed for macro-scale hydrologic simulations, uses LULC to define parameters like albedo, roughness length, and root zone depths, adopting a grid-based approach where each cell can encompass multiple LULC types (Liang et al., 1994). The soil in the model is structured into three layers: the top layer facilitates rapid soil evaporation, the middle layer captures the soil's dynamic response to rainfall, and the bottom layer depicts soil moisture behaviour (Devia et al., 2015). Lastly, the Precipitation-Runoff Modelling System (PRMS) offers a deterministic, distributed-parameter perspective. LULC influences processes from snow accumulation to runoff generation, utilising a modular approach to represent varied land covers (Leavesley, 1983).

2.3.3.3 Challenges

Despite advances in remote sensing for land surface monitoring, models often overlook the temporal dynamics of LULC, assuming static land use for extended periods. The generation of runoff from rainfall events is a spatially and temporally complex process profoundly shaped by the terrain's

topography and LULC. Modelling the effects of slope remains an unresolved issue, especially when vegetated surfaces are in play (Singh, 2017).

Many models are formulated for horizontal land surfaces (i.e., SWAT does not adjust curve numbers for slope by default). Moreover, the known morphological evolution of many catchments is frequently sidelined, either for simplification or due to data constraints (Ghomash et al., 2019). The Digital Elevation Model (DEM) quality, crucial for many applications, is influenced by various factors, including land cover and terrain slope (Zhao et al., 2010; Sulis et al., 2011; Polidori & El Hage, 2020).

Landscape connectivity, which denotes how landscapes facilitate or hinder movement across them, plays a pivotal role in runoff production (Zhao & Huang, 2022). It is vital to grasp as it affects hydrological outcomes, such as heightened flood risks or diminished groundwater recharge. With impervious structures like roads and buildings, urbanisation disrupts natural water flow, amplifying surface runoff. In contrast, natural terrains with dense vegetation promote infiltration, curbing direct runoff. The complexity of various terrains and the nuanced configurations of landforms at different scales pose additional difficulty in creating accurate hydrological models (Gao et al., 2018; Galin et al., 2019). The role of vegetation litter in influencing surface runoff and soil erosion remains an enigma (Li et al., 2014).

Further, changes such as deforestation, urbanisation, or agricultural expansion can amplify soil erosion (Nampak et al., 2018; Hu et al., 2021). Removing vegetation exposes soil to direct rainfall impact and accelerates surface runoff, which can dislodge soil particles (Zuazo & Pleguezuelo, 2009; Zhao et al., 2022). As erosion progresses, nutrient-rich topsoil is lost, potentially exposing less permeable layers like clay or bedrock (Zuazo & Pleguezuelo, 2009). This further complicates modelling as it can alter infiltration rates and increase runoff (Mohr et al., 2013; Wu et al., 2023).

Another critical yet often overlooked challenge is the phenomenon of soil hydrophobicity. The water-repellent nature of certain soils, often due to organic compounds from plant residues or microbial activity, can drastically reduce water infiltration rates. This, in turn, leads to increased surface runoff, posing challenges for accurate modelling (Orfánus et al., 2021).

Generalising hydrological processes as an empirical parameter may not be representative of actual hydrological behaviours and dynamics (Sun et al., 2017). Models, such as the SCS curve number, have been critiqued for their lack of physical justification (Beven, 2011). Numerical models such as Regression, Artificial Neural Network (ANN), Fuzzy, and Genetic Algorithms (GA) are data-driven models incapable of modelling spatially explicit relationships of hydrological responses concerning physical characteristics of the basin, like the influence of change in vegetation on various hydrological components.

2.3.4 Subsurface processes

2.3.4.1 Physical mechanisms

One of the hydrological processes that can be affected by LULC change is groundwater recharge. A recharge area can be defined as that portion of the drainage basin in which the net saturated flow of groundwater is directed away from the water table (Freeze & Cherry, 1979). Recharge can be categorised into several types, like natural groundwater recharge, artificial groundwater recharge, induced recharge, inter-aquifer recharge, and incidental recharge. Among the factors affecting recharge (climate, LULC, soil type, topography, and landforms), LULC has been found to be one of the key parameters in estimating recharge (Allison et al., 1990; Allison et al., 1994; Sandvig & Phillips, 2006; Batelaan & De Smedt, 2007; Crosbie et al., 2010; Kim & Jackson, 2012; Li et al., 2018a). The nature of the LULC, e.g., urban, agricultural, or forested area, can influence the volume, quality and type of this recharge. Seasonal LULC variations affect recharge due to the diverse recharge potential in different seasons (Siddik et al., 2022).

Urbanisation often replaces permeable surfaces with impermeable ones like asphalt, reducing natural recharge (Abdelaziz et al., 2020). Conversely, human activities and infrastructure like building artificial surface water storage structures like dams, ponds, lakes, and canals can enhance groundwater recharge by allowing water to infiltrate the soil below and enter the groundwater storage (Gale et al., 2002). Induced recharge can also occur when human activities, like heavy groundwater extraction, cause surface water to seep into aquifers (Ayotte et al., 2011).

Artificial or managed aquifer recharge can augment groundwater levels (Zhang et al., 2020; Raja Shekar & Mathew, 2023). Plantations may also help enhance groundwater recharge as planted landscapes are regularly rotated and monitored (Kristanto et al., 2022). Moreover, water extraction in plantations tends to be less extensive than in dense forests, consequently significantly reducing evapotranspiration (Geng et al., 2022). Thus, if dense forests turn to fragmented landscapes, groundwater recharge can potentially increase (Scanlon et al., 2007). In contrast, expanding impervious surfaces means less land where recharge may occur. On the other hand, fewer trees in urban areas abstract lots of water and lose it through evapotranspiration (Hornbeck et al., 1993).

In some places, water moves upward due to capillary forces, influencing soil moisture, while in areas with shallow water tables, phreatophytes might directly tap into this subsurface reservoir, extracting and releasing it via evapotranspiration (Batelaan et al., 2003; Wang et al., 2023). Incidental recharge results unintentionally from human activities like irrigation or canal seepage (Asano & Cotruvo, 2004; Wakode et al., 2018). Agricultural practices offer a dichotomy. While irrigation can enhance groundwater recharge (Zhang et al., 2023), the expansive agricultural areas often extract groundwater

at rates surpassing the recharge. Moreover, these practices can lead to soil issues, such as salinisation, which impede natural recharge (Kulmatov et al., 2020).

In vegetated systems, root characteristics such as form, diameter, depth, distribution, and developmental state significantly influence their function (Collins & Bras, 2007; McCormack et al., 2015; Coleman & Aubrey, 2018). Consequently, recharge rates demonstrate variability primarily attributed to the diverse root distributions characteristic of various topographical features, including tablelands, upslopes, midslopes, and downslopes (Collins & Bras, 2007; Li et al., 2018a).

Root depth and distribution are key to how plants manage soil moisture, particularly in water-limited ecosystems (Collins & Bras, 2007). Deep-rooted vegetation can significantly affect groundwater recharge, especially in areas with shallow water tables (Barua et al., 2021). Due to evolutionary adaptation, e.g., osmotic adjustment or hydraulic redistribution, arid and semi-arid native vegetation is capable of making better use of soil moisture and accessing deeper soil water reserves as compared to crops (Scanlon et al., 2005; Chen & Jiang, 2010; Sardans & Peñuelas, 2014). Water limitations in arid and semi-arid regions lead to a general trend where evapotranspiration rates among different vegetation types tend to be more comparable than in more water-abundant environments (Owuor et al., 2016). However, within this overall trend, there are variations. Forests and shrubs, due to their deeper root systems and physiological adaptations, are typically more efficient at transpiring water than grasslands or crops, resulting in lower recharge rates (Scanlon et al., 2002; Scanlon et al., 2005; Li et al., 2018a). Consequently, non-vegetated areas, or those with less efficient water use, may experience higher recharge rates (Fitts, 2013), but this, too, is subject to the influence of other factors mentioned earlier.

2.3.4.2 Modelling approaches

Modelling subsurface hydrological processes focuses on water movement through subsurface areas, including the unsaturated (vadose) zone and saturated groundwater flow. Empirical models of recharge employ advanced techniques such as geostatistics and Markov chain models to represent the variability of subsurface attributes (Yu & Lin, 2015; Maples et al., 2020). Models like Kostiakov and Horton, which are either semi-empirical or empirical, are typically derived from field or lab data and are often represented as straightforward equations (Mishra et al., 2003; Ma et al., 2010). Moreover, machine learning models can draw connections between groundwater levels and associated rainfall amounts based on dominant patterns (Yifru et al., 2021).

Conceptual groundwater models typically utilise interconnected storage components or tanks, which are intrinsically tied to a water budget (Yifru et al., 2021). These tanks symbolise distinct storage zones in the soil, such as surface and root zone or unsaturated and saturated zone (Liu et al., 2017). Each zone has unique storage dynamics crucial to the soil water budget. These models assume one-

dimensional vertical water flow through unsaturated zones, considering single or multiple noninteracting soil columns (Healy, 2010). Transfer functions transport drainage from the bottom of the root zone to the groundwater. Conceptual models may explicitly account for plant growth, water uptake from soil by plant roots, and release of that water to the atmosphere through leaf stomata (Fischer et al., 2008; Healy, 2010).

In contrast, physically based models offer a more comprehensive view of subsurface processes. Notably, the Richards equation and the Green–Ampt model are among the most prevalent physically based models (Ma et al., 2010). The Green-Ampt model is primarily designed to describe soil infiltration (Green & Ampt, 1911; Chen et al., 2015). While the Green-Ampt model does not inherently incorporate LULC factors, it can be integrated with other models or systems considering LULC changes.

Other groups of physical models rely on Darcy's law for the saturated domain, and the Richards equation for the unsaturated conditions, which describes the vertical movement of water in response to capillary and gravitational forces. LULC and root characteristics can be integrated into models based on the Richards equation by specifying distinct zones within the soil profile where hydraulic properties like conductivity and water retention curves are altered. The hydraulic conductivity itself may also be modified in root-affected zones to account for changes in soil structure (Kutílek, 2004). Additionally, plant water uptake can be modelled as a sink term in the equation, with the rate of uptake influenced by both root density and soil moisture conditions (Yadav & Mathur, 2008). Finally, spatial variability in vegetation types and root characteristics can be integrated into using LULC data, thus making the Richards equation-based model more adept at capturing the complex interactions between root systems and soil moisture dynamics.

2.3.4.3 Challenges

The relationship between LULC and groundwater recharge is often non-linear and influenced by various interacting factors like soil properties, climate, and human activities, making it challenging to capture these complex interactions accurately. Estimating infiltration at different spatial scales grows more intricate due to the natural variability in soil hydraulic properties and the range of rainfall patterns (Morbidelli et al., 2012). Adding LULC to groundwater and recharge models introduces an additional layer of complexity to this challenge, requiring an interdisciplinary, context-sensitive approach. However, by incorporating dynamic LULC data, groundwater models can become more reliable, versatile, and applicable for various temporal and spatial scales.

The integration of LULC data into subsurface process modelling is critically hampered by the limited availability of high-resolution LULC data, especially detailed information on root systems and soil interactions (Sun & Li, 2023). This deficiency is significant since vegetation, a key element of LULC,

substantially affects subsurface moisture dynamics. Specifically, plant roots can extract water from deeper soil layers, thereby influencing moisture balance. These interactions are complex and vary widely across different spatial and temporal scales (Beven et al., 2014; Xie et al., 2022). For example, root structures undergo seasonal variations, and external climatic factors further complicate these changes.

Adding to the complexity is the dynamic nature of LULC, which can change over time due to factors like urbanisation, agriculture, and deforestation. Rapid or extensive LULC changes can profoundly alter subsurface water pathways, storage, and availability (Foley et al., 2005; Owuor et al., 2016; Xie et al., 2022). This requires models to incorporate time-series data, a resource that is not always readily available. However, this inclusion also adds new parameters that require additional calibration, validation and uncertainty assessment, especially in areas where observational data are sparse. Further complicating is the mismatch in spatial and temporal scales between groundwater processes and changes. This scale mismatch can result in misleading or inaccurate model outcomes if not adequately addressed (Xie et al., 2022).

Some LULCs, like urban areas, pose challenges in balancing water due to altering natural drainage patterns and widely distributed new abstraction points in the urbanised region (Wakode et al., 2018). Calculating overall recharge can be achieved by combining separate estimates of natural recharge from precipitation with recharge from water supply and wastewater systems (Lerner, 2002; Wakode et al., 2018). However, the challenge here is unpermitted water extraction. These unlicensed groundwater abstractions introduce unknown variables, leading to inaccuracies and uncertainties in model predictions.

Moreover, specific LULC alterations, such as certain agricultural practices or the deployment of heavy machinery, can induce soil compaction, thereby affecting its porosity and permeability and, consequently, the subsurface water movement. Legacy effects from past LULC changes, like deforestation or wetland drainage, can persistently influence subsurface water dynamics (Lamichhane & Shakya, 2019; Guo et al., 2020; Lamichhane & Shakya, 2020). The repercussions of historical land management decisions can reverberate, affecting subsurface hydrological processes for extended periods. Given these complexities, relying exclusively on empirical equations might fall short of accurately capturing the multifaceted impacts of LULC variability. While climate change and land cover shifts can significantly impact shallow groundwater systems, how future recharge will influence these systems is unclear (Mussa et al., 2020). Changes, particularly in built-up areas, have been a focal point in many studies, but alterations in agricultural practices often go unnoticed. In regions with intensive agriculture, a shift in crop type can significantly affect water recharge. It is essential to account for both transient (like vegetation shifts) and permanent (like urban expansion) changes (Adhikari et al., 2022).

While fundamental to vadose zone hydrology, the Richards equation has been critiqued for its inability to capture the intricacies and heterogeneities of soil water flow, prompting calls for a re-evaluation and the development of more comprehensive measurement techniques. It assumes a soil continuum in basic form, potentially missing small-scale soil variations. The equation excludes tortuous water pathways, air entrapment, and plant root effects. Its reliance on the Darcy-based relationship for unsaturated flow also overlooks specific kinematic effects and dynamics between liquid and gas phases (Beven & Germann, 1982; Beven, 2011; Beven & Germann, 2013; Beven, 2018). It also may not capture preferential flow paths in soils with features like cracks (Beven, 1989; Binley et al., 1989a; Binley et al., 1989b). Beven (2019a) states that the Richards equation should be reconsidered, rooted in an experiment that ignored preferential flows. This stance is backed by both experimental evidence and inherent physics, especially considering soil property heterogeneity (Beven & Germann, 1982; Beven, 2011; Beven & Germann, 2013; Beven, 2018). Flows, in reality, can be localised, variable, and have spatial-temporal complexities (Freer et al., 1997; Jencso et al., 2009; McGuire & McDonnell, 2010; Klaus & Jackson, 2018). Yet, we lack effective measurement techniques for studying such flows. Instead of focusing on intricate details, there is a suggestion to develop measurement techniques for larger scales that encapsulate these details (Beven & Germann, 1982; Beven, 2011; Beven & Germann, 2013; Beven, 2018).

2.4 Discussion

2.4.1 LULC data

Space agencies are deploying satellites equipped with advanced sensors for LULC mapping, utilising Earth Observation (EO) data (Petrişor et al., 2010; Diaz-Pacheco & Gutiérrez, 2014; Pandey et al., 2021). Satellite imagery is characterised by various attributes, including spatial, spectral, and temporal resolutions, which determine their suitability for diverse applications. Higher spatial resolution enhances mapping accuracy by providing detailed images, while increased spectral resolution assists in distinguishing different features (Pandey et al., 2021). Temporal resolution is equally important for detecting changes and understanding dynamics over time. For instance, seasonal resolution is vital for monitoring agricultural cycles, while annual resolution helps in urban and forest cover studies. Increasing remote sensing data has led to the emergence of new classification systems for evaluating LULC and spatial changes. Understanding the input dimensions, types of remotely sensed data, and the correct implementation of classifiers in LULC mapping is essential. This understanding enables one to effectively assess the advantages and limitations of various approaches and their combinations as applied in the study (Pandey et al., 2021). Detailed information regarding Earth observation data sources and classifiers can be found in the study by (Pandey et al., 2021).

Various sources of LULC data exist worldwide (Pérez-Hoyos et al., 2012; Szarek-Iwaniuk, 2021). Among the most prominent ones are the Corine Land Cover (CLC) system, developed by the European Environment Agency for Europe's environmental monitoring (Büttner, 2014); the United States Geological Survey (USGS) Land Use and Land Cover Classification System (LULC) (Witmer, 1978), used in the United States for standardised land classification; and the FAO Land Cover Classification System (LCCS) (Herold & Schmullius, 2004), offering a flexible framework adaptable to various regions and scales. Additionally, the Modified UNESCO Classification (Becker et al., 1998), the International Geosphere-Biosphere Programme (IGBP) Land Cover Classification (Loveland et al., 2010), the Global Land Cover (GLC) project (Bartholome & Belward, 2005), and the MODIS Land Cover Type play crucial roles in supporting global environmental research and providing comprehensive land cover data (Friedl et al., 2002).

While LULC products are diverse and accessible, they have limitations like limited coverage (both temporal and spatial), data validity, detail level, and inconsistent nomenclatures. LULC databases are updated inconsistently and may not meet current research demands (Pandey et al., 2021; Szarek-Iwaniuk, 2021). Moreover, many landscapes and sensors have spawned varied classification techniques, complicating comparative analyses. Further, many LULC maps are overly generalised, lacking the detail needed for specific research (Pandey et al., 2021; Szarek-Iwaniuk, 2021). This simplified categorisation disregards the inherent variations within the same category, which can significantly influence vegetation's water storage and transportation mechanisms. These factors impose constraints on the efficacy of hydrological models, potentially causing them to succeed in specific case studies while yielding suboptimal results in others.

A crucial improvement lies in augmenting the current LULC data with additional information to enhance surface characterisation. Without that, sparsely vegetated boreal evergreen needleleaf forests could be functionally interchangeable with a coastal temperate evergreen needleleaf forest as they may fall into the same LULC category. Even if labelled similarly, LULC can exhibit vastly different hydrological behaviours depending on the context, such as variations in the understorey and litter layers and temporal factors like seasonal changes. This generic categorisation often results in models exhibiting sensitivity based on parameter settings and temporal scales (Huang et al., 2013; Jin et al., 2019).

Advancements in satellite remote sensing have ushered in a new era for monitoring evapotranspiration, particularly on broader scales with heightened spatiotemporal precision (McShane et al., 2017). While these technological strides provide significant insights, ground observation data continues to be pivotal for the calibration of such imagery, solidifying the trustworthiness of subsequent forecasts (Chia et al., 2020). Beyond mere data collection, remote sensing has proven instrumental in discerning snow cover nestled within forest canopies, offering a

more profound understanding of snow interception dynamics (Allen et al., 2020). This improvement in satellite innovation and ground observations is a promising pathway to refine and enhance hydrological models.

Yet, despite advancements in vegetation understanding and remote sensing, many models inadequately incorporate LULC dynamics (Sun et al., 2017). Even with data allowing for LULC temporal variations, many models persistently use static LULC. However, it is essential to integrate continuous LULC changes for accurate LULC-climate-hydrology interactions in a rapidly changing world (Castillo et al., 2014). Accurate and consistent mapping of change dynamics requires attention to aspects from spatial to spectral and temporal dimensions. In large-scale hydrological studies, pre-modelling data analysis is crucial to understanding the dynamics and inconsistencies between LULC datasets (Kauffeldt et al., 2013). Analysing different datasets independently aids in forming robust conclusions on choosing the best model to get the desired outcome (Juston et al., 2013; Magnusson et al., 2015).

2.4.2 Selecting the appropriate model

While modelling every physical process is not viable, it is essential to understand desired outputs and choose an optimal model structure based on data and budget constraints. Process simplification results from limited knowledge and data, imprecise measurements, and involvement of multiple scales and interactive processes. These simplifications introduce uncertainty and make it an intrinsic property of any model (Moges et al., 2020). More intricate models prove beneficial for exploring natural hydrological principles and mirroring real-world processes with higher fidelity (Zhao et al., 2013).

However, model performance does not always indicate increased accuracy; outcomes can significantly vary based on factors like the specific hydrological variable (e.g., runoff vs. soil moisture), hydrological conditions (floods vs. droughts), and temporal scale (Orth et al., 2015). Complex models may suffer from over-parametrization but miss relevant processes if they are too simple (Orth et al., 2015). For example, Lopez et al. (2020) demonstrated that setting up an energy-balance model with a simplified snowpack structure can provide nearly identical performance as a much more complex snow-physics model.

Model complexity is vital while evaluating the ability of the models to simulate the desired LULC and climate change scenarios. However, when more detailed results are needed, a fully distributed and/or physically based approach may be required, and it may be necessary to collect detailed data to apply the model (Bormann et al., 2009; Elfert & Bormann, 2010). Besides spatial discretisation, the model's temporal resolution, which may be restricted to specific intervals (e.g., sub-daily, daily, monthly), significantly impacts data availability and model complexity (Chien et al., 2013).

Differences in simulation quality among models arise from uncertainties in input data, calibration approaches, parameterisation, and model structures (Cornelissen et al., 2013; Dwarakish et al., 2015). Therefore, it is essential to be aware of the assumptions, trade-offs, and sources of error inherent to each downscaled data set and understand how those issues might apply to the particular question and location (Singh, 2017). Researchers must apply models judiciously, re-evaluating processes like the Buckingham–Richards as suggested by Beven (2019a). Beven further underscores that uncertainties are a fundamental characteristic of hydrological data (Beven, 2019b; Beven, 2019a). These uncertainties are frequently treated as aleatory, a classification largely driven by the ease of applying statistical techniques for analysis.

The broader modelling landscape, especially related to LULC, is undergoing significant shifts. For instance, the widespread online availability of hydrological data facilitates expansive and efficient simulations with platforms like Google Earth Engine. This accessibility, combined with diverse modelling approaches, not only refines our comprehension of hydrological processes but also elucidates the nuanced interplay between LULC changes and climate shifts (Cornelissen et al., 2013).

Moreover, while it is challenging to account for all processes associated with LULC, their effects are evident in the data. Advanced analytical techniques, enhanced by data-mining innovations, have the potential to offer more universally relevant solutions and introduce alternative process perspectives. Given the limitations of empirical, physical-based, and conceptual models, there is a growing interest in advanced data-driven models, including machine learning (ML) and deep learning (DL) (Jehanzaib et al., 2022).

2.4.3 Enhancing model mechanisms

While remote sensing offers qualitative insights into landscape patterns, they carry epistemic uncertainties (e.g., rainfall and soil moisture estimation). Complexities arise in capturing soil variations, antecedent moisture, infiltration, topography, and rainfall distribution. Further, dealing with human-made infrastructures and vegetation is still associated with many uncertainties. LULC significantly impacts hydrological processes in models with natural LULC changes typically evolve gradually because of ecological processes. In contrast, human activities like deforestation, agricultural expansion, and urbanisation cause rapid LULC alterations. Significant natural shifts, such as those from bushfires or floods, can arise due to extreme climate events.

These rapid changes, whether from human activity like dam construction or natural events like bushfires, can profoundly impact landscapes and the water balance of an area (Singh, 2017). The rapid and significant changes in vegetation and climate violate the prevailing assumption of a long-term steady water balance in hydrological models. This presumption, which does not account for abrupt or substantial environmental shifts, introduces considerable uncertainty in water balance,

particularly in regions experiencing extensive LULC transformations (Devia et al., 2015; Liu et al., 2019).

Understanding the hydrological response to rapid LULC changes is challenging (Dwarakish et al., 2015). In many studies, large and frequent inconsistencies between climate datasets and observed discharge showed clear spatial patterns, possibly caused by anthropogenic influences (e.g. inter-basin transfers, irrigation and reservoirs) (Devia et al., 2015; Liu et al., 2019). Infrastructure and urbanisation can alter surface connectivity, potentially increasing runoff and flooding risks (Wang et al., 2022).

While some changes may seem minor or localised, their ripple effects on the hydrological processes can be substantial. For instance, the escalation of erosion due to deforestation in sloped areas results in an accumulation of sediments in aquatic systems (Brandolini et al., 2018; Kumar et al., 2023). This process alters flow regimes and storage capacities and degrades water quality, presenting additional challenges in hydrological modelling and water resource management.

One of the challenges in incorporating dynamic LULC is that LULC changes impact hydrological components across varied timeframes. For example, deforestation instantly eliminates interception, but its effects on groundwater recharge manifest later. Enhancing the quality and quantity of hydrological data on both spatial and temporal scales is pivotal to capturing these nuances.

The intricacies of evapotranspiration, especially in forests, remain an area for enhancement in hydrological models. Transpiration is dominant, yet interception evaporation, especially in forests, can sometimes surpass it (Wang-Erlandsson et al., 2014; Wei et al., 2017). Modern modelling often overlooks forests' ability to store heat and vapour across multiple layers, from the air column to the soil (Coenders-Gerrits et al., 2020). Studies should delve deeper into the canopy interactions and understand water, vapour, and heat dynamics to better grasp forest evaporation. Future efforts should prioritise understanding the interactions among leaf growth, abscission, leaf litter dynamics, and evaporation partitioning (Mert, 2021). Additionally, understanding the processes within and beneath the canopy and how evaporation splits between interception, transpiration, and soil evaporation is crucial (Dubbert et al., 2013; Van den Hoof et al., 2013). Incorporating stable water isotopes can aid in comprehensive modelling from vegetation top to forest floor.

LULC influences the hydrological processes through manifold (Afonso de Oliveira Serrão et al., 2022; Siddik et al., 2022). Land cover dictates soil erosion, with forests acting as protective barriers. Urbanisation complicates channel flows, while deforestation affects snowpack dynamics. LULC also modulates water quality, with agricultural lands potentially introducing nutrients and urban zones contributing to pollutants (Roy et al., 2022; Gu & Li, 2024). Drained or altered wetlands disrupt regional

water balances and flood mitigation. Soil moisture, key to the critical zone and, hence, the hydrology, is directly linked to LULC.

Moreover, critical aspects like hydraulic conductivity of aquifers and roughness of the land surface are inadequately addressed spatially. While these challenges are recognised, hydrological models might miss some nuances. For instance, the temporal dynamics of soil hydrophobicity, the micro-scale impacts of LULC on soil structure, or the feedback loops between erosion, landscape connectivity, and local hydrology might not be fully captured (Blume et al., 2009; Stephens et al., 2021; Vereecken et al., 2022). Addressing these gaps requires a holistic approach, integrating interdisciplinary knowledge and continuously updating models based on new findings.

The modelling community needs to access web services from data providers and improve the spatial resolution of data to account for the great variability in climate, topography and land cover (Sitterson et al., 2018). The availability of the model and data to the public increases their usefulness, reduces duplication of efforts, and saves time and money (Sitterson et al., 2018). Also, novel remote sensing products such as vegetation optical depth may provide additional useful information on global scales of canopy structure (Rodríguez-Fernández et al., 2018). Overall, capturing LULC nuances in hydrological models is essential for accurate predictions, urging continued improvements in understanding these interplays. Future studies should examine potential shifts in the LULC pattern, considering both biophysical and socio-economic factors in a catchment with diverse vegetation (Dwarakish et al., 2015).

2.4.4 Scale issue in Hydrological modelling

Hydrological models are inherently sensitive to the spatial and temporal scales at which data are acquired, processed, and applied. At the most fundamental level, scale relates to the resolution (both spatial and temporal) and the extent over which key hydrological processes, parameters, and data inputs are represented (Blöschl & Sivapalan, 1995). Understanding scale dependencies is essential when incorporating LULC information into hydrological models, as different scales highlight different facets of hydrological behaviour and produce varying outcomes in model simulations (Beven, 2001). Large catchments typically encompass considerable heterogeneity in climate, soils, topography, and vegetation, necessitating more aggregated representations of LULC and hydrological parameters (Locke, 2024; Tetzlaff et al., 2010). These models often face challenges related to data consistency and the computational complexity of integrating diverse datasets. Conversely, smaller catchments allow for the use of high-resolution data, enabling more detailed and localised modelling.

Remotely sensed imagery or national land use datasets, for example, often provide broad-brush classifications of land cover that overlook finer spatial details and changes (Zhang & Li, 2022). While this generalised approach is computationally manageable and aids in regional decision-making, it

may overlook fine-scale patterns—such as localised irrigation practices or small patches of riparian vegetation—that can exert disproportionate influences on local runoff and evapotranspiration. In contrast, smaller catchments can be studied at finer resolutions, enabling the capture of subtle LULC gradients and more nuanced parameterisation of hydrological models (Blöschl & Sivapalan, 1995). The hydrological responses of small catchments can be highly sensitive to land use changes (Forio et al., 2020). Enhanced spatial detail often comes at the cost of greater data demands and the need for frequent updates to ensure that temporal changes—such as land cover transitions due to deforestation or agricultural expansion—are accurately represented.

Blöschl and Sivapalan (1995) highlight the importance of scale issues in hydrological modelling, noting that integrating formulations at different scales remains an unresolved challenge in the field. This issue is critical as many hydrological processes are nonlinear and vary spatially and temporally, making their study in isolation at smaller scales only somewhat insightful for their behaviour at larger catchment scales. Hydrological models need to reconstruct these complex processes to validate their representations and interactions at different scales and to test which conceptualisations of these processes are consistent with observations.

The temporal scale is also important in capturing dynamic LULC effects. Changes in vegetation cover, crop cycles, and land management practices occur at seasonal to decadal times, influencing hydrological processes such as infiltration, interception, and transpiration (Li et al., 2019). High-frequency observations can reveal rapid shifts in hydrological responses following land use changes, allowing for more responsive and adaptive model structures. Conversely, long-term datasets can explain trends in catchment behaviour under evolving climatic conditions and land management regimes, supporting strategic decision-making at the basin scale (Yang et al., 2024). Balancing the demands of temporal detail with computational feasibility and data availability remains a persistent challenge.

A key unresolved issue in hydrological science is translating the knowledge gained at fine scales to broader extents—so-called “scaling up”—while maintaining process fidelity (Blöschl & Sivapalan, 1995). Many hydrological processes exhibit nonlinear behaviours and interactions that do not simply aggregate from small to large scales. Studies at small catchments can offer valuable process understanding. However, applying these insights at larger scales can be problematic if models fail to integrate complex spatial patterns and temporal dynamics effectively. Researchers should incorporate multi-scale observations, experiments, and models that explicitly consider how land use patterns and their parameters vary through space and time (Dube et al., 2023). Scale considerations must remain at the forefront of model selection, calibration, and validation efforts, ensuring that hydrological models capture the complexity of real-world systems as faithfully and usefully as possible.

2.4.5 Model evaluation and calibration

In the calibration process of hydrological models, the direct alteration of LULC data is not typical. Instead, the focus is usually on adjusting model parameters rather than improving the representation of process dynamics (Rajat & Athira, 2021). However, aspects connected to LULC are often fine-tuned or more deeply scrutinised to achieve optimal results (Sai Veena et al., 2019). That may improve the reproduction of discharge without change, albeit not always for the right reasons (Beven, 2019a). For instance, the available LULC data might be reclassified or adjusted to fit the model's specific requirements or resolution better. Obtaining better results for the wrong reasons may lead to misleading interpretations, especially when simulating the impacts of LULC change (Merz et al., 2011; Peel & Blöschl, 2011; Hollaway et al., 2018).

The poor process dynamics in the model reduce its predictive power (Rajat & Athira, 2021). Several hydrological parameters, such as curve numbers or Manning's 'n' values, are intrinsically tied to specific LULC types. These parameters can be refined during calibration to improve model fit.

Hydrological systems are nonlinear and complex, and we have few techniques for studying patterns of processes at the catchment scale. In many instances, models have shown different sets of calibration parameters for different periods (Merz et al., 2011). Therefore, identifying and understanding the time stability of catchment model parameters and how they may change with time needs to be understood better (Wagener et al., 2010).

Traditionally, hydrological models have assumed stationary conditions (the model parameters do not change with time). Therefore, accounting for temporal changes in the model parameters is not straightforward (Peel & Blöschl, 2011). This is mainly because it is not easy to find a unique relationship between the changing parameters and complex correlations among the parameters and with various catchment characteristics (Wagener, 2007; Merz et al., 2011). All these assumptions can produce significant errors in the simulation process if climate and/or catchment conditions change much over time (Merz et al., 2011). These errors potentially extend with increasing the scale and time lag between the calibration and simulation periods.

Incorporating dynamic LULC into hydrological models substantially influences the calibration process, offering both challenges and advantages. Dynamic LULC introduces the need for time-variable parameters, ensuring that associated hydrological parameters like runoff coefficients evolve correspondingly as land cover changes. This necessitates a calibration dataset that spans diverse temporal conditions, capturing the intricacies of changing landscapes. While this more realistic portrayal of land changes enhances the model's applicability, it complicates calibration by increasing the number of tenable parameters, potentially elevating model uncertainty. Such increased complexity

demands a rigorous validation process, testing the model's proficiency across various LULC change periods.

Furthermore, the risk of overfitting emerges, where the model might echo the calibration data closely but falter with new independent datasets (Fowler et al., 2016; Dakhlaoui et al., 2017; Pool et al., 2017; Fowler et al., 2018). As the model's sensitivity to parameters can oscillate with changing LULC, periodic sensitivity analyses become pivotal. Merging data from assorted sources, like remote sensing and land surveys, can pose challenges, emphasising the need for consistent scale, resolution, and accuracy. Calibrating a model with point data and assuming that some simple power law will hold over the range of the data is essentially misleading (Westerberg et al., 2020). Lastly, dynamic LULC often ushers in scenario-based calibrations, enabling the exploration of potential land management or future trajectories. While undeniably intricate, including dynamic LULC ensures models stay in step with real-world land changes, granting them enhanced relevance and reliability when appropriately calibrated (Yonaba et al., 2021).

Regions with substantial LULC shifts during the calibration period necessitate acknowledging these changes for accurate modelling (Birhanu et al., 2019). For instance, Birhanu et al. (2019) demonstrated that in regions undergoing significant LULC changes, the HBV model—which was both accurately calibrated and validated—exhibited only minor and insignificant fluctuations (±5%) in projected water balance components like discharge, evapotranspiration, soil moisture, and groundwater recharge. However, when the actual discharge data was statistically assessed, noticeable increasing trends were observed throughout the study. It shows that static data can impede successful calibration if a model does not factor in such dynamics and there are notable LULC alterations.

Further nuances, like distinct management practices on similar land covers, might also be incorporated to boost calibration accuracy. While LULC data is rarely manipulated directly, its associated parameters and processes are vital in refining hydrological models.

2.5 Conclusions

This article has endeavoured to present an overview of LULC-related mechanisms involved in hydrological processes, their modelling approach and the shortcomings of the models in representing processes.

Physically based semi-distributed and distributed models have gained prominence for their efficacy in studying the impacts of heterogeneous LULC patterns. Nonetheless, the field of hydrology continues to face substantial constraints due to limitations in observational data. The responses of

hydrological processes to LULC changes are notably diverse, shaped by a multitude of factors, including geographical attributes and other physical factors such as slope and soil characteristics.

This complexity is further compounded by human interventions and the nuanced relationship between evaporative factors and vegetation canopies, posing significant challenges for the modelling community. In addressing these challenges, contemporary research leverages a combination of field data, experimental studies, and sophisticated modelling techniques. The advent of remote sensing has markedly enhanced our comprehension of LULC dynamics. However, fully grasping the hydrological implications of changes requires an interdisciplinary strategy that extends beyond conventional methodologies. Embracing innovative technologies and integrated modelling approaches will be instrumental in advancing watershed management practices.

Despite the progress in hydrological modelling, several challenges persist. Current models, while insightful, struggle to overcome observational constraints and often fall short in effectively utilising remote sensing data or accurately representing hydrological complexities. Traditional empirical formulas, born in data scarcity, impede modern modelling efforts, particularly in rapidly changing landscapes. Specific processes, such as snow-related interception, evapotranspiration, and soil moisture estimation, remain inadequately represented, particularly in multi-layered environments like forest areas.

Models integrate various physical processes with certain simplifications and empirical elements, making them a hybrid of purely empirical and fully physically based models. However, balancing between them is essential as this hugely impacts all subsequent processes. For example, existing limitations in soil water extraction functions hamper the full potential of the Penman-Monteith method.

To move forward, hydrological science requires a standardised LULC classification system to facilitate uniform modelling and enhance comparison across studies. A comprehensive modelling approach is essential, incorporating extensive validation, innovative process depiction, uncertainty management, and a nuanced recognition of data constraints. Continued exploration into the responses of hydrological processes to LULC changes, coupled with refined uncertainty quantification in parameter estimates and modelling, will remain at the forefront of hydrological research.

As we progress, it becomes imperative to adopt a more critical perspective on modelling practices, acknowledging the constraints imposed by data availability, study scope, desired output, and resource allocation. A concerted effort within the hydrological community is necessary to advance these models as viable hypotheses, fostering new process representations and effectively managing predictive uncertainties. A systematic evaluation of potential error sources, encompassing input data, boundary conditions, model design, and software assumptions, is crucial for developing reliable simulation

models. The journey through hydrological research is replete with uncharted territories, from pioneering observational techniques to theoretical breakthroughs and explorations of diverse ecological landscapes. The path ahead for LULC and hydrological modelling is one of embracing technological advancements and methodological rigour, ensuring our strategies are comprehensive and genuinely representative of the multifaceted realities we seek to simulate.

2.6 References

Abbott, M. B., Bathurst, J. C., Cunge, J. A., O'Connell, P. E., & Rasmussen, J. (1986). An introduction to the European Hydrological System — Systeme Hydrologique Europeen, "SHE", 1: History and philosophy of a physically-based, distributed modelling system. Journal of Hydrology, 87(1–2), 45–59. https://doi.org/10.1016/0022-1694(86)90114-9

Abdelaziz, K. K., Nicaise, Y., Séguis, L., Ouattara, I., Moussa, O., Auguste, K., Kamagaté, B., & Diakaria, K. (2020). Influence of land use land cover change on groundwater recharge in the continental terminal area of Abidjan, Ivory Coast. Journal of Water Resource and Protection, 12(05), 431–453. https://doi.org/10.4236/jwarp.2020.125026

Adhikari, R. K., Yilmaz, A. G., Mainali, B., Dyson, P., & Imteaz, M. A. (2022). Methods of groundwater recharge estimation under climate change: A review. Sustainability (Switzerland), 14(23), 15619. https://doi.org/10.3390/su142315619

Afonso de Oliveira Serrão, E., Silva, M. T., Ferreira, T. R., Paiva de Ataide, L. C., Assis dos Santos, C., Meiguins de Lima, A. M., de Paulo Rodrigues da Silva, V., de Assis Salviano de Sousa, F., & Cardoso Gomes, D. J. (2022). Impacts of land use and land cover changes on hydrological processes and sediment yield determined using the SWAT model. International Journal of Sediment Research, 37(1), 54–69. https://doi.org/10.1016/j.ijsrc.2021.04.002

Aghsaei, H., Mobarghaee Dinan, N., Moridi, A., Asadolahi, Z., Delavar, M., Fohrer, N., & Wagner, P. D. (2020). Effects of dynamic land use/land cover change on water resources and sediment yield in the Anzali wetland catchment, Gilan, Iran. Science of the Total Environment, 712, 136449. https://doi.org/10.1016/j.scitotenv.2019.136449

Alem, B. B. (2022). The nexus between land use land cover dynamics and soil erosion hotspot area of Girana Watershed, Awash Basin, Ethiopia. Heliyon, 8(2). https://doi.org/10.1016/j.heliyon.2022.e08916

Allen, S. T., Aubrey, D. P., Bader, M. Y., Coenders-Gerrits, M., Friesen, J., Gutmann, E. D., Guillemette, F., Jiménez-Rodríguez, C., Keim, R. F., Klamerus-Iwan, A., Mendieta-Leiva, G., Porada, P., Qualls, R. G., Schilperoort, B., Stubbins, A., & Van Stan, J. T. (2020). Key questions on the evaporation and transport of intercepted precipitation. In Precipitation Partitioning by Vegetation: A Global Synthesis (pp. 268–279). Springer. https://doi.org/10.1007/978-3-030-29702-2_16

Allison, G. B., Cook, P. G., Barnett, S. R., Walker, G. R., Jolly, I. D., & Hughes, M. W. (1990). Land clearance and river salinisation in the western Murray Basin, Australia. Journal of Hydrology, 119(1–4), 1–20. https://doi.org/10.1016/0022-1694(90)90030-2

Allison, G. B., Gee, G. W., & Tyler, S. W. (1994). Vadose-zone techniques for estimating groundwater recharge in arid and semiarid regions. Soil Science Society of America Journal, 58(1), 6–14. https://doi.org/10.2136/sssaj1994.03615995005800010002x

Asano, T., & Cotruvo, J. A. (2004). Groundwater recharge with reclaimed municipal wastewater: Health and regulatory considerations. Water Research, 38(8), 1941–1951. https://doi.org/10.1016/j.watres.2004.01.023

Ayotte, J. D., Szabo, Z., Focazio, M. J., & Eberts, S. M. (2011). Effects of human-induced alteration of groundwater flow on concentrations of naturally-occurring trace elements at water-supply wells. Applied Geochemistry, 26(5), 747–762. https://doi.org/10.1016/j.apgeochem.2011.01.033

Bagley, J. E., Kueppers, L. M., Billesbach, D. P., Williams, I. N., Biraud, S. C., & Torn, M. S. (2017). The influence of land cover on surface energy partitioning and evaporative fraction regimes in the US Southern Great Plains. Journal of Geophysical Research: Atmospheres, 122(11), 5793–5807. https://doi.org/10.1002/2017JD026740

Baier, W., & Robertson, G. W. (1966). A new versatile soil moisture budget. Canadian Journal of Plant Science, 46(3), 299–315. https://doi.org/10.4141/cjps66-049

Baldocchi, D., Falge, E., Gu, L., Olson, R., Hollinger, D., Running, S., Anthoni, P., Bernhofer, C., Davis, K., Evans, R., Fuentes, J., Goldstein, A., Katul, G., Law, B., Lee, X., Malhi, Y., Meyers, T., Munger, W., Oechel, W., ... Wofsy, S. (2001). FLUXNET: A new tool to study the temporal and spatial variability of ecosystem-scale carbon dioxide, water vapor, and energy flux

densities. Bulletin of the American Meteorological Society, 82(11), 2415–2434. https://doi.org/10.1175/1520-0477(2001)082<2415:FANTTS>2.3.CO;2
Bartholome, E., & Belward, A. S. (2005). GLC2000: A new approach to global land cover mapping from earth observation data. International Journal of Remote Sensing, 26(9), 1959–1977. https://doi.org/10.1080/01431160412331291297
Barua, S., Cartwright, I., Evan Dresel, P., & Daly, E. (2021). Using multiple methods to investigate the effects of land-use changes on groundwater recharge in a semi-arid area. Hydrology and Earth System Sciences, 25(1), 89–104. https://doi.org/10.5194/hess-25-89-2021
Batelaan, O., & De Smedt, F. (2007). GIS-based recharge estimation by coupling surface-subsurface water balances. Journal of Hydrology, 337(3–4), 337–355. https://doi.org/10.1016/j.jhydrol.2007.02.001
Batelaan, O., De Smedt, F., & Triest, L. (2003). Regional groundwater discharge: Phreatophyte mapping, groundwater modelling and impact analysis of land-use change. Journal of Hydrology, 275(1–2), 86–108. https://doi.org/10.1016/S0022-1694(03)00018-0
Becker, M. L., Congalton, R. G., Budd, R., & Fried, A. (1998). A GLOBE collaboration to develop land cover data collection and analysis protocols. Journal of Science Education and Technology, 7(1), 85–96. https://doi.org/10.1023/A:1022540300914
Belay, T., & Mengistu, D. A. (2021). Impacts of land use/land cover and climate changes on soil erosion in Muga watershed, Upper Blue Nile basin (Abay), Ethiopia. Ecological Processes, 10(1), 1–23. https://doi.org/10.1186/s13717-021-00339-9
Bergstrom, S. (1976). Development and application of a conceptual runoff model for Scandinavian catchments. https://urn.kb.se/resolve?urn=urn:nbn:se:smhi:diva-5738
Bergstrom, S., Forsman, A., (1973). Development of a conceptual deterministic rainfall-runoff model. Nordic Hydrol., 4(3 (1973)), 147–170. https://doi.org/10.2166/nh.1973.0012
Beven, K. (1989). Changing ideas in hydrology - The case of physically-based models. Journal of Hydrology, 105(1–2), 157–172. https://doi.org/10.1016/0022-1694(89)90101-7
Beven, K. (2001). How far can we go in distributed hydrological modelling? Hydrology and Earth System Sciences, 5(1), 1–12. https://doi.org/10.5194/hess-5-1-2001
Beven, K. (2011). Rainfall-runoff modelling: The primer. John Wiley & Sons.
Beven, K. (2018). A century of denial: Preferential and nonequilibrium water flow in soils, 1864-1984. Vadose Zone Journal, 17(1), 1–17. https://doi.org/10.2136/vzj2018.08.0153
Beven, K. (2019a). How to make advances in hydrological modelling. *Hydrology Research, 50*(6), 1481–1494. https://doi.org/10.2166/nh.2019.134
Beven, K. (2019b). Towards a methodology for testing models as hypotheses in the inexact sciences. Proceedings of the Royal Society A: Mathematical, Physical and Engineering Sciences, 475(2224), 20180862. https://doi.org/10.1098/rspa.2018.0862
Beven, K. J., & Kirkby, M. J. (1979). A physically based, variable contributing area model of basin hydrology. Hydrological Sciences Bulletin, 24(1), 43–69. https://doi.org/10.1080/02626667909491834
Beven, K., & Germann, P. (1982). Macropores and water flow in soils. Water Resources Research, 18(5), 1311–1325. https://doi.org/10.1029/WR018i005p01311
Beven, K., & Germann, P. (2013). Macropores and water flow in soils revisited. Water Resources Research, 49(6), 3071–3092. https://doi.org/10.1002/wrcr.20156
Beven, K., Cloke, H., Pappenberger, F., & Others. (2015). Hyperresolution information and hyperresolution ignorance in modelling the hydrology of the land surface. *Science China Earth Sciences, 58*(1), 25–35. https://doi.org/10.1007/s11430-014-5003-4
Beven, K., Kirkby, M., E. Freer, J., & Lamb, R. (2021). A history of TOPMODEL. Hydrology and Earth System Sciences, 25(2), 527–549. https://doi.org/10.5194/hess-25-527-2021
Bhark, E. W., & Small, E. E. (2003). Association between plant canopies and the spatial patterns of infiltration in shrubland and grassland of the Chihuahuan desert, New Mexico. Ecosystems, 6(2), 185–196. https://doi.org/10.1007/s10021-002-0210-9
Bicknell, B. R., Imhoff, J. C., Kittle Jr, J. L., Donigian Jr, A. S., & Johanson, R. C. (1997). Hydrological simulation program—FORTRAN user's manual for version 11 (EPA/600/R-97/080). U.S. Environmental Protection Agency, Athens, GA.

Binley, A., Beven, K., & Elgy, J. (1989a). A physically based model of heterogeneous hillslopes: 2. Effective hydraulic conductivities. *Water Resources Research, 25*(6), 1227–1233. https://doi.org/10.1029/WR025i006p01227

Binley, A., Elgy, J., & Beven, K. (1989b). A physically based model of heterogeneous hillslopes: 1. Runoff production. *Water Resources Research, 25*(6), 1219–1226. https://doi.org/10.1029/WR025i006p01219

Birhanu, A., Masih, I., van der Zaag, P., Nyssen, J., & Cai, X. (2019). Impacts of land use and land cover changes on hydrology of the Gumara catchment, Ethiopia. Physics and Chemistry of the Earth, 112, 165–174. https://doi.org/10.1016/j.pce.2019.01.006

Blöschl, G., & Montanari, A. (2010). Climate change impacts—throwing the dice? *Hydrological Processes, 24*(3), 374–381. https://doi.org/10.1002/hyp.7574

Blöschl, G., & Sivapalan, M. (1995). Scale issues in hydrological modelling: A review. Hydrological Processes, 9(3–4), 251–290. https://doi.org/10.1002/hyp.3360090305

Blume, T., Zehe, E., & Bronstert, A. (2009). Use of soil moisture dynamics and patterns at different spatio-temporal scales for the investigation of subsurface flow processes. Hydrology and Earth System Sciences, 13(7), 1215–1234. https://doi.org/10.5194/hess-13-1215-2009

Bormann, H., Breuer, L., Gräff, T., Huisman, J. A., & Croke, B. (2009). Assessing the impact of land use change on hydrology by ensemble modelling (LUCHEM) IV: Model sensitivity to data aggregation and spatial (re-)distribution. Advances in Water Resources, 32(2), 171–192. https://doi.org/10.1016/j.advwatres.2008.01.002

Bormann, H., Diekkrüger, B., & Richter, O. (1996). Effects of data availability on estimation of evapotranspiration. *Physics and Chemistry of the Earth, 21*(3), 171–175. https://doi.org/10.1016/S0079-1946(97)85580-2

Brandolini, P., Pepe, G., Capolongo, D., Cappadonia, C., Cevasco, A., Conoscenti, C., Marsico, A., Vergari, F., & Del Monte, M. (2018). Hillslope degradation in representative Italian areas: Just soil erosion risk or opportunity for development? Land Degradation and Development, 29(9), 3050–3068. https://doi.org/10.1002/ldr.2999

Breuer, L., Eckhardt, K., & Frede, H. G. (2003). Plant parameter values for models in temperate climates. Ecological Modelling, 169(2–3), 237–293. https://doi.org/10.1016/S0304-3800(03)00274-6

Bussière, F., Solmon, F., & Fouéré, A. (2002). Implementation and evaluation of DROP, a model for the simulation of rainfall distribution below plants described in 3D. Agronomie, 22(1), 93–103. https://doi.org/10.1051/agro:2001002

Büttner, G. (2014). CORINE land cover and land cover change products. In I. Manakos & M. Braun (Eds.), Remote Sensing and Digital Image Processing (Vol. 18, pp. 55–74). Springer Netherlands. https://doi.org/10.1007/978-94-007-7969-3_5

Cartwright, I., Cendón, D., Currell, M., & Meredith, K. (2017). A review of radioactive isotopes and other residence time tracers in understanding groundwater recharge: Possibilities, challenges, and limitations. Journal of Hydrology, 555, 797–811. https://doi.org/10.1016/j.jhydrol.2017.10.053

Castillo, C. R., Güneralp, I., & Güneralp, B. (2014). Influence of changes in developed land and precipitation on hydrology of a coastal Texas watershed. Applied Geography, 47, 154–167. https://doi.org/10.1016/j.apgeog.2013.12.009

Chen, H., & Jiang, J. G. (2010). Osmotic adjustment and plant adaptation to environmental changes related to drought and salinity. Environmental Reviews, 18(1), 309–319. https://doi.org/10.1139/A10-014

Chen, L., Xiang, L., Young, M. H., Yin, J., Yu, Z., & Genuchten, M. T. Van. (2015). Optimal parameters for the Green-Ampt infiltration model under rainfall conditions. Journal of Hydrology and Hydromechanics, 63(2), 93–101. https://doi.org/10.1515/johh-2015-0012

Chen, Y., Li, P., Xu, C., Song, Z., Sun, K., Li, W., Hu, X., & An, Q. (2023). Retrieving leaf area index from FY-3D MERSI-II data using a sensor-adaptive algorithm. International Journal of Remote Sensing, 44(7), 2317–2341. https://doi.org/10.1080/01431161.2023.2201383

Cheng, Z., & Yu, B. (2019). Effect of land clearing and climate variability on streamflow for two large basins in Central Queensland, Australia. *Journal of Hydrology, 578*, 124041. https://doi.org/10.1016/j.jhydrol.2019.124041

Chia, M. Y., Huang, Y. F., Koo, C. H., & Fung, K. F. (2020). Recent advances in evapotranspiration estimation using artificial intelligence approaches with a focus on hybridization techniques—A review. Agronomy, 10(1), 101. https://doi.org/10.3390/agronomy10010101

Chien, H., Yeh, P. J. F., & Knouft, J. H. (2013). Modeling the potential impacts of climate change on streamflow in agricultural watersheds of the Midwestern United States. *Journal of Hydrology, 491,* 73–88. https://doi.org/10.1016/j.jhydrol.2013.03.026

Coenders-Gerrits, M., Schilperoort, B., & Jiménez-Rodríguez, C. (2020). Evaporative processes on vegetation: An inside look. In Precipitation Partitioning by Vegetation: A Global Synthesis (pp. 34–47). Springer. https://doi.org/10.1007/978-3-030-29702-2_3

Coleman, M. D., & Aubrey, D. P. (2018). Stand development and other intrinsic factors largely control fine-root dynamics with only subtle modifications from resource availability. Tree Physiology, 38(12), 1805–1819. https://doi.org/10.1093/treephys/tpy033

Collins, D. B. G., & Bras, R. L. (2007). Plant rooting strategies in water-limited ecosystems. *Water Resources Research, 43*, W06407. https://doi.org/10.1029/2006WR005541

Cornelissen, T., Diekkrüger, B., & Giertz, S. (2013). A comparison of hydrological models for assessing the impact of land use and climate change on discharge in a tropical catchment. Journal of Hydrology, 498, 221–236. https://doi.org/10.1016/j.jhydrol.2013.06.016

Crawford, N. H., & Linsley, R. K. (1966). *Digital simulation in hydrology: Stanford Watershed Model IV* (Technical Report No. 39). Department of Civil and Environmental Engineering, Stanford University. https://searchworks.stanford.edu/view/1172854

Crosbie, R. S., Jolly, I. D., Leaney, F. W., & Petheram, C. (2010). Can the dataset of field based recharge estimates in Australia be used to predict recharge in data-poor areas? Hydrology and Earth System Sciences, 14(10), 2023–2038. https://doi.org/10.5194/hess-14-2023-2010

Daba, M. H., & You, S. (2020). Assessment of climate change impacts on river flow regimes in the upstream of Awash Basin, Ethiopia: Based on IPCC fifth assessment report (ar5) climate change scenarios. *Hydrology, 7,* 1–22. https://doi.org/10.3390/hydrology7040098

Dakhlaoui, H., Ruelland, D., Tramblay, Y., & Bargaoui, Z. (2017). Evaluating the robustness of conceptual rainfall-runoff models under climate variability in northern Tunisia. Journal of Hydrology, 550, 201–217. https://doi.org/10.1016/j.jhydrol.2017.04.032

Dawson, C. W., & Wilby, R. L. (2001). Hydrological modelling using artificial neural networks. Progress in Physical Geography, 25(1), 80–108. https://doi.org/10.1177/030913330102500104

de Groen, M. M. (2002). *Modelling interception and transpiration at monthly time steps: Introducing daily variability through Markov chains*. CRC Press. https://books.google.com/books?id=-birGVG44nkC&pgis=1

de Groen, M. M., & Savenije, H. H. G. (2006). A monthly interception equation based on the statistical characteristics of daily rainfall. *Water Resources Research, 42*, W12417. https://doi.org/10.1029/2006WR005013

Devia, G. K., Ganasri, B. P., & Dwarakish, G. S. (2015). A review on hydrological models. Aquatic Procedia, 4, 1001–1007. https://doi.org/10.1016/j.aqpro.2015.02.126

Dey, P., & Mishra, A. (2017). Separating the impacts of climate change and human activities on streamflow: A review of methodologies and critical assumptions. Journal of Hydrology, 548, 278–290. https://doi.org/10.1016/j.jhydrol.2017.03.014

Dhara, C. (2020). Constraining global changes in temperature and precipitation from observable changes in surface radiative heating. Geophysical Research Letters, 47(9), e2020GL087576. https://doi.org/10.1029/2020GL087576

Diaz-Pacheco, J., & Gutiérrez, J. (2014). Exploring the limitations of CORINE land cover for monitoring urban land-use dynamics in metropolitan areas. Journal of Land Use Science, 9(3), 243–259. https://doi.org/10.1080/1747423X.2012.761736

Dile, Y. T., Tekleab, S., Kaba, E. A., Gebrehiwot, S. G., Worqlul, A. W., Bayabil, H. K., Yimam, Y. T., Tilahun, S. A., Daggupati, P., Karlberg, L., & Srinivasan, R. (2018). Advances in water resources research in the Upper Blue Nile basin and the way forward: A review. Journal of Hydrology, 560, 407–423. https://doi.org/10.1016/j.jhydrol.2018.03.042

Dubbert, M., Cuntz, M., Piayda, A., Maguás, C., & Werner, C. (2013). Partitioning evapotranspiration - Testing the Craig and Gordon model with field measurements of oxygen isotope ratios of

evaporative fluxes. Journal of Hydrology, 496, 142–153. https://doi.org/10.1016/j.jhydrol.2013.05.033
Dube, T., Seaton, D., Shoko, C., & Mbow, C. (2023). Advancements in earth observation for water resources monitoring and management in Africa: A comprehensive review. Journal of Hydrology, 623, 129738. https://doi.org/10.1016/j.jhydrol.2023.129738
Duveiller, G., Hooker, J., & Cescatti, A. (2018). The mark of vegetation change on Earth's surface energy balance. Nature Communications, 9(1), 679. https://doi.org/10.1038/s41467-017-02810-8
Dwarakish, G. S., & Ganasri, B. P. (2015). Impact of land use change on hydrological systems: A review of current modeling approaches. Cogent Geoscience, 1(1), 1115691. https://doi.org/10.1080/23312041.2015.1115691
Elfert, S., & Bormann, H. (2010). Simulated impact of past and possible future land use changes on the hydrological response of the Northern German lowland "Hunte" catchment. Journal of Hydrology, 383(3–4), 245–255. https://doi.org/10.1016/j.jhydrol.2009.12.040
Ershadi, A., McCabe, M. F., Evans, J. P., Chaney, N. W., & Wood, E. F. (2014). Multi-site evaluation of terrestrial evaporation models using FLUXNET data. Agricultural and Forest Meteorology, 187, 46–61. https://doi.org/10.1016/j.agrformet.2013.11.008
Essery, R., Pomeroy, J., Ellis, C., & Link, T. (2008). Modelling longwave radiation to snow beneath forest canopies using hemispherical photography or linear regression. Hydrological Processes, 22(15), 2788–2800. https://doi.org/10.1002/hyp.6930
Fischer, B., Goldberg, V., & Bernhofer, C. (2008). Effect of a coupled soil water-plant gas exchange on forest energy fluxes: Simulations with the coupled vegetation-boundary layer model HIRVAC. Ecological Modelling, 214(2–4), 75–82. https://doi.org/10.1016/j.ecolmodel.2008.02.037
Fitts, C. R. (2013). Hydrology and Geology. In C. R. Fitts (Ed.), Groundwater Science (pp. 123–186). Academic Press. https://doi.org/10.1016/b978-0-12-384705-8.00005-4
Flügel, W.-A. (1995). Delineating hydrological response units by geographical information system analyses for regional hydrological modelling using PRMS/MMS in the drainage basin of the River Bröl, Germany. *Hydrological Processes, 9*(3–4), 423–436.
Foley, J. A., DeFries, R., Asner, G. P., Barford, C., Bonan, G., Carpenter, S. R., Chapin, F. S., Coe, M. T., Daily, G. C., Gibbs, H. K., Helkowski, J. H., Holloway, T., Howard, E. A., Kucharik, C. J., Monfreda, C., Patz, J. A., Prentice, I. C., Ramankutty, N., & Snyder, P. K. (2005). Global consequences of land use. Science, 309(5734), 570–574. https://doi.org/10.1126/science.1111772
Forio, M. A. E., De Troyer, N., Lock, K., Witing, F., Baert, L., Saeyer, N. De, Rîșnoveanu, G., Popescu, C., Burdon, F. J., Kupilas, B., Friberg, N., Boets, P., Volk, M., McKie, B. G., & Goethals, P. (2020). Small Patches of Riparian Woody Vegetation Enhance Biodiversity of Invertebrates. Water, 12(11), 3070. https://doi.org/10.3390/w12113070
Förster, K., Garvelmann, J., Meißl, G., & Strasser, U. (2018). Modelling forest snow processes with a new version of WaSiM. Hydrological Sciences Journal, 63(10), 1540–1557. https://doi.org/10.1080/02626667.2018.1518626
Forzieri, G., Miralles, D. G., Ciais, P., Alkama, R., Ryu, Y., Duveiller, G., Zhang, K., Robertson, E., Kautz, M., Martens, B., Jiang, C., Arneth, A., Georgievski, G., Li, W., Ceccherini, G., Anthoni, P., Lawrence, P., Wiltshire, A., Pongratz, J., … Cescatti, A. (2020). Increased control of vegetation on global terrestrial energy fluxes. Nature Climate Change, 10(4), 356–362. https://doi.org/10.1038/s41558-020-0717-0
Fowler, K. J. A., Peel, M. C., Western, A. W., Zhang, L., & Peterson, T. J. (2016). Simulating runoff under changing climatic conditions: Revisiting an apparent deficiency of conceptual rainfall-runoff models. Water Resources Research, 52(3), 1820–1846. https://doi.org/10.1002/2015WR018068
Fowler, K., Coxon, G., Freer, J., Peel, M., Wagener, T., Western, A., Woods, R., & Zhang, L. (2018). Simulating runoff under changing climatic conditions: A framework for model improvement. Water Resources Research, 54(12), 9812–9832. https://doi.org/10.1029/2018WR023989

Frank, J. M., Massman, W. J., Ewers, B. E., & Williams, D. G. (2019). Bayesian analyses of 17 winters of water vapor fluxes show bark beetles reduce sublimation. Water Resources Research, 55(2), 1598–1623. https://doi.org/10.1029/2018WR023054

Freer, J., Mcdonnell, J., Beven, K. J., Brammer, D., Burns, D., Hooper, R. P., & Kendal, C. (1997). Hydrological processes - Letters: Topographic controls on subsurface storm flow at the hillslope scale for Two hydrologically distinct small catchments. Hydrological Processes, 11(9), 1347–1352. https://doi.org/10.1002/(sici)1099-1085(199707)11:9<1347::aid-hyp592>3.0.co;2-r

Freeze, R. A., & Cherry, J. A. (1979). *Groundwater*. Prentice Hall.

Freudiger, D., Kohn, I., Seibert, J., Stahl, K., & Weiler, M. (2017). Snow redistribution for the hydrological modeling of alpine catchments. Wiley Interdisciplinary Reviews: Water, 4(5). https://doi.org/10.1002/WAT2.1232

Friedl, M. A., McIver, D. K., Hodges, J. C. F., Zhang, X. Y., Muchoney, D., Strahler, A. H., Woodcock, C. E., Gopal, S., Schneider, A., Cooper, A., Baccini, A., Gao, F., & Schaaf, C. (2002). Global land cover mapping from MODIS: Algorithms and early results. Remote Sensing of Environment, 83(1–2), 287–302. https://doi.org/10.1016/S0034-4257(02)00078-0

Gabbi, J., Carenzo, M., Pellicciotti, F., Bauder, A., & Funk, M. (2014). A comparison of empirical and physically based glacier surface melt models for long-term simulations of glacier response. *Journal of Glaciology, 60*(224), 1140–1154. https://doi.org/10.3189/2014JoG14J011

Gale, I., Neumann, I., Calow, R., & Moench, M. (2002). The effectiveness of artificial recharge of groundwater: A review (CR/02/108N). British Geological Survey. https://nora.nerc.ac.uk/id/eprint/527471

Galin, E., Guérin, E., Peytavie, A., Cordonnier, G., Cani, M. P., Benes, B., & Gain, J. (2019). A review of digital terrain modeling. Computer Graphics Forum, 38(2), 553–577. https://doi.org/10.1111/cgf.13657

Gao, H., Sabo, J. L., Chen, X., Liu, Z., Yang, Z., Ren, Z., & Liu, M. (2018). Landscape heterogeneity and hydrological processes: a review of landscape-based hydrological models. Landscape Ecology, 33(9), 1461–1480. https://doi.org/10.1007/s10980-018-0690-4

Gash, J. H. C. (1979). An analytical model of rainfall interception by forests. Quarterly Journal of the Royal Meteorological Society, 105(443), 43–55. https://doi.org/10.1002/qj.49710544304

Gash, J. H. C., & Morton, A. J. (1978). An application of the Rutter model to the estimation of the interception loss from Thetford Forest. Journal of Hydrology, 38(1–2), 49–58. https://doi.org/10.1016/0022-1694(78)90131-2

Geng, J., Li, H., Pang, J., Zhang, W., & Shi, Y. (2022). The effects of land-use conversion on evapotranspiration and water balance of subtropical forest and managed tea plantation in Taihu Lake Basin, China. Hydrological Processes, 36(8), e14652. https://doi.org/10.1002/hyp.14652

Gerrits, A. M. J., & Savenije, H. H. G. (2011). Forest floor interception. In Forest hydrology and biogeochemistry (pp. 445–454). Springer. https://doi.org/10.1007/978-94-007-1363-5_22

Gerrits, A. M. J., Pfister, L., & Savenije, H. H. G. (2010). Spatial and temporal variability of canopy and forest floor interception in a beech forest. Hydrological Processes, 24(21), 3011–3025. https://doi.org/10.1002/hyp.7712

Gerrits, A. M. J., Savenije, H. H. G., Hoffmann, L., & Pflster, L. (2007). New technique to measure forest floor interception - An application in a beech forest in Luxembourg. Hydrology and Earth System Sciences, 11(2), 695–701. https://doi.org/10.5194/hess-11-695-2007

Gerrits, A. M. J., Savenije, H. H. G., Veling, E. J. M., & Pfister, L. (2009). Analytical derivation of the Budyko curve based on rainfall characteristics and a simple evaporation model. Water Resources Research, 45(4). https://doi.org/10.1029/2008WR007308

Gerten, D., Schaphoff, S., Haberlandt, U., Lucht, W., & Sitch, S. (2004). Terrestrial vegetation and water balance - Hydrological evaluation of a dynamic global vegetation model. Journal of Hydrology, 286(1–4), 249–270. https://doi.org/10.1016/j.jhydrol.2003.09.029

Ghomash, S.K.B, Caviedes-Voullieme, D., & Hinz, C. (2019). Effects of erosion-induced changes to topography on runoff dynamics. Journal of Hydrology, 573, 811–828. https://doi.org/10.1016/j.jhydrol.2019.04.018

Goel, M.K. (2011). Interception of Snow. In: Singh, V.P., Singh, P., Haritashya, U.K. (Eds) Encyclopedia of Snow, Ice and Glaciers. Encyclopedia of Earth Sciences Series. Springer, Dordrecht. https://doi.org/10.1007/978-90-481-2642-2_297

Goodrich, D. C., Burns, I. S., Unkrich, C. L., Semmens, D. J., Guertin, D. P., Hernandez, M., ... & Levick, L. R. (2012). KINEROS2/AGWA: Model use, calibration, and validation. Transactions of the ASABE, 55(4), 1561-1574.

Gouttevin, I., Lehning, M., Jonas, T., Gustafsson, D., & Mölder, M. (2015). A two-layer canopy model with thermal inertia for an improved snowpack energy balance below needleleaf forest (model SNOWPACK, version 3.2.1, revision 741). Geoscientific Model Development, 8(8), 2379–2398. https://doi.org/10.5194/gmd-8-2379-2015

Green, K., Kempka, D., & Lackey, L. (1994). Using remote sensing to detect and monitor land-cover and land-use change. Photogrammetric Engineering and Remote Sensing, 60(3), 331–337.

Green, W. H., & Ampt, G. (1911). Studies on soil physics. *Journal of Agricultural Science, 4,* **1–24.** https://doi.org/10.1017/S0021859600001441

Gu, S., & Li, S. (2024). Riparian habitat quality as an indicator of land use/land cover effects on riverine water quality. Geography and Sustainability, 5(1), 135–143. https://doi.org/10.1016/j.geosus.2023.11.005

Gu, S., Tang, Y., Cui, X., Kato, T., Du, M., Li, Y., & Zhao, X. (2005). Energy exchange between the atmosphere and a meadow ecosystem on the Qinghai-Tibetan Plateau. Agricultural and Forest Meteorology, 129(3–4), 175–185. https://doi.org/10.1016/j.agrformet.2004.12.002

Guo, Y., Fang, G., Xu, Y. P., Tian, X., & Xie, J. (2020). Identifying how future climate and land use/cover changes impact streamflow in Xinanjiang Basin, East China. Science of the Total Environment, 710, 136275. https://doi.org/10.1016/j.scitotenv.2019.136275

Gutmann, E. D. (2020). Global modeling of precipitation partitioning by vegetation and their applications. In J. Van Stan II, E. Gutmann, & J. Friesen (Eds.), *Precipitation partitioning by vegetation* (pp. 161-175). Springer. https://doi.org/10.1007/978-3-030-29702-2_7

Ha, W., Kolb, T. E., Springer, A. E., Dore, S., O'Donnell, F. C., Martinez Morales, R., Masek Lopez, S., & Koch, G. W. (2015). Evapotranspiration comparisons between eddy covariance measurements and meteorological and remote-sensing-based models in disturbed ponderosa pine forests. Ecohydrology, 8(7), 1335–1350. https://doi.org/10.1002/eco.1586

Hammerle, A., Haslwanter, A., Tappeiner, U., Cernusca, A., & Wohlfahrt, G. (2008). Leaf area controls on energy partitioning of a temperate mountain grassland. Biogeosciences, 5(2), 421–431. https://doi.org/10.5194/bg-5-421-2008

Hangen, E., Buczko, U., Bens, O., Brunotte, J., & Hüttl, R. F. (2002). Infiltration patterns into two soils under conventional and conservation tillage: Influence of the spatial distribution of plant root structures and soil animal activity. Soil and Tillage Research, 63(3–4), 181–186. https://doi.org/10.1016/S0167-1987(01)00234-3

Hardy, J. P., Davis, R. E., Jordan, R., Li, X., Woodcock, C., Ni, W., & McKenzie, J. C. (1997). Snow ablation modeling at the stand scale in a boreal jack pine forest. Journal of Geophysical Research Atmospheres, 102(24), 29397–29405. https://doi.org/10.1029/96jd03096

Hargreaves, G. H., & Samani, Z. A. (1985). Reference crop evapotranspiration from ambient air temperature. *Paper - American Society of Agricultural Engineers, 1*(2), 96–99.

Healy, R. W., Winter, T. C., LaBaugh, J. W., & Franke, O. L. (2007). Water budgets: Foundations for effective water-resources and environmental management. *U.S. Geological Survey Circular 1308*. U.S. Geological Survey. https://pubs.usgs.gov/circ/2007/1308/

Healy, R.W., 2010. Estimating groundwater recharge. Cambridge University Press, United Kingdom. https://doi.org/10.1017/CBO9780511780745.

Herold, M., & Schmullius, C. (2004). Report on the harmonization of global and regional land cover products. *Workshop report at the Food and Agriculture Organization, Rome, Italy*. http://www.gofcgold.wur.nl/sites/harmon.php

Herwitz, S. R., & Slye, R. E. (1995). Three-dimensional modeling of canopy tree interception of wind-driven rainfall. Journal of Hydrology, 168(1–4), 205–226. https://doi.org/10.1016/0022-1694(94)02643-P

Hock, R. (1999). A distributed temperature-index ice- and snowmelt model including potential direct solar radiation. Journal of Glaciology, 45(149), 101–111. https://doi.org/10.3189/s0022143000003087

Hollaway, M. J., Beven, K. J., Benskin, C. McW. H., Collins, A. L., Evans, R., Falloon, P. D., Forber, K. J., Hiscock, K. M., Kahana, R., Macleod, C. J. A., Ockenden, M. C., Villamizar, M. L.,

Wearing, C., Withers, P. J. A., Zhou, J. G., Barber, N. J., & Haygarth, P. M. (2018). The challenges of modelling phosphorus in a headwater catchment: Applying a 'limits of acceptability' uncertainty framework to a water quality model. Journal of Hydrology, 558, 607–624. https://doi.org/10.1016/j.jhydrol.2018.01.063

Hornbeck, J. W., Adams, M. B., Corbett, E. S., Verry, E. S., & Lynch, J. A. (1993). Long-term impacts of forest treatments on water yield: a summary for northeastern USA. Journal of Hydrology, 150(2–4), 323–344. https://doi.org/10.1016/0022-1694(93)90115-P

Horton, R. E. (1941). An approach toward a physical interpretation of infiltration-capacity. Soil Science Society of America Journal, 5(C), 399–417. https://doi.org/10.2136/sssaj1941.036159950005000c0075x

Hu, X., Næss, J. S., Iordan, C. M., Huang, B., Zhao, W., & Cherubini, F. (2021). Recent global land cover dynamics and implications for soil erosion and carbon losses from deforestation. Anthropocene, 34, 100291. https://doi.org/10.1016/j.ancene.2021.100291

Huang, J., Zhou, P., Zhou, Z., & Huang, Y. (2013). Assessing the influence of land use and land cover datasets with different points in time and levels of detail on watershed modeling in the north river watershed, china. International Journal of Environmental Research and Public Health, 10(1), 144–157. https://doi.org/10.3390/ijerph10010144

Jehanzaib, M., Ajmal, M., Achite, M., & Kim, T. W. (2022). Comprehensive review: advancements in rainfall-runoff modelling for flood mitigation. Climate, 10(10), 147. https://doi.org/10.3390/cli10100147

Jencso, K. G., McGlynn, B. L., Gooseff, M. N., Wondzell, S. M., Bencala, K. E., & Marshall, L. A. (2009). Hydrologic connectivity between landscapes and streams: Transferring reach- and plot-scale understanding to the catchment scale. Water Resources Research, 45(4). https://doi.org/10.1029/2008WR007225

Jin, X., Jin, Y., Yuan, D., & Mao, X. (2019). Effects of land-use data resolution on hydrologic modelling, a case study in the upper reach of the Heihe River, Northwest China. Ecological Modelling, 404, 61–68. https://doi.org/10.1016/j.ecolmodel.2019.02.011

Jost, G., Weiler, M., Gluns, D. R., & Alila, Y. (2007). The influence of forest and topography on snow accumulation and melt at the watershed-scale. Journal of Hydrology, 347(1–2), 101–115. https://doi.org/10.1016/j.jhydrol.2007.09.006

Juston, J. M., Kauffeldt, A., Montano, B. Q., Seibert, J., Beven, K. J., & Westerberg, I. K. (2013). Smiling in the rain: Seven reasons to be positive about uncertainty in hydrological modelling. Hydrological Processes, 27(7), 1117–1122. https://doi.org/10.1002/hyp.9625

Kala, J., Decker, M., Exbrayat, J. F., Pitman, A. J., Carouge, C., Evans, J. P., Abramowitz, G., & Mocko, D. (2014). Influence of leaf area index prescriptions on simulations of heat, moisture, and carbon fluxes. Journal of Hydrometeorology, 15(1), 489–503. https://doi.org/10.1175/JHM-D-13-063.1

Kauffeldt, A., Halldin, S., Rodhe, A., Xu, C. Y., & Westerberg, I. K. (2013). Disinformative data in large-scale hydrological modelling. Hydrology and Earth System Sciences, 17(7), 2845–2857. https://doi.org/10.5194/hess-17-2845-2013

Kim, J. H., & Jackson, R. B. (2012). A global analysis of groundwater recharge for vegetation, climate, and soils. *Vadose Zone Journal, 11*(1), vzj2011.0021RA. https://doi.org/10.2136/vzj2011.0021ra

Kim, J., Warnock, A., Ivanov, V. Y., & Katopodes, N. D. (2012). Coupled modeling of hydrologic and hydrodynamic processes including overland and channel flow. Advances in Water Resources, 37, 104–126. https://doi.org/10.1016/j.advwatres.2011.11.009

Klamerus-Iwan, A., Link, T. E., Keim, R. F., & Van Stan, J. T. (2020). Storage and routing of precipitation through canopies. In Precipitation Partitioning by Vegetation: A Global Synthesis (pp. 16–33). Springer. https://doi.org/10.1007/978-3-030-29702-2_2

Klaus, J., & Jackson, C. R. (2018). Interflow is not binary: A continuous shallow perched layer does not imply continuous connectivity. Water Resources Research, 54(9), 5921–5932. https://doi.org/10.1029/2018WR022920

Kleidon, A. (2019). Energy Balance. In B. Fath (Ed.), Encyclopedia of Ecology: Volume 1-4, Second Edition (Vol. 4, pp. 50–63). Elsevier. https://doi.org/10.1016/B978-0-12-409548-9.00927-1

Kokkonen, T., Koivusalo, H., & Karvonen, T. (2001). A semi-distributed approach to rainfall-runoff modelling: A case study in a snow-affected catchment. *Environmental Modelling & Software, 16*(5), 481–493. https://doi.org/10.1016/S1364-8152(01)00028-7

Kristanto, Y., Tarigan, S., June, T., Wahjunie, E. D., & Sulistyantara, B. (2022). Water regulation ecosystem Sservices of multifunctional landscape dominated by monoculture plantations. Land, 11(6), 818. https://doi.org/10.3390/land11060818

Kulmatov, R., Mirzaev, J., Abuduwaili, J., & Karimov, B. (2020). Challenges for the sustainable use of water and land resources under a changing climate and increasing salinization in the Jizzakh irrigation zone of Uzbekistan. Journal of Arid Land, 12(1), 90–103. https://doi.org/10.1007/s40333-020-0092-8

Kumar, S., David Raj, A., Kalambukattu, J. G., & Chatterjee, U. (2022). Climate change impact on land degradation and soil erosion in hilly and mountainous landscape: Sustainability issues and adaptation strategies. In *Springer Climate* (pp. 119–155). Springer. https://doi.org/10.1007/978-3-031-15501-7_5

Kutílek, M. (2004). Soil hydraulic properties as related to soil structure. *Soil and Tillage Research, 79*(2), 175–184. https://doi.org/10.1016/j.still.2004.07.006

Lamichhane, S., & Shakya, N. M. (2019). Alteration of groundwater recharge areas due to land use/cover change in Kathmandu Valley, Nepal. Journal of Hydrology: Regional Studies, 26. https://doi.org/10.1016/j.ejrh.2019.100635

Lamichhane, S., & Shakya, N. M. (2020). Shallow aquifer groundwater dynamics due to land use/cover change in highly urbanized basin: The case of Kathmandu Valley. Journal of Hydrology: Regional Studies, 30. https://doi.org/10.1016/j.ejrh.2020.100707

Lan, X., Li, Y., Shao, R., Chen, X., Lin, K., Cheng, L., Gao, H., & Liu, Z. (2021). Vegetation controls on surface energy partitioning and water budget over China. Journal of Hydrology, 600, 125646. https://doi.org/10.1016/j.jhydrol.2020.125646

Leavesley, G. H., Lichty, R. W., Troutman, B. M., & Saindon, L. G. (1983). *Precipitation-runoff modeling system: User's manual* (Report No. 83-4238). U.S. Geological Survey. https://doi.org/10.3133/wri834238

Lerner, D. N. (2002). Identifying and quantifying urban recharge: A review. Hydrogeology Journal, 10(1), 143–152. https://doi.org/10.1007/s10040-001-0177-1

Levia, D. F., Carlyle-Moses, D., & Tanaka, T. (Eds.). (2011). *Forest hydrology and biogeochemistry: Synthesis of past research and future directions.* Springer. https://doi.org/10.1007/978-94-007-1363-5

Li, H., Si, B., & Li, M. (2018a). Rooting depth controls potential groundwater recharge on hillslopes. Journal of Hydrology, 564, 164–174. https://doi.org/10.1016/j.jhydrol.2018.07.002

Li, W., Wang, J., Zhang, Y., Yin, Q., Wang, W., Zhou, G., & Huo, Z. (2023). Combining texture, color, and vegetation index from unmanned aerial vehicle multispectral images to estimate winter wheat leaf area index during the vegetative growth stage. *Remote Sensing, 15,* 5715. https://doi.org/10.3390/rs15245715

Li, X., Niu, J., Xie, B., 2014. The effect of leaf litter cover on surface runoff and soil erosion in Northern China. PLoS One 9, e107789. https://doi.org/10.1371/journal.pone.0107789.

Li, X., Xiao, Q., Niu, J., Dymond, S., McPherson, E. G., van Doorn, N., Yu, X., Xie, B., Zhang, K., & Li, J. (2017). Rainfall interception by tree crown and leaf litter: An interactive process. Hydrological Processes, 31(20), 3533–3542. https://doi.org/10.1002/hyp.11275

Li, Y., Chang, J., Luo, L., Wang, Y., Guo, A., Ma, F., & Fan, J. (2019). Spatiotemporal impacts of land use land cover changes on hydrology from the mechanism perspective using SWAT model with time-varying parameters. Hydrology Research, 50(1), 244–261. https://doi.org/10.2166/nh.2018.006

Li, Y., Piao, S., Li, L. Z. X., Chen, A., Wang, X., Ciais, P., Huang, L., Lian, X., Peng, S., Zeng, Z., Wang, K., & Zhou, L. (2018b). Divergent hydrological response to large-scale afforestation and vegetation greening in China. Science Advances, 4(5), eaar4182. https://doi.org/10.1126/sciadv.aar4182

Li, Z. L., Tang, R., Wan, Z., Bi, Y., Zhou, C., Tang, B., Yan, G., & Zhang, X. (2009). A review of current methodologies for regional Evapotranspiration estimation from remotely sensed data. Sensors, 9(5), 3801–3853. https://doi.org/10.3390/s90503801

Liang, X., Lettenmaier, D. P., Wood, E. F., & Burges, S. J. (1994). A simple hydrologically based model of land surface water and energy fluxes for general circulation models. Journal of Geophysical Research: Atmospheres, 99(D7), 14415–14428. https://doi.org/10.1029/94JD00483

Lindström, G., Gardelin, M., & Persson, M. (1994). Conceptual modelling of evapotranspiration for simulations of climate change effects. SMHI. https://urn.kb.se/resolve?urn=urn:nbn:se:smhi:diva-2678

Liu, N., Harper, R. J., Smettem, K. R. J., Dell, B., & Liu, S. (2019). Responses of streamflow to vegetation and climate change in southwestern Australia. Journal of Hydrology, 572, 761–770. https://doi.org/10.1016/j.jhydrol.2019.03.005

Liu, W., Wang, L., Zhou, J., Li, Y., Sun, F., Fu, G., Li, X., & Sang, Y. F. (2016). A worldwide evaluation of basin-scale evapotranspiration estimates against the water balance method. Journal of Hydrology, 538, 82–95. https://doi.org/10.1016/j.jhydrol.2016.04.006

Liu, Z., Wang, Y., Xu, Z., & Duan, Q. (2017). Conceptual hydrological models. In Q. Duan, F. Pappenberger, J. Thielen, A. Wood, H. Cloke, & J. Schaake (Eds.), *Handbook of hydrometeorological ensemble forecasting* (pp. 1–23). Springer. https://doi.org/10.1007/978-3-642-40457-3_22-1

Locke, K. A. (2024). Modelling relationships between land use and water quality using statistical methods: A critical and applied review. Journal of Environmental Management, 362, 121290. https://doi.org/10.1016/j.jenvman.2024.121290

Lopez, M. G., Vis, M. J. P., Jenicek, M., Griessinger, N., & Seibert, J. (2020). Assessing the degree of detail of temperature-based snow routines for runoff modelling in mountainous areas in central Europe. Hydrology and Earth System Sciences, 24(9), 4441–4461. https://doi.org/10.5194/hess-24-4441-2020

Loveland, T. R., Reed, B. C., Ohlen, D. O., Brown, J. F., Zhu, Z., Yang, L., & Merchant, J. W. (2000). Development of a global land cover characteristics database and IGBP DISCover from 1 km AVHRR data. International Journal of Remote Sensing, 21(6–7), 1303–1330. https://doi.org/10.1080/014311600210191

Lundberg, A., & Halldin, S. (2001). Snow interception evaporation: Review of measurement techniques, processes, and models. *Theoretical and Applied Climatology, 70*(1–4), 117–133. https://doi.org/10.1007/s007040170010

Lundquist, J. D., Dickerson-Lange, S. E., Lutz, J. A., & Cristea, N. C. (2013). Lower forest density enhances snow retention in regions with warmer winters: A global framework developed from plot-scale observations and modeling. Water Resources Research, 49(10), 6356–6370. https://doi.org/10.1002/wrcr.20504

Luo, S., He, Y., Li, Q., Jiao, W., Zhu, Y., & Zhao, X. (2020). Nondestructive estimation of potato yield using relative variables derived from multi-period LAI and hyperspectral data based on weighted growth stage. Plant Methods, 16(1), 150. https://doi.org/10.1186/s13007-020-00693-3

Ma, N., Niu, G. Y., Xia, Y., Cai, X., Zhang, Y., Ma, Y., & Fang, Y. (2017). A systematic evaluation of Noah-MP in simulating land-atmosphere energy, water, and carbon exchanges over the continental United States. *Journal of Geophysical Research: Atmospheres, 122*(22), 12,212–12,245. https://doi.org/10.1002/2017JD027597

Ma, Y., Feng, S., Su, D., Gao, G., & Huo, Z. (2010). Modeling water infiltration in a large layered soil column with a modified Green-Ampt model and HYDRUS-1D. *Computers and Electronics in Agriculture, 71*(Supplement 1), S40–S47. https://doi.org/10.1016/j.compag.2009.07.006

Madsen, H. (2000). Automatic calibration of a conceptual rainfall-runoff model using multiple objectives. Journal of Hydrology, 235(3–4), 276–288. https://doi.org/10.1016/S0022-1694(00)00279-1

Magnusson, J., Wever, N., Essery, R., Helbig, N., Winstral, A., & Jonas, T. (2015). Evaluating snow models with varying process representations for hydrological applications. Water Resources Research, 51(4), 2707–2723. https://doi.org/10.1002/2014WR016498

Maples, S. R., Foglia, L., Fogg, G. E., & Maxwell, R. M. (2020). Sensitivity of hydrologic and geologic parameters on recharge processes in a highly heterogeneous, semi-confined aquifer system. Hydrology and Earth System Sciences, 24(5), 2437–2456. https://doi.org/10.5194/hess-24-2437-2020

McCormack, M. L., Dickie, I. A., Eissenstat, D. M., Fahey, T. J., Fernandez, C. W., Guo, D., Helmisaari, H. S., Hobbie, E. A., Iversen, C. M., Jackson, R. B., Leppälammi-Kujansuu, J., Norby, R. J., Phillips, R. P., Pregitzer, K. S., Pritchard, S. G., Rewald, B., & Zadworny, M. (2015). Redefining fine roots improves understanding of below-ground contributions to terrestrial biosphere processes. New Phytologist, 207(3), 505–518. https://doi.org/10.1111/nph.13363

McGuire, K. J., & McDonnell, J. J. (2010). Hydrological connectivity of hillslopes and streams: Characteristic time scales and nonlinearities. *Water Resources Research, 46*. https://doi.org/10.1029/2010WR009341

McShane, R. R., Driscoll, K. P., & Sando, R. (2017). A review of surface energy balance models for estimating actual evapotranspiration with remote sensing at high spatiotemporal resolution over large extents. *Scientific Investigations Report 2017–5087*. U.S. Geological Survey. https://doi.org/10.3133/sir20175087

Meili, N., Manoli, G., Burlando, P., Carmeliet, J., Chow, W. T. L., Coutts, A. M., Roth, M., Velasco, E., Vivoni, E. R., & Fatichi, S. (2021). Tree effects on urban microclimate: Diurnal, seasonal, and climatic temperature differences explained by separating radiation, evapotranspiration, and roughness effects. *Urban Forestry & Urban Greening, 58,* 126970. https://doi.org/10.1016/j.ufug.2020.126970

Mert, O. (2021). The impact of vegetation on the partitioning of evaporation in conceptual hydrological models. TUDelft Repository. http://repository.tudelft.nl/

Merz, R., Parajka, J., & Blöschl, G. (2011). Time stability of catchment model parameters: Implications for climate impact analyses. *Water Resources Research, 47.* https://doi.org/10.1029/2010WR009505

Milly, P. C. D., Betancourt, J., Falkenmark, M., Hirsch, R. M., Kundzewicz, Z. W., Lettenmaier, D. P., & Stouffer, R. J. (2008). Climate change. Stationarity is dead: Whither water management? *Science, 319*(5863), 573–574. https://doi.org/10.1126/science.1151915

Mintz, Y., & Walker, G. K. (1993). Global fields of soil moisture and land surface evapotranspiration derived from observed precipitation and surface air temperature. Journal of Applied Meteorology, 32(8), 1305–1334. https://doi.org/10.1175/1520-0450(1993)032<1305:GFOSMA>2.0.CO;2

Mishra, S. K., & Singh, V. P. (2003). SCS-CN method. In *Soil Conservation Service Curve Number (SCS-CN) methodology* (pp. 23–47). Springer. https://doi.org/10.1007/978-94-017-0147-1_2

Mishra, S. K., Tyagi, J. V., & Singh, V. P. (2003). Comparison of infiltration models. Hydrological Processes, 17(13), 2629–2652. https://doi.org/10.1002/hyp.1257

Moges, E., Demissie, Y., Larsen, L., & Yassin, F. (2021). Review: Sources of hydrological model uncertainties and advances in their analysis. Water (Switzerland), 13(1). https://doi.org/10.3390/w13010028

Mohr, C. H., Coppus, R., Iroumé, A., Huber, A., & Bronstert, A. (2013). Runoff generation and soil erosion processes after clear cutting. Journal of Geophysical Research: Earth Surface, 118(2), 814–831. https://doi.org/10.1002/jgrf.20047

Molotch, N. P., Blanken, P. D., Williams, M. W., Turnipseed, A. A., Monson, R. K., & Margulis, S. A. (2007). Estimating sublimation of intercepted and sub-canopy snow using eddy covariance systems. Hydrological Processes, 21(12), 1567–1575. https://doi.org/10.1002/hyp.6719

Monteith, J. L. (1965). Evaporation and environment. *Symposia of the Society for Experimental Biology, 19,* 205–234. https://repository.rothamsted.ac.uk/item/8v5v7/evaporation-and-environment

Morbidelli, R., Corradini, C., Saltalippi, C., & Brocca, L. (2012). Initial soil water content as input to field-scale infiltration and surface runoff models. Water Resources Management, 26(7), 1793–1807. https://doi.org/10.1007/s11269-012-9986-3

Morbidelli, R., Corradini, C., Saltalippi, C., Flammini, A., Dari, J., & Govindaraju, R. S. (2018). Rainfall infiltration modeling: A review. Water (Switzerland), 10(12), 1873. https://doi.org/10.3390/w10121873

Mueller, B., Hirschi, M., Jimenez, C., Ciais, P., Dirmeyer, P. A., Dolman, A. J., Fisher, J. B., Jung, M., Ludwig, F., Maignan, F., Miralles, D. G., McCabe, M. F., Reichstein, M., Sheffield, J., Wang, K., Wood, E. F., Zhang, Y., & Seneviratne, S. I. (2013). Benchmark products for land

evapotranspiration: LandFlux-EVAL multi-data set synthesis. Hydrology and Earth System Sciences, 17(10), 3707–3720. https://doi.org/10.5194/hess-17-3707-2013

Murray, S. J. (2014). Trends in 20th century global rainfall interception as simulated by a dynamic global vegetation model: Implications for global water resources. Ecohydrology, 7(1), 102–114. https://doi.org/10.1002/eco.1325

Mussa, K. R., Mjemah, I. C., & Muzuka, A. N. N. (2020). A review on the state of knowledge, conceptual and theoretical contentions of major theories and principles governing groundwater flow modeling. Applied Water Science, 10(6), 149. https://doi.org/10.1007/s13201-020-01202-6

Muzylo, A., Llorens, P., Valente, F., Keizer, J. J., Domingo, F., & Gash, J. H. C. (2009). A review of rainfall interception modelling. Journal of Hydrology, 370(1–4), 191–206. https://doi.org/10.1016/j.jhydrol.2009.02.058

Nampak, H., Pradhan, B., Mojaddadi Rizeei, H., & Park, H. J. (2018). Assessment of land cover and land use change impact on soil loss in a tropical catchment by using multitemporal SPOT-5 satellite images and Revised Universal Soil Loss Equation model. *Land Degradation & Development, 29,* 3440–3455. https://doi.org/10.1002/ldr.3112

Neitsch, S. L., Arnold, J. G., Kiniry, J. R., & Williams, J. R. (2011). *Soil and water assessment tool theoretical documentation: Version 2009*. Texas Water Resources Institute. https://swat.tamu.edu/docs/

Nelson, G. C., & Geoghegan, J. (2002). Deforestation and land use change: sparse data environments. Agricultural Economics, 27(3), 201–216. https://doi.org/10.1111/j.1574-0862.2002.tb00117.x

Noszczyk, T. (2019). A review of approaches to land use changes modeling. *Human and Ecological Risk Assessment: An International Journal, 25*(6), 1377–1405. https://doi.org/10.1080/10807039.2018.1468994

Orfánus, T., Zvala, A., Čierniková, M., Stojkovová, D., Nagy, V., & Dlapa, P. (2021). Peculiarities of infiltration measurements in water-repellent forest soil. Forests, 12(4), 472. https://doi.org/10.3390/f12040472

Orlandini, S., & Rosso, R. (1996). Diffusion wave modeling of distributed catchment dynamics. *Journal of Hydrologic Engineering, 1*(3), 103–113. https://doi.org/10.1061/(ASCE)1084-0699(1996)1:3(103)

Orth, R., Staudinger, M., Seneviratne, S. I., Seibert, J., & Zappa, M. (2015). Does model performance improve with complexity? A case study with three hydrological models. Journal of Hydrology, 523, 147–159. https://doi.org/10.1016/j.jhydrol.2015.01.044

Owuor, S. O., Butterbach-Bahl, K., Guzha, A. C., Rufino, M. C., Pelster, D. E., Díaz-Pinés, E., & Breuer, L. (2016). Groundwater recharge rates and surface runoff response to land use and land cover changes in semi-arid environments. Ecological Processes, 5(1). https://doi.org/10.1186/s13717-016-0060-6

Pandey, P. C., Koutsias, N., Petropoulos, G. P., Srivastava, P. K., & Ben Dor, E. (2021). Land use/land cover in view of earth observation: data sources, input dimensions, and classifiers—a review of the state of the art. Geocarto International, 36(9), 957–988. https://doi.org/10.1080/10106049.2019.1629647

Paniconi, C., & Putti, M. (2015). Physically based modeling in catchment hydrology at 50: Survey and outlook. Water Resources Research, 51(9), 7090–7129. https://doi.org/10.1002/2015WR017780

Pechlivanidis, I. G., Jackson, B. M., McIntyre, N. R., & Wheater, H. S. (2011). Catchment scale hydrological modelling: A review of model types, calibration approaches and uncertainty analysis methods in the context of recent developments in technology and applications. *Global NEST Journal, 13*(3), 193–214. https://doi.org/10.30955/gnj.000778

Peel, M. C., & Blöschl, G. (2011). Hydrological modelling in a changing world. Progress in Physical Geography, 35(2), 249–261. https://doi.org/10.1177/0309133311402550

Pellicciotti, F., Ragettli, S., Carenzo, M., & McPhee, J. (2014). Changes of glaciers in the Andes of Chile and priorities for future work. Science of the Total Environment, 493, 1197–1210. https://doi.org/10.1016/j.scitotenv.2013.10.055

Pérez-Hoyos, A., García-Haro, F. J., & San-Miguel-Ayanz, J. (2012). Conventional and fuzzy comparisons of large scale land cover products: Application to CORINE, GLC2000, MODIS and GlobCover in Europe. ISPRS Journal of Photogrammetry and Remote Sensing, 74, 185–201. https://doi.org/10.1016/j.isprsjprs.2012.09.006

Petrişor, A. I., Ianoş, I., & Tălângă, C. (2010). Land cover and use changes focused on the urbanization processes in Romania. Environmental Engineering and Management Journal, 9(6), 765–771. https://doi.org/10.30638/eemj.2010.102

Pitman, A. J. (2003). The evolution of, and revolution in, land surface schemes designed for climate models. International Journal of Climatology, 23(5), 479–510. https://doi.org/10.1002/joc.893

Polidori, L., & El Hage, M. (2020). Digital elevation model quality assessment methods: A critical review. *Remote Sensing, 12*(21), 1–36. https://doi.org/10.3390/rs12213522

Pomeroy, J. W., Gray, D. M., Hedstrom, N. R., & Janowicz, J. R. (2002). Prediction of seasonal snow accumulation in cold climate forests. Hydrological Processes, 16(18), 3543–3558. https://doi.org/10.1002/hyp.1228

Pomeroy, J. W., Marks, D., Link, T., Ellis, C., Hardy, J., Rowlands, A., & Granger, R. (2009). The impact of coniferous forest temperature on incoming longwave radiation to melting snow. Hydrological Processes, 23(17), 2513–2525. https://doi.org/10.1002/hyp.7325

Pool, S., Vis, M. J. P., Knight, R. R., & Seibert, J. (2017). Streamflow characteristics from modeled runoff time series: Importance of calibration criteria selection. *Hydrology and Earth System Sciences, 21*(11), 5443–5457. https://doi.org/10.5194/hess-21-5443-2017

Porada, P., Van Stan, J. T., & Kleidon, A. (2018). Significant contribution of non-vascular vegetation to global rainfall interception. Nature Geoscience, 11(8), 563–567. https://doi.org/10.1038/s41561-018-0176-7

Poyatos, R., Latron, J., & Llorens, P. (2003). Land use and land cover change after agricultural abandonment: The case of a Mediterranean Mountain area (Catalan Pre-Pyrenees). Mountain Research and Development, 23(4), 362–368. https://doi.org/10.1659/0276-4741(2003)023[0362:LUALCC]2.0.CO;2

Prashanth, M., Kumar, A., Dhar, S., Verma, O., Rai, S. K., & Kouser, B. (2023). Land use/land cover change and its implication on soil erosion in an ecologically sensitive Himachal Himalayan watershed, Northern India. Frontiers in Forests and Global Change, 6, 1124677. https://doi.org/10.3389/ffgc.2023.1124677

Priestly, C. H. B., & Taylor, R. J. (1972). On the assessment of surface heat flux and evaporation using large-scale parameters. Monthly Weather Review, 100(2), 81–92. https://doi.org/10.1175/1520-0493(1972)100<0081:otaosh>2.3.co;2

Raja Shekar, P., & Mathew, A. (2023). Assessing groundwater potential zones and artificial recharge sites in the monsoon-fed Murredu river basin, India: An integrated approach using GIS, AHP, and Fuzzy-AHP. Groundwater for Sustainable Development, 23, 100994. https://doi.org/10.1016/j.gsd.2023.100994

Rajat, & Athira, P. (2021). Calibration of hydrological models considering process interdependence: A case study of SWAT model. Environmental Modelling and Software, 144, 105131. https://doi.org/10.1016/j.envsoft.2021.105131

Refsgaard, J. C., & Storm, B. (1995). MIKE SHE. In V. P. Singh (Ed.), *Computer models of watershed hydrology* (pp. 809-846). Water Resources Publications.

Ren, Y., & Liu, S. (2019). A simple regional snow hydrological process-based snow depth model and its application in the Upper Yangtze River Basin. Hydrology Research, 50(2), 672–690. https://doi.org/10.2166/nh.2019.079

Rindfuss, R. R., Walsh, S. J., Turner, B. L., Fox, J., & Mishra, V. (2004). Developing a science of land change: Challenges and methodological issues. Proceedings of the National Academy of Sciences of the United States of America, 101(39), 13976–13981. https://doi.org/10.1073/pnas.0401545101

Ritchie, J. T. (1972). Model for predicting evaporation from a row crop with incomplete cover. Water Resources Research, 8(5), 1204–1213. https://doi.org/10.1029/WR008i005p01204

Rodríguez-Fernández, N. J., Mialon, A., Mermoz, S., Bouvet, A., Richaume, P., Al Bitar, A., Al-Yaari, A., Brandt, M., Kaminski, T., Le Toan, T., Kerr, Y. H., & Wigneron, J. P. (2018). An evaluation of SMOS L-band vegetation optical depth (L-VOD) data sets: High sensitivity of L-VOD to

above-ground biomass in Africa. Biogeosciences, 15(14), 4627–4645. https://doi.org/10.5194/bg-15-4627-2018
Rossi, G. (1994). Historical development of flood analysis methods. In G. Rossi, N. Harmancioğlu, & V. Yevjevich (Eds.), *Coping with floods* (pp. 3-25). Springer. https://doi.org/10.1007/978-94-011-1098-3_2
Roy, P. S., Ramachandran, R. M., Paul, O., Thakur, P. K., Ravan, S., Behera, M. D., Sarangi, C., & Kanawade, V. P. (2022). Anthropogenic Land Use and Land Cover Changes—A Review on Its Environmental Consequences and Climate Change. Journal of the Indian Society of Remote Sensing, 50(8), 1615–1640. https://doi.org/10.1007/s12524-022-01569-w
Sai Veena, S., Varma, M. R. R., Srinivasa Raju, K., & Swathi, V. (2019). Automatic calibration of SWMM using NSGA-III and the effects of delineation scale on an urban catchment. *Journal of Hydroinformatics, 21,* 781–797. https://doi.org/10.2166/hydro.2019.033
Sandvig, R. M., & Phillips, F. M. (2006). Ecohydrological controls on soil moisture fluxes in arid to semiarid vadose zones. Water Resources Research, 42(8). https://doi.org/10.1029/2005WR004644
Sardans, J., & Peñuelas, J. (2014). Hydraulic redistribution by plants and nutrient stoichiometry: Shifts under global change. Ecohydrology, 7(1), 1–20. https://doi.org/10.1002/eco.1459
Satterlund, D. R., & Haupt, H. F. (1967). Snow catch by Contier Crowns. Water Resources Research, 3(4), 1035–1039. https://doi.org/10.1029/WR003i004p01035
Satterlund, D. R., & Haupt, H. F. (1970). The Disposition of Snow Caught by Conifer Crowns. Water Resources Research, 6(2), 649–652. https://doi.org/10.1029/WR006i002p00649
Savenije, H. H. G. (2004). The importance of interception and why we should delete the term evapotranspiration from our vocabulary. Hydrological Processes, 18(8), 1507–1511. https://doi.org/10.1002/hyp.5563
Scanlon, B. R., Healy, R. W., & Cook, P. G. (2002). Choosing appropriate techniques for quantifying groundwater recharge. Hydrogeology Journal, 10(1), 18–39. https://doi.org/10.1007/s10040-001-0176-2
Scanlon, B. R., Reedy, R. C., & Tachovsky, J. A. (2007). Semiarid unsaturated zone chloride profiles: Archives of past land use change impacts on water resources in the southern High Plains, United States. Water Resources Research, 43(6). https://doi.org/10.1029/2006WR005769
Scanlon, B. R., Reedy, R. C., Stonestrom, D. A., Prudic, D. E., & Dennehy, K. F. (2005). Impact of land use and land cover change on groundwater recharge and quality in the southwestern US. Global Change Biology, 11(10), 1577–1593. https://doi.org/10.1111/j.1365-2486.2005.01026.x
Schmidt, R. A., & Gluns, D. R. (1991). Snowfall interception on branches of three conifer species. Canadian Journal of Forest Research, 21(8), 1262–1269. https://doi.org/10.1139/x91-176
Schmidt, R. A., & Pomeroy, J. W. (1990). Bending of a conifer branch at subfreezing temperatures: implications for snow interception. Canadian Journal of Forest Research, 20(8), 1250–1253. https://doi.org/10.1139/x90-165
Schmutz, S., & Moog, O. (2018). Riverine ecosystem management. In S. Schmutz & O. Moog (Eds.), *Riverine ecosystem management* (pp. 111–127). Springer. https://doi.org/10.1007/978-3-319-73250-3
Sellers, W. D. (1969). A global climatic model based on the energy balance of the earth-atmosphere system. *Journal of Applied Meteorology and Climatology, 8*(3), 392–400. https://doi.org/10.1175/1520-0450(1969)008%3C0392:AGCMBO%3E2.0.CO;2
Shadmehri Toosi, A., Calbimonte, G. H., Nouri, H., & Alaghmand, S. (2019). River basin-scale flood hazard assessment using a modified multi-criteria decision analysis approach: A case study. Journal of Hydrology, 574, 660–671. https://doi.org/10.1016/j.jhydrol.2019.04.072
Shi, Z., Xu, D., Yang, X., Jia, Z., Guo, H., & Zhang, N. (2012). Ecohydrological impacts of eucalypt plantations: A review. Journal of Food, Agriculture and Environment, 10(3–4), 1419–1426.
Shuster, W. D., Bonta, J., Thurston, H., Warnemuende, E., & Smith, D. R. (2005). Impacts of impervious surface on watershed hydrology: A review. Urban Water Journal, 2(4), 263–275. https://doi.org/10.1080/15730620500386529
Sicart, J. E., Pomeroy, J. W., Essery, R. L. H., Hardy, J., Link, T., & Marks, D. (2004). A sensitivity study of daytime net radiation during snowmelt to forest canopy and atmospheric conditions.

Journal of Hydrometeorology, 5(5), 774–784. https://doi.org/10.1175/1525-7541(2004)005<0774:ASSODN>2.0.CO;2
Siddik, M. S., Tulip, S. S., Rahman, A., Islam, M. N., Haghighi, A. T., & Mustafa, S. M. T. (2022). The impact of land use and land cover change on groundwater recharge in northwestern Bangladesh. Journal of Environmental Management, 315, 115130. https://doi.org/10.1016/j.jenvman.2022.115130
Singh, V. P. (1997). *Kinematic wave modeling in water resources: Environmental hydrology.* John Wiley & Sons.
Singh, V. P. (2017). *Handbook of applied hydrology* (2nd ed.). McGraw-Hill Education. https://www.accessengineeringlibrary.com/content/book/9780071835091
Sitterson, J., Knightes, C., Parmar, R., Wolfe, K., Muche, M., & Avant, B. (2018). An overview of rainfall-runoff model types (EPA/600/R-14/152). *International Congress on Environmental Modelling and Software*, 4–10. https://nepis.epa.gov/Exe/ZyPURL.cgi?Dockey=P100WLPI.TXT
Sood, A., & Smakhtin, V. (2015). Revue des modèles hydrologiques globaux. Hydrological Sciences Journal, 60(4), 549–565. https://doi.org/10.1080/02626667.2014.950580
Stephens, C. M., Lall, U., Johnson, F. M., & Marshall, L. A. (2021). Landscape changes and their hydrologic effects: Interactions and feedbacks across scales. Earth-Science Reviews, 212, 103466. https://doi.org/10.1016/j.earscirev.2020.103466
Storck, P., Lettenmaier, D. P., & Bolton, S. M. (2002). Measurement of snow interception and canopy effects on snow accumulation and melt in a mountainous maritime climate, Oregon, United States. Water Resources Research, 38(11), 5–16. https://doi.org/10.1029/2002wr001281
Strasser, U., Warscher, M., & Liston, G. E. (2011). Modeling snow-canopy processes on an idealized mountain. Journal of Hydrometeorology, 12(4), 663–677. https://doi.org/10.1175/2011JHM1344.1
Sulis, M., Paniconi, C., & Camporese, M. (2011). Impact of grid resolution on the integrated and distributed response of a coupled surface-subsurface hydrological model for the des Anglais catchment, Quebec. Hydrological Processes, 25(12), 1853–1865. https://doi.org/10.1002/hyp.7941
Sun, L., Yang, L., Hao, L., Fang, D., Jin, K., & Huang, X. (2017). Hydrological effects of vegetation cover degradation and environmental implications in a semiarid temperate steppe, China. *Sustainability (Switzerland, 9)*(2), 281. https://doi.org/10.3390/su9020281
Sun, X., & Li, J. (2023). Tree root-soil interaction: field study of the effect of trees on soil moisture and ground movement in an urban environment. Plant and Soil, 1–21. https://doi.org/10.1007/s11104-023-06307-w
Svoma, B. M. (2016). Difficulties in determining snowpack sublimation in complex terrain at the macroscale. Advances in Meteorology, 2016, 1–10. https://doi.org/10.1155/2016/9695757
Szarek-Iwaniuk, P. (2021). A comparative analysis of spatial data and land use/land cover classification in urbanized areas and areas subjected to anthropogenic pressure for the example of Poland. *Sustainability (Switzerland, 13)*(6), 3070. https://doi.org/10.3390/su13063070
Teklay, A., Dile, Y. T., Setegn, S. G., Demissie, S. S., & Asfaw, D. H. (2019). Evaluation of static and dynamic land use data for watershed hydrologic process simulation: A case study in Gummara watershed, Ethiopia. Catena, 172, 65–75. https://doi.org/10.1016/j.catena.2018.08.013
Tetzlaff, D., Carey, S. K., Laudon, H., & McGuire, K. (2010). Catchment processes and heterogeneity at multiple scales—benchmarking observations, conceptualization and prediction. Hydrological Processes, 24(16), 2203–2208. https://doi.org/10.1002/hyp.7784
Thomas, H. A. Jr. (1981). Improved methods for national water assessment (Water Resources Contract No. WR15249270). *Harvard Water Resources.* https://doi.org/10.3133/70046351
Todini, E. (1988). Rainfall-runoff modeling - Past, present and future. Journal of Hydrology, 100(1–3), 341–352. https://doi.org/10.1016/0022-1694(88)90191-6
Van den Hoof, C., Vidale, P. L., Verhoef, A., & Vincke, C. (2013). Improved evaporative flux partitioning and carbon flux in the land surface model JULES: Impact on the simulation of land surface processes in temperate Europe. Agricultural and Forest Meteorology, 181, 108–124. https://doi.org/10.1016/j.agrformet.2013.07.011

Van Der Ent, R. J., Wang-Erlandsson, L., Keys, P. W., & Savenije, H. H. G. (2014). Contrasting roles of interception and transpiration in the hydrological cycle - Part 2: Moisture recycling. Earth System Dynamics, 5(2), 471–489. https://doi.org/10.5194/esd-5-471-2014

van Meerveld, I., Seibert, J., 2024. Reforestation effects on low flows: Review of public perceptions and scientific evidence. WIREs Water. https://doi.org/10.1002/wat2.1760

Van Meter, K., Thompson, S. E., & Basu, N. B. (2016). Human impacts on stream hydrology and water quality. In *Stream ecosystems in a changing environment* (pp. 441–490). https://doi.org/10.1016/B978-0-12-405890-3.00011-7

Van Stan II, J. T., & Friesen, J. (2020). Precipitation partitioning, or to the surface and back again: Historical overview of the first process in the terrestrial hydrologic pathway. In J. T. Van Stan II, E. Gutmann, & J. Friesen (Eds.), *Precipitation partitioning by vegetation* (pp. 1–15). Springer. https://doi.org/10.1007/978-3-030-29702-2_1

Van Stan II, J. T., & Pypker, T. G. (2015). A review and evaluation of forest canopy epiphyte roles in the partitioning and chemical alteration of precipitation. *Science of the Total Environment, 536,* 813–824. https://doi.org/10.1016/j.scitotenv.2015.07.134

Van Stan, J. T., Coenders-Gerrits, M., Dibble, M., Bogeholz, P., & Norman, Z. (2017). Effects of phenology and meteorological disturbance on litter rainfall interception for a Pinus elliottii stand in the Southeastern United States. Hydrological Processes, 31(21), 3719–3728. https://doi.org/10.1002/hyp.11292

Van Stan, J. T., Gutmann, E., & Friesen, J. (2020). Precipitation partitioning by vegetation: A global synthesis. In *Precipitation partitioning by vegetation: A global synthesis*. Springer. https://doi.org/10.1007/978-3-030-29702-2

Vereecken, H., Amelung, W., Bauke, S. L., Bogena, H., Brüggemann, N., Montzka, C., Vanderborght, J., Bechtold, M., Blöschl, G., Carminati, A., Javaux, M., Konings, A. G., Kusche, J., Neuweiler, I., Or, D., Steele-Dunne, S., Verhoef, A., Young, M., & Zhang, Y. (2022). Soil hydrology in the Earth system. Nature Reviews Earth and Environment, 3(9), 573–587. https://doi.org/10.1038/s43017-022-00324-6

Wagener, T. (2007). Can we model the hydrological impacts of environmental change? Hydrological Processes, 21(23), 3233–3236. https://doi.org/10.1002/hyp.6873

Wagener, T., Sivapalan, M., Troch, P. A., McGlynn, B. L., Harman, C. J., Gupta, H. V, Kumar, P., Rao, P. S. C., Basu, N. B., & Wilson, J. S. (2010). The future of hydrology: An evolving science for a changing world. Water Resources Research, 46(5). https://doi.org/10.1029/2009WR008906

Wakode, H. B., Baier, K., Jha, R., & Azzam, R. (2018). Impact of urbanization on groundwater recharge and urban water balance for the city of Hyderabad, India. International Soil and Water Conservation Research, 6(1), 51–62. https://doi.org/10.1016/j.iswcr.2017.10.003

Walter, M. T., Brooks, E. S., McCool, D. K., King, L. G., Molnau, M., & Boll, J. (2005). Process-based snowmelt modeling: Does it require more input data than temperature-index modeling? Journal of Hydrology, 300(1–4), 65–75. https://doi.org/10.1016/j.jhydrol.2004.05.002

Wang, K., & Dickinson, R. E. (2012). A review of global terrestrial evapotranspiration: Observation, modeling, climatology, and climatic variability. *Reviews of Geophysics, 50*(2), RG2005. https://doi.org/10.1029/2011RG000373

Wang, Q., Liu, S., Liu, Y., Wang, F., Liu, H., & Yu, L. (2022). Effects of urban agglomeration and expansion on landscape connectivity in the river valley region, Qinghai-Tibet Plateau. Global Ecology and Conservation, 34, e02004. https://doi.org/10.1016/j.gecco.2022.e02004

Wang, T., Wu, Z., Wang, P., Wu, T., Zhang, Y., Yin, J., Yu, J., Wang, H., Guan, X., Xu, H., Yan, D., & Yan, D. (2023). Plant-groundwater interactions in drylands: A review of current research and future perspectives. Agricultural and Forest Meteorology, 341, 109636. https://doi.org/10.1016/j.agrformet.2023.109636

Wang, W., Lee, X., Xiao, W., Liu, S., Schultz, N., Wang, Y., Zhang, M., & Zhao, L. (2018). Global lake evaporation accelerated by changes in surface energy allocation in a warmer climate. Nature Geoscience, 11(6), 410–414. https://doi.org/10.1038/s41561-018-0114-8

Wang-Erlandsson, L., Van Der Ent, R. J., Gordon, L. J., & Savenije, H. H. G. (2014). Contrasting roles of interception and transpiration in the hydrological cycle - Part 1: Temporal characteristics over land. Earth System Dynamics, 5(2), 441–469. https://doi.org/10.5194/esd-5-441-2014

Wei, Z., Yoshimura, K., Wang, L., Miralles, D. G., Jasechko, S., & Lee, X. (2017). Revisiting the contribution of transpiration to global terrestrial evapotranspiration. Geophysical Research Letters, 44(6), 2792–2801. https://doi.org/10.1002/2016GL072235

Westerberg, I. K., Sikorska-Senoner, A. E., Viviroli, D., Vis, M., & Seibert, J. (2020). Hydrological model calibration with uncertain discharge data. Hydrological Sciences Journal, 67(16), 2441–2456. https://doi.org/10.1080/02626667.2020.1735638

Whitaker, A. C., & Sugiyama, H. (2005). Seasonal snowpack dynamics and runoff in a cool temperate forest: Lysimeter experiment in Niigata, Japan. Hydrological Processes, 19(20), 4179–4200. https://doi.org/10.1002/hyp.6059

Witmer, R. E. (1978). U.S. Geological Survey land-use and land-cover classification system. Journal of Forestry, 76(10), 661–666. https://doi.org/10.1093/jof/76.10.661

Wu, S., Chen, L., Wang, N., & Assouline, S. (2023). Modeling rainfall-infiltration-runoff processes on sloping surfaces subject to rapidly changing soil properties during seal formation. Journal of Hydrology, 619, 129318. https://doi.org/10.1016/j.jhydrol.2023.129318

Wu, S., Zhao, J., Wang, H., & Sivapalan, M. (2021). Regional patterns and physical controls of streamflow generation across the Conterminous United States. Water Resources Research, 57(6). https://doi.org/10.1029/2020WR028086

Xie, Y., Love, A. J., Simmons, C. T., Costar, A., & Wu, J. (2022). Groundwater age persistence in topography-driven groundwater flow over paleohydrogeologic time scales. Geology, 50(6), 731–735. https://doi.org/10.1130/G49842.1

Xu, J., Quackenbush, L. J., Volk, T. A., & Im, J. (2020). Forest and crop leaf area index estimation using remote sensing: Research trends and future directions. Remote Sensing, 12(18), 2934. https://doi.org/10.3390/RS12182934

Yadav, A., Sonje, A., Mathur, P., & Jain, D. (2012). A review on artificial groundwater recharge. *International Journal of Pharmaceutical and Biological Sciences, 3*(3), 304-311.

Yadav, B. K., & Mathur, S. (2008). Modeling soil water uptake by plants using nonlinear dynamic root density distribution function. *Journal of Irrigation and Drainage Engineering, 134*(4), 430–436. https://doi.org/10.1061/(ASCE)0733-9437(2008)134:4(430)

Yang, L., Xu, Y., Cao, Q., Niu, Z., Luo, Z., & Wang, L. (2024). Hydrological response to future changes in climate and land use/land cover in the Hanjiang River Basin. Natural Hazards. https://doi.org/10.1007/s11069-024-06992-5

Yifru, B. A., Chung, I. M., Kim, M. G., & Chang, S. W. (2021). Assessing the effect of land/use land cover and climate change on water yield and groundwater recharge in east African Rift Valley using integrated model. Journal of Hydrology: Regional Studies, 37, 100926. https://doi.org/10.1016/j.ejrh.2021.100926

Yifru, B. A., Chung, I. M., Kim, M. G., & Chang, S. W. (2021). Assessing the effect of land use/land cover and climate change on water yield and groundwater recharge in East African Rift Valley using integrated model. *Journal of Hydrology: Regional Studies, 37*, 100926. https://doi.org/10.1016/j.ejrh.2021.100926

Yin, J., Calabrese, S., Daly, E., & Porporato, A. (2019). The energy side of Budyko: Surface-energy partitioning from hydrological observations. Geophysical Research Letters, 46(13), 7456–7463. https://doi.org/10.1029/2019GL083373

Yonaba, R., Biaou, A. C., Koïta, M., Tazen, F., Mounirou, L. A., Zouré, C. O., Queloz, P., Karambiri, H., & Yacouba, H. (2021). A dynamic land use/land cover input helps in picturing the Sahelian paradox: Assessing variability and attribution of changes in surface runoff in a Sahelian watershed. Science of the Total Environment, 757, 143792. https://doi.org/10.1016/j.scitotenv.2020.143792

Yu, H. L., & Lin, Y. C. (2015). Analysis of space-time non-stationary patterns of rainfall-groundwater interactions by integrating empirical orthogonal function and cross wavelet transform methods. Journal of Hydrology, 525, 585–597. https://doi.org/10.1016/j.jhydrol.2015.03.057

Zeinivand, H., & Smedt, F. (2009). Hydrological modeling of snow accumulation and melting on river basin scale. Water Resources Management, 23(11), 2271–2287. https://doi.org/10.1007/s11269-008-9381-2

Zeng, Y., Yang, X., Fang, N., & Shi, Z. (2020). Large-scale afforestation significantly increases permanent surface water in China's vegetation restoration regions. *Agricultural and Forest Meteorology, 290*, 108001. https://doi.org/10.1016/j.agrformet.2020.108001

Zeng, Z., Piao, S., Li, L. Z. X., Zhou, L., Ciais, P., Wang, T., Li, Y., Lian, X., Wood, E. F., Friedlingstein, P., Mao, J., Estes, L. D., Myneni, R. B., Peng, S., Shi, X., Seneviratne, S. I., & Wang, Y. (2017). Climate mitigation from vegetation biophysical feedbacks during the past three decades. Nature Climate Change, 7(6), 432–436. https://doi.org/10.1038/nclimate3299

Zhang, C., & Li, X. (2022). Land Use and Land Cover Mapping in the Era of Big Data. Land, 11(10), 1692. https://doi.org/10.3390/land11101692

Zhang, H., Xu, Y., & Kanyerere, T. (2020a). A review of the managed aquifer recharge: Historical development, current situation and perspectives. Physics and Chemistry of the Earth, 118–119, 102887. https://doi.org/10.1016/j.pce.2020.102887

Zhang, K., Kimball, J. S., & Running, S. W. (2016). A review of remote sensing based actual evapotranspiration estimation. WIREs Water, 3(6), 834–853. https://doi.org/10.1002/wat2.1168

Zhang, M., & Wei, X. (2021). Deforestation, forestation, and water supply. Science, 371(6533), 990–991. https://doi.org/10.1126/science.abe7821

Zhang, X., Chen, J., Zhan, L., Ma, F., Yan, J., & Wang, T. (2023). Study on groundwater recharge based on chloride mass balance and hydrochemistry in the irrigated agricultural area, North China Plain. Environmental Earth Sciences, 82(3), 70. https://doi.org/10.1007/s12665-022-10682-5

Zhang, X., Gu, S., Zhao, X., Cui, X., Zhao, L., Xu, S., Du, M., Jiang, S., Gao, Y., Ma, C., & Tang, Y. (2010). Radiation partitioning and its relation to environmental factors above a meadow ecosystem on the Qinghai-Tibetan Plateau. *Journal of Geophysical Research: Atmospheres, 115*, D10104. https://doi.org/10.1029/2009JD012373

Zhao, J., Wang, Z., Dong, Y., Yang, Z., & Govers, G. (2022). How soil erosion and runoff are related to land use, topography and annual precipitation: Insights from a meta-analysis of erosion plots in China. Science of the Total Environment, 802, 149665. https://doi.org/10.1016/j.scitotenv.2021.149665

Zhao, L., Xia, J., yu Xu, C., Wang, Z., Sobkowiak, L., & Long, C. (2013). Evapotranspiration estimation methods in hydrological models. Journal of Geographical Sciences, 23(2), 359–369. https://doi.org/10.1007/s11442-013-1015-9

Zhao, X., & Huang, G. (2022). Exploring the impact of landscape changes on runoff under climate change and urban development: Implications for landscape ecological engineering in the Yangmei River Basin. Ecological Engineering, 184, 106794. https://doi.org/10.1016/j.ecoleng.2022.106794

Zhao, Z., Benoy, G., Chow, T. L., Rees, H. W., Daigle, J. L., & Meng, F. R. (2010). Impacts of accuracy and resolution of conventional and LiDAR based DEMs on parameters used in hydrologic modeling. Water Resources Management, 24(7), 1363–1380. https://doi.org/10.1007/s11269-009-9503-5

Zheng, Z., Gao, J., Ma, Z., Wang, Z., Yang, X., Luo, X., Jacquet, T., & Fu, G. (2016). Urban flooding in China: Main causes and policy recommendations. Hydrological Processes, 30(7), 1149–1152. https://doi.org/10.1002/hyp.10717

Zhou, K. (2022). Urban water dissipation calculation based on the improved water balance models. Journal of Water and Climate Change, 13(1), 372–382. https://doi.org/10.2166/wcc.2021.330

Zuazo, V. H. D., & Pleguezuelo, C. R. R. (2009). Soil-erosion and runoff prevention by plant covers: A review. In E. Lichtfouse, M. Navarrete, P. Debaeke, S. Véronique, & C. Alberola (Eds.), Sustainable Agriculture (pp. 785–811). Springer Netherlands. https://doi.org/10.1007/978-90-481-2666-8_48

CHAPTER 3

THREE DECADES OF LAND COVER CHANGE IN THE MURRAY DARLING BASIN: INSIGHTS AND IMPLICATIONS

Highlights:

Floods and droughts have a strong regional impact on land cover change.

Large parts of MDB showed increases in natural bare and artificial surfaces.

The western part of MDB showed a decreasing trend in the cultivated area.

Impacts of policy change are not discernible in land cover change.

Land use data shows irrigated agriculture expanding despite limiting policies.

Three decades of land cover change in the Murray Darling Basin: Insights and implications

A. Shadmehri Toosi[1*], O. Batelaan[1], M. Shanafield[1], H. Guan[1], N. Crossman[2]

1. Flinders University, National Centre for Groundwater Research and Training, College of Science and Engineering, Bedford Park, 5042, Australia
2. Flinders University, College of Business, Government and Law, Bedford Park, 5042, Australia

*Corresponding author

Email: amirh.shadmehr@flinders.edu.au

3.1 Abstract

Temporal and spatial variability of land cover data plays a crucial role in understanding the changes that are taking place in our landscape over time. These changes can significantly impact ecosystem health, the economy, and society; thus, it is crucial to identify and understand them. This study focuses on the Murray Darling Basin, Australia's most important agricultural region, and examines the changes in land cover over 31 years (1990-2021). The dynamics between each land cover class were investigated using the latest Geoscience Australia level 3 land cover dataset. Further, we evaluated the effects of water recovery initiatives and infrastructure developments on agricultural land use at the sub-catchment scale. The Sustainable Diversion Limit (SDL) units (closely aligned with sub-catchment boundaries) with the highest total water recovery were investigated using Australian Bureau of Agricultural and Resource Economics (ABARES) land use data. The results revealed a significant increase in the natural bare surface and a notable decline in the Basin's water bodies. There was a decreasing trend in cultivated terrestrial vegetation across the western part of the Basin. Although the magnitude of changes substantially varied across the catchments, the eastern part of the Murray Darling Basin has undergone fewer changes overall. Climate, rainfall variability and terrain were strong drivers of land cover spatiotemporal variability in the Murray Darling Basin. The land use data indicates an expansion of irrigated agriculture in the SDL units with the highest total water recovery, suggesting that improvements in water use efficiency may have enabled an increase in agricultural land, indicative of a rebound effect. This study provides a comprehensive understanding of the Basin's temporal land cover variability. It contributes to improved decision-making, formulating

effective policy options, and predicting the likely impact of changes to preserve the region's natural resources.

Keywords: Land cover dynamics, Land conversion, Environmental management, Murray Darling Basin, Land-use policy

3.2 Introduction

Land use - land cover change is occurring at the global scale with numerous physical, ecological, and socio-economic consequences (Teklay et al., 2019; Zeng et al., 2020). The changing landscape impacts processes ranging from local water supply to global water balance and carbon cycling (Obahoundje et al., 2017; Dile et al., 2018; Li et al., 2018; Saddique et al., 2020). In recent decades, global population growth and urbanisation have exacerbated land cover change to meet the demands for food and habitable spaces. To accurately describe the interactions between land use, climate, and hydrology, we first need to understand the land use - land cover change dynamics (Castillo et al., 2014). Therefore, monitoring and comprehending the extent of these changes is crucial for effective environmental management and sustainable development.

Land cover change has been recorded over Australia in the past decades, with significant impacts on basin hydrologic characteristics such as streamflow, recharge rate, temperature, and precipitation (Saha et al., 2019; Tulbure & Broich, 2019; Lane et al., 2023). The assessment of land cover changes largely relies on classified spatial data, typically accompanied by additional, complementary variables (Hasegawa et al., 2017; Calderón-Loor et al., 2021b). This information is used to assess land cover changes over time. Numerous coarse-resolution, global land-cover products exist, such as the 250 m resolution MODIS Land Cover dataset (Friedl et al., 2010), the 300 m resolution GLOBCOVER, the 5 ha resolution Corine Land Cover (Bossard et al., 2000), and others (Hansen et al., 2000; Loveland et al., 2010; Bontemps et al., 2013; Calderón-Loor et al., 2021a). However, these datasets are usually limited by spatial resolution and temporal range. In addition, inconsistent classification systems can make using and integrating data from various sources difficult, particularly in regions with dynamic environments, hindering efforts to track changes in land cover and understand its interaction with hydrological processes.

Land cover change monitoring has advanced due to the increasing availability of high and medium-resolution satellite imagery and the emergence of cloud-computing services (Xiong et al., 2017). High computational costs generally restrict the analysis of consistent high-resolution land-cover maps over large areas. However, the emergence of proprietary, web-based platforms such as Google Earth Engine drastically reduces computation times and expands the potential for analysing and accessing massive geospatial data (Gorelick et al., 2017; Calderón-Loor et al., 2021a).

Land cover change is a critical issue in Australia, driven by various factors, including agricultural expansion, urbanisation, and climate change. Understanding these changes is

essential for effective land management and conservation efforts. One of the areas that has experienced the greatest potential for change is the Murray Darling Basin (MDB). The MDB is notable for being home to Australia's most fertile agricultural regions (Postel, 2000), which contributes $30 billion to the Australian economy every year (MDBA, 2023c). Furthermore, the Basin plays a critical role in delivering water resources in Australia, with its rivers and groundwater systems contributing to over 70% of the country's total irrigation water (Gonzalez et al., 2020; Fu et al., 2022). However, the development of the basin for water supply and agriculture has impacted its ecosystems, leading to altered flow regimes, water pollution, habitat loss, and biodiversity decline (Alexandra, 2018; Hart et al., 2020; McLoughlin et al., 2020). To balance anthropogenic use with ecosystem health, the MDB has received significant public investment to modernise irrigation infrastructure and implement strategic water policies, including the 2007 Water Act and the 2012 MDB Plan (Alexandra, 2018; Grafton & Wheeler, 2018). The goal has been to reduce the amount of water extracted for irrigation and return water to the environment to improve river and wetland ecosystem health.

Given its significance, management of natural resources in the MDB will benefit from a long-term, comprehensive analysis of land-cover change using high-resolution land cover data to better understand whether MDB policy has impacted key land system processes and the intricate patterns involved in local land cover change (Hoskins et al., 2016; Klotz et al., 2016). Integrating this knowledge is crucial for tackling the challenges related to water quality and quantity within the Basin, ensuring both ecological stability and resource sustainability (Holland et al., 2015; Papas, 2018; Hart et al., 2020). This includes an awareness of the variability in these changes and an assessment of the primary trends over time. Although several studies have explored national-scale land-use changes, they often do not provide consistent temporal coverage and lack detailed regional insights. For example, Bryan et al. (2009) offer valuable insights into the land use dynamics in the MDB, but the data is now over two decades old and covers only a brief period before the 2007 Water Act and 2012 MDB Plan. Among few studies investigating land use and land cover dynamics in MDB, no previous study has employed complete spatiotemporal land cover and land use data to examin changes within the MDB throughly.

Utilising Digital Earth Australia level 3 land cover data with a resolution of 25 m, the study examines annual changes over the 31-year period from 1990 to 2020. By examining the land cover changes and their spatial and temporal characteristics, this study aims to provide insights into the drivers of land cover change in the MDB and discuss their potential impacts. Additionally, we evaluate the potential effects of water recovery initiatives and irrigation infrastructure developments on agricultural land use at the Sustainable Diversion Limit (SDL)

units level (commensurate with sub-catchments) using land use data. Drawing on prior studies, this research provides valuable perspectives to the discourse on sustainable water resource management in arid and semi-arid regions globally.

3.3 Methods and material

3.3.1 Study area

The MDB covers more than a million square km (~106 million hectares). It spans across four states - Queensland, New South Wales, Victoria, and South Australia - and the Australian Capital Territory. The MDB is an extensive and interconnected system of rivers, consisting of 22 catchments extending over 1365 km from north to south and 1250 km from east to west (Figure 3.1). Most of the Basin is characterised by extensive floodplains and low-rolling terrain. However, the western slopes of the Great Dividing Range and Snowy Mountains are included in the Basin towards the east and southeast (Camilleri et al., 2010).

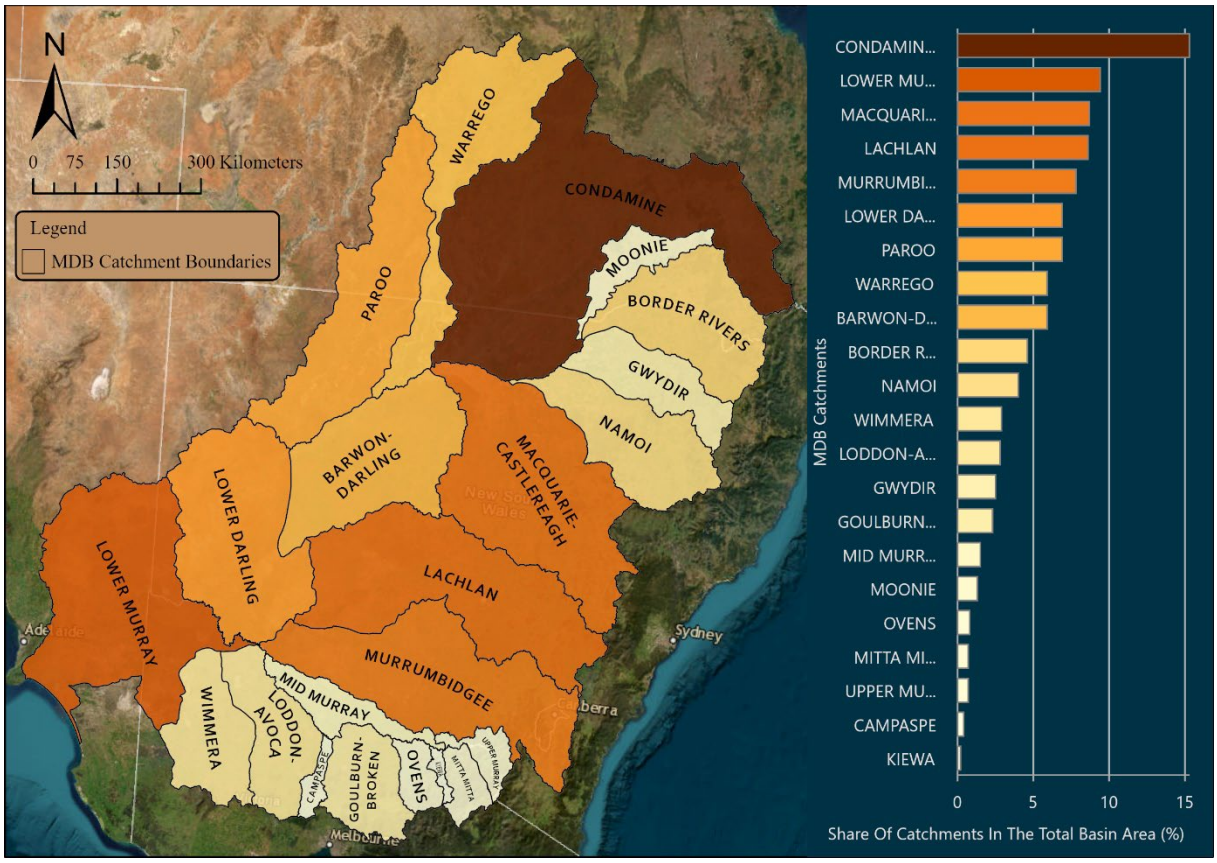

Figure 3.1: Murray Darling Basin and its 22 catchments with their catchment area as a percentage of the total Basin area.

The sub-catchments of the MDB play a vital function in producing the source water of the main rivers of the Basin, the Murray and Darling Rivers. Each sub-catchment has unique characteristics; for example, the Upper Murray River has primarily higher elevation and

forested land, while the Lower Murray River has mostly flat and agricultural land. The sub-catchments, therefore, play a critical role in water management for irrigation, hydroelectric power generation, and environmental conservation. With over 40% of Australia's annual agricultural production coming from the MDB, it is the country's most intensive agricultural region (Pink, 2008).

The Basin is home to diverse ecosystems and habitats, including wetlands, forests, and grasslands, making it a vital area for preserving the health of rivers, lakes, and wetlands for future generations. However, many of the sub-catchments have been impacted by climate change and increased climate variability, particularly the low river flows in the 2000s Millenium Drought (Cai & Cowan, 2008; Pink, 2008) and the recent 2018-2020 drought. The increasing human use of the waterways for agriculture has also contributed to the decline of the Basin's health (Williams et al., 2022). Additionally, over the past several decades, extensive clearing of native vegetation for agriculture has occurred (Hart et al., 2020; Walker & Prosser, 2021), including some of the highest clearing rates in the northern portions of the Basin in the last decade (Reside et al., 2017; Pickering & Guglyuvatyy, 2019).

3.3.2 Data

3.3.2.1 Land Cover data

Digital Earth Australia (DEA) is a national platform that offers access to a vast array of geospatial data, including land use and land cover datasets (Tissott & Mueller, 2022). DEA Land Cover is based on the Food and Agriculture Organization's (FAO) Land Cover Classification System (LCCS) taxonomy version 2, which is globally applicable (Gregrio & Jansen, 2000). The DEA Land Cover classifications are generated by combining qualitative or quantitative environmental information obtained from the annual composites of Landsat satellite sensor data, resulting in annual classifications of Australia's land cover from 1990 to 2020. The DEA Land Cover product consists of eight datasets: the base (level 3) classification, seven additional descriptor layers (which can be either quantitative or qualitative environmental information), and the final (level 4) classification that combines the base classes with the associated descriptors. In this study, we used the base classification to comprehensively understand the data set (Tissott & Mueller, 2022).

DEA Land Cover provides metadata explaining the land cover; however, interpretation can be complex as the same terminology is used to report on land use. The Cultivated Terrestrial Vegetation (CTV) category in the DEA Land Cover map refers to areas where active cultivation has been observed, including crop planting, harvesting (including grass production), fertilisation, and ploughing. In the DEA dataset, only herbaceous cultivation is depicted and

encompasses vegetation with varying cover levels, from bare (ploughed) areas to fully-grown crops. These agricultural areas may transition between cultivated and natural covers as management practices change, moving from actively cropped or grazed to fallow, low cover due to climate effects such as drought or other covers based on the dominant conditions during the year. The Natural Terrestrial Vegetation (NTV) category represents areas that possess the characteristics of natural or semi-natural herbaceous or woody vegetation (based primarily on floristics, structure, function, and dynamic characteristics). This approach considers NTV primarily vegetated if a pixel's vegetated fraction is more than 30%. The vegetation can transition between photosynthetic vegetation fraction and non-photosynthetic fraction states throughout the year. When urban regions contain vegetation such as suburbs with trees, they are categorised as NTV only if the vegetation proportion in the pixel is greater than or equal to 30% and as Artificial Surfaces (AS) if it is less than that. The approach enables the incorporation of semi-natural vegetation, such as native grasslands or pasture lands, into the NTV category.

Natural Aquatic Vegetation (NAV) is associated mainly with wetlands, where woody or herbaceous vegetation dominates the area. This type of vegetation is commonly seen in flooded forests, swamps, salt marshes, fens, and mangroves, with only the latter being included in the current release. Artificial Surfaces (AS) refers to areas created by human activity, composed mainly of impermeable surfaces such as industrial and urban structures, railways, and roads. These surfaces are easily recognisable when they are larger than the 25-m spatial resolution of the sensor and often include open-cut extraction sites. Natural Surfaces (NS) comprise primarily non-consolidated materials, such as mudflats or saltpans, or consolidated materials, such as bare rock or bare soil. Finally, the Water class encompasses terrestrial and coastal open water bodies, including dams, lakes, large rivers, and the coastal and near-shore zones.

DEA level 3 data provides valuable information about land cover types over MDB. DEA datasets typically provide annual coverage over the same period, derived from continuous satellite monitoring throughout the year. The exact temporal windows used by DEA may differ slightly depending on the product and acquisition availability. In practice, we assume the classification datasets represent land conditions around the focal years, recognising minor temporal offsets. However, the categorisation and classification of cover data can impact its accuracy. Disagreements often arise regarding the most suitable land cover categories, and temporal changes within a given category may not be reflected in the classification, potentially masking important ecological shifts.

Managed plantations, some orchards, and tree crops cannot currently be distinguished from semi-natural or natural terrestrial vegetation and are not included in the CTV area. There may be instances where areas of NTV, NS, or NAV are misclassified as CTV due to the variable cycles associated with events such as fires, inundation, drought, and rainfall, which can cause greening or browning of natural vegetation that resembles the seasonal or management-induced behaviour of cultivated land.

The distinction between surfaces that are mainly barren with no remaining photosynthetic vegetation and partially covered surfaces is based on the spectral reflectance difference. When vegetation coverage is very low, it should be classified as NS instead of NTV, but confusion can occur due to spectral variability in the soil reflectance compared to the sparse vegetation reflectance. There can also be some confusion between CTV and NTV due to natural variations in native vegetation throughout the year. Similarly, artificial surfaces (AS) and natural surfaces have similarities in the annual variation of spectral signatures; NS may temporarily change to or from CTV during a drought.

As per the DEA documentation, the total accuracy of the DEA dataset is 80% for a total of 12,000 samples tested for all classes in both 2010 and 2015 (Owers et al., 2021; Tissott & Mueller, 2022). Classes such as artificial surfaces, natural aquatic vegetation, and water have high accuracies. However, classifying cultivated terrestrial vegetation and bare surfaces proved difficult, resulting in the lowest accuracy among the land cover classes, with F1 scores* ranging from 0.55-0.74 and 0.62-0.67, respectively. The dataset is appropriate to use at the national scale where other more detailed land cover information is unavailable (Lucas et al., 2019; Owers et al., 2021; Tissott & Mueller, 2022).

3.3.2.2 Land use data

The Australian Land Use and Management (ALUM) Classification system offers a nationally consistent approach to collecting and presenting land use information, catering to a broad user base across Australia (ABARES, 2021; ABARES, 2022). National-scale land use data were available for multiple years, from which we chose 1996–97, 2000–01, 2005–06, 2010–11, and 2015–16. Since national land use data was unavailable for 2020, we used 2020 catchment scale land use data, which uses the same classification method but offers higher resolution. We assume that this dataset represents accurately the land use for 1995, 2000, 2005, 2010, 2015, and 2020. Its products are typically derived from remote sensing imagery (e.g., Landsat), agricultural statistics, field surveys, and expert knowledge, ensuring a robust

* The “F1 score” is a combination of precision and recall and an overall measure of accuracy. “Precision” refers to the ability of a classification model to return only relevant instances. “Recall” refers to the ability to identify all relevant instances.

foundation for understanding land use patterns. To validate the classification, ALUM datasets undergo ground-truthing, expert review, and cross-referencing against high-resolution imagery, topographic maps, agricultural census records, orthophotos, and ancillary geospatial layers.

In this study, we employed the primary classes of ALUM land use, which consisted of six primary classes: Conservation and natural environments, land primarily used for conserving essentially natural ecosystems; Production from relatively natural environments, land mainly utilised for primary production with minimal alterations to native vegetation; Production from dryland agriculture and plantations, land predominantly employed for primary production based on dryland farming systems; Production from irrigated agriculture and plantations, land mostly used for primary production involving irrigated farming; Intensive uses, land extensively modified for residential, commercial, or industrial purposes; and Water, which includes bodies of water.

ABARES reports that overall classification accuracy for broad land use categories is generally greater than 80% at national scales, though specific accuracy figures can vary regionally depending on data availability and land use complexity. Uncertainties in land use datasets include classification errors, often due to the challenge of distinguishing between visually or spectrally similar land uses in imagery (Dong et al., 2015). Uncertainties persist due to factors such as temporal discrepancies in data acquisition, image quality variations, spectral similarities between certain land cover types, and limited ground-reference data in remote regions. Land use data is typically updated every five years and may not accurately reflect the most recent state of land use. It should be noted that there is a difference in resolution between older and newer datasets. In this study, we assume that the chosen datasets are representative and sufficiently accurate for the purpose of capturing broad-scale land use patterns over time. We further assume that, collectively, these datasets accurately reflect land use patterns for the periods of interest (i.e., 1995, 2000, 2005, 2010, 2015, and 2020). While some degree of uncertainty remains inherent in any classification product, the ALUM datasets provide one of the most reliable, systematically produced land use information sources available for the MDB.

3.3.3 Preprocessing and analysis

Land cover data were downloaded from Amazon Web Services (AWS). ArcGIS (Esri, 2020) was used for mosaicking data, combining multiple individual images or datasets into a seamless image to analyse land use patterns or monitor changes over time. The projection of all images was GDA94 / Australian Albers, which is EPSG:3577 (https://epsg.io/3577).

The Tabulate Area tool in ArcGIS Pro was used to summarise data and get insights into land cover patterns within the study area. We summarised the land cover dynamics for Level 3 DEA Land Cover (Landsat) for the whole Basin and 22 catchments in MDB. Similarly, the Tabulate Area tool was employed to summarise land use data throughout the Basin and within individual SDL units. Additionally, the reported total water recovery figures were normalised by the area of each SDL unit, allowing for a more accurate comparison.

The "Unique" method in ArcGIS Pro was used to identify the unchanged land covers across the time axis. This method can be used to identify pixels with unique values within the time axis of the multidimensional dataset, showing the unchanged pixels and pixels that vary between several land cover classes over time. For example, if the same value always appears for the given pixels, those pixels are unchanged. If different values occur in one pixel across time, then this pixel has experienced other land cover classes.

We conducted a trend analysis to examine the temporal changes in land cover. First, we estimated the total area of each land cover for each year across the entire Basin, providing a comprehensive view of the overall land cover changes over time. Next, the analysis was repeated for catchments to see if there was any pattern in the trend of change and in which catchments. Here, Mann-Kendall trend analysis was used to measure the degree of monotonic association between the data and time and indicates whether there is an upward or downward trend in the data (Mann, 1945; Kendall, 1975).

Test statistic S is used to calculate the p-value, which quantifies the likelihood of observing a data trend as pronounced as the one identified, assuming that no actual trend exists in the data. Essentially, it assesses whether the observed trend could have occurred by random chance. If the p-value is below a certain significant level (in this case, 0.05), it was concluded that there is an indication of a trend in the data. The data were organised into a time series format, with the dependent variable (e.g., percentage of each land cover) recorded for each time. The Mann-Kendall tau statistic measures the degree of monotonic association between the data and time. A positive Kendall's tau indicates an upward trend, while a negative Kendall's tau indicates a downward trend (Salehi et al., 2020). Further, the Sen slope was used to estimate the slope of a trend in data, validate the results, and provide a more comprehensive analysis of the data (Sen, 1968). The Sen slope test works by dividing the data into multiple segments and calculating the median slope for each segment. The overall trend is then estimated as the median of the slopes of all segments. The Sen slope estimator is robust to outliers and less sensitive to the assumption of normality than other regression methods. However, it is not suitable for detecting non-monotonic trends.

To calculate water recovery in millimetres (mm) per SDL unit, we utilised the total registered surface water recovery data under the Basin Plan (as of 30 September 2023), expressed in gigaliters (GL). Following unit conversion, the total water volume was divided by the SDL unit area to determine the water recovery for each SDL unit in mm. This approach standardises the measure of water recovery, enabling comparisons across different units. The top six units with the highest recovery numbers were selected for further investigation.

3.4 Results

3.4.1 Land cover change in the whole Basin

The pixel analysis map shows the number of changes, though it is unclear what the frequency is, when, and how the change has happened (Figure 3.2). 27% of the Basin was associated with only one land cover class over the 31 years, indicating that no land cover change has happened during this period. Comparing these results with the CSIRO-reported broad land use in 1996/97 and 2000/01 shows that many areas with one unique land cover type are categorised as Conservation and Other Minimal Use (Bryan & Marvanek, 2004). For 34% of the MDB, land cover transitions were primarily between two categories, NTV and CTV, suggesting a tendency for areas to switch between these two land covers. This percentage was 38% and 1.4% for the area that changed between 3 and 4 classes, respectively. On average, over 31 years, NTV constitutes 68% of the whole Basin, followed by CTV at 21% and NS at 11% of the Basin. The Water coverage was 0.7% and less than 0.03% for other Land covers. On average, the highest relative standard deviations were observed in the whole Basin over 31 years for NTV, CTV, and NS, with 6.2%, 5.4%, and 6.3%.

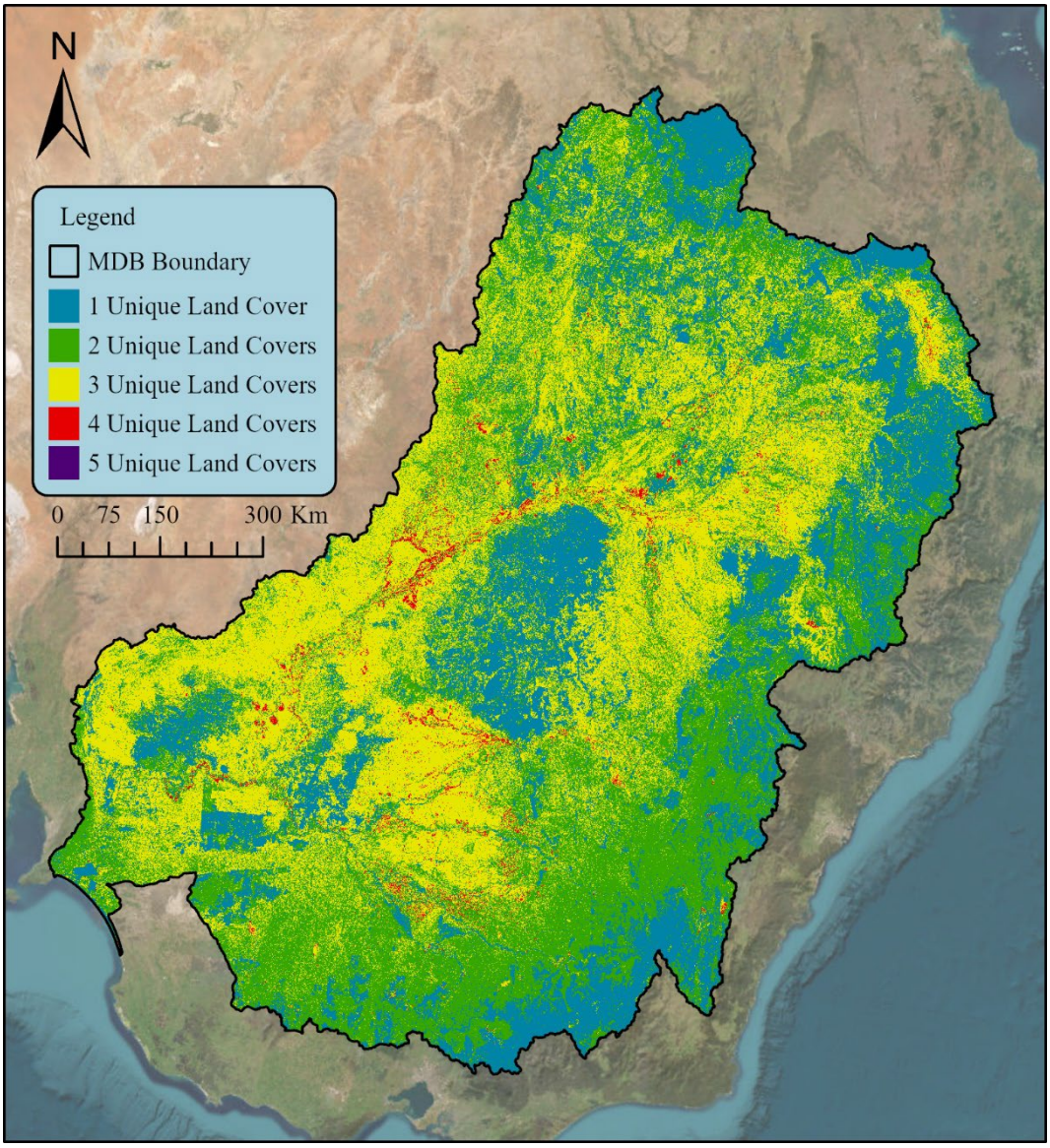

Figure 3.2: Number of land covers per pixel occurring within 31 years, between 1990-2020.

NTV was the dominant land cover over all years, and its peaks corresponded to a decline in NS and CTV (Figure 3.3, Table A.1). In 1990, NTV comprised 64% of the MDB, followed by CTV, constituting 33% of the whole Basin. Further, NS and Water accounted for 1.7 and 1.5% of the MDB, respectively. In 2020, NTV was still the dominant land cover, accounting for 57% of the Basin. Similarly, CTV remained the second significant land cover, declining by nearly 9% from 1990, while Water fell to 0.6%. In contrast, NS increased significantly from 1.7 to 18%. Artificial surfaces gradually increase each year (300% increase over 31 years), though they constitute a very small proportion of the basin. Finally, the percentage of NO data (N/A) decreased over time.

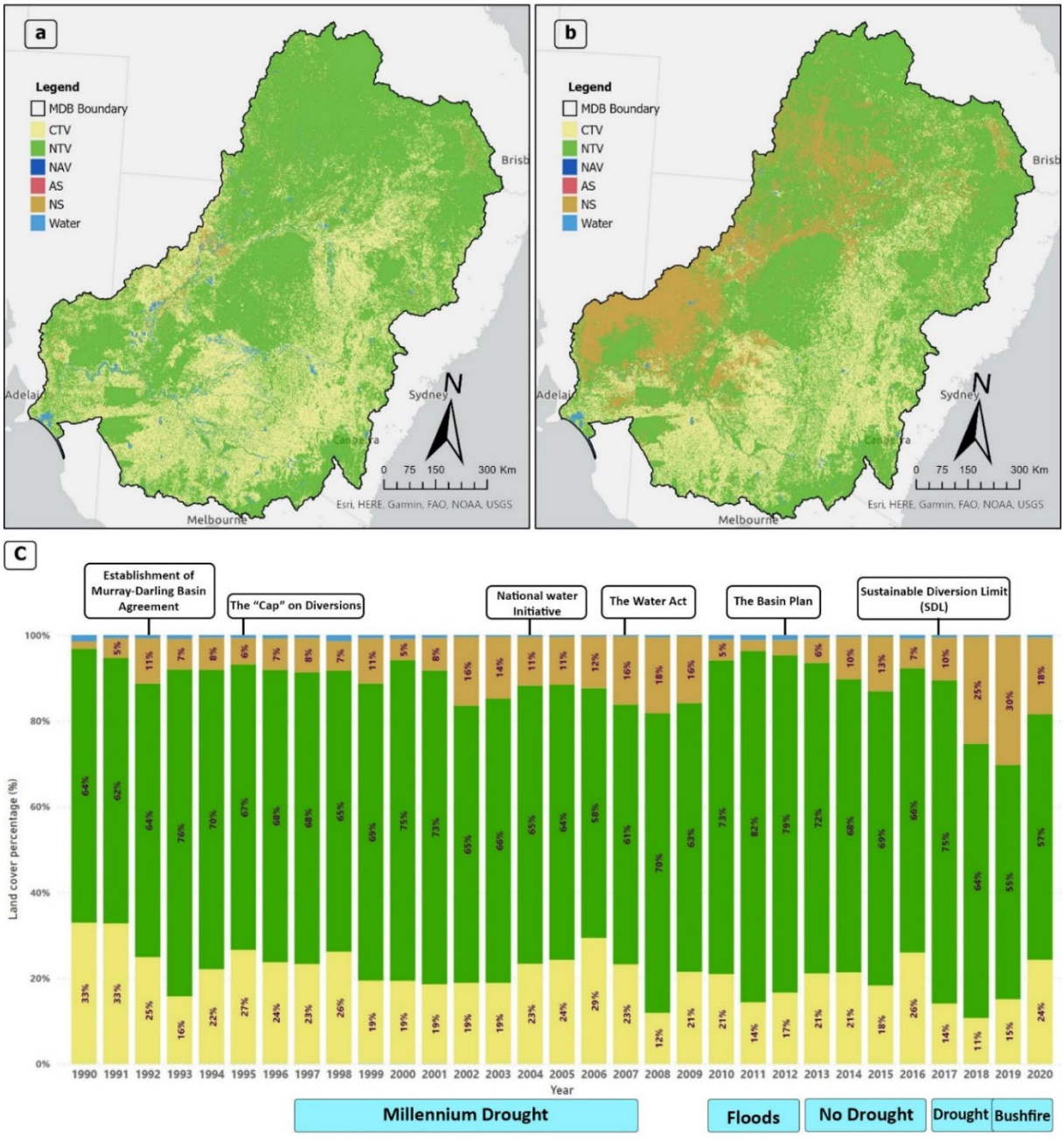

Figure 3.3: (a) Land cover map for 1990; (b) Land cover map for 2020; (c) Areal percentage of different land cover classes per year from 1990 till 2020; the important policies that may have impacted land cover are listed on top of the chart and the important climatic events are listed below the chart (NTV: Natural Terrestrial Vegetation, CTV: Cultivated Terrestrial Vegetation, NAV: Natural Aquatic Vegetation, AS: Artificial Surface, NS: Natural Bare Surface).

The results from the analysis of the spatiotemporal variation of land use in the MDB culminated in some areas of considerable landscape alteration between 1990 and 2020. Figure 3.4 highlights an area adjacent to Lake Victoria in the southwestern New South Wales Riverina region, where notable changes in land cover have occurred annually. The analysis for this region revealed a negative correlation between NS (-0.79) and Water, as well as NTV (-0.54). We further investigated Level 4 land cover data for this small area to investigate changes

between land cover classes. “NS bare area, unvegetated” showed a -0.73 correlation with “Non-perennial water (1-3 months),” which was reflected in level 3 data too. Additionally, there was a -0.8 correlation between “NS bare area, unvegetated” and “NTV herbaceous open (15 to 40%)” and a 0.66 correlation between “CTV herbaceous sparse (54% to 15%)” and “NTV herbaceous scattered (1 to 4%)”. Furthermore, there was a -0.61 correlation between “CTV herbaceous closed (>65%)” and “NS very sparsely vegetated area”, which may indicate the abandonment of agricultural land in certain years.

The land cover maps show that for the whole basin, the NS area has grown steadily from a low of 1.2% in 1990 to a peak of 30% in 2019. A noticeable variation in NS cover can be seen in Figure 3.3, wherein NS land cover is more notable in the dry years. In 2011, the peak in NTV coverage of 82% of the entire Basin occurred, which may have been associated with the La Niña wet period. The percentage of NTV again dipped to 55% by 2019, a year after another period of below-average rainfall and low water flows. CTV ranged from 11% to 33%, with a peak value recorded in 1990 and a minimum in 2018. Most variations in the percentage of land cover were observed between NTV and CTV, with NS experiencing a comparatively smaller share of this variation (Figure 3.2).

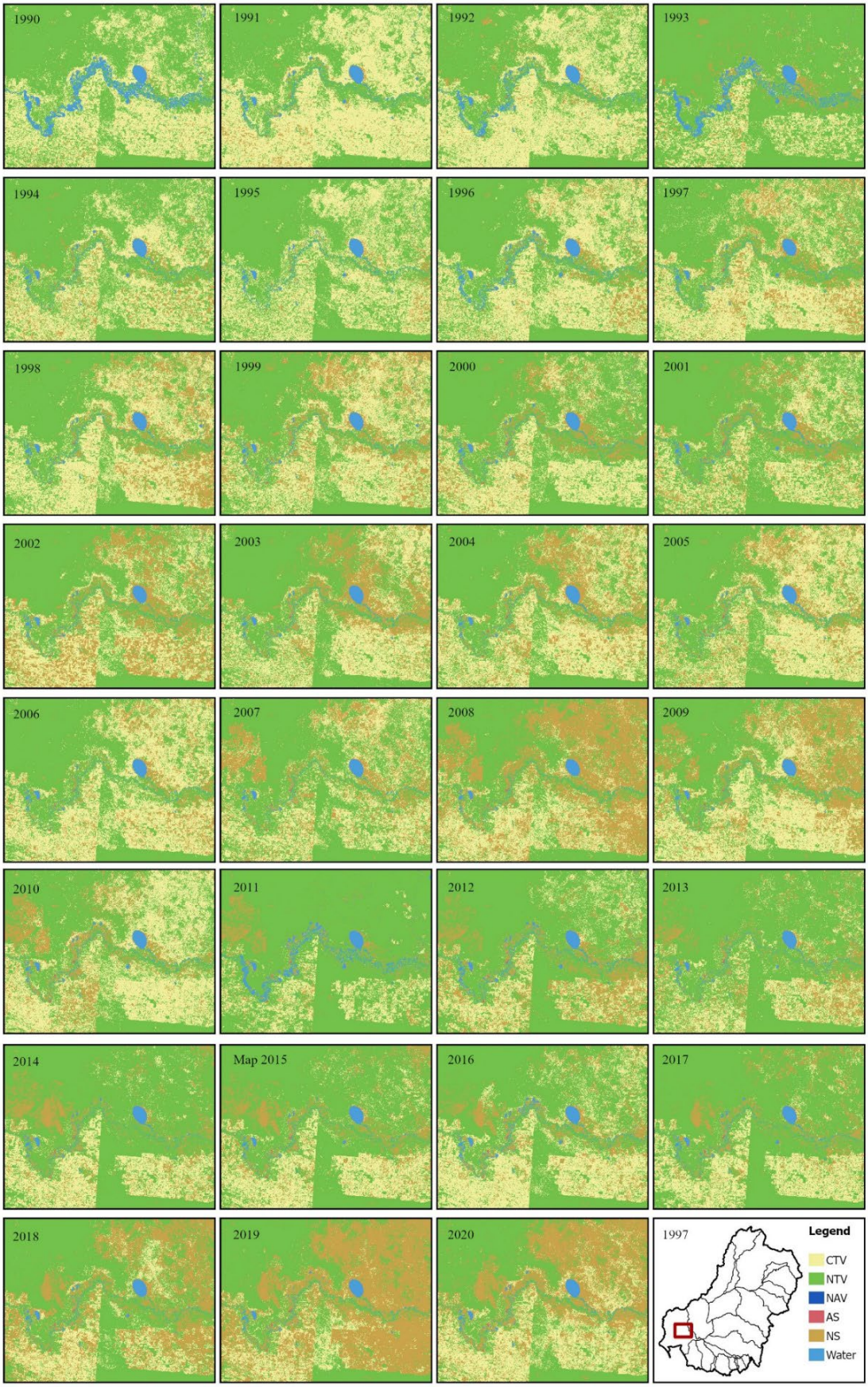

Figure 3.4: Land cover dynamics between 1990 and 2020 for a 22,222 km2 area near Lake Victoria, the western Riverina region of southwestern New South Wales, Australia.

The Mann-Kendall test signalled a decreasing trend in CTV and Water and a considerably increasing trend in NS and AS areas (Table 3.1). The Sen Slopes were highest for CTV (-0.3) followed by NS (0.35). The decreasing trend for CTV may be partly explained by the decline in rainfall after 1990. Further, the Spearman correlation analysis revealed a positive correlation of 0.38 between mean rainfall and NTV, indicating that NTV also tends to increase as rainfall increases. Interestingly, when NTV was shifted by one year, the correlation increased to 0.72, suggesting that NTV takes approximately one year to respond to changes in rainfall. In contrast, NS showed a negative correlation of -0.59 with mean rainfall, while water exhibited a strong positive correlation of 0.70.

Table 3.1:Trend analysis tests for the MDB.

	Mann Kendal's test result					Sen's Slope test result
Land cover	Kendall's tau statistic	Mann-Kendal's score	Trend	p-value	Slope	intercept
CTV	0.3462	-161	decreasing	0.0065	-0.301	25.857
NTV	-0.230	-107.000	no trend	0.072	-0.041	67.118
NAV	0.092	43.000	no trend	0.475	0.000	0.000
AS	0.841	391.000	increasing	0.000	0.001	0.009
NS	0.325	151.000	increasing	0.011	0.349	4.574
Water	-0.299	-139.000	decreasing	0.019	-0.014	0.845

3.4.2 Land cover changes in catchments

Considering the Basin-scale heterogeneity, the results are also presented at the catchment scale to identify better regional variation and controlling factors. The percentage of areas in the Murray-Darling catchments that have not changed land cover between 1990 and 2020 ranged from 10 to 71% for each catchment over 31 years (Figure 3.5). The Lower Darling was the only catchment that showed significant oscillation between at least three land cover classes, and more than 70% of its area had three land covers or more. Further, in more than 90% of six south-eastern catchments (Ovens, Mitta Mitta, Upper Murray, Kiewa, Campaspe, and Goulburn Broken), the land cover only changed between two land cover classes or remained unchanged. Very few pixels changed between five classes in all catchments.

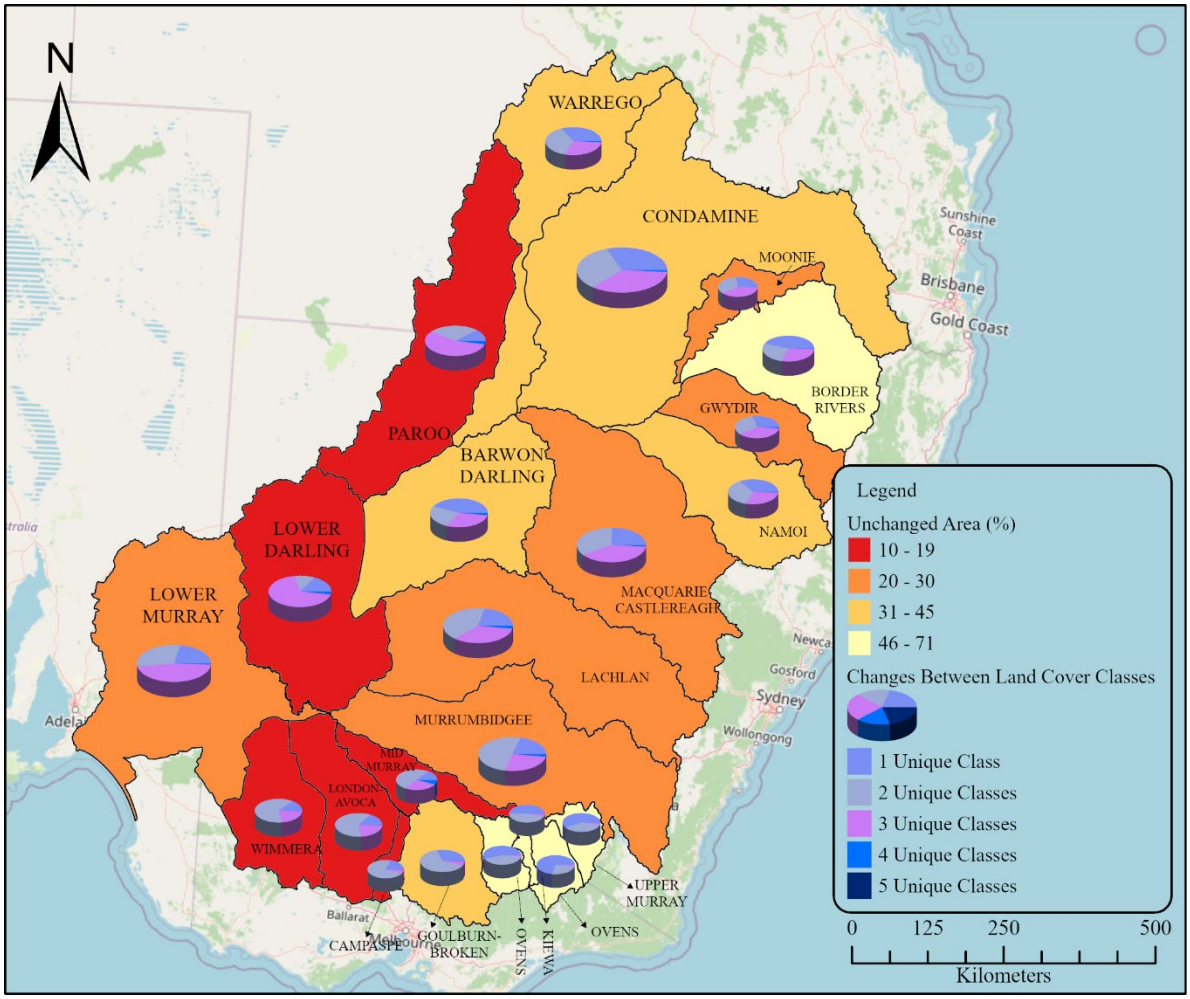

Figure 3.5: Percentage of area categorised as pixels with 1,2, 3, 4, and 5 land cover classes over 31 years, and the percentage of unchanged land cover area per catchment.

Considering the changes in land cover per catchment between 1990-2020, the area of NS increased significantly since 1990 in all catchments (Figure 3.6). The largest increases (more than 3% of whole MDB) were recorded in the Lower Darling, Lower Murray, and Condamine catchments. Moreover, there was a decrease in water area (ranging between 0.01 and 0.22%) between 1990-2020 in all catchments, with Lachlan and Lower Darling accounting for the largest share of change (Figure 3.6). Investigation of changes in NTV and CTV from 1990 to 2020 revealed that most MDB catchments experienced a decline in CTV, with NTV decreasing in near half of them. Only three catchments (Condamine, London-Avoca, and Wimmera) exhibited a slight increase in CTV. For NTV, several catchments noted slight rises, with the most significant being in Murrumbidgee corresponding to 0.69% of NTV change between 1990-2020. A reduction in NTV and CTV appeared to correspond to increase in NS in most catchments (Figure A.1). For example, from 1990-2020 in Condamine NS increased by 3.24%, while NTV and CTV decreased by 2.74% and 0.52%, respectively. Further, a rise in NTV percentage was observed in the area where CTV decreased. For example, between 1990-

2020 in Murrumbidgee CTV decreased by -0.78%, while NTV and NS increased by 0.69% and 0.17%, respectively.

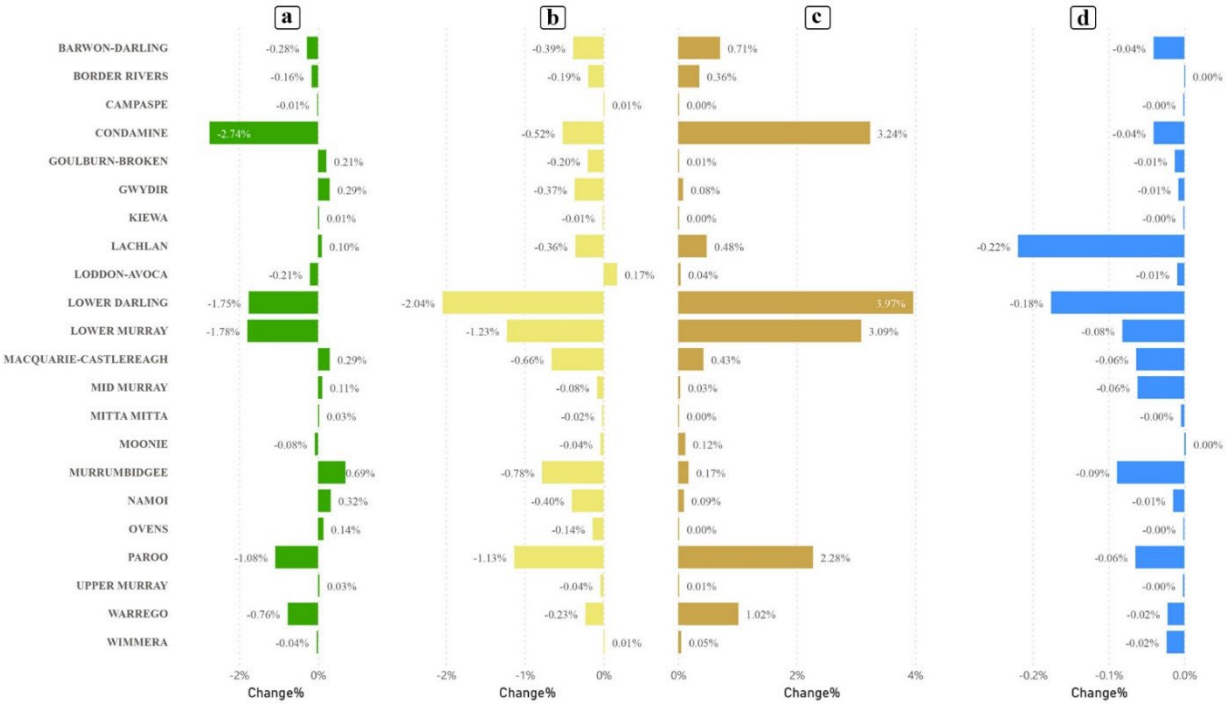

Figure 3.6: 1990-2020 change in land cover as percentage of the total MDB for (a) Natural Terrestrial Vegetation (NTV); (b) Cultivated Terrestrial Vegetation (CTV); (c) Natural Bare Surface (NS); (d) Water.

Small catchments such as Kiewa corresponded to less than 1% of land cover changes in the whole Basin (Figure 3.6). However, CTV and NTV in Kiewa changed by roughly 6%, showing that CTV has turned to NTV during this period. Wimmera, Murrumbidgee, MD Murray, London Avoca, and Lachlan catchments were highly cultivated in 1990, and CTV underwent only a negligible change by 2020. NS covered a significant part of the Warrego, Lower Murray, and Lower Darling catchments in 2020, although it was negligible in 1990 (Figure 3.7).

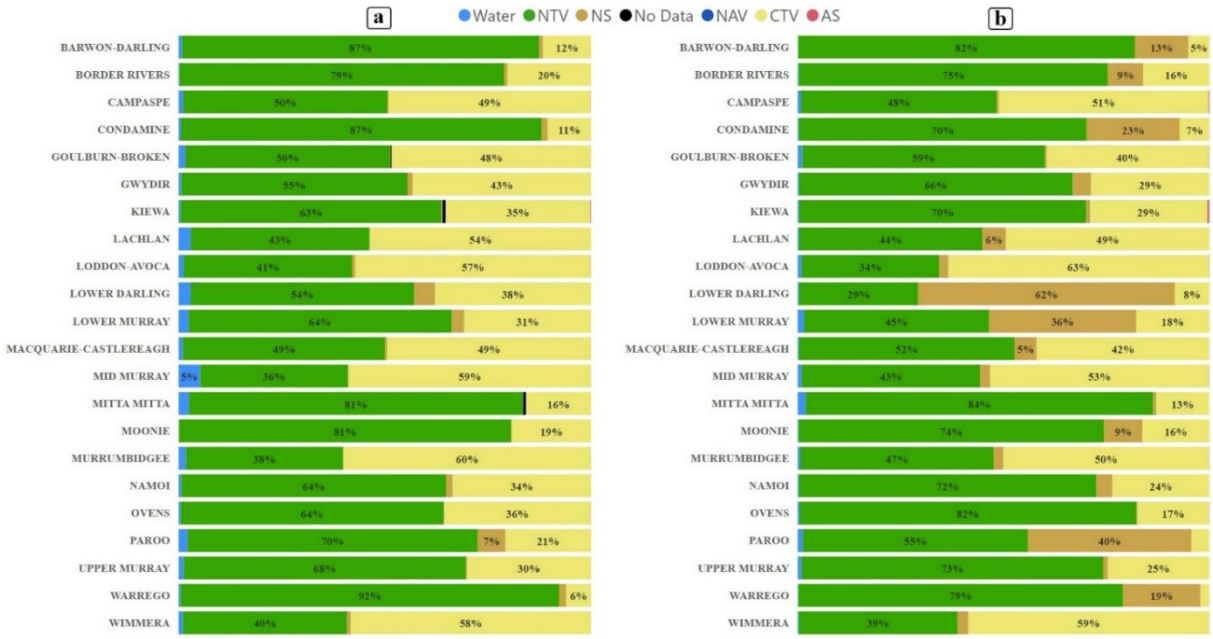

Figure 3.7: Distribution of different land covers over MDB in (a) 1990 and (b) 2020.

We applied trend analysis tests for each catchment to get more insight into the trend of land cover change over the MDB. The Mann-Kendall and Sen's slope tests for all the catchments showed a decreasing trend in CTV for all western catchments (Figure 3.8, Table A.2). The largest Sen's slope was found in Lower Darling and Lower Murray, respectively -0.765 and -0.613. Further, the results showed an increasing trend in NS, particularly in the northern and southern catchments. In contrast, no trend has been observed in the central catchments of the MDB for NS. Moreover, except for the Border Rivers catchment, which showed a decreasing trend, no trend was observed in all other catchments for NTV areas. This may indicate that Mann-Kendall is not suitable when there are non-monotonic trends.

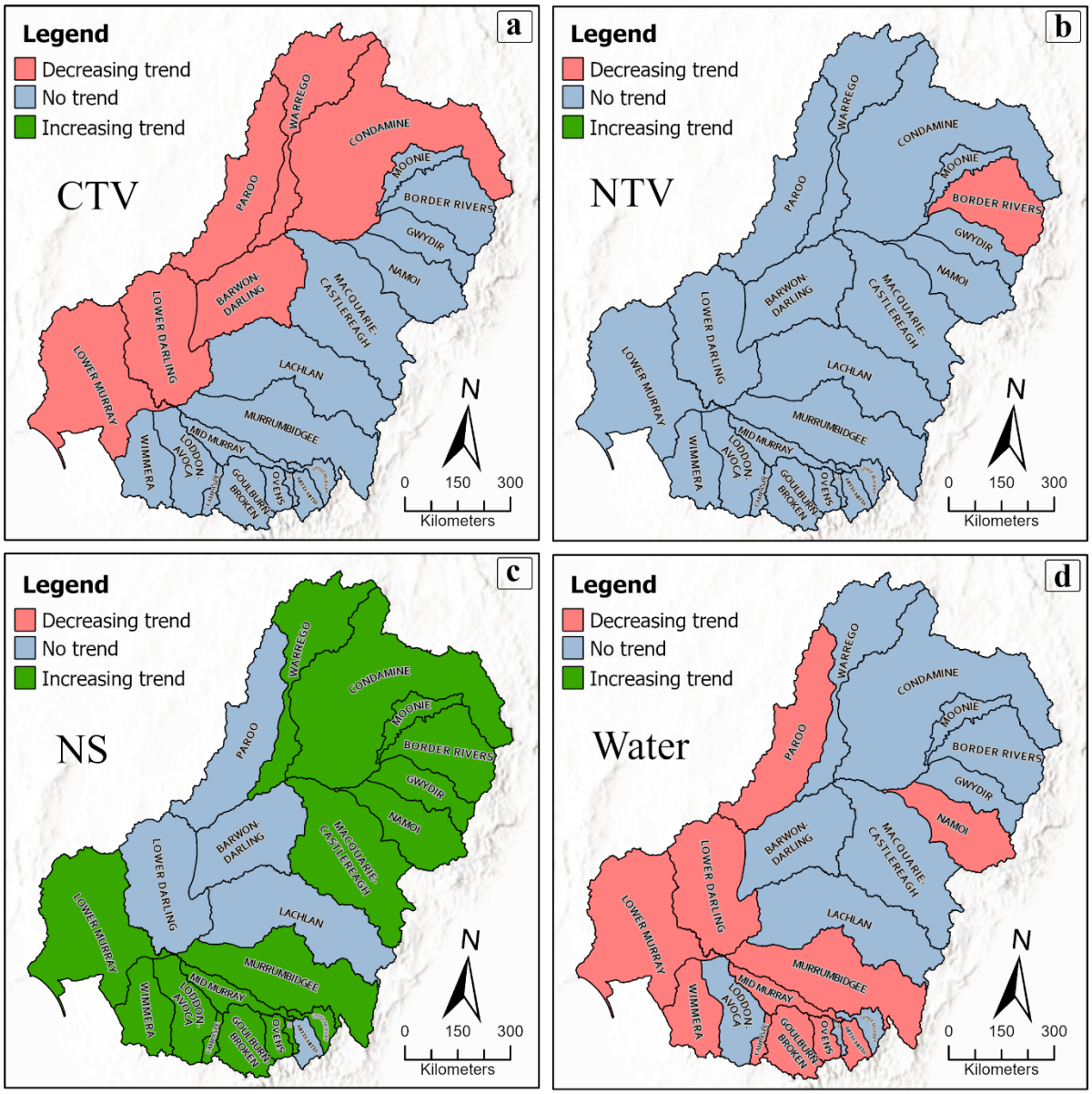

Figure 3.8: 1990-2020 trend analysis of land cover classes for all catchments. (a) NTV: Natural Terrestrial Vegetation, (b) CTV: Cultivated Terrestrial Vegetation, (c) NS: Natural Bare Surface, (d) Water.

3.4.3 Land use change over Murray-Darling Basin

3.4.3.1 Overall land use change

The land use data were used to investigate changes in agricultural areas across the MDB. The conservation and natural environment areas in the whole basin gradually increased from 7% in 1995 to a peak of 15% in 2010 before declining to 9% by 2020 (Figure 3.9). In contrast, in the first decade, production from relatively natural environments was under 20%, surged to 45% in 2005, after that maintaining levels above 26 to 35% towards the end of the period. The share of land utilised for dryland agriculture and plantations started at 75%, witnessed a

minimum of 41%, then recovered but failed to reach the initial decade's levels, stabilising below 60%.

Production from irrigated agriculture and plantations, represented in orange, exhibited significant fluctuations, starting below 2% before reaching a peak of 3% in 2020. Water resources followed a similar trend, remaining below 2% but spiking to 3% in 2010 and 2015, only to drop below 2% again by 2020. Intensive land uses stayed under 1% until it gradually increased, surpassing the 1% mark by 2010.

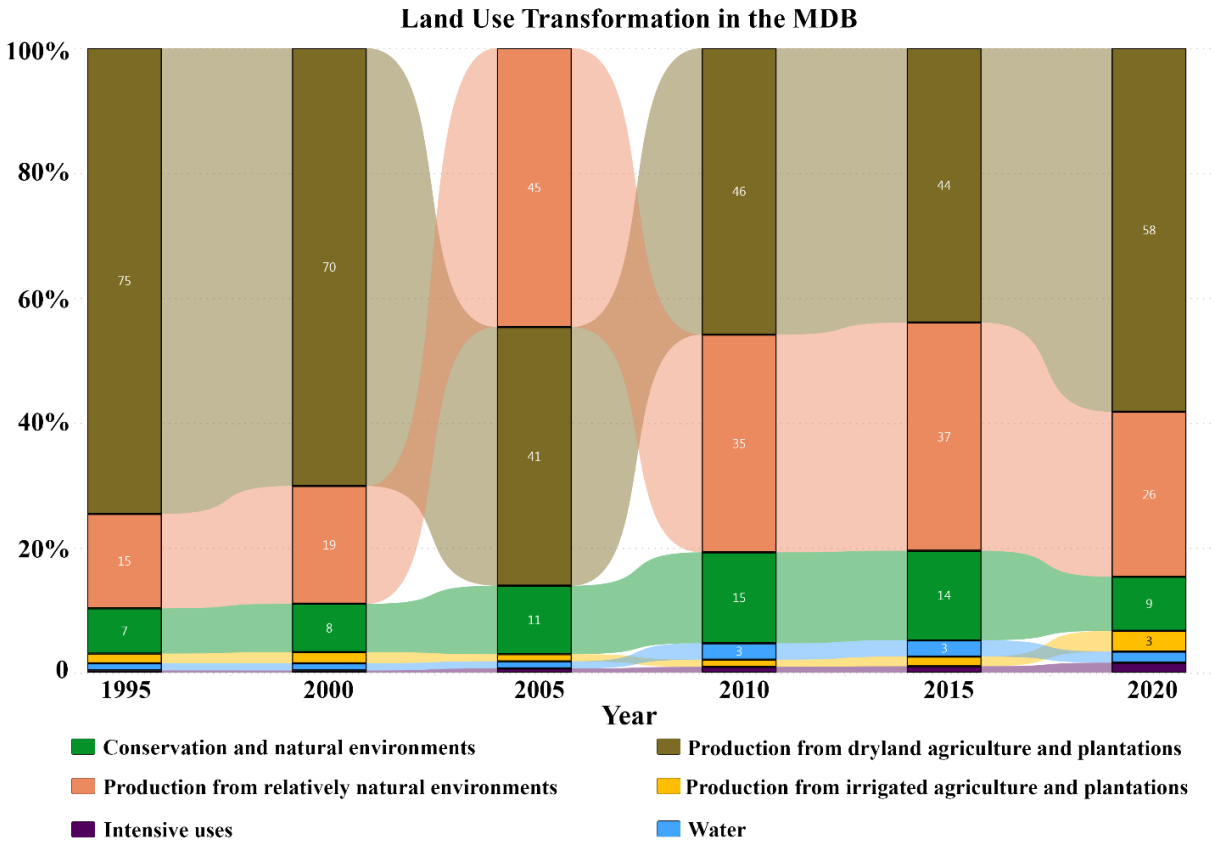

Figure 3.9: Temporal dynamics of land use in the Murray-Darling Basin: 1995-2020.

3.4.3.2 Water recovery over MDB Sustainable Diversion Limits (SDL) units

The Murray-Darling Basin Authority (MDBA) reports show a general upward trend in total water recovery for the environment across SDL units (Figure A.2). In the beginning, direct purchases of water entitlements were the main type of water recovery. However, over time, there is a noticeable shift towards off-farm and on-farm infrastructure efficiency investments as a way to recover water for the environment (Figure A.2). Water recovery volumes experienced a significant increase from the 2013-14 period onwards, reaching a plateau in 2019 and remaining at that level through 2023.

Looking at the total water recovery map (Figure 3.10), distinct regional patterns emerge when considering the Northern Basin and Southern Basin separately. Over 80% of recovery takes place in South Australian Murray, New South Wales Murray, Goulburn, Victorian Murray and Murrumbidgee. Analysing total water recovery normalised by SDL unit areas revealed that the Murrumbidgee, New South Wales Murray, Goulburn, Victorian Murray, South Australian Murray and Barwon-Darling Watercourse had higher recoveries, with respective figures of 5, 14, 19, 24, 60 mm, and the highest at 420 mm (Figure 3.10).

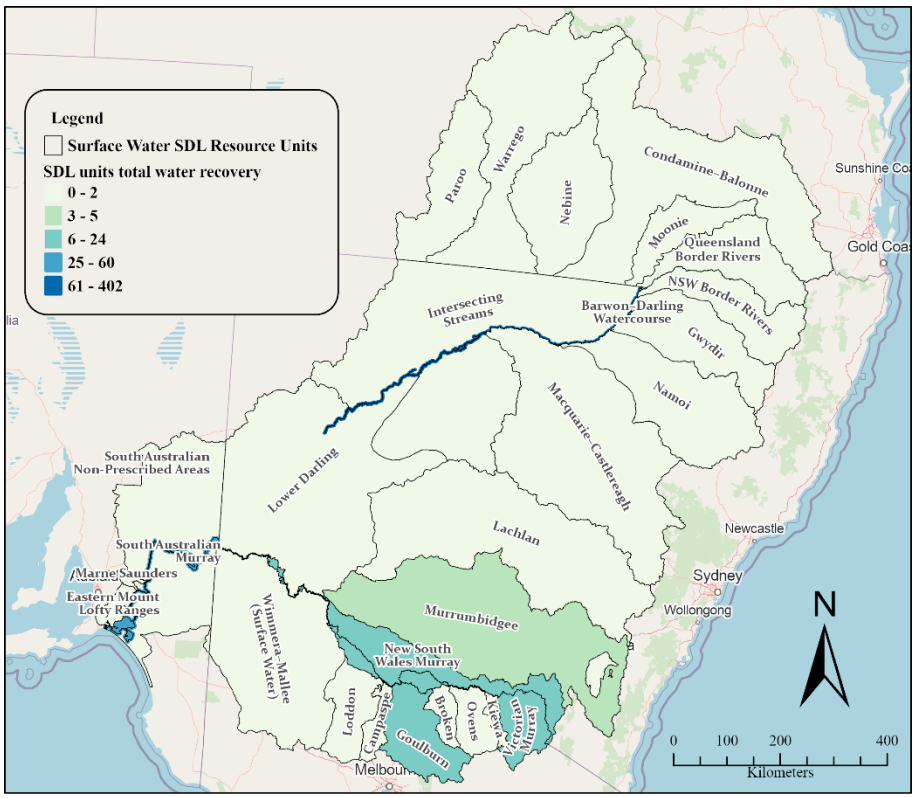

Figure 3.10: Total water recovery (mm) per unit area in surface water SDL Resource Units.

3.4.3.3 Land use change over SDL units with the highest water recovery

Over the examined period (1995-2020), there has been a discernible fluctuation in the total area dedicated to agriculture. Overall, the area under production for dryland agriculture and plantations has declined in most of the SDL catchments, especially after 2005 (Figure 3.11). On the other hand, the area of production from irrigated agriculture and plantations has increased in most SDL units with the highest water recovery levels. The increase in production rate from irrigated agriculture and plantations differed between SDLs' units.

The data on intensive land use also indicate a steady rise towards the end of the period studied, particularly in the Goulburn area, which increased from 1% in 1995 to 8% by 2020. Furthermore, the expansion of the water-covered regions is evident after 2010 in the majority of the SDL units with the highest water recovery.

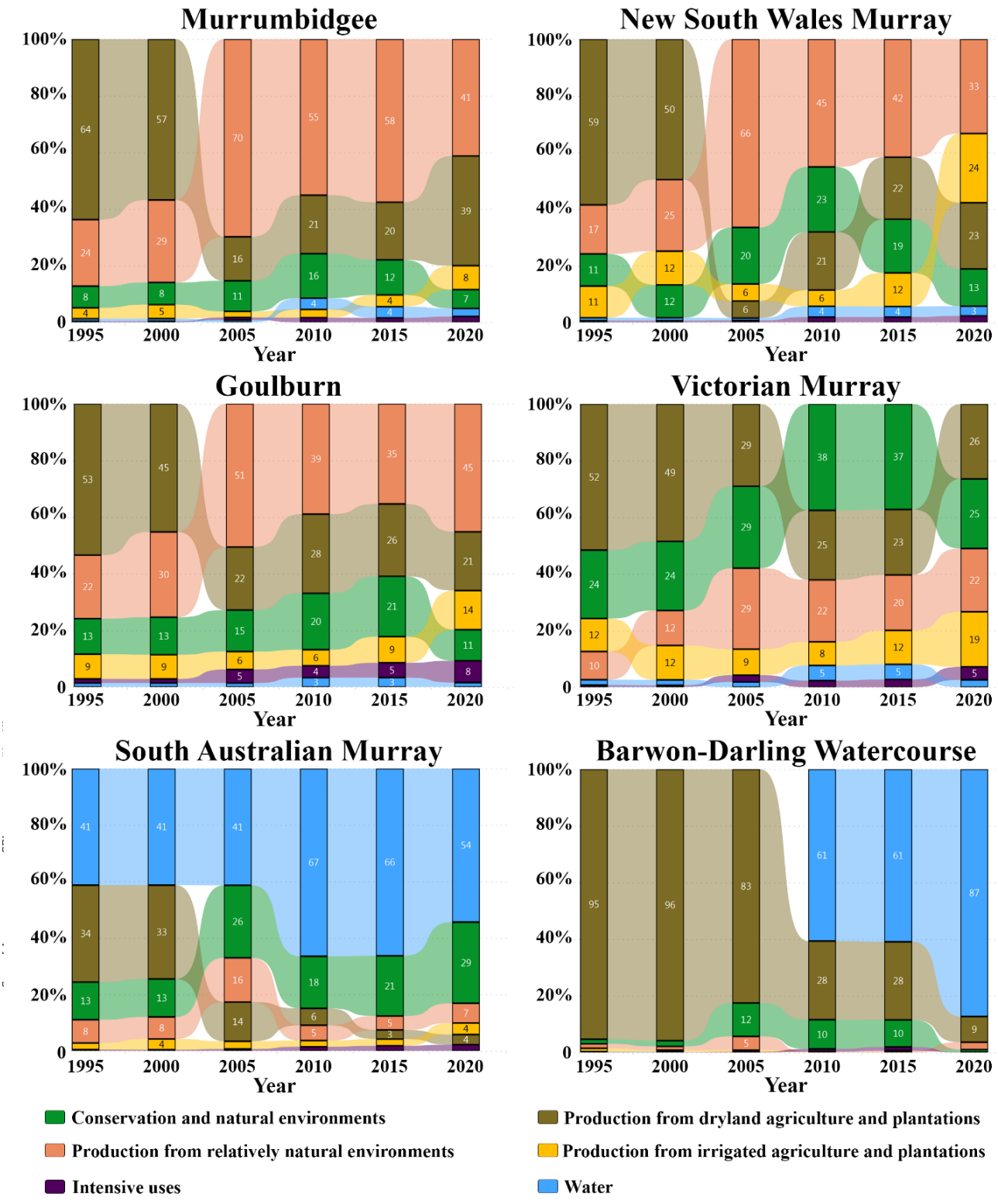

Figure 3.11: Comparative analysis of land use trends across regions with highest water recovery in the Murray-Darling Basin: 1995-2020.

3.5 Discussion

Land cover plays a vital role in shaping the hydrology of a catchment, exerting a significant influence on the overall water cycle (Gebremicael et al., 2019; Jose et al., 2021). Evaluating land cover dynamics is necessary for sustainable resource management and economic growth. This study analysed various aspects of land cover distribution and dynamics in the MDB, examining basin and catchment level statistics to understand the changes in land cover across the region. To achieve this, the DEA level 3 landcover dataset was used to get a general overview of the dominant land cover types and the overall distribution of land cover in the Basin. This top-down approach allowed us to understand the land cover patterns at both a broad and a detailed scale.

The extent of land cover change in the Murray-Darling Basin varied significantly among catchments, with some catchments displaying minimal year-to-year fluctuations and a higher percentage of unchanged land cover. This included Border Rivers, Upper Murray, Ovens and Kiewa. Since 1990, the western part of the Murray-Darling Basin has experienced a decreasing trend in Cultivated Terrestrial Vegetation (CTV). On the other hand, the Natural Bare Surface (NS) expanded in several catchments, particularly in the Lower Darling, Lower Murray, and Condamine catchments. (Semi-)Natural Terrestrial Vegetation (NTV) consistently dominated the land cover throughout the years, with its peaks corresponding to declines in NS and CTV. Additionally, there has been a decline in water areas across 11 catchments, with the most significant proportional decrease occurring in the Lachlan and Lower Darling catchments.

In the subsequent sections, we will examine the factors driving land cover change over time, focusing on the prevailing climate and policy conditions. However, we acknowledge that these are not the sole drivers. We will also summarise the environmental implications of the observed changes in specific land cover types.

3.5.1 Decadal land cover change

3.5.1.1 Land cover change 1990-2000

Climate shifts have played a significant role in rainfall after 1990. Between 1977 and 1990, persistent, blocking high-pressure systems in the south of Australia along longitude 140°E with a low to its north were observed, leading to high rainfall in the MDB (Callaghan, 2019). In 1990, the water land cover class was at its highest level in 31 years in the Basin, accounting for 1.49% of the total area. In contrast, in 1990, the percentage of NS, indicating areas with sparse or no vegetation cover, was at its lowest level, 1.71% of the Basin. Since the 1990s, climate change has decreased cool-season rainfall in the southern Murray-Darling Basin,

which has affected the Basin's agricultural region (Speer et al., 2021). Due to climate variability and changes in land cover management practices, irrigated agriculture in the Murray Darling Basin has experienced significant shifts (Grafton et al., 2014). Following a peak in 1991, the percentage of CTV experienced a decline and maintained values below 28% toward the end of 2000 (Figure 3.3). Particularly after the start of the millennium drought in 1997, it declined to 19% and remained at that level for several years. The decrease in cropland from 1990 to 2000 in the MDB is consistent with the results reported by (Yao et al., 2017).

3.5.1.2 Land cover change 2000-2010

Changes in climate patterns and droughts significantly impacted the land cover across the MDB between 2000 and 2010 (Speer et al., 2021). During the Millennium Drought, which lasted from 1997 to 2009, there were prolonged periods, specifically from 2001 to 2004 and 2004 to 2007, when there was no occurrence of La Niña or negative Indian Ocean Dipole event (King et al., 2020). The millennium drought caused stress to communities and ecosystems (Ashton et al., 2009; van Dijk et al., 2013). This is reflected in the percentage of water area in the whole Basin, ranging from 1.5% to 0.3%, with the lowest recorded in 2007 and the highest in 1990. Total storage did not recover until the unusually wet La Niña period in early 2010 (van Dijk et al., 2013). The water land cover class increased to more than 1% in 2010 after being below 0.7% of the Basin area for around seven years. It suggests that the Basin function required above-average rainfall conditions to be restored (McKernan, 2005).

Furthermore, the NS cover was more than 11% of the total area during the Millennium Drought except for the first two years. During the Millennium drought, distinct ecosystems within the Basin experienced harm due to high salinity levels in the water (MDBA, 2023b). In many cases, water was too saline to be used for drinking or watering animals and crops, resulting in reduced crop production and agricultural land abandonment (Alcantara et al., 2013). An increase in bare surfaces can also be linked to an increase in salinity, as long periods of high salinity may harm the natural environment, crops, and livestock (Warrence et al., 2002; Shrivastava & Kumar, 2015). On the other hand, the decrease in water supply led to lower crop yields, changes in the types of crops grown in the region, and a decline in some agricultural industries (Bryan & Marvanek, 2004). This may explain the reduction in CTV during these years, especially in the western part of the study area.

Between 2000 and 2010, Australia's population experienced a steady growth rate of around 16% over the decade (ABS, 2011). Population growth increased the demand for land to support housing, infrastructure, and economic activities (Avtar et al., 2019). From 2000 to 2010, the increase in AS accounted for less than 0.01% of the total Basin area. Although the

percentage of AS is small compared to other land cover classes, the need for food and other agricultural commodities can increase AS in the MDB, the agricultural hub of Australia (Pollino et al., 2021; Lane et al., 2023). In the eastern part of the study area, there was an increase in CTV toward the end of the decade, which is in line with Hu et al. (2020). Expansion of agricultural lands, including large-scale commercial agriculture, smallholder farming, and shifting cultivation, can lead to deforestation, conversion of natural habitats to croplands, and changes in land use patterns (Pendrill et al., 2022; Tao et al., 2023), which is evident from the dynamic of land cover classes CTV, NTV and NS during this period (Figure A.1).

3.5.1.3 Land cover change 2010-2021

Climate-driven natural disasters, such as bushfires, floods, and droughts, have significantly influenced land cover changes from 2010-2021. In 2010, negative phases of the Interdecadal Pacific Oscillation (IPO) and positive phases of the Southern Oscillation Index caused high rainfall (Callaghan, 2019). This led to significant flooding within the northern MDB, including in the Warrego, Paroo, Nebine, Moonie, Maranoa, Balonne, Condamine, Culgoa, and Weir Rivers (MDBA, 2010). These events were reflected by a significant increase in the water land cover class, which jumped from 0.3% in 2009 to 1% in 2010 and to a rise in NTV from 62% to 73% during the same period.

In 2016, widespread rainfall in the MDB was caused by a negative Indian Ocean Dipole event, whereby anomalously warm sea surface temperatures in the east Indian Ocean gave rise to dynamic and thermodynamic conditions (King et al., 2020). The winter of 2016 was particularly wet in southeast Australia and ranked the fourth wettest for the MDB since 1900, the start of the instrumental record (King et al., 2020). The observed increase in NTV and decrease in NS, as depicted in Figure 3.3, aligns with the impact of this phenomenon. These results were also supported by changes in land cover patterns observed in a small section of the study area near Lake Victoria in the western Riverina region of southwestern New South Wales (Figure 3.4).

After 2016, there were unusually dry conditions in the MDB, the most prolonged since 1900. Large swaths of Australia, particularly the MDB region of south-eastern Australia, were in drought from 2017-2020 (King et al., 2020). In 2019-2020, extensive bushfires burned large parts of forested and rural regions in southeast NSW and north-eastern Victoria (Biswas et al., 2021). Nearly one-third of the 15,000 km2 forested and rural areas of the Upper Murray catchment in south-east NSW and north-eastern Victoria were burnt during the 2019-2020 fire season (Joehnk et al., 2020). Bushfires had significant impacts on the land cover in the MDB, reflected in the percentage of NS and decrease in NTV. The highest percentage of NS was

observed in 2019 (30%), while NTV went under 60%. This is likely because 2018-20 was an arid year, and much land (CTV and NTV) would have been bare in 2020, also reflected in Water land cover (Figure 3.3a, b and Figure 3.6). Between 2010 and 2020, the expansion of artificial surfaces surged to 0.015% from less than 0.01% between 2000 and 2010.

3.5.2 Unveiling the dynamic nature of major land cover types

3.5.2.1 Natural terrestrial vegetation

The northern and southern parts of the MDB showed distinct spatial and temporal variations in the impact of land cover change. The cross-correlation analysis unveiled a correlation, without a time lag, between NTV and precipitation in the northern part of the Basin. However, in the southern part of the MDB, a one-year time lag was required for the correlation to reach significance (Table A.3). This could be due to the variability in rainfall seasonality within the MDB catchments (BOM, 2020). In the northern part, the rainfall tends to be more concentrated in the summer months (December to February) due to the influence of monsoonal systems (Gallant et al., 2012; BOM, 2020). Southern parts of the Basin typically experience a more evenly distributed rainfall throughout the year, with a peak in winter (June to August) due to the passage of cold fronts and mid-latitude weather systems (Murphy & Timbal, 2008; Speer et al., 2021). Further, the northern Basin is mainly flat, with few hills or mountain ranges. The water in the northern Basin moves slowly in wide, shallow rivers and evaporates more quickly, and there are fewer places to store large volumes of water (MDBA, 2023a). Additionally, the northern region of the MDB is typically hotter and drier than its southern counterpart. This can result in sparse vegetation, reducing the landscape's ability to retain water (Chen et al., 2021).

In most southern catchments, introducing a one-year lag reveals a persistent correlation between NTV and rainfall, with the correlation strength increasing in some catchments (Figure A.1). NTV typically shows a gradual decrease in vegetation cover in response to the depletion of terrestrial water storage (TWS) (Chen et al., 2021). Topographic differences help form natural reservoirs and channels that can hold and direct water, which may explain the increase in correlation between precipitation and NTV with a one-year lag.

The southern Basin receives higher levels of rainfall, which often results in vegetation being less reliant on precipitation (MDBA, 2023a), as the minimum water requirement is usually fulfilled. Precipitation was not the limiting factor for the occurrence of NTV in five catchments that received the highest amount of precipitation: the Goulburn-Broken, Kiewa, Upper Murray, Campaspe, Ovens and Mitta Mitta (Figure A.1). In these catchments, the correlation between NTV and precipitation was low.

3.5.2.2 Cultivated terrestrial vegetation

The CTV area comprised a lower percentage than NTV. The observed reduction in CTV during the millennium drought can be attributed directly to the decline in river inflows and consequent declines in reservoir storage and released volumes (van Dijk et al., 2013). Overall, the reduction in CTV and water areas and the increase in NS areas corroborated the results of the Mann-Kendall trend test. The decreasing CTV trend in the western part of the study area could be attributed to its mainly dryland agriculture. The drier interior regions of the MDB have low returns from agriculture per hectare (Bryan & Marvanek, 2004). Although the total volume of water used for irrigation drastically decreased during the Millennium drought, the value derived from each unit of water used increased significantly (Kirby et al., 2014). This is attributed to notable advancements in irrigation efficiency at the farm level and irrigation water supply systems (Kirby et al., 2012; Kirby et al., 2014), reflecting higher economic efficiency and a shift towards more valuable crops per unit of water used. Irrigated agriculture is widespread in the MDB, including the Murrumbidgee catchment, Murray Valley, and Goulburn Valley. In remote sensing imagery, cultivation practices often lead to highly dynamic spectral signals within and between years and regular transitions between vegetation and bare soil (Tissott & Mueller, 2022). This can be inferred from the standard deviation of the remote sensing-based estimated CTV in these areas. CTV's highest standard deviation over time was in the Goulburn-Broken, Mitta Mitta, and Upper Murray catchments (Table A.4), corresponding to high rainfall variation in those catchments (Table A.5). Dryland agriculture is common in this part of the Basin (van Dijk et al., 2009), and the response to the weather can be seen in the variability of CTV.

Greater diversity of land cover occurs in the southern part of the MDB, hosting the most profitable agricultural regions, including Goulburn (Vic) and the Murrumbidgee (NSW). In these areas, it is common for irrigated and/or high-value agricultural land uses to be adjacent to low-value land uses such as beef and sheep grazing and cereals (Bryan & Marvanek, 2004). The southern regions are also the most intensively farmed part of the MDB, making it particularly vulnerable to the impacts of climate change on agriculture and food production. These changes are anticipated to considerably impact fluctuations in surface runoff, evapotranspiration, groundwater recharge, and hence the water balance on both spatial and temporal scales (Lawrence & Vandecar, 2015; Cohn et al., 2019; Adhikari et al., 2020).

3.5.2.3 Natural bare surfaces

The increasing area of natural bare surfaces in the MDB has far-reaching implications for the environment, water quality, air quality, and agriculture. NS leaves the soil exposed and one of the major implications is the increased risk of erosion, as bare soils are more susceptible to erosion by wind and water. An increase in NS can significantly increase the risk of flooding,

as these surfaces reduce the land's ability to absorb and retain rainwater. Therefore, the loss of natural vegetation and soil, combined with an increase in impervious surfaces, can considerably impact the amount and timing of water entering rivers and streams, ultimately leading to an increased risk of flooding. The loss of vegetation cover can also disrupt the balance of the ecosystem, affecting wildlife habitat and biodiversity. The lower reaches of the MDB are a hotspot for freshwater biodiversity (Hammer et al., 2013); loss of vegetation cover associated with the observed increase in NS indicates increased stress on the region's ecosystems. There was a declining trend in water areas in 11 of the 22 catchments. Almost all are located in the western and southern parts of MDB. The findings align with other reports which attributed the below-average annual rainfall in the southern Basin to climate change (Hope, 2017; Speer et al., 2021; CSIRO & BOM, 2022). Previous studies have shown that the southeastern region of the Basin has been particularly affected by climate change (Pittock & Connell, 2010; Pittock & Finlayson, 2011). This is consistent with the results of rainfall trend analysis, which reveal a declining trend in four catchments situated in the southeast part of the MDB - Upper Murray, Ovens, Mitta Mitta, and Goulburn-Broken and also for the Namoi catchment, which is located in the eastern part of the Basin (Table A.6).

3.5.3 Impact of water management policies on land use dynamics in the MDB

While land cover data, especially CTV, has proven effective in delineating the general extent of cultivated areas, its utility is constrained when it comes to pinpointing specific land use traits, such as areas under irrigation. Even at Level 4, DEA land cover data elaborates on cover density but falls short of offering granular insights into irrigation practices. Therefore, land use data was used to discuss the impact of policy. From 1995 to 2020, the MDB experienced significant land use changes, heavily influenced by climatic events such as the millennium drought and subsequent periods of substantial rainfall. Moreover, policy interventions have also played a crucial role in land use transitions by influencing the allocation and management of resources and offering incentives or subsidies for sustainable practices.

During the Millennium Drought, the increased demand for scarce water supplies for agriculture, urban, industrial, and environmental uses shifted the national policy focus toward more sustainable management of Australia's water resources (Ashton et al., 2009). The impact of drought became evident during the middle of the drought in 2005, marked by significant land use changes, particularly a notable decline in dryland agriculture and plantations. The National Water Initiative (2004) and Water Act (2007) focused on balancing the needs of different stakeholders and reforming the water agenda to address issues related to water management, allocation and sustainability (Connell & Grafton, 2011; Garrick et al., 2012; Dyson, 2021; Kirsch et al., 2021).

Since 2010, the MDB has experienced a remarkable environmental shift, largely due to substantial rainfall that dramatically reversed previous dry conditions (MDBA, 2010; Callaghan, 2019). This shift was evidenced by a rapid increase in water storage levels, rising from 26% at the beginning of 2010 to 80% by early 2011 (Wei et al., 2011). Concurrently, significant policy reforms were implemented, focusing on sustainable water management (Hart, 2016; MDBA, 2018). These reforms encompassed both financial allocations for improving irrigation efficiency and the implementation of the Basin Plan in 2012, which introduced Sustainable Diversion Limits (SDL) to enhance water management and mitigate over-allocation and environmental degradation in the MDB (Crossman et al., 2010; Wheeler et al., 2013). Consequently, these measures necessitated a reduction in water allocations for irrigated agriculture. Additionally, subsidies were provided for developing more efficient agricultural infrastructure, enabling farmers to utilise water resources more effectively.

Theoretically, improvements in irrigation efficiency, infrastructure, and agricultural policies promoting water-saving technologies were expected to enable the expansion of irrigated land while reducing water use (Wei et al., 2011). However, the practical effectiveness of these measures in terms of return flows and increased stream flows remains debatable (Grafton & Wheeler, 2018). Over recent decades, MDB irrigators have extensively upgraded their systems with private and government subsidies to boost agricultural productivity and environmental outcomes (Meyer, 2005; Crossman et al., 2010; Wheeler et al., 2013; DAWR, 2019a). Nevertheless, research indicates that these subsidies have inadvertently increased water extractions, altered crop patterns, and intensified on-farm water use (Steinfield & Kingsford, 2013; Slattery et al., 2019). Additional concerns include the construction of new private dams, funded by subsidies, which capture overland flows and potentially increase water extractions beyond the Cap limits (Slattery et al., 2019). The cost-effectiveness of subsidising irrigation infrastructure versus buying direct water entitlements is contentious. Although the former is more costly, its actual impact on water savings and environmental outcomes has been questioned, sometimes leading to expanded irrigated areas or shifts to more water-intensive crops (Grafton & Wheeler, 2018; Wheeler et al., 2020; Wheeler, 2022). These issues highlight the critical need to reassess the effectiveness of these financial outlays in achieving their intended environmental benefits compared to the reported water savings (Grafton & Williams, 2019).

The SDL units that have achieved the greatest levels of water recovery are located along the main channel of the Murray River and its significant tributaries within the MDB, more particularly, the four units, Murrumbidgee, New South Wales Murray, Goulburn and Victorian Murray, which are all located in the southeast of the MDB. Detailed analysis of individual units

reveals unique patterns of land use change, each reflecting local environmental, economic, and policy influences. For example, in Goulburn and Victorian Murray, agricultural productivity is a major economic driver known for its dairy and crop production. In Goulburn, there is a decrease in 'Production from dryland agriculture and plantation' and an increase in 'Production from irrigated agriculture and plantations', which could indicate the adoption of more water-efficient but intensive farming practices, possibly reflecting a rebound effect. The rebound effect on water use occurs when the increase in water demand from improved water productivity surpasses the technical efficiency savings, leading to higher water extractions (Wheeler et al., 2020). The Victorian Murray unit shows a general increase in 'Conservation and natural environments' with a simultaneous decline in 'Production from dryland agriculture and plantations' while the water shows the highest percentage in 2010 and 2015; at the same time, irrigated agriculture increased.

The volume of water that farmers buy, or sell is influenced by rainfall, water allocations, and storage, which in turn impacts agricultural practices. There has been a significant shift towards market-based water management in the region. The establishment of water trading mechanisms allows for the reallocation of water towards higher-value uses, which may explain the shift away from traditional dryland agriculture towards more water-efficient agricultural practices and conservation efforts. For example, at low water allocation prices, dairy farmers typically use their own water allocations to grow pasture. However, as prices increase (above AUD$220/ML), it becomes more profitable for them to purchase supplemental feed or 'dry out' their cows and sell their available water (Grafton et al., 2016). This suggests a transformation that might be associated with changes in water policy and agricultural strategies (Grafton et al., 2014).

Although the irrigated area experienced reductions during dry years, data, particularly from after 2010, indicate an increase in irrigated lands. This trend may highlight a sustained shift towards more perennial types of land use, suggesting a long-term adaptation to the availability of subsidies and the economic benefits associated with perennial crops. Adamson and Loch (2014) noted that subsidies led to an expansion of the area under irrigated cultivation and prompted a shift towards more perennial planting. These subsidies facilitated the adoption of perennial plants such as trees, vines, nuts, and stone fruits, requiring significant initial investments and long-term commitments due to their consistent water needs (Grafton et al., 2016). However, these crops also have lower water requirements and yield higher net returns (Grafton et al., 2016).

Our research indicated an increase rather than a decrease in intensive uses and production from irrigated agriculture and plantations across several SDL units, alongside a reduction of

conservation and natural environments. This pattern confirms the rebound effect, where efforts to enhance irrigation efficiency and promote water recovery are not translating into the anticipated environmental benefits. Indeed, despite substantial governmental incentives aimed at boosting irrigation efficiency, these improvements have paradoxically led to increased water extractions, particularly under conditions of water scarcity, minimal idle capacity, subsidised irrigation infrastructure, and low water and energy costs (Grafton et al., 2018; Ward & Pulido-Velazquez., 2008; Loch & Adamson, 2015; Wheeler et al., 2020). The subsidies encouraged expanding irrigated areas and using diverse water sources, raising concerns about the actual environmental benefits versus the reported water savings.

The coincidence of heavy rain events in 2010 and 2016 could have impacted both water availability and recovery. While superficially suggesting successful water recovery, this increase may reflect the coincidental interplay between favourable climate conditions and water policy implementations, making it difficult to distinguish the true drivers (ABARES, 2020). The temporal delay in observable changes in land cover post-policy implementation, coupled with the complexities of climate variability, land management practices, and socio-economic dynamics, complicates the accurate assessment of policy impacts.

3.6 Conclusion and future insights

This study provides a detailed analysis of land cover and land use changes in the Murray Darling Basin (MDB), examining annual land cover data from 1990 to 2020 and land use data at five-year intervals from 1995 to 2020. The land cover changes were investigated across 22 MDB catchments using the Geoscience Australia level 3 land cover dataset, while land use changes were assessed across Sustainable Diversion Limit (SDL) units based on ABARES data. Significant findings include an increase in natural bare surfaces and a decrease in water bodies, alongside shifts in agricultural land use driven by water recovery initiatives and infrastructure developments.

Various factors, including climate variability, agricultural expansion, changes in water management, and natural disasters influenced land cover changes across catchments. Their distribution and magnitude varied due to regional and local factors like topography, climate, and land management practices.

The cross-correlation analysis identified a direct correlation between (Semi-)Natural Terrestrial Vegetation (NTV) and precipitation in the northern Basin, while a one-year lag is necessary to observe a significant correlation in the southern part of the MDB. This highlights the varied influence of environmental drivers throughout the basin. Climate change is

anticipated to impact the northern and southern regions of the MDB differently. Although the southern region will experience effects from climate change, these are expected to be less severe due to the region's higher rainfall and greater water availability compared to the north.

Trend analysis results indicated a decrease in Cultivated Terrestrial Vegetation (CTV) in MDB's western region and an increase in Natural Bare Surface (NS) across majority of catchments. The increasing stress on the ecosystem due to the rise in NS points towards a greater risk of erosion and potential impacts on water and air quality. Reducing CTV areas risks the local economy and food security; thus, promoting sustainable farming and investing in climate-resilient crops is essential in the dryer part of the MDB. The evaluation of land use changes in the Murray-Darling Basin indicates a notable expansion of irrigated and intensively used areas, particularly in SDL units with significant water recovery. Initiatives such as the Water Act and the Basin Plan were originally introduced to reallocate water from consumptive uses back to the environment. Measures aimed at increasing irrigation efficiency and implementing water buybacks were intended as practical means to achieve these environmental recovery targets. However, outcomes have frequently deviated from expectations, leading to increased irrigation rather than containment. Evidence from previous research and our study suggests a rebound effect, where enhancements in water efficiency paradoxically expand agricultural land use (Loch & Adamson, 2015; Wheeler et al., 2020).

In formulating policies, special attention should be given to the management of irrigated land cover, recognising its significance in altering hydrology and addressing associated risks such as increased recharge, nutrient leaching, elevated water tables, waterlogging, and soil salinisation (Stewardson et al., 2021; Beavis et al., 2023; Lane et al., 2023). While acknowledging the positive impacts of water efficiency measures, policy development should consider broader implications and complexities, including regional variations, technological limitations, behavioural factors, rebound effects, and complex interactions. Policy and technical complacency and reliance on inadequate data have hampered informed water management and policy decisions in the MDB (Wheeler & Garrick, 2020). Rebound effects resulting from efficiency improvements must be mitigated to prevent unsustainable water practices (Wheeler et al., 2020). Improved monitoring through the use of satellite imagery, metered data, and standardised data collection is an aspect to ensure effective and sustainable land cover and land use management (Turner et al., 2019).

The Digital Earth Australia (DEA) platform's LCCS Level 3 data provides insights into the land cover changes across the MDB. On the other hand, national land use data offers broader details at a lower resolution, proving invaluable for monitoring agricultural changes and assessing the impact of policies on a large scale. The findings from this research indicate that

high-level national land use and land cover data are useful for understanding overall trends and climatic impacts, prioritising conservation efforts, and making informed land-use decisions. Continued monitoring and research are crucial for a deeper understanding of the long-term effects of the Basin Plan on land cover and ecosystem health within the MDB.

Under the existing cap, irrigators may acquire additional water from others, leveraging efficiency gains and water harvesting practices to intensify land and water use. Such infrastructure can intercept flows that would otherwise enter river systems, effectively redistributing water availability and enabling new or expanded irrigation enterprises without exceeding the overall 1995 diversion limit. Although this does not increase the total volume of water diverted, it can lead to localised intensifications in production, thereby introducing complexity and unintended outcomes to environmental water recovery efforts. The challenge lies in achieving sustainable agricultural expansion while acknowledging that improvements in water-use efficiency and related infrastructure can reshape water allocation patterns. These highlight the importance of strategies that consider market dynamics, infrastructural influences, and socio-economic behaviours to safeguard environmental objectives.

Uncertainty in datasets, such as difficulties in distinguishing spectrally similar land use and land cover or temporal inconsistencies, could result in errors in identifying specific land use and land cover patterns. This might lead to over- or underestimation of key land use and land cover changes, affecting conclusions about regional development, conservation priorities, or policies. Future research should focus on refining the spatial and temporal resolution of land cover and land use data to capture their changes. Additionally, applying advanced remote sensing methods and machine learning algorithms is crucial for identifying land use and land cover transitions and minimising classification errors.

3.7 References

ABARES. (2020). ABARES Insights: Analysis of water recovery in the Murray-Darling Basin. https://www.agriculture.gov.au/abares/products/insights/economic-effects-of-water-recovery-in-murray-darling-basin#effects-of-different-drivers-can-be-complex-and-difficult-to-observe, (Accessed 09 July 2024).

ABARES. (2021). Catchment scale land use of Australia – update December 2020, Australian Bureau of Agricultural and Resource Economics and Sciences, Canberra, February, CC BY 4.0. https://doi.org/10.25814/aqjw-rq15

ABARES. (2022). Land use of Australia 2010–11 to 2015–16, 250 m, Australian Bureau of Agricultural and Resource Economics and Sciences, Canberra, September, CC BY 4.0. https://doi.org/10.25814/7ygw-4d64.

ABS. (2011). 1370.0.55.001 - Measures of Australia's progress: summary indicators. https://www.abs.gov.au/ausstats/abs@.nsf/Lookup/by%20Subject/1370.0.55.001~2011~Main%20Features~Population~3, (Accessed 09 July 2024).

ABS. (2008). Water and the Murray Darling Basin: A statistical profile (Chapter 5: Natural resource management in the Murray-Darling). Canberra, ACT: Australian Bureau of Statistics, 115–125.

ABS. (2012). Measures of Australia's Progress: Summary indicators, 2012. Catalogue Number 1370.0.55.001. http://www.abs.gov.au/ausstats/abs@.nsf/Lookup/by Subject/1370.0.55.001~2012~Main Features~Productivity~20

Adamson, D., & Loch, A. (2014). Possible negative feedbacks from "gold-plating" irrigation infrastructure. Agricultural Water Management, 145, 134–144. https://doi.org/10.1016/j.agwat.2013.09.022

Adhikari, R. K., Mohanasundaram, S., & Shrestha, S. (2020). Impacts of land-use changes on the groundwater recharge in the Ho Chi Minh city, Vietnam. Environmental Research, 185, 109440. https://doi.org/10.1016/j.envres.2020.109440

Alcantara, C., Kuemmerle, T., Baumann, M., Bragina, E. V., Griffiths, P., Hostert, P., Knorn, J., Müller, D., Prishchepov, A. V., Schierhorn, F., Sieber, A., & Radeloff, V. C. (2013). Mapping the extent of abandoned farmland in Central and Eastern Europe using MODIS time series satellite data. Environmental Research Letters, 8(3), 35035. https://doi.org/10.1088/1748-9326/8/3/035035

Alexandra, J. (2018). Evolving governance and contested water reforms in Australia's Murray Darling Basin. Water (Switzerland), 10(2), 113. https://doi.org/10.3390/w10020113

Ashton, D., Oliver, M., Hooper, S., Mackinnon, D., & Mallawaarachchi, T. (2009). Irrigated agriculture in the Murray-Darling Basin: A farm level analysis by region and industry. Issues Insights 09.4, 14. http://www.abare.gov.au/publications_html/ins/insights_09/a4.pdf

Avtar, R., Tripathi, S., Aggarwal, A. K., & Kumar, P. (2019). Population-urbanization-energy nexus: A review. Resources, 8(3), 136. https://doi.org/10.3390/resources8030136

Beavis, S. G., Wong, V. N. L., Mosley, L. M., Baldwin, D. S., Latimer, J. O., Lane, P., & Lal, A. (2023). Water quality risks in the Murray-Darling basin. Australian Journal of Water Resources, 27(1), 85–102. https://doi.org/10.1080/13241583.2022.2163475

Biswas, T. K., Karim, F., Kumar, A., Wilkinson, S., Guerschman, J., Rees, G., McInerney, P., Zampatti, B., Sullivan, A., Nyman, P., Sheridan, G. J., & Joehnk, K. (2021). 2019–2020 Bushfire impacts on sediment and contaminant transport following rainfall in the Upper Murray River catchment. Integrated Environmental Assessment and Management, 17(6), 1203–1214. https://doi.org/10.1002/ieam.4492

BOM. (2020). Trends and historical conditions in the Murray-Darling Basin. https://www.mdba.gov.au/sites/default/files/pubs/bp-eval-2020-BOM-trends-and-historical-conditions-report.pdf

Bontemps, S., Defourny, P., Radoux, J., Van Bogaert, E., Lamarche, C., Achard, F., Mayaux P., Boettcher, M., Brockmann, C., Kirches, G., Zülkhe, M., Kalogirou, V., Seifert, F.M., Arino, O., 2013. Consistent global land cover maps for climate modelling communities:

Current achievements of the ESA's land cover CCI. Proceedings of the ESA Living Planet Symposium, Edinburgh, pp. 9-13.
Bossard, M., Feranec, J., & Otahel, J. (2000). CORINE land cover technical guide – Addendum 2000 part I state-of-play production methods of the CORINE land cover database (Vol. 40). European Environment Agency Copenhagen.
Bryan, B. A., Barry, S., & Marvanek, S. (2009). Agricultural commodity mapping for land use change assessment and environmental management: An application in the Murray-Darling Basin, Australia. Journal of Land Use Science, 4(3), 131–155. https://doi.org/10.1080/17474230802618722
Bryan, B.A., & Marvanek, S. 2004). Quantifying and valuing land use change for integrated catchment management evaluation in the Murray-Darling Basin 1996/97-2000/01: stage 2 report to the Murray-Darling Basin commission. CSIRO Land and Water, Australia. http://www.clw.csiro.au/publications/consultancy/2004/MDBC_stage2_report.pdf
Cai, W., & Cowan, T. (2008). Dynamics of late autumn rainfall reduction over southeastern Australia. Geophysical Research Letters, 35(9). https://doi.org/10.1029/2008GL033727
Calderón-Loor, M., Hadjikakou, M., & Bryan, B. A. (2021). High-resolution wall-to-wall land-cover mapping and land change assessment for Australia from 1985 to 2015. Remote Sensing of Environment, 252. https://doi.org/10.1016/j.rse.2020.112148
Callaghan, J. (2019). A comparison of weather systems in 1870 and 1956 leading to extreme floods in the Murray–Darling Basin. Journal of Southern Hemisphere Earth Systems Science, 69(1), 84. https://doi.org/10.1071/ES19003
Camilleri, S., Thomson, J. R., & Mac Nally, R. (2010). The interaction between land use and catchment physiognomy: understanding avifaunal patterns of the Murray–Darling Basin, Australia. Journal of Biogeography, 37(2), 293–304. https://doi.org/10.1111/j.1365-2699.2009.02212.x
Castillo, C. R., Güneralp, I., & Güneralp, B. (2014). Influence of changes in developed land and precipitation on hydrology of a coastal Texas watershed. Applied Geography, 47, 154–167. https://doi.org/10.1016/j.apgeog.2013.12.009
Chen, A., Guan, H., & Batelaan, O. (2021). Seesaw terrestrial wetting and drying between eastern and western Australia. Earth's Future, 9(5). https://doi.org/10.1029/2020EF001893
Cohn, A. S., Bhattarai, N., Campolo, J., Crompton, O., Dralle, D., Duncan, J., & Thompson, S. (2019). Forest loss in Brazil increases maximum temperatures within 50 km. Environmental Research Letters, 14(8). https://doi.org/10.1088/1748-9326/ab31fb
Connell, D., & Grafton, R. Q. (2011). Water reform in the Murray-Darling Basin. Water Resources Research, 47(4). https://doi.org/10.1029/2010WR009820
Crossman, N. D., Connor, J. D., Bryan, B. A., Summers, D. M., & Ginnivan, J. (2010). Reconfiguring an irrigation landscape to improve provision of ecosystem services. Ecological Economics, 69(5), 1031–1042. https://doi.org/10.1016/j.ecolecon.2009.11.020
CSIRO, BOM, 2022. State of Climate 2022. http://www.bom.gov.au/state-of-the-climate/, (Accessed 09 July 2024).
Dile, Y. T., Tekleab, S., Kaba, E. A., Gebrehiwot, S. G., Worqlul, A. W., Bayabil, H. K., Yimam, Y. T., Tilahun, S. A., Daggupati, P., Karlberg, L., & Srinivasan, R. (2018). Advances in water resources research in the Upper Blue Nile basin and the way forward: A review. Journal of Hydrology, 560, 407–423. https://doi.org/10.1016/j.jhydrol.2018.03.042
Dong, M., Bryan, B. A., Connor, J. D., Nolan, M., & Gao, L. (2015). Land use mapping error introduces strongly-localised, scale-dependent uncertainty into land use and ecosystem services modelling. Ecosystem Services, 15, 63–74. https://doi.org/10.1016/j.ecoser.2015.07.006
Dyson, M. (2020). Current water resources policy and planning in the Murray–Darling Basin. In Murray-Darling Basin, Australia: Its future management (pp. 163–184). Elsevier. https://doi.org/10.1016/B978-0-12-818152-2.00008-5

ESRI. (2023). ArcGIS Pro: Release 3.1.3. Redlands, CA: Environmental Systems Research Institute. In ArcGIS Pro: Release 3.1.3. Redlands, CA: Environmental Systems Research Institute.

Fu, G., Rojas, R., & Gonzalez, D. (2022). Trends in groundwater levels in alluvial aquifers of the Murray–Darling Basin and their attributions. Water (Switzerland), 14(11), 1808. https://doi.org/10.3390/w14111808

Gallant, A. J. E., Kiem, A. S., Verdon-Kidd, D. C., Stone, R. C., & Karoly, D. J. (2012). Understanding hydroclimate processes in the Murray-Darling Basin for natural resources management. Hydrology and Earth System Sciences, 16(7), 2049–2068. https://doi.org/10.5194/hess-16-2049-2012

Garrick, D., Bark, R., Connor, J., & Banerjee, O. (2012). Environmental water governance in federal rivers: Opportunities and limits for subsidiarity in Australia's Murray-Darling River. Water Policy, 14(6), 915–936. https://doi.org/10.2166/wp.2012.120

Gebremicael, T. G., Mohamed, Y. A., & Van der Zaag, P. (2019). Attributing the hydrological impact of different land use types and their long-term dynamics through combining parsimonious hydrological modelling, alteration analysis and PLSR analysis. Science of the Total Environment, 660, 1155–1167. https://doi.org/10.1016/j.scitotenv.2019.01.085

Gonzalez, D., Dillon, P., Page, D., & Vanderzalm, J. (2020). The potential for water banking in Australia's Murray–darling basin to increase drought resilience. Water (Switzerland), 12(10), 1–24. https://doi.org/10.3390/w12102936

Gorelick, N., Hancher, M., Dixon, M., Ilyushchenko, S., Thau, D., & Moore, R. (2017). Google Earth Engine: Planetary-scale geospatial analysis for everyone. Remote Sensing of Environment, 202, 18–27. https://doi.org/10.1016/j.rse.2017.06.031

Grafton, R. Q., & Wheeler, S. A. (2018). Economics of water recovery in the Murray-Darling Basin, Australia. Annual Review of Resource Economics, 10, 487–510. https://doi.org/10.1146/annurev-resource-100517-023039

Grafton, R. Q., Pittock, J., Williams, J., Jiang, Q., Possingham, H., & Quiggin, J. (2014). Water planning and hydro-climatic change in the Murray-Darling Basin, Australia. Ambio, 43(8), 1082–1092. https://doi.org/10.1007/s13280-014-0495-x

Grafton, R. Q., Williams, J., Perry, C. J., Molle, F., Ringler, C., Steduto, P., Udall, B., Wheeler, S. A., Wang, Y., Garrick, D., & Allen, R. G. (2018). The paradox of irrigation efficiency. Science, 361(6404), 748–750. https://doi.org/10.1126/science.aat9314

Grafton, R.Q., Horne, J., & Wheeler, S.A. (2016). On the marketisation of water: evidence from the Murray-Darling Basin, Australia. Water Resour. Manag. 30, 913–926. https://doi.org/10.1007/s11269-015-1199-0.

Gregrio, A., & Jansen, J. (2000). Land cover classification system (LCCS); classification concepts and user manual for software version 2. https://www.fao.org/4/y7220e/y7220e00.htm, (Accessed 09 July 2024).

Hammer, M. P., Bice, C. M., Hall, A., Frears, A., Watt, A., Whiterod, N. S., Beheregaray, L. B., Harris, J. O., & Zampatti, B. P. (2013). Freshwater fish conservation in the face of critical water shortages in the southern Murray-Darling Basin, Australia. Marine and Freshwater Research, 64(9), 807–821. https://doi.org/10.1071/MF12258

Hansen, M.C., Defries, R.S., Townshend, J.R.G., & Sohlberg, R. (2000). Global land cover classification at 1 km spatial resolution using a classification tree approach. International Journal of Remote Sensing, 21(6–7), 1331–1364. https://doi.org/10.1080/014311600210209

Hart, B. T. (2016). The Australian Murray–Darling Basin Plan: challenges in its implementation (part 1). International Journal of Water Resources Development, 32(6), 819–834. https://doi.org/10.1080/07900627.2015.1083847

Hart, B., Walker, G., Katupitiya, A., & Doolan, J. (2020). Salinity management in the Murray-Darling Basin, Australia. Water (Switzerland), 12(6), 1829. https://doi.org/10.3390/w12061829

Hasegawa, T., Fujimori, S., Ito, A., Takahashi, K., & Masui, T. (2017). Global land-use allocation model linked to an integrated assessment model. Science of the Total Environment, 580, 787–796. https://doi.org/10.1016/j.scitotenv.2016.12.025

Holland, J. E., Luck, G. W., & Max Finlayson, C. (2015). Threats to food production and water quality in the Murray-Darling Basin of Australia. Ecosystem Services, 12, 55–70. https://doi.org/10.1016/j.ecoser.2015.02.008

Hope, P., Timbal, B., Hendon, H., Ekström, M., & Potter, N. (2017). A synthesis of findings from the Victorian Climate Initiative (VicCI). Bureau of Meteorology, 56pp, Australia. http://www.bom.gov.au/research/projects/vicci/, (Accessed 09 July 2024).

Hoskins, A. J., Bush, A., Gilmore, J., Harwood, T., Hudson, L. N., Ware, C., Williams, K. J., & Ferrier, S. (2016). Downscaling land-use data to provide global 30" estimates of five land-use classes. Ecology and Evolution, 6(9), 3040–3055. https://doi.org/10.1002/ece3.2104

Hu, Q., Xiang, M., Chen, D., Zhou, J., Wu, W., & Song, Q. (2020). Global cropland intensification surpassed expansion between 2000 and 2010: A spatio-temporal analysis based on GlobeLand30. Science of the Total Environment, 746, 141035. https://doi.org/10.1016/j.scitotenv.2020.141035

Joehnk, K., Biswas, T., Karim, F., Kumar, A., Guerschman, J., Wilkinson, S., Rees, G., McInerney, P., Zampatti, B., Sullivan, A., Nyman, P., & Tk, B. (2020). Water quality responses and mitigation options for post 2019-20 bushfires floods in south eastern Australia – a catchment scale analysis. A technical report for the csiro strategic bushfire project 2020. CSIRO Report No. 2020/EP206475. Canberra, Australia: CSIRO.

Jose, D. M., Makhdumi, W., & Dwarakish, G. S. (2021). Hydrological modelling to study the impacts of climate and LULC change at basin scale: A review. In R. Jha, V. P. Singh, V. Singh, L. B. Roy, & R. Thendiyath (Eds.), Water resources management and reservoir operation : Hydraulics, water resources and coastal engineering (pp. 13–26). Springer International Publishing. https://doi.org/10.1007/978-3-030-79400-2_2

King, A. D., Pitman, A. J., Henley, B. J., Ukkola, A. M., & Brown, J. R. (2020). The role of climate variability in Australian drought. Nature Climate Change, 10(3), 177–179. https://doi.org/10.1038/s41558-020-0718-z

Kirby, M., Bark, R., Connor, J., Qureshi, M. E., & Keyworth, S. (2012). The economic impact of water reductions during the Millennium Drought in the Murray-Darling Basin. In *Proceedings of the AARES Conference* (March 2016). https://doi.org/10.22004/ag.econ.124490

Kirby, M., Bark, R., Connor, J., Qureshi, M. E., & Keyworth, S. (2014). Sustainable irrigation: How did irrigated agriculture in Australia's Murray-Darling Basin adapt in the Millennium Drought? Agricultural Water Management, 145, 154–162. https://doi.org/10.1016/j.agwat.2014.02.013

Kirsch, E., Colloff, M. J., & Pittock, J. (2021). Lacking character? A policy analysis of environmental watering of Ramsar wetlands in the Murray-Darling Basin, Australia. Marine and Freshwater Research, 73(10), 1225–1240. https://doi.org/10.1071/MF21036

Klotz, M., Kemper, T., Geiß, C., Esch, T., & Taubenböck, H. (2016). How good is the map? A multi-scale cross-comparison framework for global settlement layers: Evidence from Central Europe. Remote Sensing of Environment, 178, 191–212. https://doi.org/10.1016/j.rse.2016.03.001

Lane, P. N. J., Benyon, R. G., Nolan, R. H., Keenan, R. J., & Zhang, L. (2023). Forests, fire and vegetation change impacts on Murray-Darling Basin water resources. Australian Journal of Water Resources, 27(1), 68–84. https://doi.org/10.1080/13241583.2023.2179555

Lawrence, D., & Vandecar, K. (2015). Effects of tropical deforestation on climate and agriculture. Nat. Clim. Chang. 5, 27–36. https://doi.org/10.1038/nclimate2430.

Li, Y., Piao, S., Li, L. Z. X., Chen, A., Wang, X., Ciais, P., Huang, L., Lian, X., Peng, S., Zeng, Z., Wang, K., & Zhou, L. (2018). Divergent hydrological response to large-scale afforestation and vegetation greening in China. Science Advances, 4(5), eaar4182. https://doi.org/10.1126/sciadv.aar4182

Loch, A., & Adamson, D. (2015). Drought and the rebound effect: A Murray–Darling Basin example. Natural Hazards, 79(3), 1429–1449. https://doi.org/10.1007/s11069-015-1705-y

Loveland, T. R., Reed, B. C., Ohlen, D. O., Brown, J. F., Zhu, Z., Yang, L., & Merchant, J. W. (2000). Development of a global land cover characteristics database and IGBP DISCover from 1 km AVHRR data. International Journal of Remote Sensing, 21(6–7), 1303–1330. https://doi.org/10.1080/014311600210191

Lucas, R., Mueller, N., Siggins, A., Owers, C., Clewley, D., Bunting, P., Kooymans, C., Tissott, B., Lewis, B., Lymburner, L., & Metternicht, G. (2019). Land cover mapping using digital earth Australia. Data, 4(4), 143. https://doi.org/10.3390/data4040143

Mann, H. B. (1945). Nonparametric tests against trend. Econometrica, 13(3), 245. https://doi.org/10.2307/1907187

McKernan, M. (2005). Drought: The Red Marauder. Allen and Unwin.

McLoughlin, C. A., Thoms, M. C., & Parsons, M. (2020). Reflexive learning in adaptive management: A case study of environmental water management in the Murray Darling Basin, Australia. River Research and Applications, 36(4), 681–694. https://doi.org/10.1002/rra.3607

MDBA. (2010). Murray Darling Basin Authority annual report 2009–10. https://www.mdba.gov.au/sites/default/files/publications/annual-report-2009-10-mdba.pdf, (Accessed 09 July 2024).

MDBA. (2018). EY Report: Analysis of efficiency measures in the Murray–Darling Basin. EY, p. 307. https://www.mdba.gov.au/sites/default/files/publications/ey-report-analysis-efficiency-measures-2018.pdf, (Accessed 09 July 2024).

MDBA. (2023a). A guide to water management in the Murray–Darling Basin. https://www.mdba.gov.au/water-management/river-murray-operations/how-water-managed, (Accessed 09 July 2024).

MDBA. (2023b). Impact of salinity. https://www.mdba.gov.au/climate-and-river-health/water-quality/salinity/impact-salinity, (Accessed 09 July 2024).

MDBA. (2023c). Why the Murray–Darling Basin matters. https://www.mdba.gov.au/basin/why-murray-darling-basin-matters, (Accessed 09 July 2024).

Murphy, B. F., & Timbal, B. (2008). A review of recent climate variability and climate change in Southeastern Australia. International Journal of Climatology, 28(7), 859–879. https://doi.org/10.1002/joc.1627

Obahoundje, S., Ofosu, E. A., Akpoti, K., & Kabo-bah, A. T. (2017). Land use and land cover changes under climate uncertainty: Modelling the impacts on hydropower production in Western Africa. Hydrology, 4(1), 2. https://doi.org/10.3390/hydrology4010002

Owers, C. J., Lucas, R. M., Clewley, D., Planque, C., Punalekar, S., Tissott, B., Chua, S. M. T., Bunting, P., Mueller, N., & Metternicht, G. (2021). Living Earth: Implementing national standardised land cover classification systems for Earth Observation in support of sustainable development. Big Earth Data, 5(3), 368–390. https://doi.org/10.1080/20964471.2021.1948179

Papas, M. (2018). Supporting sustainable water management: Insights from Australia's reform journey and future directions for the Murray-Darling Basin. Water (Switzerland), 10(11), 1649. https://doi.org/10.3390/w10111649

Pendrill, F., Gardner, T. A., Meyfroidt, P., Persson, U. M., Adams, J., Azevedo, T., Lima, M. G. B., Baumann, M., Curtis, P. G., De Sy, V., Garrett, R., Godar, J., Goldman, E. D., Hansen, M. C., Heilmayr, R., Herold, M., Kuemmerle, T., Lathuillière, M. J., Ribeiro, V., Tyukavina, A., Weisse, M.J., & West, C. (2022). Disentangling the numbers behind agriculture-driven tropical deforestation. Science, 377(6611), eabm9267. https://doi.org/10.1126/science.abm9267

Pickering, C., & Guglyuvatyy, E. (2019). Negative impact of land clearing and deforestation on the Great Barrier Reef: Assessing the effectiveness of Queensland's Vegetation Management Act 1999 (Qld). Carbon and Climate Law Review, 13(3), 195–207. https://doi.org/10.21552/cclr/2019/3/6

Pink, B. (2008). Water and the Murray Darling Basin-A statistical profile, ABS Catalogue No. 4610.0.55.007, Canberra, ACT: Australian Bureau of Statistics. https://www.abs.gov.au/ausstats/abs@.nsf/mf/4610.0.55.007, (Accessed 09 July 2024).

Pittock, J., & Connell, D. (2010). Australia demonstrates the planet's future: Water and climate in the Murray-Darling basin. International Journal of Water Resources Development, 26(4), 561–578. https://doi.org/10.1080/07900627.2010.519522

Pittock, J., & Finlayson, C. M. (2011). Australia's MurrayDarling Basin: Freshwater ecosystem conservation options in an era of climate change. Marine and Freshwater Research, 62(3), 232–243. https://doi.org/10.1071/MF09319

Pollino, C. A., Hart, B. T., Nolan, M., Byron, N., & Marsh, R. (2020). Rural and regional communities of the Murray–Darling Basin. In B. T. Hart, N. R. Bond, N. Byron, C. A. Pollino, & M. J. Stewardson (Eds.), Murray-Darling Basin, Australia: Its Future Management (Vol. 1, pp. 21–46). Elsevier. https://doi.org/10.1016/B978-0-12-818152-2.00002-4

Postel, S. L. (2000). Entering an era of water scarcity: The challenges ahead. Ecological Applications, 10(4), 941–948. https://doi.org/10.1890/1051-0761(2000)010[0941:EAEOWS]2.0.CO;2

Quentin Grafton, R., Horne, J., & Wheeler, S. A. (2016). On the Marketisation of Water: Evidence from the Murray-Darling Basin, Australia. Water Resources Management, 30(3), 913–926. https://doi.org/10.1007/s11269-015-1199-0

Reside, A. E., Beher, J., Cosgrove, A. J., Evans, M. C., Seabrook, L., Silcock, J. L., Wenger, A. S., & Maron, M. (2017). Ecological consequences of land clearing and policy reform in Queensland. Pacific Conservation Biology, 23(3), 219–230. https://doi.org/10.1071/PC17001

Saddique, N., Mahmood, T., & Bernhofer, C. (2020). Quantifying the impacts of land use/land cover change on the water balance in the afforested River Basin, Pakistan. Environmental Earth Sciences, 79(19), 448. https://doi.org/10.1007/s12665-020-09206-w

Saha, P. P., Zeleke, K., & Hafeez, M. (2019). Impacts of land use and climate change on streamflow and water balance of two sub-catchments of the Murrumbidgee River in South Eastern Australia. In A. M. Melesse, W. Abtew, & G. Senay (Eds.), Extreme Hydrology and Climate Variability: Monitoring, Modelling, Adaptation and Mitigation (pp. 175–190). Elsevier. https://doi.org/10.1016/B978-0-12-815998-9.00015-4

Salehi, S., Dehghani, M., Mortazavi, S. M., & Singh, V. P. (2020). Trend analysis and change point detection of seasonal and annual precipitation in Iran. International Journal of Climatology, 40(1), 308–323. https://doi.org/10.1002/joc.6211

Sen, P. K. (1968). Estimates of the regression coefficient based on Kendall's Tau. Journal of the American Statistical Association, 63(324), 1379–1389. https://doi.org/10.1080/01621459.1968.10480934

Shrivastava, P., & Kumar, R. (2015). Soil salinity: A serious environmental issue and plant growth promoting bacteria as one of the tools for its alleviation. Saudi Journal of Biological Sciences, 22(2), 123–131. https://doi.org/10.1016/j.sjbs.2014.12.001

Speer, M. S., Leslie, L. M., MacNamara, S., & Hartigan, J. (2021). From the 1990s climate change has decreased cool season catchment precipitation reducing river heights in Australia's southern Murray-Darling Basin. Scientific Reports, 11(1), 16136. https://doi.org/10.1038/s41598-021-95531-4

Stewardson, M. J., Walker, G., & Coleman, M. (2021). Hydrology of the Murray–Darling Basin. In Murray-Darling Basin, Australia (pp. 47–73). Elsevier.

Tao, H., Al-Hilali, A. A., Ahmed, A. M., Mussa, Z. H., Falah, M. W., Abed, S. A., Deo, R., Jawad, A. H., Abdul Maulud, K. N., Latif, M. T., & Yaseen, Z. M. (2023). Statistical and spatial analysis for soil heavy metals over the Murray-Darling river basin in Australia. Chemosphere, 317, 137914. https://doi.org/10.1016/j.chemosphere.2023.137914

Teklay, A., Dile, Y. T., Setegn, S. G., Demissie, S. S., & Asfaw, D. H. (2019). Evaluation of static and dynamic land use data for watershed hydrologic process simulation: A case study in Gummara watershed, Ethiopia. Catena, 172, 65–75. https://doi.org/10.1016/j.catena.2018.08.013

Tissott, B., & Mueller, N. (2022). DEA Land Cover 25m. Geoscience Australia, Canberra. https://doi.org/10.26186/146090

Tulbure, M. G., & Broich, M. (2019). Spatiotemporal patterns and effects of climate and land use on surface water extent dynamics in a dryland region with three decades of Landsat satellite data. Science of the Total Environment, 658, 1574–1585. https://doi.org/10.1016/j.scitotenv.2018.11.390

Turner, G., Vanderbyl, T., & Kumar, S. (2019). Final report of the independent panel's review of the Sustainable Diversion Limit (SDL) Water Accounting Framework. https://figshare.utas.edu.au/articles/report/Final_Report_of_the_Independent_Panel_s_Review_of_the_Sustainable_Diversion_Limit_SDL_Water_Accounting_Framework/23170937

Van Dijk, A. I. J. M., Beck, H. E., Crosbie, R. S., De Jeu, R. A. M., Liu, Y. Y., Podger, G. M., Timbal, B., & Viney, N. R. (2013). The Millennium Drought in southeast Australia (2001-2009): Natural and human causes and implications for water resources, ecosystems, economy, and society. Water Resources Research, 49(2), 1040–1057. https://doi.org/10.1002/wrcr.20123

Van Dijk, A., Renzullo, L., King, E., & Guerschman, J.-P. (2009). The Australian water resources assessment system. Blending water cycle observations and models at local to continental scale. GEWEX/ILEAPS "Water in a Changing Climate."

Walker, G., & Prosser, I. P. (2021). Water quality: Land use impacts on salinity, sediments, and nutrients. In Murray-Darling Basin, Australia: Its Future Management (pp. 109–135). Elsevier. https://doi.org/10.1016/B978-0-12-818152-2.00006-1

Ward, F. A., & Pulido-Velazquez, M. (2008). Water conservation in irrigation can increase water use. Proceedings of the National Academy of Sciences, 105(47), 18215–18220. https://doi.org/10.1073/pnas.0805554105

Warrence, N.J., Bauder, J.W., & Pearson, K.E. (2002). Basics of salinity and sodicity effects on soil physical properties. Department of Land Resources and Environmental Sciences, Montana State University-Bozeman, MT, 129: 1-29. https://waterquality.montana.edu/energy/cbm/background/soil-prop.html (Accessed 09 July 2024).

Weber, E. (1977). Kendall, M.: Multivariate analysis. Charles Griffin b Co. LTD. London, High Wycombe 1975. 210 s., 9 Abb., 27 Tab., 1 Anhang, £ 6,80. Biometrical J. 19, 309–309. https://doi.org/10.1002/bimj.4710190413.

Wei, Y., Langford, J., Willett, I. R., Barlow, S., & Lyle, C. (2011). Is irrigated agriculture in the Murray Darling Basin well prepared to deal with reductions in water availability? Global Environmental Change, 21(3), 906–916. https://doi.org/10.1016/j.gloenvcha.2011.04.004

Wheeler, S. A. (2022). Debunking Murray-Darling Basin water trade myths. Australian Journal of Agricultural and Resource Economics, 66(4), 797–821. https://doi.org/10.1111/1467-8489.12490

Wheeler, S. A., Carmody, E., Grafton, R. Q., Kingsford, R. T., & Zuo, A. (2020). The rebound effect on water extraction from subsidising irrigation infrastructure in Australia. Resources, Conservation and Recycling, 159, 104755. https://doi.org/10.1016/j.resconrec.2020.104755

Wheeler, S., & Garrick, D.E. (2020). A tale of two water markets in Australia: lessons for understanding participation in formal water markets. Oxford Rev. Econ. Policy 36, 132–153. https://doi.org/10.1093/oxrep/grz032.

Wheeler, S., Zuo, A., & Bjornlund, H. (2013). Farmers' climate change beliefs and adaptation strategies for a water scarce future in Australia. Global Environmental Change, 23(2), 537–547. https://doi.org/10.1016/j.gloenvcha.2012.11.008

Williams, J., Colloff, M. J., Grafton, R. Q., Khan, S., Paydar, Z., & Wyrwoll, P. (2023). The three-infrastructures framework and water risks in the Murray-Darling Basin, Australia. Australian Journal of Water Resources, 27(1), 47–67. https://doi.org/10.1080/13241583.2022.2151106

Xiong, J., Thenkabail, P. S., Tilton, J. C., Gumma, M. K., Teluguntla, P., Oliphant, A., Congalton, R. G., Yadav, K., & Gorelick, N. (2017). Nominal 30-m cropland extent map of continental Africa by integrating pixel-based and object-based algorithms using

Sentinel-2 and Landsat-8 data on google earth engine. Remote Sensing, 9(10), 1065. https://doi.org/10.3390/rs9101065
Yao, Z., Zhang, L., Tang, S., Li, X., & Hao, T. (2017). The basic characteristics and spatial patterns of global cultivated land change since the 1980s. Journal of Geographical Sciences, 27(7), 771–785. https://doi.org/10.1007/s11442-017-1405-5
Zeng, F., Ma, M. G., Di, D. R., & Shi, W. Y. (2020). Separating the impacts of climate change and human activities on runoff: A review of method and application. Water (Switzerland), 12(8), 2201. https://doi.org/10.3390/W12082201

CHAPTER 4

UNCOVERING EVAPOTRANSPIRATION PATTERNS IN THE MURRAY DARLING BASIN OVER TWO DECADES: A LAND COVER PERSPECTIVE

Highlights:

CMRSET performed better than MODIS AET in long-term basin water balance.

Significant differences in AET among MDB catchments.

Temporal AET variability is dominated by rainfall in most catchments.

Significant differences in AET/P between major land covers were unusual.

Uncovering evapotranspiration patterns in the Murray Darling Basin over two decades: A land cover perspective

A. Shadmehri Toosi[1,2*], O. Batelaan[1,2], M. Shanafield[1,2], H. Guan1[1,2]

1. Flinders University, National Centre for Groundwater Research and Training, College of Science and Engineering, Bedford Park, 5042, Australia

2. National Centre for Groundwater Research and Training, Flinders University, GPO Box 2100, Adelaide, SA 5001, Australia

*Corresponding author

Email: amirh.shadmehr@flinders.edu.au

4.1 Abstract

The Murray Darling Basin (MDB) is one of Australia's most important water and land resources, contributing significantly to the country's economy. Actual evapotranspiration (AET) plays a critical role in the water balance of the Basin, influencing water availability for irrigation and other uses. Understanding the dynamics of AET in the MDB under changing land cover and climate is essential for managing water resources sustainably, predicting water availability for agriculture, and ensuring the long-term sustainability of the region's economy and ecosystems. This study provides a comprehensive analysis of the long-term changes in AET over the MDB at both the Basin and catchment levels over the two-decade period 2001-2020. To investigate the dynamics of AET within various land cover types, high-resolution Digital Earth Australia (DEA) Land Cover data was employed alongside the MODIS and CMRSET AET datasets.

While the MODIS dataset showed limitations in water balance assessment compared to CMRSET, overall, both datasets generally agreed on AET patterns despite variations in magnitude. Rainfall was the primary driver of variability in AET across most catchments. There were significant differences in average AET across three major land cover classes within most MDB catchments, except for a few in the northern part. The results of this study highlight the importance of comparing and testing AET products. Furthermore, the study highlights the need for regional studies given diverse hydrological characteristics and the significant influence of regional climate, terrain, and land cover changes on AET.

Keywords: CMRSET, MODIS, Actual Evapotranspiration (AET), land cover, ecohydrology

4.2 Introduction

Evapotranspiration (ET) is the sum of the water lost to the atmosphere through transpiration by vegetation and evaporation from wet canopy, soil, and surface water bodies (Irmak, 2008). Actual Evapotranspiration (AET) is the amount of water that is evaporated and transpired from the land surface and vegetation, whereas Potential Evapotranspiration (PET) is the maximum amount of water that could be evaporated and transpired under ideal (non-water limited) conditions (Jin et al., 2017). Understanding AET and PET is important for effective water resource management, as it helps quantify water use and assess the impacts of climate and land cover changes on water availability.

Researchers have long assumed that there is a significant difference in average evapotranspiration between different land cover classes, as vegetation types and densities can influence the amount of water that transpires and evaporates (Liu et al., 2010; Chen et al., 2011; Yang et al., 2022). Land use and land cover changes, such as deforestation or urbanisation, can significantly alter the rate and pattern of AET, which in turn can affect the availability of water resources for human and ecological needs (He et al., 2008; Pal et al., 2021). Conversion of natural vegetation to croplands and other forms of human development has reduced vegetation cover. Reducing vegetation cover diminishes evapotranspiration, affecting moisture recycling and surface runoff patterns (Wierik et al., 2021). This disruption to the water cycle and recharge processes can result in water stress in certain regions.

Leaf area, root depth, and stomatal conductance can influence the evapotranspiration rates (Garrigues et al., 2015; Yang et al., 2023). Climate conditions also impact evapotranspiration rates, including temperature, humidity, solar radiation, and wind speed (McColl et al., 2019). Moreover, soil properties such as texture and water-holding capacity, topography and land management practices affect water availability for evapotranspiration (Pradhan, 2019; Zhao et al., 2019). Incorporating all these variables over a large scale to estimate evapotranspiration poses challenges due to data availability, spatial heterogeneity, temporal variability, model complexity, and computational requirements.

Many studies have concentrated on the variability in AET under different climates and its change. Wei et al. (2021) showed that climate change plays a dominant role in affecting water yield (calculated as the annual precipitation minus the annual actual evapotranspiration), while land use and land cover change have a small impact. Feng et al. (2020) indicated that the dominant factor of AET variability depended on the timescale and dry-wet conditions. Brümmer et al. (2012) studied various sites across Canada from 2003 to 2006. Despite varied annual precipitation (250−1450 mm) across sites, evapotranspiration consistently ranged

between 400 and 500 mm when precipitation exceeded 700 mm and never went below 200 mm. Beaulieu et al. (2016) found that the response of land plants to climate change in the future seems only slightly to affect water resources. They also emphasised the current deficiencies and constraints in simulating and assessing the effects of climate change.

In large catchments, accurately tracking water use and allocations is essential for effective water management, especially during drought and water scarcity (Bretreger et al., 2020). To achieve this, comprehensive monitoring and metering are required to ensure equitable distribution of limited water resources among stakeholders (Nguyen et al., 2020). However, monitoring ET on a large scale can be challenging (Karimi et al., 2019; Bretreger et al., 2020; Simons et al., 2020). Remote sensing has become a valuable tool for estimating AET at regional and global scales (Dimitriadou & Nikolakopoulos, 2020). However, the accuracy of remote sensing AET products can vary depending on factors such as the type of remote sensing data used, the algorithm employed for ET estimation, and the spatial and temporal resolution of the data (Zhang et al., 2016; McShane et al., 2017).

Several remote sensing-based AET datasets are available, each with its strengths and limitations. Among these datasets, MODIS (Moderate Resolution Imaging Spectroradiometer) AET has been widely applied in research in various fields, including hydrology, agriculture, ecology, and climate science (Petus et al., 2013; Running et al., 2019; Dimitriadou & Nikolakopoulos, 2020; Deus & Gloaguen, 2013; Zhang & Chen, 2017; Liu et al., 2019; 2022).

Guerschman et al. (2009) developed the CMRSET model for estimating AET at monthly and 1 km spatial resolutions across Australia. Using MODIS reflectance data, the model adjusts potential evapotranspiration with vegetation indices to compute AET. This model has been extensively validated and applied in various studies (Swaffer et al., 2020; Crosbie & Rachakonda, 2021; Gelsinari et al., 2021; Kunnath-Poovakka et al., 2021; Peña-Arancibia et al., 2021a; 2021b). It was found to provide the best result among five satellite-driven remote sensing AET products when benchmarked against independent evaluation datasets in Australia (King et al., 2011). In the latest data release, the spatial resolution and temporal frequency of CMRSET have been enhanced, and data were calibrated using an enhanced collection of observed AET from eddy covariance flux towers (Guerschman et al., 2022). These characteristics make CMRSET particularly well-suited for monitoring agriculture, irrigation, and wetlands and providing input for assessing structural and policy improvements (Guerschman et al., 2022).

While land cover and climate changes exert complex and varying influences on AET, there remains a significant gap in comprehensively understanding the response of ET to specific

vegetation change drivers, with model-based estimations of these responses marked by considerable uncertainty (Liu et al., 2013; Wang et al., 2021; Li et al., 2022; Yang et al., 2023). This research examined long-term shifts in the CMRSET AET within a large Australian catchment of agricultural and ecological significance, focusing on both the Basin and catchment scales. By utilising the high-resolution Digital Earth Australia (DEA) Level 3 25 m Land Cover data, this study meticulously examines AET in relation to land cover changes over a two-decade period (2001-2020). The primary objectives of this study are:

1. To compare the CMRSET and MODIS datasets in estimating AET.
2. To evaluate the trend and dynamics of AET across different land cover types over time across the MDB.
3. To test whether there is a significant difference in AET between major LULC types.

4.3 Methods and material

4.3.1 Study area

The Murray Darling Basin (MDB) spans an area of over one million km^2, encompassing four Australian states - Queensland, New South Wales, Victoria, and South Australia - along with the Australian Capital Territory (Figure 4.1). The Basin consists of 22 catchments (Table B.1), with over 30,000 kilometres of rivers, creeks, and streams. The MDB's rainfall patterns are strongly influenced by the El Niño, La Niña, Indian Ocean Dipole, and the Southern Annular Mode (King et al., 2020). The MDB transitions from subtropical in the north to a dry, arid climate in the south, with a large rainfall spatial variability (Shen et al., 2017).

In the early 2000s, the Basin experienced severe droughts, record-low rainfall, and high temperatures (Leblanc et al., 2009; 2012). More recently, the drought also established the preconditions for the catastrophic 2019–20 bushfires (Wang & Cai, 2020), which were followed by floods in 2022/2023 (Gissing et al., 2022; Alexandra, 2023; Beavis et al., 2023). Climate proxies demonstrate that the alternating patterns of droughts and floods are characteristic features of the MDB's climate (Gallant & Gergis, 2011; Alexandra, 2023). Climate change can potentially intensify the flood-drought oscillations in the MDB, set against an overarching trend of increasing aridity (CSIRO, 2022). These climatic conditions have markedly affected agriculture in the MDB and strained the region's water resources (Leblanc et al., 2012; Dreverman, 2013). This change is important, as the Basin is home to over two million people and provides the country with food, water, important economic activities, and high ecological values. Given the significance of agriculture in the Basin and the impacts of high water demand on the ecology, a comprehensive water management plan was established in 2012 (Hart, 2016; MDBA, 2018), which targets an environmental water recovery of 2,075 GL/y.

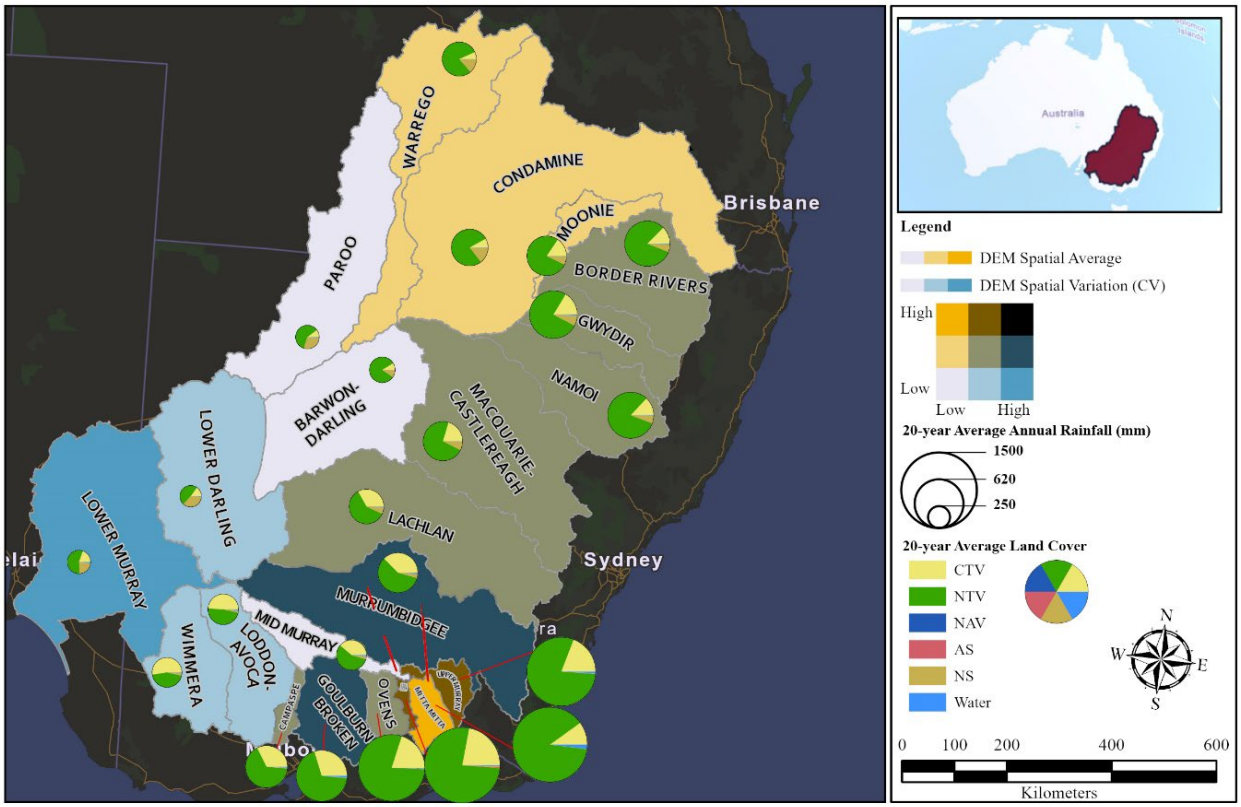

Figure 4.1: Study area; Murray-Darling Basin within Australia with catchments and elevation (mAHD).

4.3.2 Data

In this study, the level 3 (base classification) Digital Earth Australia (DEA) Land Cover data with a spatial resolution of 25 m were used (Tissott & Mueller 2022). DEA land cover data is based on the Food and Agriculture Organization's (FAO) Land Cover Classification System (LCCS) taxonomy Version 2, which is globally applicable (Di Gregorio & Jansen, 1998; 2000; Di Gregorio, 2005). DEA Land Cover is produced by combining qualitative and quantitative environmental information derived from Landsat satellite sensor data, resulting in annual classifications of Australia's land cover from 1988 to 2020 (Tissott & Mueller 2022). It consists of seven descriptor layers: Cultivated Terrestrial Vegetation (CTV), (Semi-)Natural Terrestrial Vegetation (NTV), Natural Aquatic Vegetation (NAV), Artificial Surface (AS), Natural Bare Surface (NS), and Water. This study concentrated on three major land cover classes: CTV, NTV and NS. The selection of these specific classes was driven by their significant relevance to AET studies. Moreover, these classes collectively constitute over 97% of the total Basin area, rendering them the predominant land cover types within the study's scope.

CMRSET evapotranspiration dataset provides AET for Australia with a spatial resolution of 30 m and a monthly frequency. CMRSET combines reflective remote sensing indices and PET

calculated from the Bureau of Meteorology's daily meteorological data. The combination of high-resolution, low-frequency AET estimates (such as those from Landsat) with low-resolution, high-frequency AET estimates (such as those from MODIS and VIIRS) creates a dataset that is both high-resolution and high-frequency, with no gaps caused by cloud coverage. We used Google Earth Engine to download CMRSET AET for Australia by obtaining and aggregating monthly data to obtain yearly data with GDA94/Australian Albers projection.

Annual AET datasets from the MODIS early AET dataset were requested from the NASA website (https://appeears.earthdatacloud.nasa.gov/). The MOD16A3 Version 6.1 product is a yearly composite dataset that provides estimates of yearly Evapotranspiration (ET), Latent Heat Flux (LE), PET and Potential LE (PLE) along with a quality control layer. These estimates are derived from satellite data with a spatial resolution of 500 m and are available from 2001 to the present (Running & Mu, 2021). The pixel values for the two ET layers (AET and PET) are the sum for all days within the defined year.

The MOD16A2 product estimates AET using the Penman-Monteith equation and provides 8-day composite data at a spatial resolution of 1 km (Zhang et al., 2008). The model inputs include daily meteorological reanalysis data and MODIS remotely sensed data products such as vegetation property dynamics, albedo, and land cover (Running & Mu, 2021). The MODIS AET, specifically the Version 6.1 Level-1B (L1B) product, has undergone significant improvements and calibration changes compared to the preceding Version 6.0 (Running & Mu, 2021).

Daily rainfall from the Australian Gridded Climate Data (AGCD) v2 (Bureau of Meteorology), was downloaded from the National Computational Infrastructure (NCI) data catalogue (Evans et al., 2023). This dataset covers the Australian continent and surrounding regions, with a spatial resolution of approximately 0.05 degree (~5 km) (Evans et al., 2020).

4.3.3 Data preprocessing and analysis

Data were collected, mosaiced, projected and resampled to match corresponding land cover pixels to ensure that each pixel's size and extent matched. The data was also masked for the study area. All preprocessing was done in ArcGIS Pro (Esri, 2023). The zonal statistics method in ArcGIS Pro was used to calculate the average parameter of each catchment in different years.

4.3.3.1 Normalization for rainfall impact

The ratio of AET to Precipitation (P) (AET/P) provides a detailed measure of the fraction of precipitation expended through evapotranspiration over a year. To calculate the AET/P ratio,

the MODIS dataset MOD16A3, which provides annual AET estimates, is utilised alongside the CMRSET dataset, which has been aggregated on a yearly basis. These annual AET values from both datasets are then divided by the corresponding gridded precipitation data for the same period. The resulting values were spatially averaged to produce maps representing the AET/P ratio at both the Basin and catchment scales.

4.3.3.2 Coefficient of variation

The coefficient of variation for temporal variability for each catchment was calculated as follows:

$$Temporal\ Coefficient\ of\ Variation = \frac{\frac{1}{n}\sum_{t=1}^{20} \bar{X}_i}{\sqrt{\frac{1}{n-1}\left(\sum_{t=1}^{20} \bar{X}_i - \mu_{\bar{X}_i}\right)^2}} \qquad \text{Eq. 1}$$

Where:

n is the number of years the AET or AET/P values.

$\bar{X}_i$ is the average of all AET or AET/P pixel values within the i-th catchment on an annual basis.

$\mu_{\bar{X}i}$ is the mean of the yearly averages of AET or AET/P for all pixels within the same catchment.

The coefficient of variatizon for spatial variability is formulated as:

$$Spatial\ coefficient\ of\ variation\ = \frac{1}{n}\sum_{t=1}^{n}\left(\frac{\bar{X}_i}{\sigma_i}\right) \qquad \text{Eq. 1}$$

Where:

σ_i is the standard deviation of AET or AET/P over all pixels for a given catchment in the given year.

4.3.3.3 Water balance

The water balance was calculated as:

$$\sum_{2001}^{2020} outflow \sim \sum_{2001}^{2020} P - \sum_{2001}^{2020} AET - \sum_{2001}^{2020} R \qquad \text{Eq. 2}$$

Where the difference between the cumulative precipitation (P) and the combined values of AET and recharge (R) for the entire Basin from 2001 to 2020 equates to the cumulative outflow. For comparison between outflow calculation for CMRSET and MODIS data, we have assumed that R is negligible across the Basin.

4.3.3.4 Trend analysis

The Mann-Kendall tau statistic was used to measure the degree of monotonic association between the data and time (Mann 1945, Kendall 1975, Gilbert 1987). A positive Kendall's tau indicates an upward trend, while a negative Kendall's tau indicates a downward trend (Salehi et al., 2020). The Sen slope was used to estimate the slopes of identified trends, validate the results, and provide a more comprehensive analysis of the data (Sen, 1968). The Sen slope test works by dividing the data into multiple segments and calculating the median slope for each segment. The overall trend was then estimated as the median of the slopes of all segments. The Sen slope estimator is robust to outliers and less sensitive to the assumption of normality than other regression methods. However, it is not suitable for detecting non-monotonic trends.

4.3.3.5 ANOVA and t-test

A two-step statistical approach was adopted to test the hypothesis that AET varies significantly across different land cover classes. A one-way ANOVA was conducted to determine if there were any statistically significant differences in AET among the three landcover classes at the basin and catchment levels. Following the ANOVA, pairwise comparisons between the land cover classes were conducted using Student's t-test (Figure 4.2). The statistical analyses were performed using the Scipy package in Python.

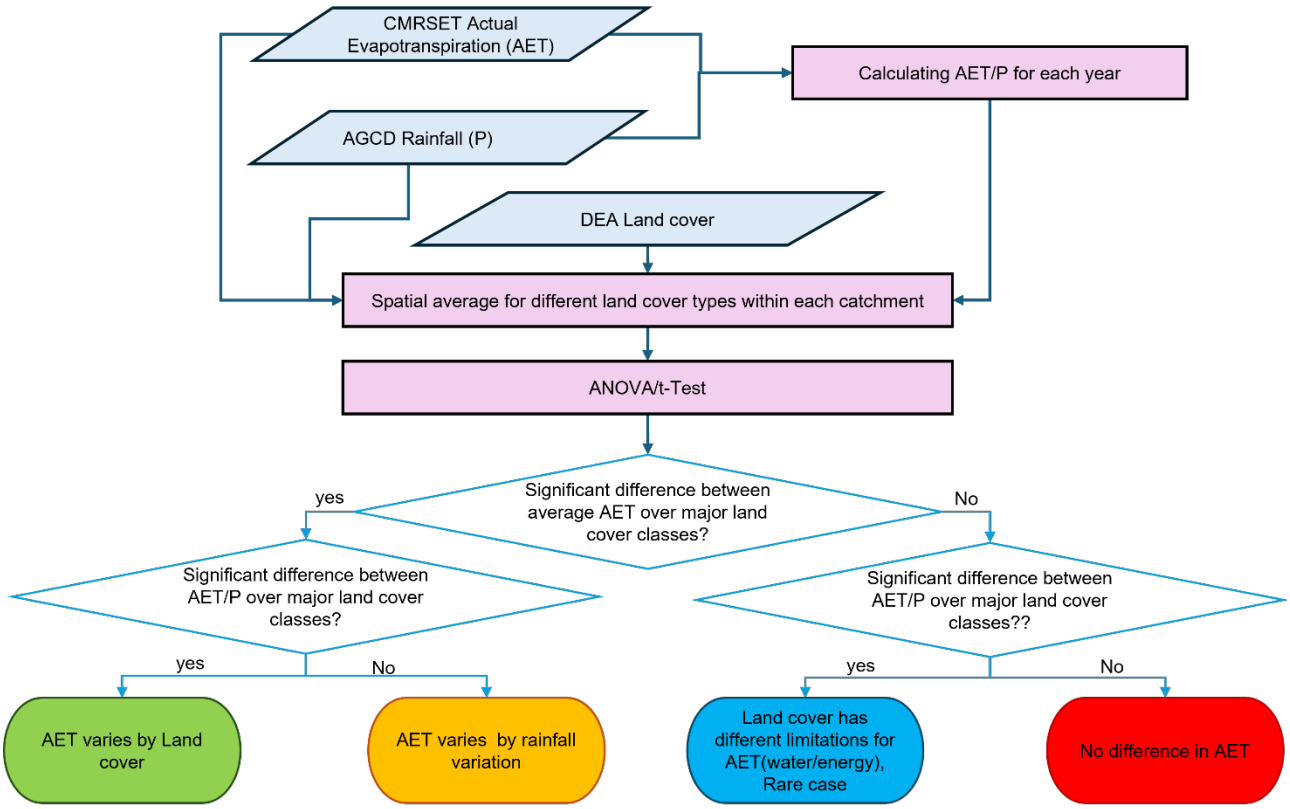

Figure 4.2: Flowchart for the systematic interpretation of ANOVA and subsequent t-test outcomes.

4.4 Results

4.4.1 Precipitation

Between 2001 and 2020, the MDB experienced an average annual precipitation of 428 mm (Figure 4.3). The Basin's average rainfall exhibits considerable year-to-year variability. While the highest recorded average annual precipitation of 810 mm occurred in 2010, the lowest was observed in 2019 at 231mm. Prior to 2010, southeastern Australia endured its driest period since 1900 (Van Dijk et al., 2013). Except for the years 2011, 2012 and 2016, the majority of the 2001-2020 period witnessed below-average precipitation compared to the 20-year average (Figure 4.3). Additionally, the data distribution skewed towards higher values, with the median often falling below the mean due to the highly variable rainfall patterns, both spatially and temporally, on the Basin scale.

There was a significant variation in average rainfall among the analysed catchments. The data revealed a broad range of precipitation, with certain catchments averaging over 900 mm, while others recorded less than 300 mm of rainfall (Figure 4.3b). Kiewa, Mitta Mitta, Upper Murray, and Ovens catchments received higher rainfall, while the Lower Darling, Lower Murray and Paroo received less rainfall than average. Out of the 22 catchments, only Goulburn-Broken,

Gwydir, Kiewa, Lower Darling, Macquarie-Castlereagh, Mid-Murray, Ovens and Warrego, have an average precipitation that is greater than that of the whole basin average.

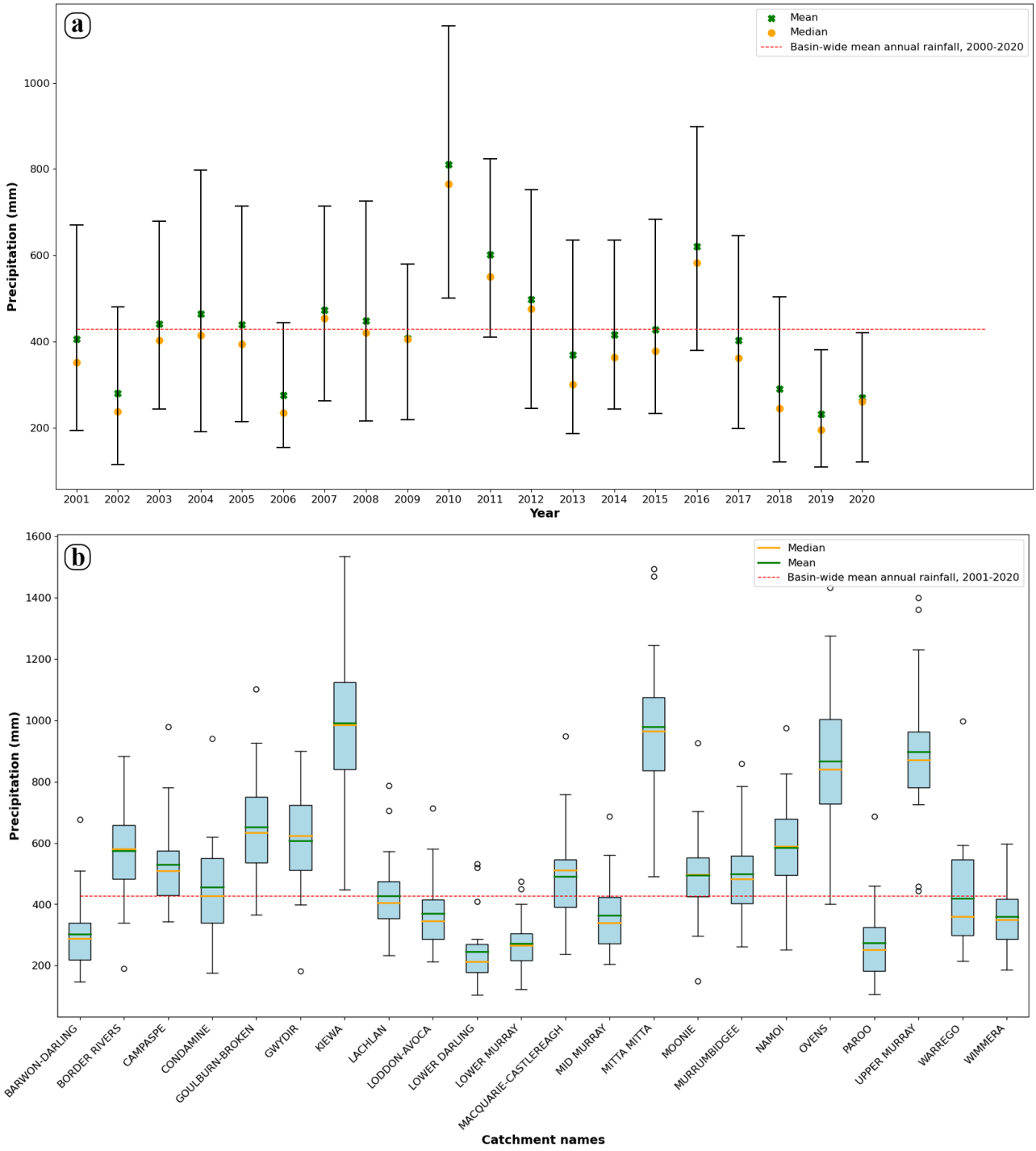

Figure 4.3: (a) Annual variability of rainfall over MDB for the years 2001 to 2020; (b) Distribution of annual rainfall across various MDB catchments during the 20-year period. Each boxplot displays the interquartile range, indicating the middle 50% of the data, with the central line representing the median rainfall. The 'whiskers' extend to the furthest points that are not considered outliers, and any data point outside of this range is represented as an open dot, which signifies a year with unusually high or low rainfall. The red dashed line across the plot denotes average rainfall over 20 years over the whole Basin.

The analysis of rainfall data in the MDB over a two-decade period revealed distinct patterns of temporal and spatial variations across the different catchments (Figure 4.4). The only catchments that showed both a high temporal and spatial variation were the northern Basin Border Rivers, Gwydir, and Namoi. The western part of the MDB, Warrego, Paroo, Lower Darling, and Barwon Darling, showed higher temporal variation in rainfall but low spatial variations. The southern catchments, especially Goulburn-Broken and Ovens, tend to exhibit low temporal but high spatial variation.

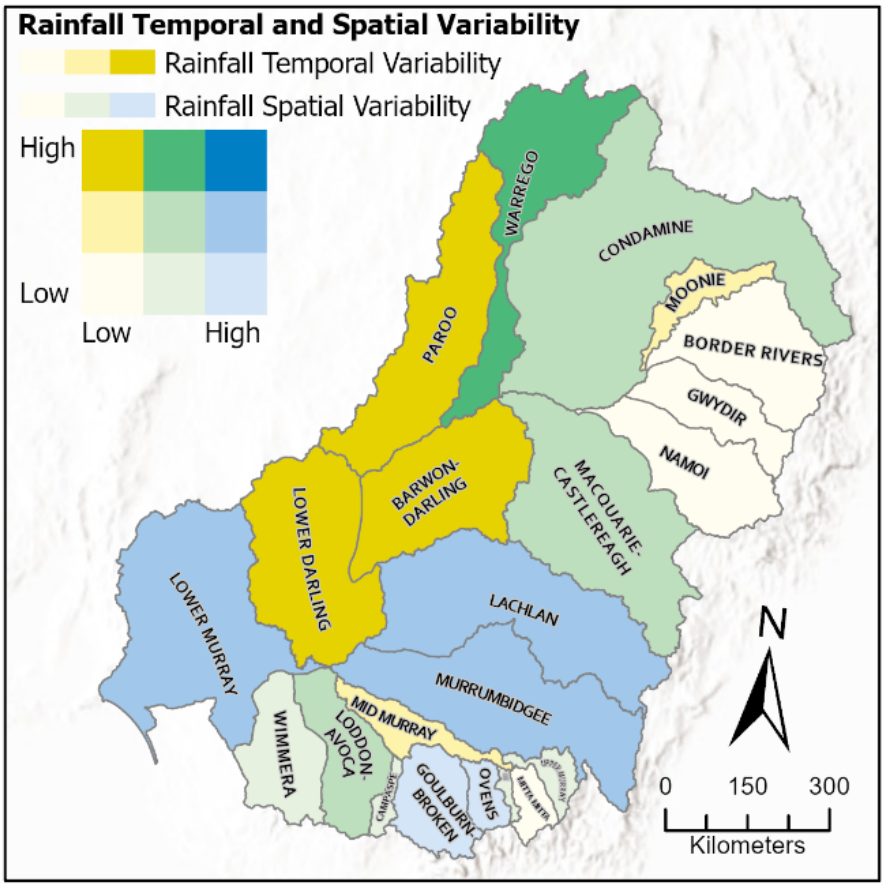

Figure 4.4: Temporal and spatial classification of the coefficient of variation for rainfall from 2001-2020, categorised into low, moderate, and high variability using Jenks natural breaks.

4.4.2 Comparative analysis of AET and AET/P: MODIS vs. CMRSET datasets

4.4.2.1 AET and AET/P changes at the whole basin scale

Using the CMRSET dataset, the time series of AET over the MDB was evaluated across various land cover classes (Figure 4.5a). For CTV, the average mean AET was recorded at 1.1 mm/day, with the minimum and maximum mean AET values at 0.78 mm/day and 1.47 mm/day, respectively (Table B.2). The NTV class exhibited a slightly higher average mean AET of 1.22 mm/day, extending from 1.10 mm/day to 1.45 mm/day. However, The NS class showed the lowest AET rates with an average mean of 0.77 mm/day and the minimum and

maximum mean values of 0.61 mm/day and 0.94 mm/day, respectively. In the CMRSET dataset, the difference between the AET of the CTV, NTV and NS classes was more noticeable than MODIS AET. Overall, there was generally good agreement between the two datasets, although there were some variations in the magnitude of the estimates.

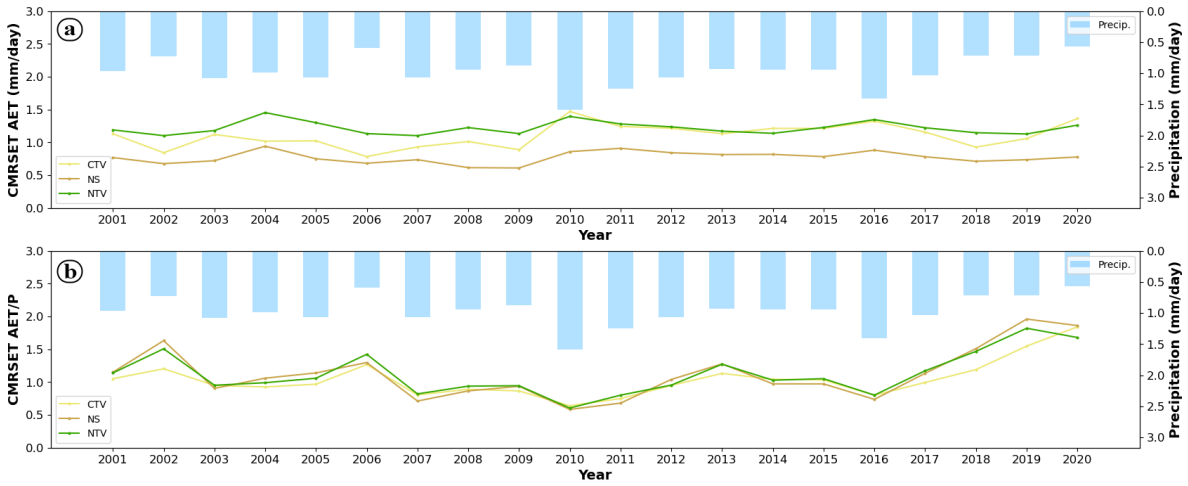

Figure 4.5: (a) AET and (b) AET/P time series 2001-2020 for CMRSET dataset (CTV: Cultivated Terrestrial Vegetation; NS: Natural Bare Surface; NTV: Natural Terrestrial Vegetation).

AET was lower than 1 mm/day in the MODIS dataset in most years (Figure B.1). In contrast, in the CMRSET dataset, AET was greater than 1 mm/day for the NTV class throughout the entire period and for many years, it was also higher than 1 mm/day for the CTV class. However, AET was less than 1 mm/day for the NS class in all years. The MODIS AET data analysis revealed a distinct variation across different land cover classes. The NTV class and CTV class exhibited higher AET rates, with the NTV class showing a range of 0.65-1.24 mm/day and an average of 0.87 mm/day, while the CTV class ranged from 0.53-1.16 mm/day with an average of 0.84 mm/day over 20 years. In contrast, the NS class demonstrated the lowest AET, ranging from 0.36-0.76 mm/day, with a basin-wide average of 0.52 mm/day from 2001 to 2020.

For Basin average AET/P time series, AET/P significantly narrowed the gap between different land cover classes for CMRSET datasets (Figure 4.5b) and MODIS (Figure B.1). However, the results demonstrate that AET/P was less than 1 for the entire period for MODIS until 2017 when it began to surpass the value of 1. On the other hand, for the CMRSET dataset, AET/P was primarily greater than 1 for most years across all land covers. The comparison of the two datasets showed that during drought years, the CMRSET dataset demonstrates a superior capacity to distinguish between CTV and NTV, as the difference in AET between CTV and NTV was more pronounced in the CMRSET dataset. Following 2010, the CTV and NTV for both datasets began to overlap, signalling a convergence in their behaviour until 2014, when

a new drought period commenced (King et al., 2020). After 2016, the MODIS and CMRSET AET/P ratios show a remarkably increasing trend. The AET/P time series minimised the difference between the land cover classes compared to the AET time series. However, in the CMRSET dataset, a subtle difference is still more apparent (Figure 4.5b). The average AET/P map for MODIS and CMRSET data revealed a different pattern over MDB (Figure B.3). The AET/P map derived from CMRSET consistently showed higher values than the MODIS map. The MODIS data showed a much smaller part of the Basin with values of AET/P exceeding 1, highlighting a discrepancy between the two datasets.

4.4.2.2 AET and AET/P changes at the catchment level

Analysis of the AET based on MODIS data across the 22 catchments revealed significant variability, with the Paroo and Barwon Darling catchments having the lowest average AET of 0.43 and 0.54 mm/day, respectively, and the Mitta Mitta and Kiewa catchments having the highest with 2.13 and 2.02 mm/day, respectively (Table 4.1). The analysis of AET based on the CMRSET data showed similar results, with the Kiewa and Mitta Mitta catchments having the highest AET values of 2.02 mm/day, while Lower Darling and Paroo had the lowest with 0.74 mm/day. Kiewa, Mitta Mitta, and Upper Murray consistently exhibited relatively high AET values, while Lower Darling and Paroo had relatively low AET values.

Table 4.1: Average AET (mm/d) and AET/precipitation ratio based on the CMRSET and MODIS datasets for different catchments of the MDB.

Catchment	AET (mm/d) (CMRSET)	AET/P (CMRSET)	AET (mm/d) (MODIS)	AET/P (MODIS)
BARWON-DARLING	0.88	1.20	0.54	0.72
BORDER RIVERS	1.50	1.06	1.03	0.68
CAMPASPE	1.41	1.07	1.21	0.91
CONDAMINE	1.22	1.11	0.76	0.62
GOULBURN-BROKEN	1.63	1.06	1.55	0.99
GWYDIR	1.60	1.08	1.09	0.69
KIEWA	2.02	0.85	2.02	0.88
LACHLAN	1.10	1.03	0.85	0.77
LODDON-AVOCA	1.08	1.17	1.00	1.08
LOWER DARLING	0.74	1.29	0.62	1.10
LOWER MURRAY	0.84	1.32	0.84	1.18
MACQUARIE-CASTLEREAGH	1.29	1.05	0.92	0.70
MID MURRAY	1.19	1.32	0.98	1.04
MITTA MITTA	2.02	0.83	2.13	0.90
MOONIE	1.18	0.96	0.75	0.58
MURRUMBIDGEE	1.25	1.04	1.10	0.87
NAMOI	1.55	1.05	1.13	0.73
OVENS	1.88	0.91	1.74	0.83
PAROO	0.74	1.20	0.43	0.67
UPPER MURRAY	1.99	0.91	1.90	0.87
WARREGO	1.08	1.08	0.59	0.54
WIMMERA	0.97	1.07	0.95	1.04

Based on the MODIS AET data, Warrego, Moonie, and Condamine catchments had AET/P values of 0.54, 0.58, and 0.62, respectively, indicating lower AET relative to precipitation. Conversely, Lower Murray, Lower Darling, and Loddon-Avoca catchments exhibited AET/P values of 1.18, 1.10, and 1.08, respectively, suggesting a relatively higher proportion of AET than precipitation. For the CMRSET data, the catchments with the lowest AET/P values were Mitta Mitta and Kiewa, with values of 0.83 and 0.85, respectively. In contrast, Lower Murray, Mid Murray, and Lower Darling catchments exhibited higher AET/P values of 1.32, 1.32, and 1.29, respectively.

The temporal and spatial variability of AET and AET/P for MODIS (Figure B.2) and CMRSET (Figure 4.6) showed distinct patterns of variability across the MDB, with few exceptions. Jenks natural breaks were used to classify the values into three groups, minimising variation within groups and maximising variation between groups. The results revealed some overlap between the two datasets but no clear overall pattern. MODIS AET/P showed less spatial and temporal variability over six catchments, primarily located in the northern part of the basin. Conversely, CMRSET data showed more dispersed variability patterns, reflecting differences in how each dataset captures AET and precipitation dynamics.

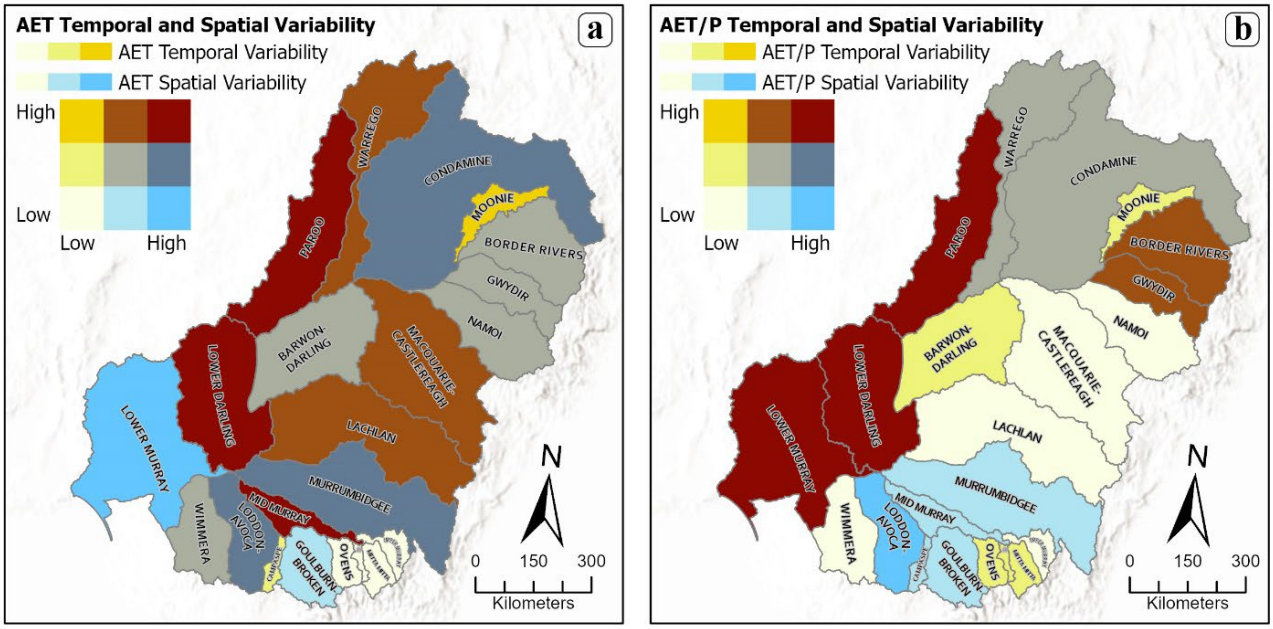

Figure 4.6: Temporal and spatial classification of the coefficient of variation for CMRSET (a) AET and (b) AET/P for 2001-2020, categorised into low, moderate, and high variability using Jenks natural breaks.

4.4.2.3 Water balance: MODIS vs CMRSET datasets

Across the Basin, a noticeable east-west gradient was observed for rainfall and AET (Figure 4.7). Mean annual precipitation ranged from over 1,000 mm in the southeast to less than 300 mm in the central and western regions of the MDB. The overall pattern of MODIS and CMERSET AET were the same. However, the spatial correlation between average 20 years MODIS AET and rainfall data was 0.27, while for CMRSET, it was much higher at 0.70.

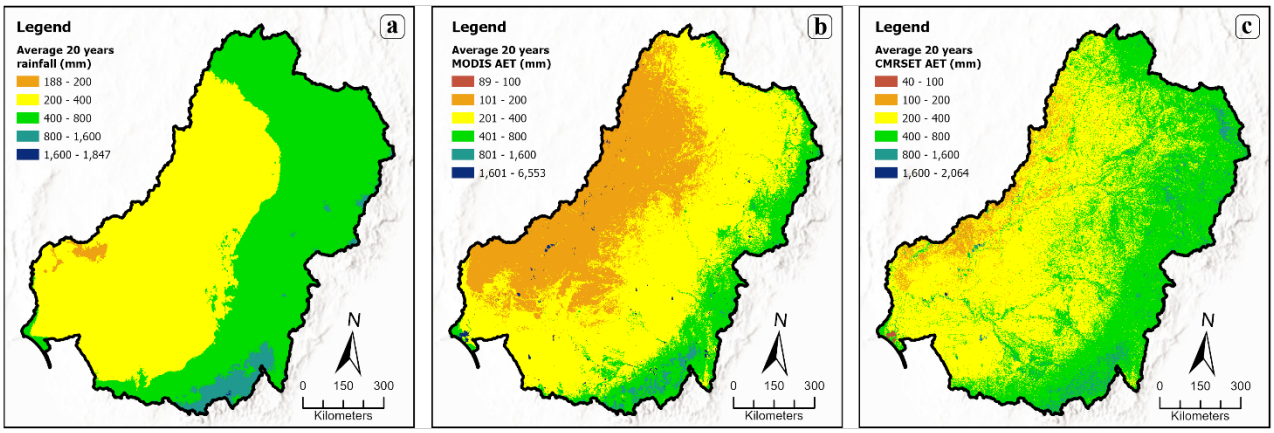

Figure 4.7: Average 20 years (2001-2020) (a) rainfall; (b) MODIS AET; (c) CMRSET AET.

The southern region of the study area exhibits low and negative precipitation values minus AET (P-AET) for the MODIS dataset (Figure 4.8). However, in the CMRSET AET product, negative values are distributed throughout the entire Basin, with the southwestern part showing a relatively greater abundance of negative P-AET values.

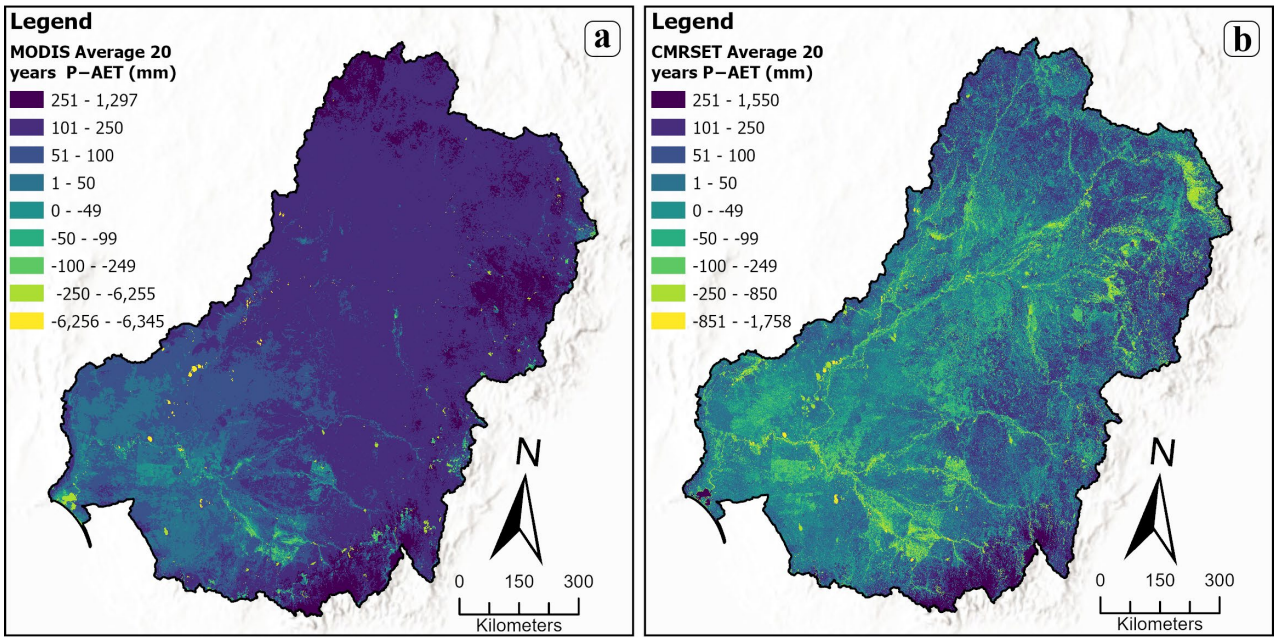

Figure 4.8: Average 20 years (2001-2020) estimated balance (P-AET) based on (a) MODIS; (b) CMRSET

The MODIS AET dataset indicated an average annual evapotranspiration of 313 mm, while the CMERSET dataset exhibited an average annual evapotranspiration of 416 mm. Dreverman (2013) reported an average runoff of 23,850 GL/year, equating to an average of 22 mm across the whole Basin. This value is in close agreement with the 20-year average for P-AET as reported by the CMRSET dataset, which is 12 mm. In contrast, the P-AET estimated using the MODIS AET dataset is significantly higher, at 115 mm. Consequently, an annual average discrepancy of approximately

93 mm was observed between the P-AET values derived from the MODIS dataset and the average outflow reported by the MDBA according to Wentworth Group of Concerned Scientists (2020).

4.4.3 Temporal dynamics of CMRSET AET and AET/P

The time series analysis of AET across various land covers demonstrated variations in AET values among different land use types (Figure B.5). However, when considering the AET/P, the discrepancies between land covers were noticeably reduced. Among the 22 catchments studied, Kiewa, Mitta Mitta, Ovens, and Upper Murray exhibited higher AET ranges and averages (typically exceeding 1.75 mm) during the study period (Figure B.6). Time series of AET demonstrated that in nearly 50% of the 22 catchments, overall, the values of AET within NTV were higher than in other land covers. AET/P reached its lowest value for all land uses in 2010, and a sharp increase in AET/P was observed in most catchments after 2016.

The analysis of AET and AET/P trends across various land covers and catchments demonstrates a predominance of stable patterns, with no significant trends in most regions. Notable exceptions were observed in the Kiewa and Mitta Mitta catchments, which displayed increasing AET trends (Table 4.2). The AET trends observed within NTV land cover in these catchments aligned with the overall increases in AET. The Lower Murray catchment showed an increasing trend in CTV, while a decreasing trend of AET was observed over NS land cover in Border River and Gwydir. No overall trend in AET/P was observed; however, an increasing trend in AET/P was identified in the Condamine-Balonne over CTV land cover and in the Moonie over NS.

Table 4.2: Significant trend analysis test statistics (2001-2020) for AET and AET/P across different land cover classes in MDB catchments. Note: Only statistically significant results are reported in this table. For all other land cover classes, no significant trends were observed.

			Mann Kendal's test result				Sen's Slope test result	
Catchment names			**Tau**	**s**	**trend**	**p**	**Slope**	**intercept**
BORDER RIVERS	AET	NS	-0.44	-84.00	decreasing	0.01	-0.02	1.54
GWYDIR	AET	NS	-0.58	-110.00	decreasing	0.00	-0.04	2.02
KIEWA	AET	NTV	0.43	82.00	increasing	0.01	0.01	1.92
MITTA MITTA	AET	NTV	0.41	78.00	increasing	0.01	0.01	1.88
LOWER MURRAY	AET	CTV	0.47	90.00	increasing	0.00	0.01	0.72
CONDAMINE	AET\P	CTV	0.33	62.00	increasing	0.05	0.02	0.81
MOONIE	AET\P	NS	0.39	74.00	increasing	0.02	0.02	0.55
KIEWA	AET	overall	0.38	72.00	increasing	0.02	0.01	1.92
MITTA MITTA	AET	overall	0.41	78.00	increasing	0.01	0.01	1.92

4.4.4 ANOVA and t-test between land covers for the CMRSET dataset

The ANOVA test results indicated significant differences in average AET across major land cover classes within all the MDB's catchments, except for the northern catchments Condamine, Border Rivers, and Gwydir (Figure 4.9). Similarly, pairwise comparison showed significant differences in average AET between NTV and NS in most catchments (Figure 4.9b). However, in the case of CTV

AET versus NS (Figure 4.9a) and CTV AET versus NTV (Figure 4.9c), many regions exhibited no statistically significant differences in average AET.

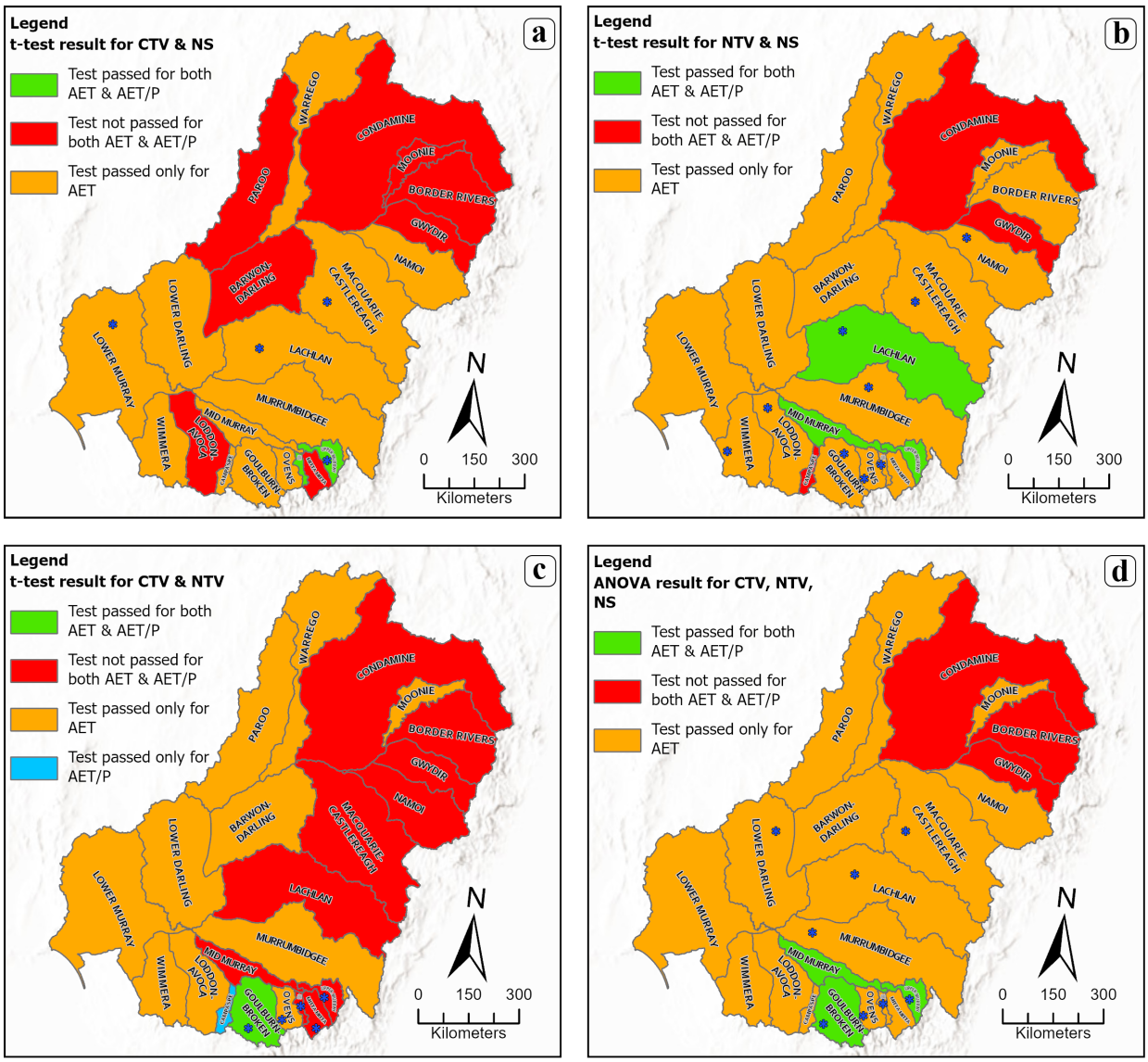

Figure 4.9: The result of ANOVA and t-test for CMRSET AET between (a) CTV (Cultivated Terrestrial Vegetation) and NS (Natural Bare Surface); (b) NTV (Natural Terrestrial Vegetation) and NS; (c) CTV and NTV; and (d) CTV, NTV and NS. (* indicates the catchments with significant differences in precipitation among given land covers)

Among the 22 catchments, Goulburn Broken, Lachlan, Mid Murray and Upper Murray are the only catchments that showed a significant difference between three major land covers, AET and AET/P ($p < 0.05$) (Figure 4.9d). Only the Gwydir and Campaspe catchments demonstrated a meaningful difference in AET/P between CTV and NTV (Figure 4.9c).

For NTV and NS, most catchments exhibited significant differences in average AET and/or AET/P (Figure 4.9b). Conversely, in 10 out of 22 catchments, CTV and NTV showed no significant divergence in both AET and AET/P (Figure 4.9c). For CTV versus NS, eight catchments displayed no substantial difference in AET and AET/P, six of them are in the northern MDB (Figure 4.9a).

Notably, the Goulburn Broken catchment showed a significant difference between CTV and NTV for AET and AET/P ($p < 0.05$) (Figure 9c).

4.5 Discussion

4.5.1 Comparison of CMRSET and MODIS AET datasets

The comparative analysis of AET and AET/P using MODIS and CMRSET datasets over the MDB highlights distinct variations in evapotranspiration dynamics across different land cover classes and spatial scales. During the dry years from 2001 to 2009, the average Actual Evapotranspiration (AET) values among CTV and NTV were more distinctly differentiated. This clearer distinction likely reflects the varied responses of these vegetation types to water stress, with CTV possibly experiencing more pronounced AET reductions due to its reliance on available moisture for agricultural productivity. However, post-2010, increased rainfall, which alleviates moisture stress across both types of vegetation, may have contributed to the distinction in AET between CTV and NTV becoming less apparent in both the MODIS and CMRSET datasets. The improved Algorithm of CMRSET seems to contribute a clearer distinction between different vegetation types, particularly during drought conditions.

Our results highlight the significant difference between 20 years of average P-AET for MODIS vs CMRSET (Figure 4.8). The MODIS data tends to underestimate AET, resulting in a consequential overestimation of water yield. The magnitude of this error was estimated to be about 50 times greater than the recovery targets outlined in the Basin Plan. This significant disparity cannot be disregarded, as it represents a substantial portion of the contracted surface water recovery estimated by the MDB Authority. Similar to our results, Wentworth Group of Concerned Scientists (2020) demonstrated that the discrepancies between observed and expected river flows under prevailing climatic conditions, including dry and drought periods from 2012/13 to 2018/19, were significantly smaller in the Northern Basin compared to the Southern Basin. The average differences were 104 GL/y and 521 GL/y, respectively.

The accuracy of AET products is heavily influenced by unique catchment characteristics, local climate, and terrain conditions, reflecting the inherent complexity in modelling these factors worldwide (Zhao et al., 2019). MODIS, despite its widespread use, has been found to systematically underestimate AET due to structural weaknesses within its algorithm, as reported in several studies (Kim et al., 2012; Velpuri et al., 2013; Hu et al., 2015; Baik et al., 2018). These weaknesses often lead to inaccurate estimates of moisture demand in arid and temperate zones, largely because MODIS relies on indices such as NDVI and LAI, which may not fully capture the environmental variability influencing AET (Baik et al., 2018). Although CMRSET has demonstrated greater accuracy in water balance, the product is not without its limitations. Bretreger et al. (2020) found that CMRSET tends to overestimate AET, especially in irrigation-intensive regions. Research by McVicar et al.

(2017) demonstrated that while the Landsat-only CMRSET AET product performed well when compared to eddy-covariance flux tower AET measurements, its accuracy declined at the catchment or reach water balance scale, showing a systematic overestimation. This discrepancy is further intensified by spectral differences between sensors and the lower temporal resolution of Landsat compared to MODIS. Blending Landsat and MODIS data has been shown to mitigate some of these errors, but CMRSET's sensitivity to these discrepancies remains a significant factor affecting its accuracy (McVicar et., 2017).

Unlike MODIS, many more regional details can be observed in P-AET in the CMRSET dataset. It is in line with Zhao et al. (2019), who found a poor consistency between AET products in northern MDB catchments (e.g., Kiewa, Upper Murray, Mitta Mitta). In the MODIS dataset, a few regions that exhibit significant negative values, contrasting sharply with the more homogeneous distribution of negative values across the Basin seen in the CMRSET dataset (Figure 4.8b). The CMRSET P-AET map is in line with the MDB Authority report stating that around 86% of the Basin contributes minimal to no runoff to the river system, except during floods (MDBA, 2021). The catchments draining the Great Dividing Range on the southeast and southern margins of the Basin make the largest contributions to total runoff, despite their smaller size (MDBA, 2023d). This is also supported by an average 20-year AET/P map (Figure B.3). CMRSET consistently depicts elevated AET/P ratios surpassing 1 across numerous pixels, indicating that a substantial portion of the Basin experiences water use exceeding precipitation inputs. This may arise from irrigation practices, where the water applied to support agricultural activities exceeds natural rainfall, thus inflating the AET values.

Based on our results, the CMRSET model has proven reliable and accurate in estimating AET, supported by a water balance estimation close to the Basin outflow. Guerschman et al. (2022) independently evaluated the CMRSET model by comparing its mean annual precipitation and AET estimates with measured streamflow data from 638 catchments in Australia. The evaluation revealed that the CMRSET model had an RMSE (root mean square error) of 0.50 mm/d (relative RMSE of 0.26) and an R^2 value of 0.70 when considering long-term differences (5 years or more).

The divergence in AET magnitudes between the CMRSET and MODIS datasets, particularly the higher AET/P ratios observed in CMRSET, can be attributed to differences in the algorithms and inputs used by these two products. For instance, Weerasinghe et al. (2020) noted that MODIS reliance on vapour pressure deficit often led to significant underestimations of AET during warmer periods. Zhao et al. (2019) found that land cover and rainfall significantly influence the reliability of AET products, particularly the areas with intensive land uses showed a higher correlation in inaccuracies of AET products. The MODIS algorithm assumes uniform biophysical parameters, without considering factors like soil water content, terrain, or subpixel variability, which impacts AET accuracy. A study by Sharma et al. (2016) showed that Landsat-derived AET estimates can explain 91% of the variability in the observed AET, in contrast to 59% by MODIS-based estimates. According

to Zhang et al. (2016) study in Jordan, MODIS data tends to underestimate AET by up to 50% in irrigated agricultural lands and also shows underestimations for sparsely vegetated areas. Given that the Murray-Darling Basin consists predominantly of natural terrestrial vegetation, along with extensive agricultural areas, these factors could contribute to the underestimation of AET using MODIS AET. Moreover, the large pixel size of MODIS and its inability to capture subpixel heterogeneities can result in inaccurate AET estimates. Intensive water uses like agricultural areas may have significant localised impacts that are missed at the 500m resolution. In contrast, the finer resolution of CMRSET is better suited for capturing these small-scale variations, which could explain the lower AET/P ratios observed in MODIS data compared to CMRSET.

The underestimation of AET can severely impact water balance calculations (Liu et al., 2020). Notably, this issue is particularly pronounced in arid and temperate regions, where such errors may lead to overestimated water availability, affecting reservoir operations, agricultural water distribution, and drought management strategies (Ruud et al., 2004). Moreover, these underestimations introduce biases into hydrological models, affecting the accuracy of soil moisture and streamflow simulations, which are crucial for long-term climate change projections (Ding et al., 2022). During model calibration, the incorporation of different AET datasets results in variable parameter estimates, influencing model sensitivity and water resource assessments (Taia et al., 2023). For instance, in arid zones where accurate water availability predictions are critical, any discrepancies can result in severe resource mismanagement based on erroneous data suggesting inflated water availability. The implications of these findings are significant, spanning water resources management and hydrological forecasting.

4.5.2 Spatiotemporal dynamics of CMRSET AET and AET/P

The Kiewa, Mitta Mitta, Ovens, and Upper Murray catchments exhibit higher rates of AET compared to other catchments. This observation is attributed to substantial rainfall and extensive forest coverage in these areas. For instance, approximately 80% of the Upper Murray is forested (MDBA, 2023f). Additionally, a higher rate of AET over CTV suggests more intensive agricultural practices. For instance, in the Kiewa catchment, which is characterised by intensive cultivation of crops such as tobacco, there is a notable increase in AET due to heightened water demands (Guang et al., 2019; MDBA, 2023b). Conversely, the Barwon-Darling, Lower Darling, Lower Murray, Paroo, and Warrego catchments display lower average AET values, corresponding to lower rainfall in these areas. The western part of MDB has a higher temporal variation of rainfall, consistent with the literature (Heimhuber et al., 2016, Evans et al., 2010). The El Niño-Southern Oscillation (ENSO) also plays a role, with El Niño events causing drier conditions and potentially exacerbating temporal variations (Freund et al., 2021).

The time series data from CMRSET demonstrates consistently high AET/P ratios, typically exceeding 1, primarily due to decreased rainfall in last two decades. The finding of Weligamage

(2023) in the Victoria, Australia showed that despite varying precipitation levels, AET remained relatively stable from the pre-drought to the Millennium Drought periods. This stability resulted in higher AET/P ratios during the drought compared to pre-drought conditions, when significant decreases in rainfall were recorded. In the MDB, the predominance of irrigated agriculture has a substantial impact on these ratios, as irrigation sustains AET levels that often surpass precipitation. The MDB's catchments, being more water-limited than energy-limited, display a greater sensitivity to rainfall fluctuations over potential energy changes. Zhang et al. (2001) identified canopy resistance and the availability of water stored in the soil as key determinants of ET in drier conditions. This sensitivity is further evidenced in the western parts of the MDB, where lower rainfall increases the variability in AET/P ratios, a finding echoed by Massari et al. (2022). They noted that changes in the rainfall-runoff relationship occur regardless of whether a catchment is water-limited or energy-limited.

Figure 4.6a from the Paroo and Lower Darling catchments illustrates the high spatial and temporal variability of AET and AET/P in arid zones, contrasting with their lower spatial but high temporal variability in rainfall. In such areas, when water is scarce, AET is limited by the available moisture, leading to similar AET levels across different land covers—whether forest, grassland, or agricultural fields. In contrast, humid areas, with their frequent and uniform rainfall, exhibit a stable relationship between precipitation and AET, resulting in lower spatial variability in AET/P ratios. This stability reflects the non-limiting nature of water, which supports consistent AET rates across the landscape.

In arid regions, the high spatial variability of AET/P is driven by sporadic and scarce precipitation, patchy vegetation, variable soil moisture, and elevated evaporative demands. These factors contribute to a heterogeneous distribution of AET, exacerbated by topographical influences that can significantly amplify variability. For instance, valleys may receive more runoff, thus exhibiting higher AET, while adjacent ridges may experience drier conditions. Conversely, more consistent water availability and homogenous vegetation cover in humid regions lead to more uniform AET patterns and lower spatial variability in AET/P ratios. Here, the consistent precipitation mitigates the impact of topographical differences on water distribution.

The AET/P time series of CMRSET data shows an increase in the AET/P ratio after 2016 (Figure 4.5b). Following 2016, there were dry conditions in the MDB, with 12 consecutive seasons of below-average rainfall, the longest since 1900 (King et al., 2020). The AET/P values exceeding 1 from 2017 to 2020 can be attributed to a pattern of exceptionally wet years followed by subsequent dry years. While AET/P ratios generally reduce disparities among various land covers, this trend is not universally observed across different catchments (Figure 4.6b, B.5). In more arid areas of MDB (e.g., Northwest), the temporal variation of AET/P is higher than in humid areas (e.g., Southeast) due to the high variation of both AET and P in the northwest regions (Figure 4.4, 4.6a). Conversely, the southeast areas exhibit a low spatial and temporal variation of AET/P (Figure 4.6b), which can be attributed to the low variation of both P and AET (Figure 4.4, 4.6a). This suggests that temporal

variability in AET and P is predominantly controlled by climatic factors. In contrast, a high spatial variability of AET/P is observed in arid areas (Figure 4.6b), driven by a high spatial variability of AET and a low variability of P, highlighting the impact of land use on AET.

Mitta Mitta, Ovens, Kiewa, and Upper Murray were the only catchments that exhibited an average AET/P ratio of less than 1. Spatial-temporal analysis indicated low temporal and low to moderate spatial variability in these catchments. This suggests a more consistent and predictable rainfall pattern over time within these areas. On the other hand, the Namoi, Gwydir, Border Rivers, and Mitta Mitta catchments displayed relatively low variability in rainfall at both temporal and spatial scales (Figure 4.4).

The analysis of AET across different land covers from 2001 to 2020 revealed significant changes. While a 20-year period may be relatively short for robust trend analysis, few catchments showed significant trends. The Kiewa and Mitta Mitta catchments (Table 4.2) showed a consistent increase in overall AET, aligning with trends observed in NTV. This pattern suggests that changes in land cover, potentially driven by commercial forest management practices, may contribute to higher evapotranspiration rates in these areas, as discussed by Sun et al. (2022). Further, In the Mitta Mitta catchment, dams alter natural flow patterns and water availability (MDBA, 2023e), further influencing evapotranspiration rates (Zhan et al., 2019). The stable AET trend over most of the catchments NTV highlights the resilience of these ecosystems, while the decreasing trend of AET over NS in Border Rivers and Gwydir points to potential changes in soil moisture. Similarly, the development of irrigated agriculture, diverse horticultural industry and dryland agriculture in the Lower Murray explain the observed increase in evapotranspiration in the CTV land cover type (MDBA, 2023c).

The observed variations in AET across CTV suggest changes in agricultural practices, including both irrigated and dryland agriculture. These fluctuations in AET are indicative of evolving agricultural practices and water management strategies. This aligns with the observations made by Xiao et al. (2024), who noted that both crop type and climatic changes collectively influence agricultural water dynamics.

The AET/P ratio showed no trend in all catchments. This implies that increases or decreases in AET are directly linked to similar changes in precipitation, keeping their ratio relatively stable. Analysing the time series data, it is evident that AET/P reduces the gap between different land cover types. This could mean that water availability from precipitation dictates the rate of evapotranspiration. It is consistent with research showing that climate change may play a role as shifts in precipitation patterns and rising temperatures can affect evapotranspiration rates (Feng et al., 2019; Konapala et al., 2020).

There was no AET/P trend within NTV in all catchments. The lack of trend in AET/P could suggest that ecosystems are adapting to changing conditions in a way that maintains a balance between

water use and water availability. In the Condamine, the rise in AET/P within CTV can be attributed to increased irrigation in the drier areas with limited water storage, where agricultural practices and irrigation intensify AET relative to precipitation. Similarly, an upward trend in AET/P over NS land cover is observed in the Moonie catchment, which can be attributed to its semi-arid climate and irregular river flows, which contribute to soil saturation and moisture availability, leading to higher AET/P. Furthermore, the impact of landscape alterations and groundwater availability may contribute to this trend (Te Wierik et al., 2021; Glanville et al., 2023).

The variations in AET and AET/P across land covers and catchments are influenced, in part, by differences in precipitation patterns associated with each land-cover type. It may appear counterintuitive that precipitation differs among CTV, NTV, and NS categories since rainfall patterns are generally expected to be spatially uniform at broader scales. However, these land-cover classes are not evenly distributed across the MDB. Each category tends to occur in regions with distinct climatic regimes, topographies, and moisture gradients. For example, areas classified as NS may be located in more arid zones with inherently lower precipitation, whereas regions dominated by CTV or NTV might coincide with river corridors, floodplains, or areas that receive comparatively greater rainfall due to local climate variability or orographic effects. Additionally, the spatial resolution and interpolation methods used in gridded precipitation datasets can introduce differences in estimated rainfall totals across varying landscapes. Thus, differences in precipitation values reflect the geographic and climatic characteristics of where each land-cover category predominantly occurs, rather than indicating that rainfall itself is intrinsically different over identical land areas.

4.5.3 Differences in AET between LULC

Large-scale AET modelling across diverse land covers is challenging due to the variability and complexity of land surface characteristics, including spatial heterogeneity, temporal changes, soil moisture variations and human impacts (Yang et al., 2023). We employed ANOVA and t-tests to evaluate the disparity in AET across major land covers to understand if the CMRSET dataset accurately reflects these differences on a larger scale. Our findings revealed a lack of significant difference between average AET over major land cover types in Gwydir, Condamine, and Border River, which can be attributed to the high value of AET over NS land cover in these catchments. For example, Gwydir's AET over NS land cover has been higher than NTV and CTV for many years (Figure B.5). Similarly, the Condamine-Balonne catchment has a high AET over NS, which can stem from water harvesting for irrigation, contributing to water availability in the soil (MDBA, 2023a). What stands out from their AET time series (Figure B.5) is the consistently higher evapotranspiration over NS compared to CTV and NTV during the millennium drought. Soil moisture levels can be uniformly low across different land covers in drought periods; this can result in similar AET rates regardless of the vegetation or land cover type (Figure B.5). Furthermore, the Gwydir catchment is characterised by summer-dominant rainfall. Under conditions of summer-dominant rainfall, bare surfaces can exhibit higher AET compared to areas with dense canopy vegetation due to the direct exposure of

soil moisture to evaporative forces and the absence of moderating microclimatic effects provided by vegetation. Vegetation under drought stress reduces transpiration through stomatal closure and decreased leaf area, thereby limiting its AET. In contrast, bare soil lacks these biological control mechanisms. Even small amounts of moisture—such as from light rainfall events or dew—evaporate directly from the soil surface. This direct evaporation can exceed the heavily curtailed transpiration of drought-stressed vegetation, leading to relatively higher AET rates for NS despite the overall scarcity of water.

The pairwise comparison of land covers shows that the catchments in the northern part of the MDB mostly lack significant differences in average AET and AET/P over land covers. Generally, the northern and western parts of the MDB tend to be drier compared to the southern part. Zhao et al. (2019) found a disparity in the consistency of AET products in drier catchments, like the Condamine-Balonne, in contrast to the greater consistency found in more humid areas, such as the Upper Murray. This may help explain the lack of significant difference in AET and AET/P between land covers. The few catchments that showed significant differences between both AET and AET/P for different land covers are in the southern part of the Basin (Figure 4.9), which generally has higher water availability and receives more precipitation. Similarly, the study by Gao et al. (2007) in a region in southeastern China demonstrated that annual AET closely follows the trend of rainfall. Despite an increase in temperature, AET exhibited a decreasing trend, mirroring the trend in rainfall.

The question arises: does the variability of AET follow that of PET? To investigate this, we analysed the AET/P and PET/P ratios across 20-year averages and spatial variability across all catchments (Figure B.4). Generally, AET/P and PET/P long-term average tend to follow each other closely, indicating a balance between actual water usage by vegetation and atmospheric water demand, given the precipitation. However, exceptions are noted in the Moonie, Goulburn-Broken, and Campaspe regions. These results, along with the t-test results (Figure 4.9 and Figure B.8), show that the land cover impact is prominent in AET. The contrasting patterns of spatial variability of PET/P and AET/P in northwest areas suggest a land use effect because AET is calculated as AET =K*PET, where K is closely related to land cover types (Figure B.4).

DEA Level 3 data provides valuable information about land cover in the MDB, but some uncertainties affect its accuracy and reliability. How data is categorised and classified can impact accuracy, leading to inconsistencies and difficulties in comparing data over time and locations. The dataset's overall accuracy is 80%, with challenges in classifying cultivated vegetation and bare surfaces (Tissott & Mueller, 2022). Limitations exist in distinguishing managed plantations and orchards from natural vegetation, and misclassifications can occur due to natural events that resemble cultivated land behaviour. Despite these uncertainties, the data remains valuable for national-scale analysis when detailed information is lacking.

4.6 Conclusions

In this study, we analysed the actual evapotranspiration in the Murray Darling Basin using CMRSET and MODIS datasets. The findings demonstrate a reasonable alignment between these datasets in overall AET patterns, yet with significant variations in magnitude. Specifically, the CMRSET dataset indicated higher AET rates for all analysed land cover types, including Natural Terrestrial vegetation, Cultivated Terrestrial Vegetation and Natural Bare Surface. A Basin-scale water balance assessment indicated that MODIS considerably underestimates AET, thereby underscoring the heightened precision of CMRSET in estimating water balances. Consequently, CMRSET was selected for further analysis.

The 2001-2020 trend analysis revealed an increasing AET trend in the southeastern catchments and the northern part of the MDB in the CMRSET dataset. In the study of AET across all analysed land cover types in the MDB, most catchments exhibited significant differences, primarily in AET values, but not in AET/P. However, this pattern was not uniform across all regions. Assuming the CMRSET dataset accurately reflects real-world evapotranspiration, the minimal variation in AET between land cover types, observed at this broad categorisation and catchment scale, could either imply a dominant role of rainfall over land cover in determining AET, or it might indicate a need for further refinement of the model employed in this analysis to more accurately detect such variations.

An observed pattern indicated that catchments exhibiting significant differences in both AET and AET/P were generally in the southern part and in those areas with higher levels of rainfall. However, it is important to note that this trend was not consistently observed across all catchments. Unique amongst these, the Campaspe catchment displayed significant differences in AET/P between CTV and NTV. This indicates a nuanced interaction of hydrological processes, which varies considerably across different catchments within the MDB.

This study illustrates the complex and varied hydrological processes across different catchments in the MDB, highlighting the need for tailored management strategies to address the Basin's diverse hydrological characteristics. It emphasises the significant influence of regional climate, terrain, and land cover changes on AET. Understanding these factors is essential for improving AET estimation, identifying product limitations, and refining calibration and validation processes, especially considering ongoing climate and land cover change. The study also stresses the importance of accurate and reliable water data, robust monitoring, and transparent reporting in the MDB. Data availability and quality can vary by source, region, and scale. Differences in data collection methods, the aggregation of information from multiple jurisdictions, and uneven reporting standards can lead to gaps and inconsistencies. Discrepancies between MDB authority outflow data and outflow estimation with MODIS data highlight the need for precise water accounting, which is critical for managing various needs and understanding crop and vegetation water requirements. Improving data

harmonisation, accessibility, and timeliness would support more effective policy evaluations and environmental management decisions.

With the MDB facing climate change challenges, including drying and warming trends, continuous monitoring and assessing water recovery targets becomes imperative for effective decision-making and climate change adaptation. Accurate quantification of AET, as a fundamental component of the water balance, is increasingly recognised as key for robust water resource management. The findings advocate for future research concentrating on detailed land cover analysis to enhance AET estimation accuracy, which is essential for developing robust water security strategies under changing climatic conditions.

4.7 References

Alexandra, J. (2023). Climate risk assessment in the MDB–a review. Australian Journal of Water Resources, 27(1), 18–30. https://doi.org/10.1080/13241583.2022.2157107

Allen, R. G., Tasumi, M., Morse, A., Trezza, R., Wright, J. L., Bastiaanssen, W., Kramber, W., Lorite, I., & Robison, C. W. (2007). Satellite-based energy balance for Mapping Evapotranspiration with Internalized Calibration (METRIC)—Applications. Journal of Irrigation and Drainage Engineering, 133(4), 395–406. https://doi.org/10.1061/(asce)0733-9437(2007)133:4(395)

Baik, J., Liaqat, U. W., & Choi, M. (2018). Assessment of satellite- and reanalysis-based evapotranspiration products with two blending approaches over the complex landscapes and climates of Australia. Agricultural and Forest Meteorology, 263, 388–398. https://doi.org/10.1016/j.agrformet.2018.09.007

Beaulieu, E., Lucas, Y., Viville, D., Chabaux, F., Ackerer, P., Goddéris, Y., & Pierret, M. C. (2016). Hydrological and vegetation response to climate change in a forested mountainous catchment. In Modeling Earth Systems and Environment (Vol. 2, Issue 4, pp. 1–15). https://doi.org/10.1007/s40808-016-0244-1

Beavis, S. G., Wong, V. N. L., Mosley, L. M., Baldwin, D. S., Latimer, J. O., Lane, P., & Lal, A. (2023). Water quality risks in the Murray-Darling basin. Australian Journal of Water Resources, 27(1), 85–102. https://doi.org/10.1080/13241583.2022.2163475

Bretreger, D., Yeo, I. Y., Hancock, G., & Willgoose, G. (2020). Monitoring irrigation using Landsat observations and climate data over regional scales in the Murray-Darling Basin. Journal of Hydrology, 590, 125356. https://doi.org/10.1016/j.jhydrol.2020.125356

Brown, P., Colloff, M. J., Slattery, M., Johnson, W., & Guarino, F. (2022). An unsustainable level of take: on-farm storages and floodplain water harvesting in the northern Murray–Darling Basin, Australia. Australian Journal of Water Resources, 26(1), 43–58. https://doi.org/10.1080/13241583.2022.2042061

Brümmer, C., Black, T. A., Jassal, R. S., Grant, N. J., Spittlehouse, D. L., Chen, B., Nesic, Z., Amiro, B. D., Arain, M. A., Barr, A. G., Bourque, C. P. A., Coursolle, C., Dunn, A. L., Flanagan, L. B., Humphreys, E. R., Lafleur, P. M., Margolis, H. A., McCaughey, J. H., & Wofsy, S. C. (2012). How climate and vegetation type influence evapotranspiration and water use efficiency in Canadian forest, peatland and grassland ecosystems. Agricultural and Forest Meteorology, 153, 14–30. https://doi.org/10.1016/j.agrformet.2011.04.008

Chen, J., Yu, Z., Zhu, Y., & Yang, C. (2011). Relationship between land use and evapotranspiration-a case study of the Wudaogou area in Huaihe River basin. Procedia Environmental Sciences, 10(PART A), 491–498. https://doi.org/10.1016/j.proenv.2011.09.080

Cleugh, H. A., Leuning, R., Mu, Q., & Running, S. W. (2007). Regional evaporation estimates from flux tower and MODIS satellite data. Remote Sensing of Environment, 106(3), 285–304. https://doi.org/10.1016/j.rse.2006.07.007

Cornish, P. M., & Vertessy, R. A. (2001). Forest age-induced changes in evapotranspiration and water yield in a eucalypt forest. Journal of Hydrology, 242(1–2), 43–63. https://doi.org/10.1016/S0022-1694(00)00384-X

Crosbie, R. S., & Rachakonda, P. K. (2021). Constraining probabilistic chloride mass-balance recharge estimates using baseflow and remotely sensed evapotranspiration: the Cambrian Limestone Aquifer in northern Australia. Hydrogeology Journal, 29(4), 1399–1419. https://doi.org/10.1007/s10040-021-02323-1

CSIRO. (2022). State of the Climate, 2022. http://www.bom.gov.au/state-of-the-climate/, (Accessed June 2024).

Deus, D., & Gloaguen, R. (2013). Remote sensing analysis of lake dynamics in semi-arid regions: Implication for water resource management. Lake Manyara, East African Rift, Northern Tanzania. Water (Switzerland), 5(2), 698–727. https://doi.org/10.3390/w5020698

Di Gregorio, A. (2005). Land cover classification system: Classification concepts and user manual: LCCS. Food and Agriculture Organization of the United Nations. https://www.fao.org/4/y7220e/y7220e00.htm, (Accessed in June 2024).

Di Gregorio, A., & Jansen, L.J. (1998). A new concept for a land cover classification system. The Land. 2, 55-65.

Di Gregorio, A., and Jansen, L. J. M. (2000). Land Cover Classification System (LCCS): Classification concepts and user manual. Fao, 53, 179.

Dimitriadou, S., & Nikolakopoulos, K. G. (2020). Remote sensing methods to estimate evapotranspiration incorporating MODIS derived data and applications over Greece: A review. In Eighth International Conference on Remote Sensing and Geoinformation of the Environment (RSCy2020) (Vol. 11524). SPIE. https://doi.org/10.1117/12.2570780

Ding, J., & Zhu, Q. (2022). The accuracy of multisource evapotranspiration products and their applicability in streamflow simulation over a large catchment of Southern China. Journal of Hydrology: Regional Studies, 41, 101092. https://doi.org/10.1016/j.ejrh.2022.101092

Dreverman, D. (2013) Murray-Darling Basin Authority/David Dreverman, Responding to extreme drought in the Murray-Darling Basin, Australia. In: Schwabe, K., Albiac, J., Connor, J., Hassan, R., Meza González, L. (Eds.), Drought in arid and semi-arid regions. Springer, Dordrecht, 2013, pp. 425–435. https://doi.org/10.1007/978-94-007-6636-5_24

ESRI. (2023). ArcGIS Pro: Release 3.1.3. Redlands, CA: Environmental Systems Research Institute.

Evans, A., Jones, D., Lellyett, S., Smalley, R., & Australia. Bureau of Meteorology. (2020). An enhanced gridded rainfall analysis scheme for Australia.

Evans, J. P., & McCabe, M. F. (2010). Regional climate simulation over Australia's Murray-Darling basin: A multitemporal assessment. Journal of Geophysical Research Atmospheres, 115(14). https://doi.org/10.1029/2010JD013816

Feng, S., Liu, J., Zhang, Q., Zhang, Y., Singh, V. P., Gu, X., & Sun, P. (2020). A global quantitation of factors affecting evapotranspiration variability. Journal of Hydrology, 584, 124688. https://doi.org/10.1016/j.jhydrol.2020.124688

Feng, X., Thompson, S. E., Woods, R., & Porporato, A. (2019). Quantifying asynchronicity of precipitation and potential evapotranspiration in Mediterranean climates. Geophysical Research Letters, 46(24), 14692–14701. https://doi.org/10.1029/2019GL085653

Foley, J. A., DeFries, R., Asner, G. P., Barford, C., Bonan, G., Carpenter, S. R., Chapin, F. S., Coe, M. T., Daily, G. C., Gibbs, H. K., Helkowski, J. H., Holloway, T., Howard, E. A., Kucharik, C. J., Monfreda, C., Patz, J. A., Prentice, I. C., Ramankutty, N., & Snyder, P. K. (2005). Global consequences of land use. Science, 309(5734), 570–574. https://doi.org/10.1126/science.1111772

Freund, M. B., Marshall, A. G., Wheeler, M. C., & Brown, J. N. (2021). Central Pacific El Niño as a precursor to summer drought-breaking rainfall over southeastern Australia. Geophysical Research Letters, 48(7), e2020GL091131. https://doi.org/10.1029/2020GL091131

Gallant, A. J. E., & Gergis, J. (2011). An experimental streamflow reconstruction for the River Murray, Australia, 1783-1988. Water Resources Research, 47(4). https://doi.org/10.1029/2010WR009832

Gao, G., Chen, D., Xu, C. Y., & Simelton, E. (2007). Trend of estimated actual evapotranspiration over China during 1960–2002. J Geophysical Res: Atmospheres, 112(D11). https://doi.org/10.1029/2006JD008010.

Garrigues, S., Olioso, A., Calvet, J. C., Martin, E., Lafont, S., Moulin, S., Chanzy, A., Marloie, O., Buis, S., Desfonds, V., Bertrand, N., & Renard, D. (2015). Evaluation of land surface model simulations of evapotranspiration over a 12-year crop succession: Impact of soil hydraulic and vegetation properties. Hydrology and Earth System Sciences, 19(7), 3109–3131. https://doi.org/10.5194/hess-19-3109-2015

Gelsinari, S., Pauwels, V. R. N., Daly, E., Van Dam, J., Uijlenhoet, R., Fewster-Young, N., & Doble, R. (2021). Unsaturated zone model complexity for the assimilation of evapotranspiration rates in groundwater modelling. Hydrology and Earth System Sciences, 25(4), 2261–2277. https://doi.org/10.5194/hess-25-2261-2021

Gilbert, R.O. (1987). Statistical methods for environmental pollution monitoring. Wiley, New York. https://doi.org/10.2307/2531935

Gissing, A., Timms, M., Browning, S., Crompton, R., & McAneney, J. (2022). Compound natural disasters in Australia: A historical analysis. Environmental Hazards, 21(2), 159–173. https://doi.org/10.1080/17477891.2021.1932405

Glanville, K., Sheldon, F., Butler, D., & Capon, S. (2023). Effects and significance of groundwater for vegetation: A systematic review. Science of the Total Environment, 875, 162577. https://doi.org/10.1016/j.scitotenv.2023.162577

Grafton, R. Q., Pittock, J., Davis, R., Williams, J., Fu, G., Warburton, M., Udall, B., Mckenzie, R., Yu, X., Che, N., Connell, D., Jiang, Q., Kompas, T., Lynch, A., Norris, R., Possingham, H., &

Quiggin, J. (2013). Global insights into water resources, climate change and governance. Nature Climate Change, 3(4), 315–321. https://doi.org/10.1038/nclimate1746

Guang, J., Shao, X., Miao, Q., Yang, X., Gao, C., Ding, F., & Yuan, Y. (2019). Effects of irrigation amount and irrigation frequency on flue-cured tobacco evapotranspiration and water use efficiency based on three-year field drip-irrigated experiments. Agronomy 9, 624. https://doi.org/10.3390/agronomy9100624

Guerschman, J. P., McVicar, T. R., Vleeshower, J., Van Niel, T. G., Peña-Arancibia, J. L., & Chen, Y. (2022). Estimating actual evapotranspiration at field-to-continent scales by calibrating the CMRSET algorithm with MODIS, VIIRS, Landsat and Sentinel-2 data. Journal of Hydrology, 605, 127318. https://doi.org/10.1016/j.jhydrol.2021.127318

Guerschman, J. P., Van Dijk, A. I. J. M., Mattersdorf, G., Beringer, J., Hutley, L. B., Leuning, R., Pipunic, R. C., & Sherman, B. S. (2009). Scaling of potential evapotranspiration with MODIS data reproduces flux observations and catchment water balance observations across Australia. Journal of Hydrology, 369(1–2), 107–119. https://doi.org/10.1016/j.jhydrol.2009.02.013

Hart, B. T. (2016). The Australian Murray–Darling Basin Plan: Challenges in its implementation (part 1). International Journal of Water Resources Development, 32(6), 819–834. https://doi.org/10.1080/07900627.2015.1083847

He, H., Zhou, J., & Zhang, W. (2008). Modelling the impacts of environmental changes on hydrological regimes in the Hei River Watershed, China. Global and Planetary Change, 61(3–4), 175–193. https://doi.org/10.1016/j.gloplacha.2007.08.012

Heimhuber, V., Tulbure, M. G., & Broich, M. (2016). Modeling 25 years of spatio-temporal surface water and inundation dynamics on large river basin scale using time series of earth observation data. Hydrology and Earth System Sciences, 20(6), 2227–2250. https://doi.org/10.5194/hess-20-2227-2016

Hu, G., Jia, L., & Menenti, M. (2015). Comparison of MOD16 and LSA-SAF MSG evapotranspiration products over Europe for 2011. Remote Sensing of Environment, 156, 510–526. https://doi.org/10.1016/j.rse.2014.10.017

Irmak, S. (2008). Evapotranspiration. In Encyclopedia of Ecology, Five-Volume Set (pp. 1432–1438). Elsevier Inc.

Jin, Z., Liang, W., Yang, Y., Zhang, W., Yan, J., Chen, X., Li, S., & Mo, X. (2017). Separating vegetation greening and climate change controls on evapotranspiration trend over the Loess Plateau. Scientific Reports, 7(1), 8191. https://doi.org/10.1038/s41598-017-08477-x

Karimi, P., Bongani, B., Blatchford, M., & de Fraiture, C. (2019). Global satellite-based ET products for the local level irrigation management: An application of irrigation performance assessment in the Sugarbelt of Swaziland. Remote Sensing, 11(6), 705. https://doi.org/10.3390/rs11060705

Kendall, M.G. (1975). Rank correlation methods, 4th Edition. Charles Griffin, London.

Kim, H. W., Hwang, K., Mu, Q., Lee, S. O., & Choi, M. (2012). Validation of MODIS 16 global terrestrial evapotranspiration products in various climates and land cover types in Asia. KSCE Journal of Civil Engineering, 16(2), 229–238. https://doi.org/10.1007/s12205-012-0006-1

King, A. D., Pitman, A. J., Henley, B. J., Ukkola, A. M., & Brown, J. R. (2020). The role of climate variability in Australian drought. Nature Climate Change, 10(3), 177–179. https://doi.org/10.1038/s41558-020-0718-z

King, E., Van-Niel, T. G., Van-Dijk, A. I. J. M., Wang, Z., Paget, M., Raupach, T., Guerschman, J., Haverd, V., McVicar, T., Miltenburg, I., Raupach, M., Renzullo, L., & Zhang, Y. (2011). Actual evapotranspiration estimates for Australia. Inter-comparison and Evaluation. Water Information Research and Development Alliance Science Symposium, Melbourne, Australia, 165. https://doi.org/10.4225/08/5852dd7484ac3

Konapala, G., Mishra, A. K., Wada, Y., & Mann, M. E. (2020). Climate change will affect global water availability through compounding changes in seasonal precipitation and evaporation. Nature Communications, 11(1), 3044. https://doi.org/10.1038/s41467-020-16757-w

Kunnath-Poovakka, A., Ryu, D., Eldho, T. I., & George, B. (2021). Parameter uncertainty of a hydrologic model calibrated with remotely sensed evapotranspiration and soil moisture. Journal of Hydrologic Engineering, 26(3), 4020070. https://doi.org/10.1061/(asce)he.1943-5584.0002055

Leblanc, M. J., Tregoning, P., Ramillien, G., Tweed, S. O., & Fakes, A. (2009). Basin-scale, integrated observations of the early 21st century multiyear drought in Southeast Australia. Water Resources Research, 45(4). https://doi.org/10.1029/2008WR007333

Leblanc, M., Tweed, S., Van Dijk, A., & Timbal, B. (2012). A review of historic and future hydrological changes in the Murray-Darling Basin. Glob. Planet. Change 80–81, 226–246. https://doi.org/10.1016/j.gloplacha.2011.10.012.

Li, G., Zhang, F., Jing, Y., Liu, Y., & Sun, G. (2017). Response of evapotranspiration to changes in land use and land cover and climate in China during 2001–2013. Science of the Total Environment, 596–597, 256–265. https://doi.org/10.1016/j.scitotenv.2017.04.080

Li, X., Zou, L., Xia, J., Dou, M., Li, H., & Song, Z. (2022). Untangling the effects of climate change and land use/cover change on spatiotemporal variation of evapotranspiration over China. Journal of Hydrology, 612, 128189. https://doi.org/10.1016/j.jhydrol.2022.128189

Lin, N., Jiang, R., Liu, Q., Yang, H., Liu, H., & Yang, Q., (2022). Quantifying the spatiotemporal variation of evapotranspiration of different land cover types and the contribution of its associated factors in the Xiliao River Plain. Remote Sens. 14, 252. https://doi.org/10.3390/rs14020252

Lin, N., Li, J., Jiang, R., Li, X., & Liu, S. (2023). Quantifying the spatiotemporal variation of NPP of different land cover types and the contribution of its associated factors in the Songnen Plain. Forests, 14(9), 252. https://doi.org/10.3390/f14091841

Liu, J., Xiong, Y., Tian, J., & Tan, Z. (2019). Spatiotemporal changes in evapotranspiration from an overexploited water resources basin in arid northern China and their implications for ecosystem management. Sustainability (Switzerland), 11(2), 445. https://doi.org/10.3390/su11020445

Liu, W., Hong, Y., Khan, S.I., Huang, M., Vieux, B., Caliskan, S., Grout, T., 2010. Actual evapotranspiration estimation for different land use and land cover in urban regions using Landsat 5 data. J. Appl. Remote Sens. 4, 041873. https://doi.org/10.1117/1.3525566.

Liu, Y., Zhuang, Q., Chen, M., Pan, Z., Tchebakova, N., Sokolov, A., Kicklighter, D., Melillo, J., Sirin, A., Zhou, G., He, Y., Chen, J., Bowling, L., Miralles, D., & Parfenova, E. (2013). Response of evapotranspiration and water availability to changing climate and land cover on the Mongolian Plateau during the 21st century. Global and Planetary Change, 108, 85–99. https://doi.org/10.1016/j.gloplacha.2013.06.008

Liu, Z., Cheng, L., Zhou, G., Chen, X., Lin, K., Zhang, W., Chen, X., & Zhou, P. (2020). Global response of evapotranspiration ratio to climate conditions and watershed characteristics in a Changing Environment. Journal of Geophysical Research: Atmospheres, 125(7). https://doi.org/10.1029/2020JD032371

Ma, Z., Yan, N., Wu, B., Stein, A., Zhu, W., & Zeng, H. (2019). Variation in actual evapotranspiration following changes in climate and vegetation cover during an ecological restoration period (2000–2015) in the Loess Plateau, China. Science of the Total Environment, 689, 534–545. https://doi.org/10.1016/j.scitotenv.2019.06.155

Mann, H. B. (1945). Nonparametric tests against trend. Econometrica, 13(3), 245. https://doi.org/10.2307/1907187

Massari, C., Avanzi, F., Bruno, G., Gabellani, S., Penna, D., & Camici, S. (2022). Evaporation enhancement drives the European water-budget deficit during multi-year droughts. Hydrology and Earth System Sciences, 26(6), 1527–1543. https://doi.org/10.5194/hess-26-1527-2022

McColl, K. A., Salvucci, G. D., & Gentine, P. (2019). Surface flux equilibrium theory explains an empirical estimate of water-limited daily evapotranspiration. Journal of Advances in Modeling Earth Systems, 11(7), 2036–2049. https://doi.org/10.1029/2019MS001685

McShane, R. R., Driscoll, K. P., & Sando, R. (2017). A review of surface energy balance models for estimating actual evapotranspiration with remote sensing at high spatiotemporal resolution over large extents. Scientific Investigations Report 2017-5087, 19. https://doi.org/10.3133/sir20175087

McVicar, T. R., Van Niel, T. G., & Lingtao, L. (2017). Remote sensing of land-use-specific actual evapotranspiration of entire catchments containing plantations. CSIRO. https://www.fwpa.com.au/images/resources/-2017/Final_Report_PNC286-1112.pdf (Accessed August 2021).

MDBA. (2018). EY Report: Analysis of efficiency measures in the Murray–Darling Basin. https://www.mdba.gov.au/publications-and-data/publications/ey-report-analysis-efficiency-measures-murray-darling-basin, (Accessed in June 2024).
MDBA. (2021). Murray Darling Basin Authorities, Climates and climate change. https://www.mdba.gov.au/importance-murray-darling-basin/environment/climate-change, (Accessed in June 2024).
MDBA. (2023a). Murray Darling Basin Authorities, Condamine–Balonne catchment. https://www.mdba.gov.au/basin/catchments/northern-basin-catchments/condamine-balonne-catchment, (Accessed in June 2024).
MDBA. (2023b). Murray Darling Basin Authorities, Kiewa catchment. https://www.mdba.gov.au/basin/catchments/southern-basin-catchments/kiewa-catchment, 2023b (Accessed in June 2024).
MDBA. (2023c). Murray Darling Basin Authorities, Lower Murray catchment. https://www.mdba.gov.au/basin/catchments/southern-basin-catchments/lower-murray-catchment, (Accessed in June 2024).
MDBA. (2023d). Murray Darling Basin Authorities, MDBA Climate. https://www.mdba.gov.au/climate-and-river-health/climate, (Accessed in June 2024).
MDBA. (2023e). Murray Darling Basin Authorities, Mitta Mitta catchment. https://www.mdba.gov.au/basin/catchments/southern-basin-catchments/mitta-mitta-catchment, (Accessed in June 2024).
MDBA (2023f). Murray Darling Basin Authorities, Upper Murray catchment. https://www.mdba.gov.au/basin/catchments/southern-basin-catchments/upper-murray-catchment, (Accessed in June 2024).
Nguyen, M. D., Baez-Villanueva, O. M., Bui, D. D., Nguyen, P. T., & Ribbe, L. (2020). Harmonization of landsat and sentinel 2 for crop monitoring in drought prone areas: Case studies of Ninh Thuan (Vietnam) and Bekaa (Lebanon). Remote Sensing, 12(2), 281. https://doi.org/10.3390/rs12020281
Pal, S., Dominguez, F., Bollatti, P., Oncley, S. P., Yang, Y., Alvarez, J., & Garcia, C. M. (2021). Investigating the effects of land use change on subsurface, surface, and atmospheric branches of the hydrologic cycle in central Argentina. Water Resources Research, 57(11), e2021WR029704. https://doi.org/10.1029/2021WR029704
Peña-Arancibia, J. L., Mahboob, M. G., Islam, A. T., Mainuddin, M., Yu, Y., Ahmad, M. D., Ibn Murad, K. F., Saha, K. K., Hossain, A., Moniruzzaman, M., Ticehurst, C., & Kong, D. (2021A). The Green revolution from space: Mapping the historic dynamics of main rice types in one of the world's food bowls. Remote Sensing Applications: Society and Environment, 21, 100460. https://doi.org/10.1016/j.rsase.2020.100460
Peña-Arancibia, J. L., McVicar, T. R., Kong, D., Guerschman, J. P., Van Niel, T. G., Vleeshower, J., & Li, L. T. (2021B). On the interchangeability of Landsat and MODIS data in the CMRSET actual evapotranspiration model – Comment on "Monitoring irrigation using Landsat observations and climate data over regional scales in the Murray-Darling Basin" by David Bretreger, In-Youn. Journal of Hydrology, 603, 127044. https://doi.org/10.1016/j.jhydrol.2021.127044
Petus, C., Lewis, M., & White, D. (2013). Monitoring temporal dynamics of Great Artesian Basin wetland vegetation, Australia, using MODIS NDVI. Ecological Indicators, 34, 41–52. https://doi.org/10.1016/j.ecolind.2013.04.009
Pradhan, N. R. (2019). Estimating growing-season root zone soil moisture from vegetation index-based evapotranspiration fraction and soil properties in the Northwest Mountain region, USA. Hydrological Sciences Journal, 64(7), 771–788. https://doi.org/10.1080/02626667.2019.1593417
Prosser, I. P., Chiew, F. H. S., & Smith, M. S. (2021). Adapting water management to climate change in the murray–darling basin, australia. Water (Switzerland), 13(18), 2504. https://doi.org/10.3390/w13182504
Running, S. W., Mu, Q., Zhao, M., & Moreno, A. (2019). MODIS global terrestrial evapotranspiration (ET) Product (MOD16A2/A3 and Year-end Gap-filled MOD16A2GF/A3GF) NASA Earth Observing System MODIS Land Algorithm. NASA EOSDIS Land Processes DAAC, 6, 1–37. https://doi.org/10.5067/MODIS/MOD16A3GF.006

Running, S., Mu, Q., & Zhao, M. (2021). MODIS/Terra gross primary productivity 8-Day L4 Global 500m SIN Grid V061, NASA EOSDIS Land Processes DAAC [data set]. In NASA EOSDIS Land Processes Distributed Active Archive Center. https://doi.org/https://doi.org/10.5067/MODIS/MOD16A2.061

Ruud, N., Harter, T., & Naugle, A. (2004). Estimation of groundwater pumping as closure to the water balance of a semi-arid, irrigated agricultural basin. Journal of Hydrology, 297(1–4), 51–73. https://doi.org/10.1016/j.jhydrol.2004.04.014

Salehi, S., Dehghani, M., Mortazavi, S. M., & Singh, V. P. (2020). Trend analysis and change point detection of seasonal and annual precipitation in Iran. International Journal of Climatology, 40(1), 308–323. https://doi.org/10.1002/joc.6211

Scanlon, B. R., Jolly, I., Sophocleous, M., & Zhang, L. (2007). Global impacts of conversions from natural to agricultural ecosystems on water resources: Quantity versus quality. Water Resources Research, 43(3). https://doi.org/10.1029/2006WR005486

Sen, P. K. (1968). Estimates of the regression coefficient based on Kendall's Tau. Journal of the American Statistical Association, 63(324), 1379–1389. https://doi.org/10.1080/01621459.1968.10480934

Sharma, V., Kilic, A., & Irmak, S. (2016). Impact of scale/resolution on evapotranspiration from Landsat and MODIS images. Water Resources Research, 52(3), 1800–1819. https://doi.org/10.1002/2015WR017772

Shen, H., Leblanc, M., Frappart, F., Seoane, L., O'Grady, D., Olioso, A., & Tweed, S. (2017). A comparative study of GRACE with continental evapotranspiration estimates in Australian semi-arid and arid basins: Sensitivity to climate variability and extremes. Water (Switzerland), 9(9), 614. https://doi.org/10.3390/w9090614

Simons, G.W.H., Bastiaanssen, W.G.M., Cheema, M.J.M., Ahmad, B., & Immerzeel, W.W. (2020). A novel method to quantify consumed fractions and non-consumptive use of irrigation water: application to the Indus Basin irrigation system of Pakistan. Agric. Water Manag. 236, 106174. https://doi.org/10.1016/j.agwat.2020.106174.

Sun, S., Liu, Y., Chen, H., Ju, W., Xu, C. Y., Liu, Y., Zhou, B., Zhou, Y., Zhou, Y., & Yu, M. (2022). Causes for the increases in both evapotranspiration and water yield over vegetated mainland China during the last two decades. Agricultural and Forest Meteorology, 324, 109118. https://doi.org/10.1016/j.agrformet.2022.109118

Swaffer, B. A., Habner, N. L., Holland, K. L., & Crosbie, R. S. (2020). Applying satellite-derived evapotranspiration rates to estimate the impact of vegetation on regional groundwater flux. Ecohydrology, 13(1), e2172. https://doi.org/10.1002/eco.2172

Taia, S., Scozzari, A., Erraioui, L., Kili, M., Mridekh, A., Haida, S., Chao, J., & El Mansouri, B. (2023). Comparing the ability of different remotely sensed evapotranspiration products in enhancing hydrological model performance and reducing prediction uncertainty. Ecological Informatics, 78, 102352. https://doi.org/10.1016/j.ecoinf.2023.102352

Tan, X., Wu, X., Huang, Z., Fu, J., Tan, X., Deng, S., Liu, Y., Gan, T. Y., & Liu, B. (2023). Increasing global precipitation whiplash due to anthropogenic greenhouse gas emissions. Nature Communications, 14(1), 2796. https://doi.org/10.1038/s41467-023-38510-9

te Wierik, S. A., Cammeraat, E. L. H., Gupta, J., & Artzy-Randrup, Y. A. (2021). Reviewing the impact of land use and land-use change on moisture recycling and precipitation patterns. Water Resources Research, 57(7), e2020WR029234. https://doi.org/10.1029/2020WR029234

Tissott, B., & Mueller, N. (2022). DEA Land Cover 25m. Geoscience Australia, Canberra. https://doi.org/10.26186/146090

Van Dijk, A.I., Beck, H.E., Crosbie, R.S., De Jeu, R.A., Liu, Y.Y., Podger, G. M., Timbal, B., & Viney, N. R. (2013). The Millennium Drought in southeast Australia (2001–2009): Natural and human causes and implications for water resources, ecosystems, economy, and society. Water Resour. Res. 49, 1040-1057. https://doi.org/10.1002/wrcr.20123.

Velpuri, N. M., Senay, G. B., Singh, R. K., Bohms, S., & Verdin, J. P. (2013). A comprehensive evaluation of two MODIS evapotranspiration products over the conterminous United States: Using point and gridded FLUXNET and water balance ET. Remote Sensing of Environment, 139, 35–49. https://doi.org/10.1016/j.rse.2013.07.013

Wang, G., & Cai, W. (2020). Two-year consecutive concurrences of positive Indian Ocean Dipole and Central Pacific El Niño preconditioned the 2019/2020 Australian "black summer" bushfires. Geoscience Letters, 7(1), 1–9. https://doi.org/10.1186/s40562-020-00168-2

Wang, Q., Cheng, L., Zhang, L., Liu, P., Qin, S., Liu, L., & Jing, Z. (2021). Quantifying the impacts of land-cover changes on global evapotranspiration based on the continuous remote sensing observations during 1982–2016. Journal of Hydrology, 598, 126231. https://doi.org/10.1016/j.jhydrol.2021.126231

Weerasinghe, I., Bastiaanssen, W., Mul, M., Jia, L., & van Griensven, A. (2020). Can we trust remote sensing evapotranspiration products over Africa? Hydrology and Earth System Sciences, 24(3), 1565–1586. https://doi.org/10.5194/hess-24-1565-2020

Wei, P., Chen, S., Wu, M., Deng, Y., Xu, H., Jia, Y., & Liu, F. (2021). Using the invest model to assess the impacts of climate and land use changes on water yield in the upstream regions of the shule river basin. Water (Switzerland), 13(9), 1250. https://doi.org/10.3390/w13091250

Weligamage, H. G., Fowler, K., Ryu, D., Saft, M., Peterson, T., & Peel, M. C. (2025). Vegetation as a driver of shifts in rainfall-runoff relationship: Synthesising hydrological evidence with remote sensing. Journal of Hydrology, 648, 132389. https://doi.org/10.1016/j.jhydrol.2024.132389

Wentworth Group of Concerned Scientists. (2020). Assessment of river flows in the Murray-Darling Basin : Observed versus expected flows under the Basin Plan 2012-2019 (Issue August, pp. 1–37). Wentworth Group of Concerned Scientists Sydney, Australia. www.wentworthgroup.org

Xiao, X., Zhang, J., & Liu, Y. (2024). Impacts of crop type and climate changes on agricultural water dynamics in Northeast China from 2000 to 2020. Remote Sens. 16, 1007. https://doi.org/10.3390/rs16061007.

Yang, L., Li, J., Sun, Z., Liu, J., Yang, Y., & Li, T. (2022). Daily actual evapotranspiration estimation of different land use types based on SEBAL model in the agro-pastoral ecotone of northwest China. PLoS ONE, 17(3 March), e0265138. https://doi.org/10.1371/journal.pone.0265138

Yang, Y., Roderick, M. L., Guo, H., Miralles, D. G., Zhang, L., Fatichi, S., Luo, X., Zhang, Y., McVicar, T. R., Tu, Z., Keenan, T. F., Fisher, J. B., Gan, R., Zhang, X., Piao, S., Zhang, B., & Yang, D. (2023). Evapotranspiration on a greening earth. Nature Reviews Earth and Environment, 4(9), 626–641. https://doi.org/10.1038/s43017-023-00464-3

Zhan, S., Song, C., Wang, J., Sheng, Y., & Quan, J. (2019). A global assessment of terrestrial evapotranspiration increase due to surface water area change. Earth's Future, 7(3), 266–282. https://doi.org/10.1029/2018EF001066

Zhang, L., Dawes, W. R., & Walker, G. R. (2001). Response of mean annual evapotranspiration to vegetation changes at catchment scale. Water Resources Research, 37(3), 701–708. https://doi.org/10.1029/2000WR900325

Zhang, H., Gorelick, S., Avisse, N., Tilmant, A., Rajsekhar, D., & Yoon, J. (2016). A new temperature-vegetation Triangle Algorithm with Variable Edges (TAVE) for Satellite-Based Actual Evapotranspiration Estimation. Remote Sensing, 8(9), 735. https://doi.org/10.3390/rs8090735

Zhang, K., Kimball, J. S., & Running, S. W. (2016). A review of remote sensing based actual evapotranspiration estimation. Wiley Interdisciplinary Reviews: Water, 3(6), 834–853. https://doi.org/10.1002/wat2.1168

Zhang, T., & Chen, Y. (2017). Analysis of dynamic spatiotemporal changes in actual evapotranspiration and its associated factors in the Pearl River Basin based on MOD16. Water (Switzerland), 9(11), 832. https://doi.org/10.3390/w9110832

Zhang, Y. Q., Chiew, F. H. S., Zhang, L., Leuning, R., & Cleugh, H. A. (2008). Estimating catchment evaporation and runoff using MODIS leaf area index and the Penman-Monteith equation. Water Resources Research, 44(10). https://doi.org/10.1029/2007WR006563

Zhao, Y., Lu, Z., & Wei, Y. (2019). An assessment of global precipitation and evapotranspiration products for regional applications. Remote Sensing, 11(9), 1077. https://doi.org/10.3390/rs11091077

CHAPTER 5

SYNTHESIS OF FINDINGS AND DIRECTIONS FOR FUTURE RESEARCH

5.1 Summary of findings

This thesis began with an overview of land cover and land use (LULC) conceptualisation in hydrological models. To identify the gaps in our understanding of LULC, we first investigated the main hydrological processes that are impacted by LULC and explored how they were conceptualised in models. Then, we discussed the processes within models that could be improved to integrate LULC dynamics effectively. This is followed by the important question of whether we have enough data to address LULC-related issues in models. Even if data is available, are the land cover dynamics significant enough that it is worth the effort of adding complexity to hydrological models? To answer these questions, we require context, so we chose the Murray-Darling Basin (MDB) as a case study. The MDB is an ideal location to study the impact of LULC dynamics on hydrological processes. It has undergone significant changes in LULC and climate, resulting in changes in its water balance, including vanishing flows that remain a mystery. The next study focused on actual evapotranspiration (AET) within the basin as the most important component in the water balance and hydrological modelling. We investigated AET over different land covers to learn how significant the differences are and what the possible drivers might be.

The key findings from each of the three specific studies are as follows:

- Hydrological modelling is further constrained by the reliance on traditional empirical formulas, which may not be suitable for rapidly changing landscapes. LULC changes can significantly influence hydrological processes with impacts that are highly diverse and influenced by factors beyond land cover alone. The scale and magnitude of these impacts can vary greatly, by factors like geographical location, slope, climate, and others, highlighting the importance of region-specific studies. Additionally, accurately modelling processes like interception and AET remains a significant challenge. LULC transformations challenge the foundational assumption of hydrological stationarity, and while dynamic LULC complicates the calibration process, it enhances model validity. Our research showed the need for a standardised LULC classification system, comprehensive modelling approaches that incorporate extensive validation. Current models often have untapped potential to fully utilise remote sensing data, which could significantly improve their accuracy and representation of real-world conditions. A critical perspective on modelling practices, acknowledging data constraints and embracing technological advancements, is essential for developing more reliable and representative simulations.
- The study revealed significant LULC changes in the MDB over 31 years. These changes, driven by climate variability, agricultural practices, water management initiatives, and natural disasters, vary substantially across the basin's catchments. Notably, there has been an increase in natural bare surfaces and a decrease in water bodies, along with shifts in agricultural land use, particularly in areas with significant water recovery efforts. A complex relationship existed

between land cover and rainfall, with differing responses observed in the northern and southern regions of the MDB. While Cultivated Terrestrial Vegetation (CTV) in land cover showed a general decreasing trend, the land use data showed that irrigated agriculture increased. It highlighted the importance of using different data sources according to the scale and purpose of the study. Further investigation into the rebound effect of water efficiency improvements is crucial for developing policies that promote truly sustainable water use. While water efficiency improvements have led to agricultural expansion, this has also resulted in a rebound effect. Although total water extractions are capped at 1995 levels, water recovered for the environment can be traded, allowing irrigators who have improved their water-use efficiency to sell part of their allocation. This market-based redistribution enables other agricultural enterprises to expand or intensify production, thus giving the appearance of increased agricultural water use despite stable overall extractions, highlighting the unintended consequences of some water recovery initiatives. The study emphasised the need for refined data, advanced monitoring techniques, and policy considerations that address the complex interactions between land use, water management, and environmental outcomes in the MDB.

- Our research highlighted the crucial sensitivity of AET products to basic water balance calculation. The CMRSET dataset, with its enhanced algorithm, more accurately differentiates AET during drought conditions compared to the MODIS dataset, which tends to underestimate AET consistently. Such underestimation by MODIS can significantly affect water flow assessments and subsequent management strategies within the MDB. Variability in AET across MDB catchments is predominantly influenced by rainfall, with only a few catchments exhibiting significant AET differences across major land cover types, highlighting the role of regional factors. Notably, an increasing AET trend was observed in only two out of 22 catchments, likely due to changes in land cover or management practices that increase evapotranspiration. Additionally, minimal variation in the AET/P ratio across most catchments indicates that rainfall is the primary driver of AET at this broad scale. Catchments showing significant differences in both AET and AET/P were generally located in the southern, higher-rainfall areas. This study highlighted the complexities involved in accurately capturing environmental variables and stressed the necessity for meticulous selection and comparative analysis of different AET datasets to effectively understand and manage hydrological processes in the MDB, especially considering the implications of climate change.

5.2 Future research directions

- **Enhancing hydrological models with advanced empirical methods:**

  While using simple empirical equations for modelling hydrological processes in models has traditionally been favoured for their ease of use and efficiency, there remains significant potential for integrating more advanced methodologies, such as machine learning, to improve LULC modelling. Despite the availability of land use data, inconsistencies in nomenclature and classification systems persist, necessitating the adoption of standardised frameworks that enhance model accuracy and applicability.

- **Dynamic representation of LULC in hydrological modelling:**

  While our understanding of hydrologically relevant LULC processes has improved, their integration into hydrological models remains inadequate. There is a critical need for research focused on developing standardised and comprehensive approaches that account for the spatial heterogeneity and temporal dynamics of LULC. Emphasising dynamic data incorporation—which varies significantly based on regional climate, topography, and land management—is vital for refining models and enhancing predictive accuracy.

- **Impact of agricultural practices on evapotranspiration:**

  Diverse agricultural practices, such as varied irrigation methods, crop rotation, and the use of cover crops, significantly impact evapotranspiration rates. Research in this area is crucial for developing sustainable agricultural strategies that optimise water use while ensuring crop productivity. Further investigation into the rebound effect of water efficiency improvements will also be pivotal in shaping policies that support sustainable water use.

- **Improving spatial and temporal data resolution:**

  Current discrepancies in AET data across different catchments underscore the need for more localised studies. Enhancing both the spatial and temporal resolution of this data is crucial, as even minor improvements in model components could lead to significant advancements in our understanding and management of hydrological processes. While large-scale water balances such as those of the MDB typically rely on aggregated data, improving spatial and temporal data resolution can still be beneficial. Even incremental enhancements in the resolution of AET and related hydrological variables can help identify critical local-scale dynamics—such as variations in land cover, irrigation practices, or microclimatic conditions—that may not be captured by more coarsely aggregated data. These refined insights support more targeted management interventions, better calibration of basin-wide models, and improved allocation decisions. By enabling more precise assessments of where and when

water is used, these finer-grained data can contribute to a more nuanced understanding of the basin's overall water balance, ultimately informing adaptive strategies under varying climatic and land-use scenarios.

- **Interdisciplinary approaches to LULC change:**

  Collaborative research that spans hydrology, ecology, and social sciences is essential to comprehensively understand the socio-economic drivers of land use changes and their hydrological impacts. Constructing comprehensive models that incorporate human behaviour and economic dynamics will inform more effective land management and policy decisions.

- **Long-term impact studies and remote sensing integration:**

  Continued long-term studies are necessary to assess the impacts of climate change on LULC dynamics and hydrological processes. Additionally, the potential of remote sensing data to improve model accuracy and representation of real-world conditions should be explored to enhance the reliability and effectiveness of hydrological models.

APPENDIX A

Table A.1: Areal percentage of different land cover for 1990 till 2020 for the whole MDB.

Year	No data	CTV	NTV	*NAV	AS	NS	Water
1990	0.02	32.91	63.87	0.00	0.01	1.71	1.49
1991	0.00	32.77	61.88	0.00	0.01	4.58	0.75
1992	0.01	24.91	63.76	0.00	0.01	10.56	0.75
1993	0.02	15.75	76.20	0.00	0.02	7.12	0.89
1994	0.04	22.05	69.80	0.00	0.01	7.50	0.60
1995	0.04	26.55	66.51	0.00	0.01	6.18	0.70
1996	0.03	23.70	68.13	0.00	0.01	7.36	0.76
1997	0.03	23.27	68.01	0.00	0.02	7.96	0.71
1998	0.01	26.16	65.50	0.00	0.02	6.92	1.40
1999	0.08	19.35	69.27	0.00	0.02	10.54	0.73
2000	0.07	19.32	74.77	0.00	0.02	4.90	0.93
2001	0.07	18.51	73.15	0.00	0.02	7.63	0.63
2002	0.02	18.89	64.59	0.00	0.02	16.07	0.41
2003	0.00	18.89	66.27	0.00	0.02	14.42	0.38
2004	0.00	23.36	64.85	0.00	0.02	11.35	0.43
2005	0.01	24.27	64.13	0.00	0.02	11.16	0.42
2006	0.00	29.39	58.21	0.00	0.02	12.05	0.33
2007	0.01	23.23	60.55	0.00	0.03	15.88	0.31
2008	0.00	11.91	69.84	0.00	0.03	17.71	0.50
2009	0.00	21.47	62.65	0.00	0.03	15.53	0.33
2010	0.00	20.96	73.14	0.00	0.02	4.81	1.06
2011	0.01	14.38	81.92	0.00	0.02	2.53	1.14
2012	0.02	16.60	78.65	0.00	0.03	3.53	1.17
2013	0.01	21.10	72.39	0.00	0.03	5.84	0.63
2014	0.01	21.35	68.34	0.00	0.03	9.81	0.46
2015	0.00	18.29	68.60	0.00	0.03	12.67	0.40
2016	0.01	25.97	66.26	0.00	0.03	6.94	0.79
2017	0.01	14.09	75.33	0.00	0.03	10.00	0.54
2018	0.01	10.68	63.94	0.00	0.03	24.96	0.37
2019	0.00	15.09	54.61	0.00	0.04	29.94	0.32
2020	0.00	24.28	57.25	0.00	0.04	17.88	0.55

*Note: The values for NAV are consistently zero, indicating negligible or non-existent coverage during the studied period.

Table A.2: Trend analysis (1990-2020) test statistics for land cover classes for MDB catchments.

		Mann Kendal's test result				Sen's Slope test result	
Catchment names		**Tau**	**s**	**trend**	**p**	**Slope**	**intercept**
GOULBURN-BROKEN	CTV	-0.148	-69.000	no trend	0.248	-0.239	39.423
GOULBURN-BROKEN	NTV	0.170	79.000	no trend	0.185	0.263	57.942
GOULBURN-BROKEN	AS	0.832	387.000	increasing	0.000	0.003	0.029
GOULBURN-BROKEN	NS	0.531	247.000	increasing	0.000	0.009	0.094
GOULBURN-BROKEN	Water	-0.454	-211.000	decreasing	0.000	-0.025	1.604
GOULBURN-BROKEN	NAV	0.000	0.000	no trend	1.000	0.000	0.000
GWYDIR	CTV	-0.110	-51.000	no trend	0.395	-0.116	19.774
GWYDIR	NTV	-0.243	-113.000	no trend	0.057	-0.149	80.010
GWYDIR	AS	0.639	297.000	increasing	0.000	0.000	0.004
GWYDIR	NS	0.320	149.000	increasing	0.012	0.131	1.116
GWYDIR	Water	-0.217	-101.000	no trend	0.089	-0.009	0.617
KIEWA	CTV	-0.088	-41.000	no trend	0.497	-0.099	25.415
KIEWA	NTV	0.075	35.000	no trend	0.563	0.096	73.422
KIEWA	AS	0.785	365.000	increasing	0.000	0.011	0.125
KIEWA	NS	0.669	311.000	increasing	0.000	0.015	0.142
KIEWA	Water	-0.131	-61.000	no trend	0.308	-0.001	0.380
LACHLAN	CTV	-0.114	-53.000	no trend	0.377	-0.250	37.362
LACHLAN	NTV	0.015	7.000	no trend	0.919	0.060	58.161
LACHLAN	AS	0.798	371.000	increasing	0.000	0.000	0.004
LACHLAN	NS	0.222	103.000	no trend	0.083	0.090	0.608
LACHLAN	Water	-0.230	-107.000	no trend	0.072	-0.011	0.503
LOWER MURRAY	CTV	-0.505	-235.000	decreasing	0.000	-0.613	31.520
LOWER MURRAY	NTV	-0.049	-23.000	no trend	0.708	-0.099	56.529
LOWER MURRAY	AS	0.897	417.000	increasing	0.000	0.001	0.013
LOWER MURRAY	NS	0.385	179.000	increasing	0.002	0.617	9.281
LOWER MURRAY	Water	-0.295	-137.000	decreasing	0.021	-0.005	1.652
LOWER MURRAY	NAV	0.090	42.000	no trend	0.486	0.000	0.001
MACQUARIE-CASTLEREAGH	CTV	-0.247	-115.000	no trend	0.053	-0.526	29.900
MACQUARIE-CASTLEREAGH	NTV	0.019	9.000	no trend	0.892	0.059	70.872
MACQUARIE-CASTLEREAGH	AS	0.781	363.000	increasing	0.000	0.001	0.007
MACQUARIE-CASTLEREAGH	NS	0.333	155.000	increasing	0.009	0.139	1.158
MACQUARIE-CASTLEREAGH	Water	-0.196	-91.000	no trend	0.126	-0.003	0.234
MITTA MITTA	CTV	-0.101	-47.000	no trend	0.434	-0.044	10.694
MITTA MITTA	NTV	0.157	73.000	no trend	0.221	0.080	86.576
MITTA MITTA	AS	0.578	269.000	increasing	0.000	0.000	0.002
MITTA MITTA	NS	0.217	101.000	no trend	0.089	0.001	0.016
MITTA MITTA	Water	-0.265	-123.000	decreasing	0.038	-0.013	2.200
NAMOI	CTV	-0.213	-99.000	no trend	0.096	-0.222	16.145
NAMOI	NTV	-0.071	-33.000	no trend	0.587	-0.057	82.501
NAMOI	AS	0.772	359.000	increasing	0.000	0.001	0.009
NAMOI	NS	0.277	129.000	increasing	0.030	0.093	0.292
NAMOI	Water	-0.286	-133.000	decreasing	0.025	-0.009	0.528
OVENS	CTV	-0.105	-49.000	no trend	0.415	-0.118	23.873
OVENS	NTV	0.110	51.000	no trend	0.395	0.122	75.492
OVENS	AS	0.798	371.000	increasing	0.000	0.003	0.029
OVENS	NS	0.587	273.000	increasing	0.000	0.005	0.064
OVENS	Water	-0.325	-151.000	decreasing	0.011	-0.005	0.501

Table A.2: Continue

		Mann Kendal's test result				Sen's Slope test result	
Catchment names		**Tau**	**s**	**trend**	**p**	**Slope**	**intercept**
PAROO	CTV	-0.333	-155.000	decreasing	0.009	-0.308	14.931
PAROO	NTV	-0.015	-7.000	no trend	0.919	-0.067	63.269
PAROO	NS	0.131	61.000	no trend	0.308	0.376	24.349
PAROO	Water	-0.256	-119.000	decreasing	0.045	-0.018	0.713
WARREGO	CTV	-0.312	-145.000	decreasing	0.014	-0.165	9.051
WARREGO	NTV	-0.187	-87.000	no trend	0.144	-0.249	87.685
WARREGO	AS	0.748	348.000	increasing	0.000	0.000	0.000
WARREGO	NS	0.265	123.000	increasing	0.038	0.387	2.914
WARREGO	Water	-0.234	-109.000	no trend	0.066	-0.003	0.191
WIMMERA	CTV	0.062	29.000	no trend	0.634	0.057	52.720
WIMMERA	NTV	-0.084	-39.000	no trend	0.518	-0.083	44.078
WIMMERA	AS	0.845	393.000	increasing	0.000	0.001	0.012
WIMMERA	NS	0.277	129.000	increasing	0.030	0.054	1.604
WIMMERA	Water	-0.346	-161.000	decreasing	0.007	-0.028	1.148
MURRUMBIDGEE	CTV	-0.127	-59.000	no trend	0.324	-0.290	44.772
MURRUMBIDGEE	NTV	0.049	23.000	no trend	0.708	0.080	55.059
MURRUMBIDGEE	AS	0.828	385.000	increasing	0.000	0.002	0.023
MURRUMBIDGEE	NS	0.385	179.000	increasing	0.002	0.048	0.070
MURRUMBIDGEE	Water	-0.368	-171.000	decreasing	0.004	-0.031	1.515
UPPER MURRAY	CTV	-0.019	-9.000	no trend	0.892	-0.016	19.934
UPPER MURRAY	NTV	0.045	21.000	no trend	0.734	0.026	78.892
UPPER MURRAY	AS	0.755	351.000	increasing	0.000	0.000	0.002
UPPER MURRAY	NS	0.419	195.000	increasing	0.001	0.003	0.020
UPPER MURRAY	Water	-0.247	-115.000	no trend	0.053	-0.008	1.058
MID MURRAY	CTV	-0.157	-73.000	no trend	0.221	-0.362	48.387
MID MURRAY	NTV	0.161	75.000	no trend	0.208	0.371	47.690
MID MURRAY	AS	0.798	371.000	increasing	0.000	0.003	0.033
MID MURRAY	NS	0.449	209.000	increasing	0.000	0.059	0.046
MID MURRAY	Water	-0.553	-257.000	decreasing	0.000	-0.109	3.614
MOONIE	CTV	-0.230	-107.000	no trend	0.072	-0.162	17.568
MOONIE	NTV	-0.161	-75.000	no trend	0.208	-0.157	83.803
MOONIE	NS	0.346	161.000	increasing	0.007	0.177	0.349
MOONIE	Water	0.243	113.000	no trend	0.057	0.003	0.104
BORDER RIVERS	CTV	-0.028	-13.000	no trend	0.838	-0.018	13.413
BORDER RIVERS	NTV	-0.316	-147.000	decreasing	0.013	-0.176	85.905
BORDER RIVERS	AS	0.699	325.000	increasing	0.000	0.000	0.003
BORDER RIVERS	NS	0.299	139.000	increasing	0.019	0.102	0.979
BORDER RIVERS	Water	0.105	49.000	no trend	0.415	0.002	0.294
BARWON-DARLING	CTV	-0.406	-189.000	decreasing	0.001	-0.365	15.184
BARWON-DARLING	NTV	0.166	77.000	no trend	0.196	0.329	76.462
BARWON-DARLING	AS	0.716	333.000	increasing	0.000	0.000	0.001
BARWON-DARLING	NS	0.058	27.000	no trend	0.659	0.062	5.809
BARWON-DARLING	Water	-0.247	-115.000	no trend	0.053	-0.003	0.159

Table A.2: Continue

		Mann Kendal's test result				Sen's Slope test result	
Catchment names		**Tau**	**s**	**trend**	**p**	**Slope**	**intercept**
LODDON-AVOCA	CTV	-0.071	-33.000	no trend	0.587	-0.111	53.542
LODDON-AVOCA	NTV	0.037	17.000	no trend	0.786	0.070	42.421
LODDON-AVOCA	AS	0.802	373.000	increasing	0.000	0.003	0.026
LODDON-AVOCA	NS	0.286	133.000	increasing	0.025	0.051	1.171
LODDON-AVOCA	Water	-0.239	-111.000	no trend	0.062	-0.010	1.061
CAMPASPE	CTV	-0.209	-97.000	no trend	0.103	-0.493	45.094
CAMPASPE	NTV	0.204	95.000	no trend	0.110	0.465	54.524
CAMPASPE	AS	0.884	411.000	increasing	0.000	0.006	0.023
CAMPASPE	NS	0.548	255.000	increasing	0.000	0.013	0.174
CAMPASPE	Water	-0.295	-137.000	decreasing	0.021	-0.013	1.155
CONDAMINE	CTV	-0.342	-159.000	decreasing	0.007	-0.183	10.216
CONDAMINE	NTV	-0.222	-103.000	no trend	0.083	-0.327	87.609
CONDAMINE	AS	0.626	291.000	increasing	0.000	0.001	0.005
CONDAMINE	NS	0.312	145.000	increasing	0.014	0.432	1.323
CONDAMINE	Water	-0.006	-3.000	no trend	0.973	0.000	0.194
LOWER DARLING	CTV	-0.402	-187.000	decreasing	0.002	-0.765	29.702
LOWER DARLING	NTV	-0.002	-1.000	no trend	1.000	-0.007	44.338
LOWER DARLING	AS	0.385	179.000	increasing	0.002	0.000	0.016
LOWER DARLING	NS	0.170	79.000	no trend	0.185	0.744	18.441
LOWER DARLING	Water	-0.312	-145.000	decreasing	0.014	-0.031	1.179

Table A.3: Correlation between land cover percentage and precipitation: Green indicates a significant correlation (p<0.05), while red denotes no significant correlation (p>0.05).

Basin	NTV 1 Lag	NTV no Lag	NS 1 lag	NS No lag	Water 1 Lag	Water No Lag
PAROO	0.612	0.506	-0.554	-0.600	0.470	0.801
BORDER RIVERS	0.519	0.522	-0.331	-0.673	0.566	0.651
MOONIE	0.550	0.631	-0.533	-0.668	0.435	0.509
CONDAMINE	0.763	0.744	-0.641	-0.704	0.648	0.607
WARREGO	0.607	0.636	-0.623	-0.666	0.456	0.761
NAMOI	0.715	0.084	-0.395	-0.718	0.630	0.617
MACQUARIE-CASTLEREAGH	0.613	0.064	-0.435	-0.591	0.378	0.647
BARWON-DARLING	0.451	0.393	-0.518	-0.424	0.654	0.592
LOWER DARLING	0.685	0.424	-0.474	-0.477	0.601	0.527
GOULBURN-BROKEN	0.294	-0.258	-0.254	-0.617	0.536	0.710
GWYDIR	0.498	0.027	-0.260	-0.706	0.710	0.642
LOWER MURRAY	0.575	0.233	-0.235	-0.398	0.420	0.478
LACHLAN	0.566	0.242	-0.535	-0.519	0.578	0.623
KIEWA	0.075	-0.292	-0.148	-0.348	0.626	0.662
WIMMERA	0.511	0.185	-0.144	-0.588	0.524	0.558
UPPER MURRAY	-0.189	-0.327	-0.053	-0.591	0.518	0.815
CAMPASPE	0.229	-0.236	-0.151	-0.610	0.612	0.504
MURRUMBIDGEE	0.504	0.139	-0.429	-0.702	0.533	0.660
MID MURRAY	0.548	-0.013	-0.257	-0.575	0.405	0.519
LODDON-AVOCA	0.525	0.102	-0.173	-0.717	0.352	0.716
OVENS	0.275	-0.287	-0.252	-0.586	0.347	0.750
MITTA MITTA	-0.098	-0.390	-0.152	-0.756	0.536	0.746

Table A.4: Standard deviation (1990-2020) of land cover (%) in MDB's catchments.

	CTV	NTV	*NAV	AS	NS	Water
BARWON-DARLING	6.58	9.19	*NA*	0.00	6.81	0.56
BORDER RIVERS	3.22	4.07	*NA*	0.00	5.45	0.14
CAMPASPE	14.84	14.79	*NA*	0.06	0.31	0.33
CONDAMINE	3.88	9.17	*NA*	0.01	9.50	0.24
GOULBURN-BROKEN	10.38	10.44	0.00	0.03	0.20	0.38
GWYDIR	7.22	6.55	*NA*	0.00	7.66	0.25
KIEWA	6.19	6.34	*NA*	0.11	0.25	0.14
LACHLAN	10.55	10.37	*NA*	0.00	6.10	0.55
LODDON-AVOCA	10.49	10.19	*NA*	0.03	1.36	0.30
LOWER DARLING	11.54	15.80	*NA*	0.00	18.58	0.78
LOWER MURRAY	8.05	7.81	0.00	0.01	9.00	0.25
MACQUARIE-CASTLEREAGH	10.87	10.58	*NA*	0.01	8.09	0.30
MID MURRAY	12.71	11.98	*NA*	0.03	3.41	1.43
MITTA MITTA	2.72	3.11	*NA*	0.00	0.11	0.37
MOONIE	6.40	8.97	*NA*		7.89	0.09
MURRUMBIDGEE	10.85	10.35	*NA*	0.02	4.05	0.47
NAMOI	6.31	6.15	*NA*	0.01	5.37	0.23
OVENS	7.84	7.87	*NA*	0.03	0.07	0.11
PAROO	6.86	14.24	*NA*		14.10	0.98
UPPER MURRAY	4.52	4.72	*NA*	0.00	0.32	0.23
WARREGO	4.66	9.01	*NA*	0.00	8.30	0.23
WIMMERA	7.68	7.64	*NA*	0.01	1.38	0.47

* Note: The entries for NAV are zero, indicating negligible coverage. NA values, where present, signify that the cover does not exist in the given catchment.

Table A.5: Summary of statistics for precipitation for the whole MDB.

Year	MIN	MAX	MEAN	STD
1990	173.2012	2418.966	529.4195	245.5769
1991	112.8271	2218.881	428.0512	229.5523
1992	227.4961	2368.462	561.3789	248.6039
1993	179.8701	2621.813	515.4917	224.3683
1994	83.93066	1514.342	325.9952	159.2186
1995	201.1992	2529.909	536.4529	228.9407
1996	136.7012	2614.265	542.5032	269.6811
1997	178.4482	1483.698	443.6373	189.82
1998	133.4893	2317.508	571.1741	247.1461
1999	162.3213	1932.66	582.4711	211.2486
2000	230.5459	2273.047	574.2423	201.8892
2001	119.6924	1941.792	405.7512	208.9133
2002	57.12988	1486.798	279.4138	165.4796
2003	149.376	2056.217	440.594	193.2744
2004	123.3887	1805.013	463.8856	235.4619
2005	96.21582	2071.034	439.7165	216.7747
2006	92.77051	1195.347	275.1724	127.0729
2007	191.4258	1926.84	472.7581	185.2628
2008	137.5879	1581.794	448.4786	200.6458
2009	124.9795	1853.406	406.9997	161.653
2010	307.3975	2740.509	810.2043	264.4522
2011	145.3691	2212.564	600.8763	203.9217
2012	151.6982	2115.126	498.0745	212.9032
2013	104.1621	2214.305	368.727	205.3108
2014	182.1055	1706.767	416.4459	181.2696
2015	125.7373	1631.637	428.1483	187.5188
2016	258.7432	2609.296	620.6371	241.7515
2017	117.749	2073.819	402.6755	202.5732
2018	57.36426	1812.829	290.4505	170.8818
2019	37.96289	1626.65	230.8489	146.4931
2020	36.0918	908.0674	269.0009	115.5498

Table A.6: Precipitation statistics per catchment (P-Mean: Average precipitation 1990-2020; P-Mean-STD: Standard Deviation of mean precipitation over Time, reflecting temporal variation; P-STD-Mean: Mean of precipitation standard deviation over time, reflecting spatial variation; P-Trend: Result of the Mann-Kendall test).

	P_mean (mm)	P_Mean_STD	P_STD_Mean	P_trend
BARWON-DARLING	331	125	54	no trend
BORDER RIVERS	604	154	109	no trend
CAMPASPE	559	157	133	no trend
CONDAMINE	484	150	114	no trend
GOULBURN-BROKEN	690	176	270	decreasing
GWYDIR	639	165	117	no trend
KIEWA	1057	271	287	no trend
LACHLAN	458	136	143	no trend
LODDON-AVOCA	392	118	103	no trend
LOWER DARLING	259	107	33	no trend
LOWER MURRAY	287	90	78	no trend
MACQUARIE-CASTLEREAGH	531	162	124	no trend
MID MURRAY	382	118	72	no trend
MITTA MITTA	1040	253	208	decreasing
MOONIE	522	155	50	no trend
MURRUMBIDGEE	529	147	214	no trend
NAMOI	627	167	117	decreasing
OVENS	921	243	283	decreasing
PAROO	307	131	61	no trend
UPPER MURRAY	951	234	233	decreasing
WARREGO	452	170	106	no trend
WIMMERA	380	106	92	no trend

Table A.7: Average (1990-2020) percentage of major land covers in MDB's catchments.

	CTV	NTV	*NAV	AS	NS	Water
BARWON-DARLING	10.04	81.01	*NA*	0.00	8.65	0.30
BORDER RIVERS	12.87	82.38	*NA*	0.01	4.39	0.36
CAMPASPE	37.30	61.28	*NA*	0.12	0.44	0.84
CONDAMINE	8.31	80.36	*NA*	0.02	11.03	0.28
GOULBURN-BROKEN	32.85	65.24	0.00	0.08	0.28	1.27
GWYDIR	17.92	75.94	*NA*	0.01	5.60	0.53
KIEWA	23.98	74.62	*NA*	0.31	0.42	0.39
LACHLAN	34.90	59.69	*NA*	0.01	4.94	0.45
LODDON-AVOCA	51.02	45.81	*NA*	0.07	2.10	0.98
LOWER DARLING	18.85	48.05	*NA*	0.02	32.12	0.95
LOWER MURRAY	22.91	56.93	0.00	0.03	18.48	1.63
MACQUARIE-CASTLEREAGH	23.17	71.14	*NA*	0.02	5.36	0.30
MID MURRAY	41.81	53.72	*NA*	0.08	2.20	2.19
MITTA MITTA	10.67	86.94	*NA*	0.00	0.07	1.95
MOONIE	15.76	78.77	*NA*		5.32	0.16
MURRUMBIDGEE	39.32	57.22	*NA*	0.06	2.48	0.90
NAMOI	15.00	80.54	*NA*	0.02	4.03	0.41
OVENS	21.86	77.42	*NA*	0.07	0.15	0.44
PAROO	10.88	60.88	*NA*		27.35	0.89
UPPER MURRAY	19.91	78.82	*NA*	0.00	0.15	0.90
WARREGO	6.92	82.18	*NA*	0.00	10.68	0.21
WIMMERA	52.46	44.17	*NA*	0.04	2.64	0.69

* Note: The entries for NAV are zero, indicating negligible coverage. NA values, where present, signify that the cover does not exist in the given catchment.

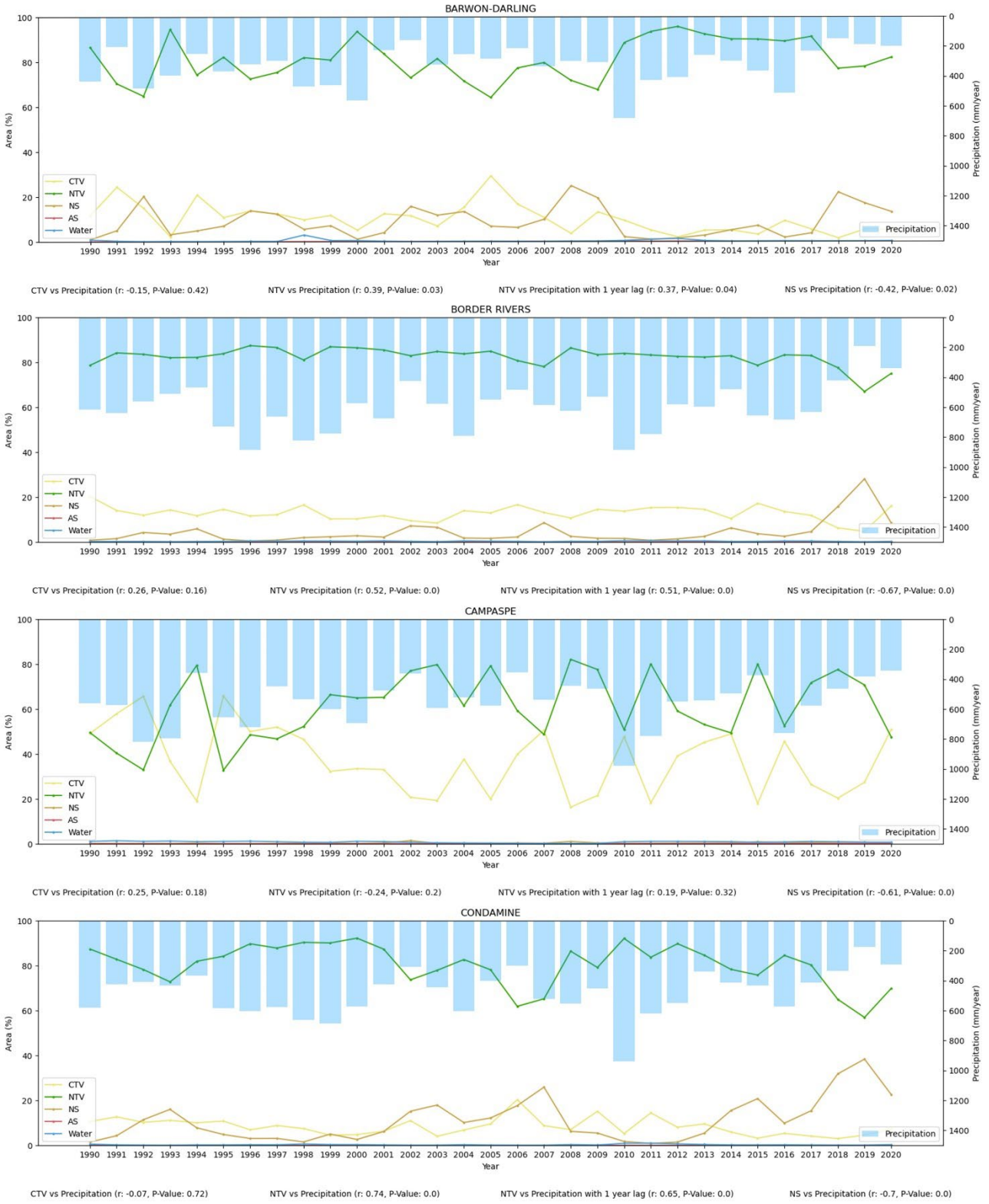

Figure A.1: Major land covers (%) in MDB catchments from 1990 to 2020.

Continuation of Figure A.1: Major land covers (%) in MDB catchments from 1990 to 2020.

Continuation of Figure A.1: Major land covers (%) in MDB catchments from 1990 to 2020

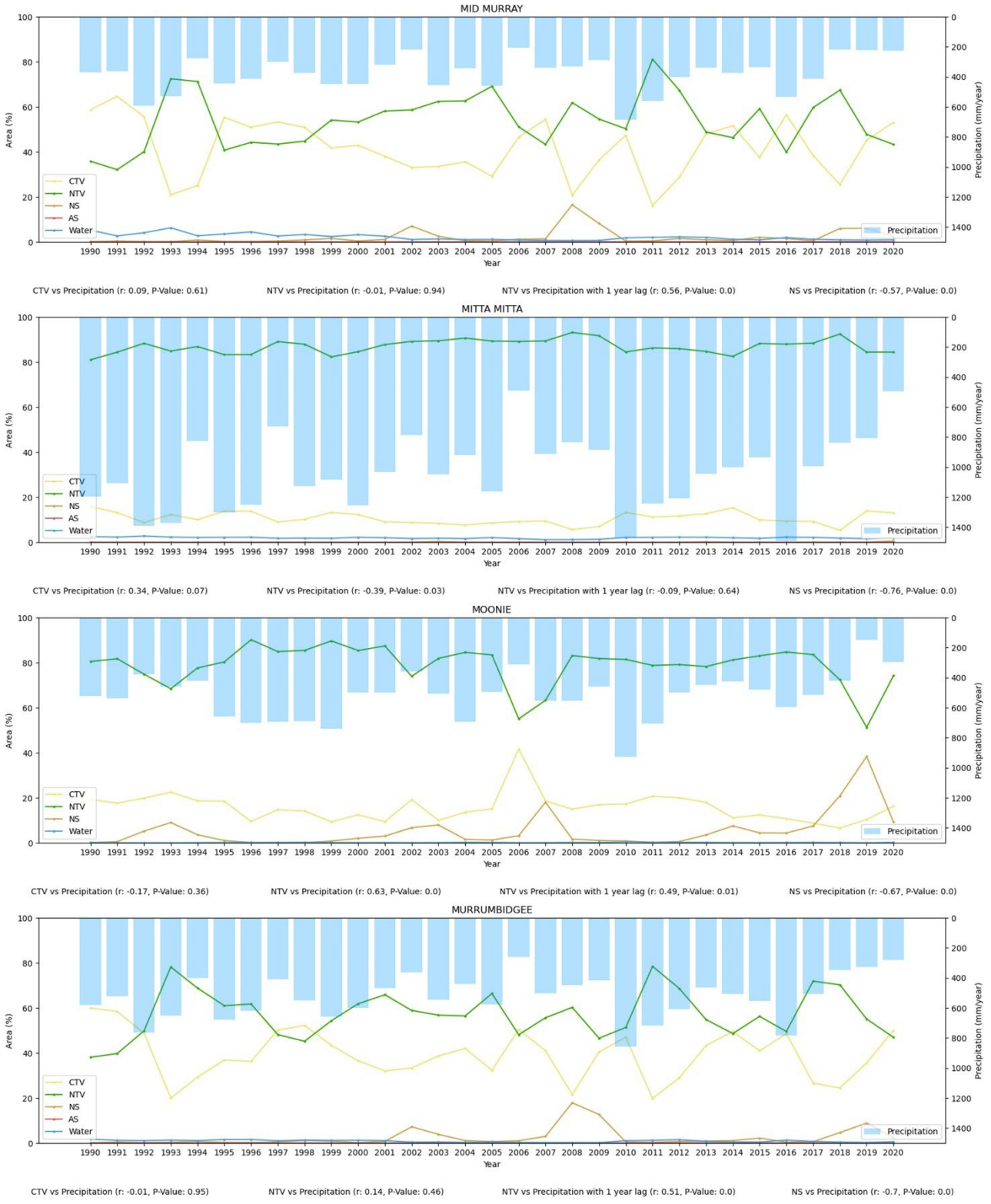

Continuation of Figure A.1 Major land cover (%) in MDB catchments from 1990 to 2020.

Continuation of Figure A.1 Major land cover (%) in MDB catchments from 1990 to 2020.

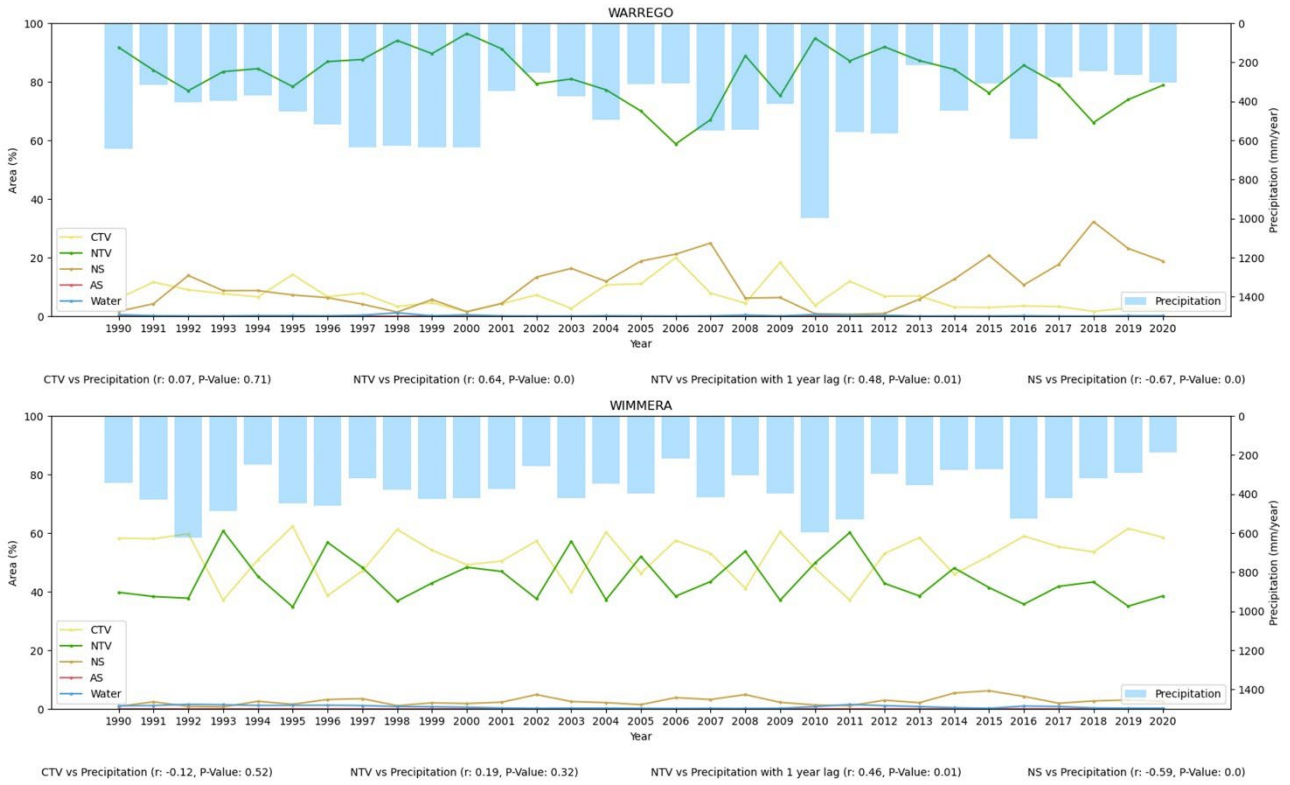

Continuation of Figure A.1 Major land cover (%) in MDB catchments from 1990 to 2020.

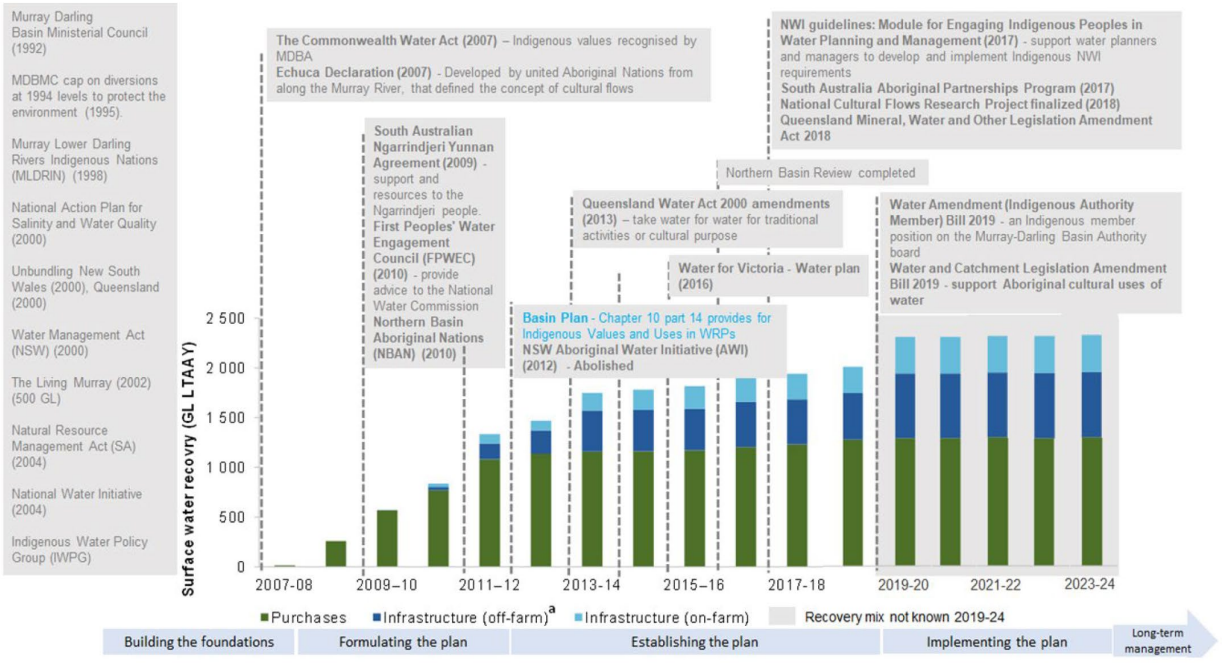

Figure A.2: Basin water reform timeline agriculture, economy and water trade themes 2007-24. Sourced from Marsden Jacob, adapted from (MDBA, 2020).

APPENDIX B

Table B.1: Descriptions of 22 catchments in the Murray-Darling Basin (MDB)

Catchment	Annual stream flow	Catchment area (% of MDB)	Contribution to Basin water (% of MDB outflow)	Major water storages	River length	Key water users
Barwon-Darling	3,500 GL/yr (Bourke)	13%	2.80%	None	1,600 km (approx.)	Urban water supply, stock, domestic and irrigation
Border Rivers	130 GL/yr (Macintyre River at Wallangra)	4%	5%	Pindari Lake (312 GL), Glenlyon Lake (261 GL), Lake Coolmunda (69 GL)		Urban centres, agriculture
Campaspe	Campaspe: 352 GL/yr	0.4%	0.90%	Lake Eppalock (304 GL) on the Campaspe; Malmsbury (18 GL), Lauriston (20 GL) and Upper Coliban (32 GL) reservoirs on the Coliban	220 km	Urban water supply, industry, stock and domestic, irrigation
Central Murray		3%	-	Yarrawonga Weir (118 GL), Torrumbarry Weir (37 GL), mid-Murray storages (58 GL), Mildura Weir (37 GL)	2,500 km total; approx. 1,200 km Hume Dam to Wentworth	Irrigated agriculture, urban water supply, stock and domestic
Condamine-Balonne	1,305 GL/yr (St George)	13%	8.50%	Beardmore Dam (94 GL), Leslie Dam (106 GL), Cooby Dam (21 GL)	1,195 km (Condamine, Balonne, and Culgoa channel)	Urban centres, agriculture
Goulburn-Broken	3,000 GL/yr	2%	11%	Goulburn River: Lake Eildon (3,334 GL), Goulburn Weir (26 GL), Waranga Basin (432 GL), Greens Lake (33 GL) Broken River: Lake Nillahcootie (40 GL)	Goulburn River: 570 km, Broken River: 174 km	Irrigated agriculture, urban water supply, industry

Gwydir	336 GL/yr (Bundarra - unregulated flow)	~ 2%	3.40%	Copeton Dam (1,364 GL)	480 km	Irrigated agriculture, urban water supply, stock and domestic, mining
Kiewa	689 GL/yr	< 0.2%		Rocky Valley Dam (28 GL)	109 km	Urban water supply, stock and domestic, hydroelectricity, irrigation
Lachlan	834 GL/yr (Cowra)	8%	6.50%	Wyangala (1,220 GL), Lake Cargelligo (36 GL), Carcoar Dam (36 GL)	1,339 km	Urban water supply, stock and domestic, irrigated agriculture, mining
Loddon-Avoca	Loddon River: 201 GL/yr (Laanecoorie Weir) Avoca River: 84 GL/yr (Coonooer Bridge)	2.3%	1.70%	Loddon River: Cairn Curran Reservoir (147 GL), Tullaroop Reservoir (73 GL), Laanecoorie Reservoir (8 GL) Avoca River: none	Loddon River: 310 km Avoca River: 270 km	2.3% of the MDB
Lower Darling		3%		Lakes Menindee, Cawndilla, Pamamaroo and Wetherell (1,730 GL)	530 km	Urban water supply, stock, domestic and irrigation
Lower Murray		9%	-	Lake Victoria (677 GL)	2,500 km total, approx. 1,000 km Wentworth to Southern Ocean	Irrigated agriculture, urban centres (including Adelaide), stock and domestic supply
Macquarie-Castlereagh	1,175 GL/yr (Macquarie at Dubbo)	7%	8.40%	Burrendong (1,190 GL), Windamere (353 GL), Oberon (45 GL), Ben Chifley (31 GL), Suma Park (18 GL)	Castlereagh River: 549 km Macquarie River: 960 km Bogan River: 590 km	Irrigated agriculture, urban water supply, industrial water supply
Mitta Mitta	900 GL/yr (into Dartmouth Dam)	0.9%	10%	Dartmouth (3,856 GL)	204 km	Urban water supply, stock and domestic, irrigation
Moonie		1.4%	0.80%	Thallon Weir (0.2 GL)	542 km	Stock and domestic, irrigation

Murrumbidgee	4,000 GL/yr (Wagga Wagga)	8%	16%	Burrinjuck (1,026 GL), Blowering (1,628 GL), Talbingo (921 GL), Tantangara (254 GL), Googong (125 GL)	1,485 km	Irrigated agriculture, hydroelectricity, urban water supply
Namoi	696 GL/yr (Gunnedah)	4%	3.20%	Keepit Dam (426 GL), Split Rock Dam (397 GL), Chaffey Dam (101 GL)	700 km	Irrigated agriculture, urban water supply, stock and domestic, mining
Ovens	1,775 GL/yr (at Peechelba)	0.7%	6%	Lake Buffalo (24 GL), Lake William Hovell (14 GL)	191 km	Irrigated agriculture, urban water supply, stock and domestic
Paroo	445 GL/yr (Calwarro gauge)	3%	2%	None	600 km	Stock and domestic
Upper Murray	2,550 GL/yr (Hume Dam unregulated inflow)	2%	17%	Hume Dam (3,005 GL), Khancoban Pondage (26 GL), Geehi Reservoir (21 GL) and Tooma Reservoir (26 GL)	2,500 km in total; 300 km source to Hume Dam	Hydroelectricity, urban water supply, stock and domestic
Warrego	422 GL/yr (Wyandra stream gauging station)	7%	< 1%	Cunnamulla Weir (4.8 GL)	900 km	Stock and domestic
Wimmera	206 GL/yr (at Mackenzie River confluence)	3%	1.70%	Lake Bellfield (79 GL), Lake Fyans (19 GL), Lake Lonsdale (66 GL), Lake Wartook (29 GL), Taylors Lake (27 GL), Rocklands Reservoir (348 GL), Lake Toolondo (92 GL)	278 km	Urban water supply, industry, stock and domestic, irrigation

Table B.2: Comparison of AET statistics between MODIS and CMRSET datasets average across various land cover classes over 20 years (2001-2020)

	MODIS			CMRSET		
	MEAN	Min	Max	MEAN	Min	Max
Cultivated Terrestrial Vegetation (CTV)	0.84	0.53	1.16	1.11	0.78	1.47
(Semi-)Natural Terrestrial Vegetation (NTV)	0.87	0.65	1.24	1.22	1.10	1.45
Natural Aquatic Vegetation (NAV)	9.13	5.03	11.25	2.45	1.45	3.03
Artificial Surface (AS)	8.67	7.77	9.46	1.64	1.48	1.83
Natural Bare Surface (NS)	0.53	0.36	0.76	0.77	0.61	0.94
water	8.54	5.33	10.91	3.74	2.95	4.15
Grand Total	4.45	0.36	11.25	1.94	0.61	4.15

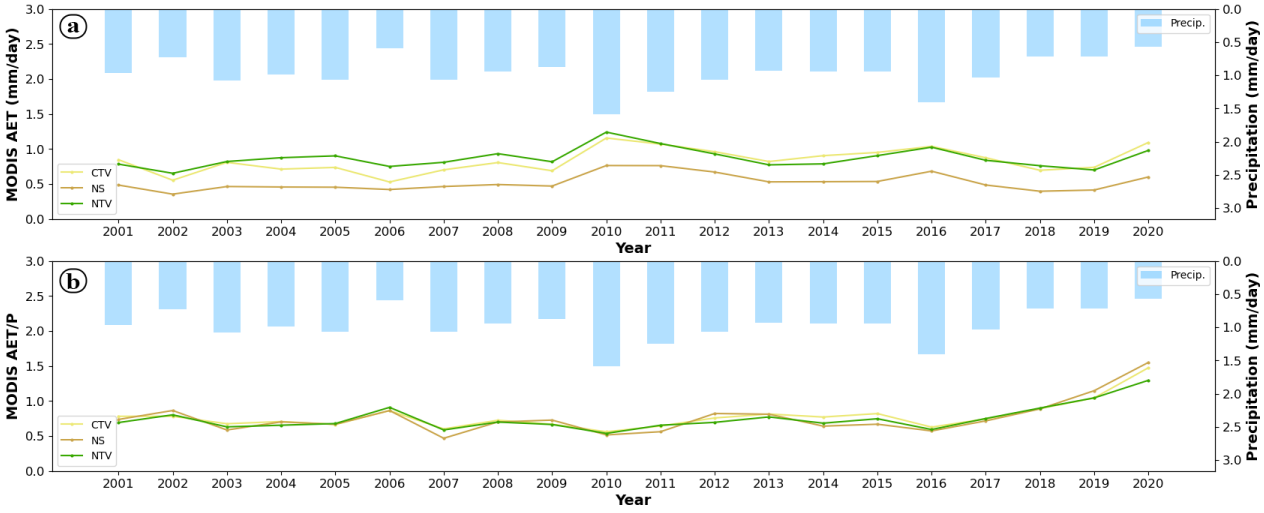

Figure B.1: (a) AET; and (b) AET/P time series for MODIS dataset 2001-2020

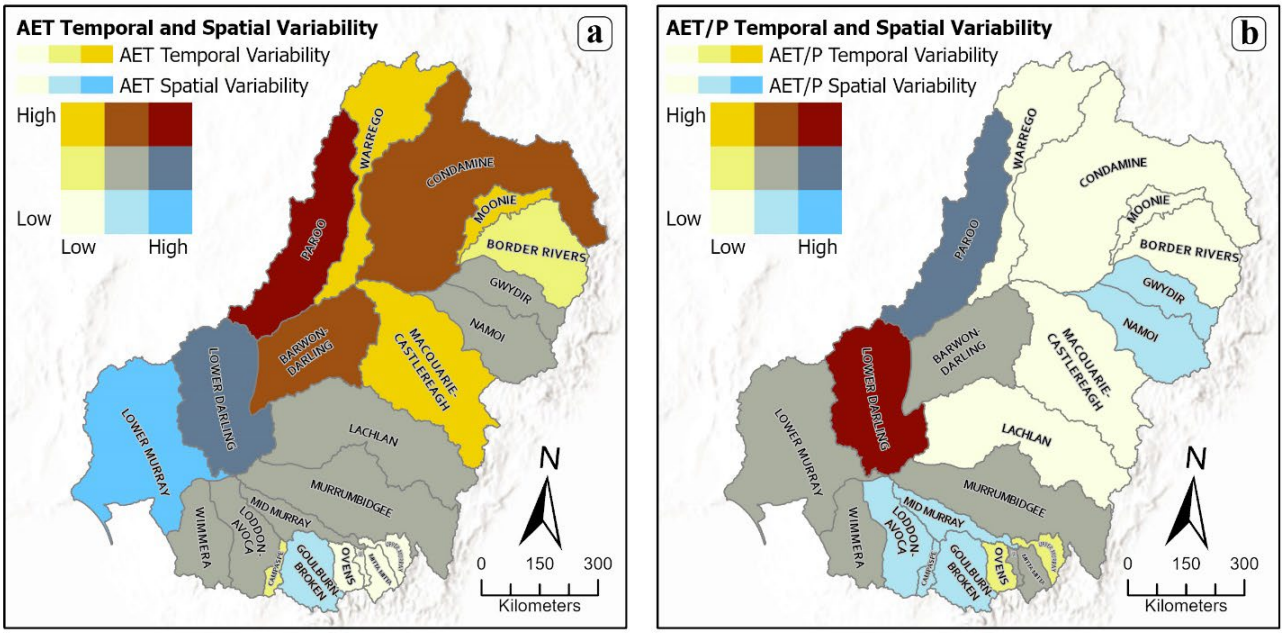

Figure B.2: Temporal and spatial classification of the coefficient of variation for MODIS (a) AET and (b) AET/P for 2001-2020, categorised into low, moderate, and high variability using Jenks natural breaks.

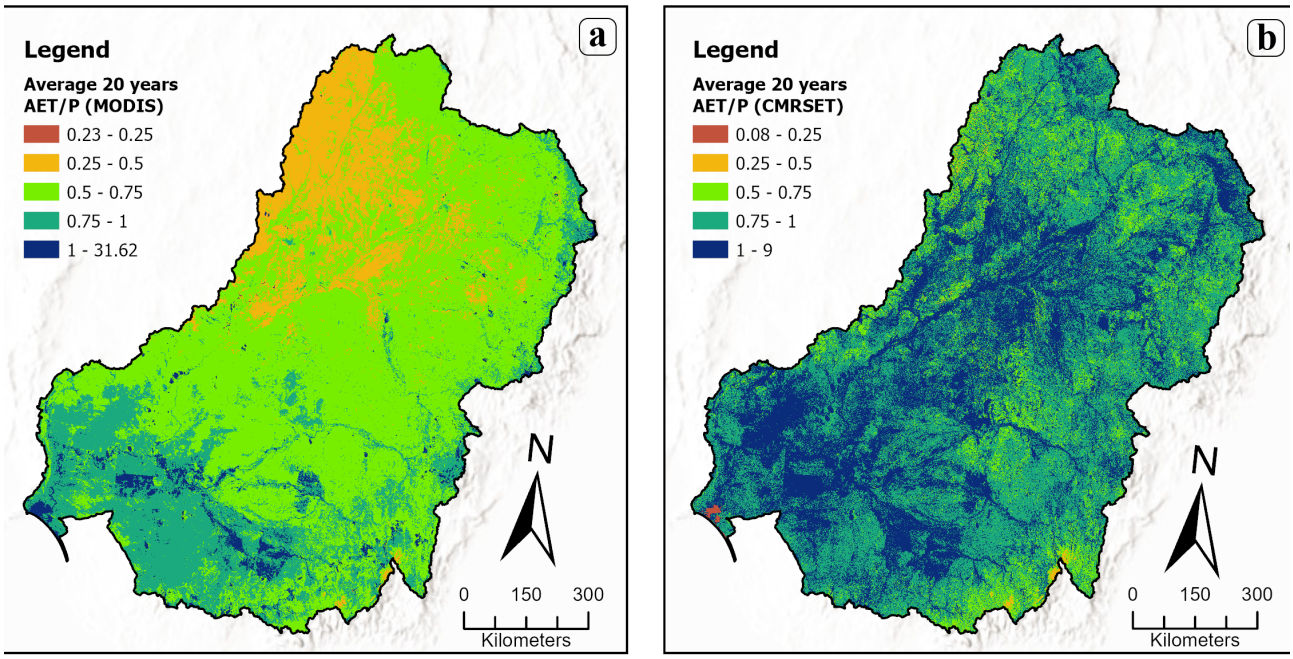

Figure B.3: Average 20 years (2001-2020) AET/P (a) MODIS; (b) CMRSET

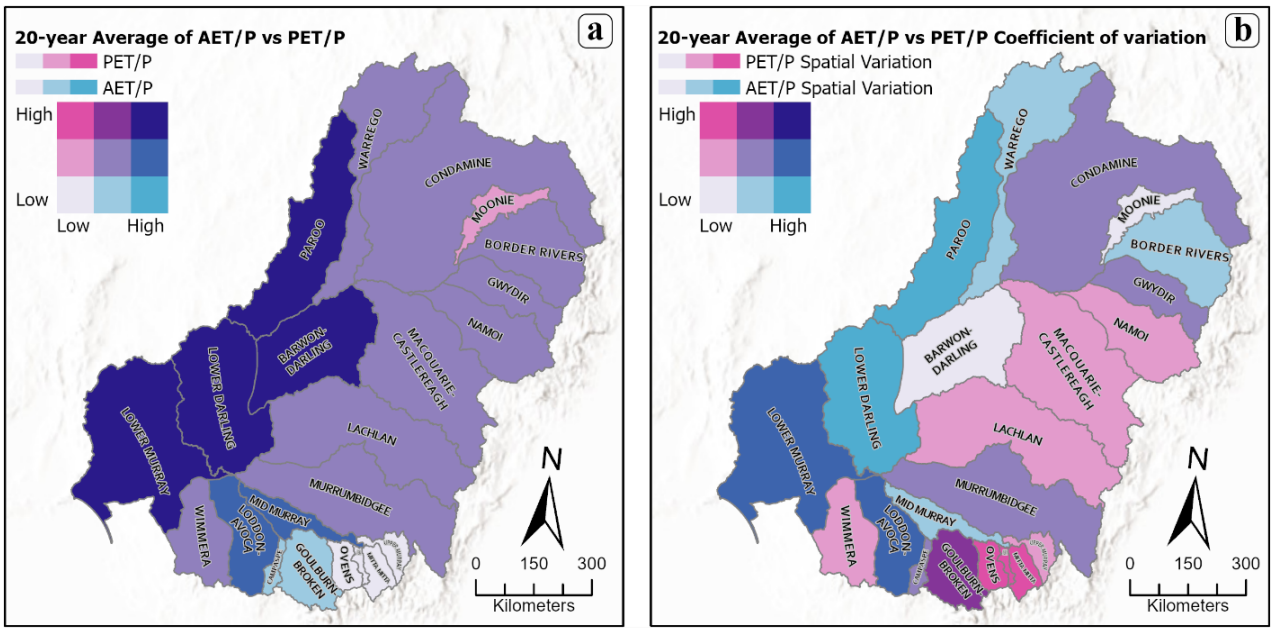

Figure B.4: (a) 20-year average of AET/P and PET/P, categorised into low, moderate, and high (b) Spatial classification of the coefficient of variation for CMRSET AET and MODIS PET/P for 2001-2020 using Jenks natural breaks.

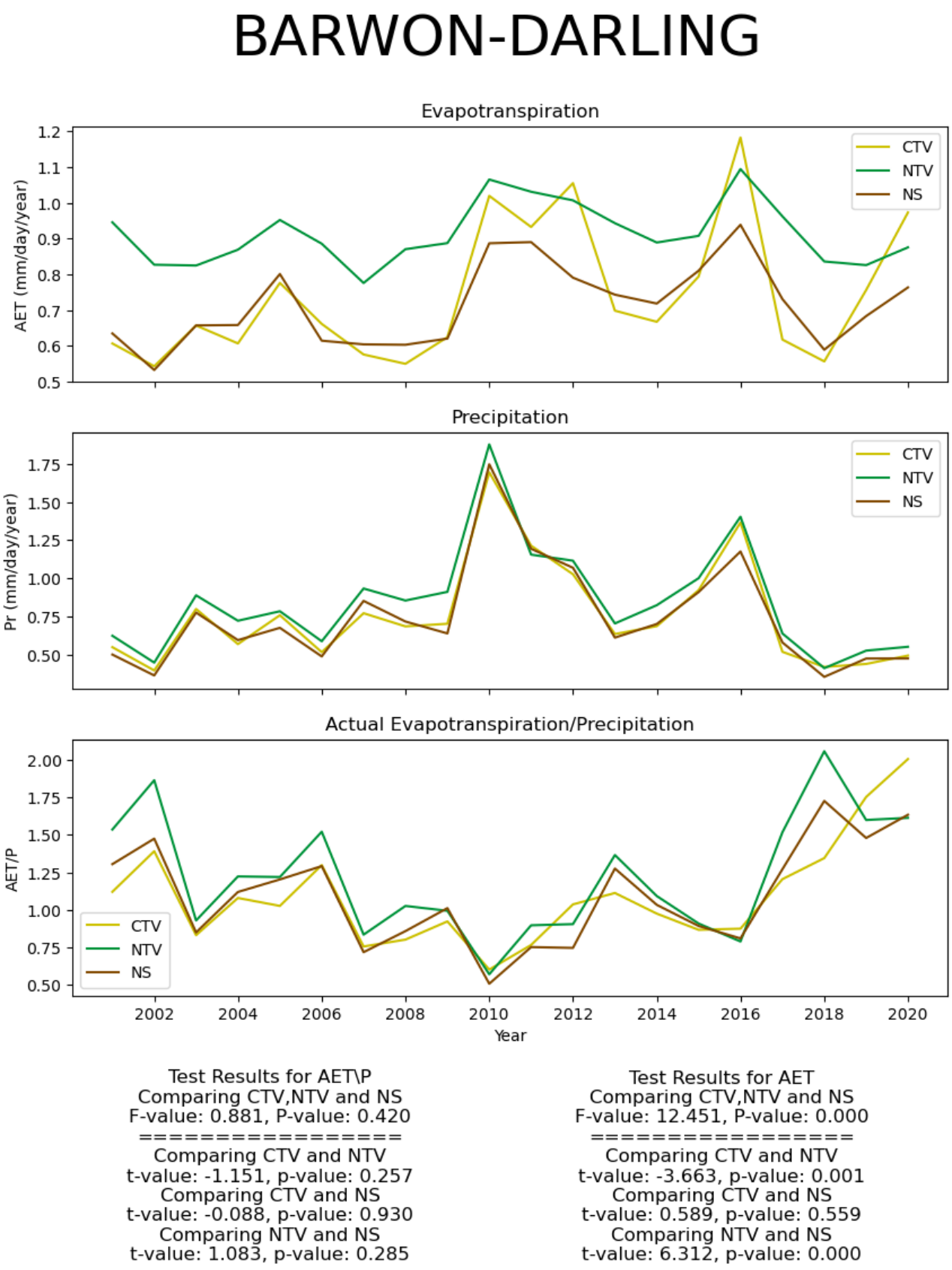

Figure B.5: AET, P and AET/P time series (2001-2020) for CMRSET dataset for different catchments

BORDER_RIVERS

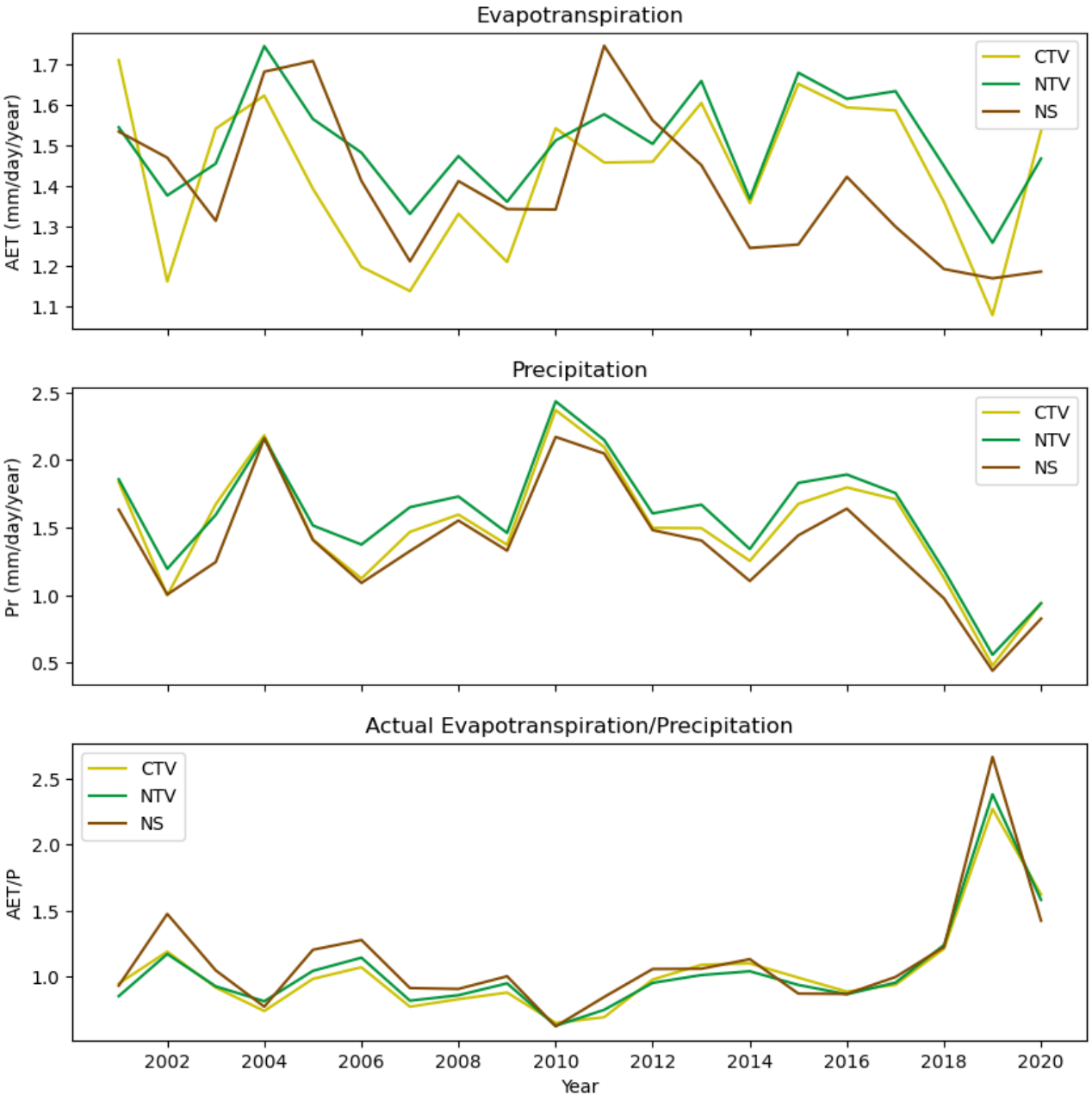

Test Results for AET\P
Comparing CTV,NTV and NS
F-value: 0.240, P-value: 0.787
==========
Comparing CTV and NTV
t-value: -0.068, p-value: 0.946
Comparing CTV and NS
t-value: -0.620, p-value: 0.539
Comparing NTV and NS
t-value: -0.548, p-value: 0.587

Test Results for AET
Comparing CTV,NTV and NS
F-value: 2.103, P-value: 0.132
==========
Comparing CTV and NTV
t-value: -1.481, p-value: 0.147
Comparing CTV and NS
t-value: 0.500, p-value: 0.620
Comparing NTV and NS
t-value: 2.153, p-value: 0.038

Figure B.5: Continued

CAMPASPE

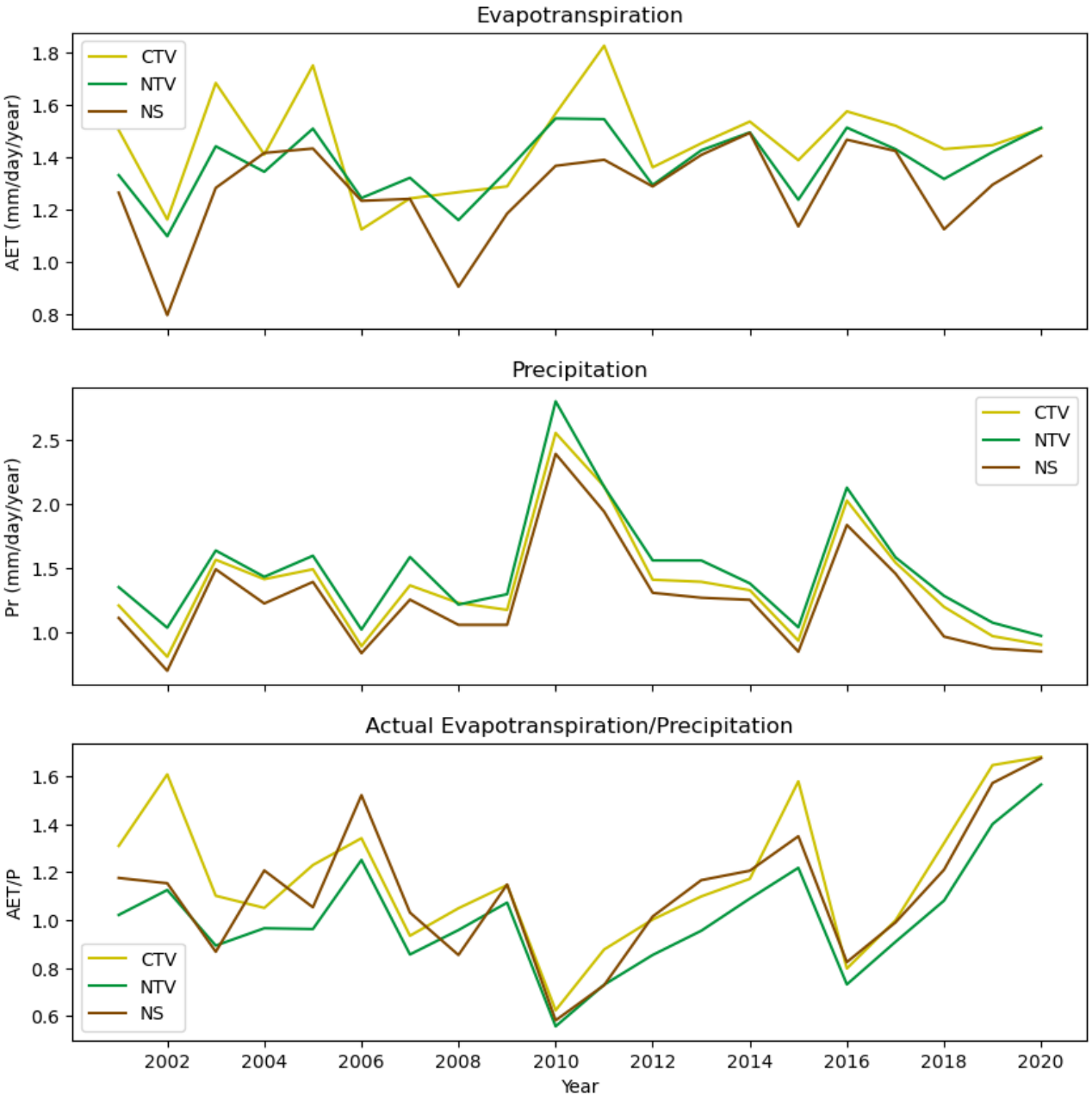

Test Results for AET\P
Comparing CTV,NTV and NS
F-value: 2.023, P-value: 0.142
==========
Comparing CTV and NTV
t-value: 2.025, p-value: 0.050
Comparing CTV and NS
t-value: 0.689, p-value: 0.495
Comparing NTV and NS
t-value: -1.316, p-value: 0.196

Test Results for AET
Comparing CTV,NTV and NS
F-value: 5.515, P-value: 0.006
==========
Comparing CTV and NTV
t-value: 1.502, p-value: 0.141
Comparing CTV and NS
t-value: 3.022, p-value: 0.004
Comparing NTV and NS
t-value: 1.989, p-value: 0.054

Figure B.1: Continued

CONDAMINE

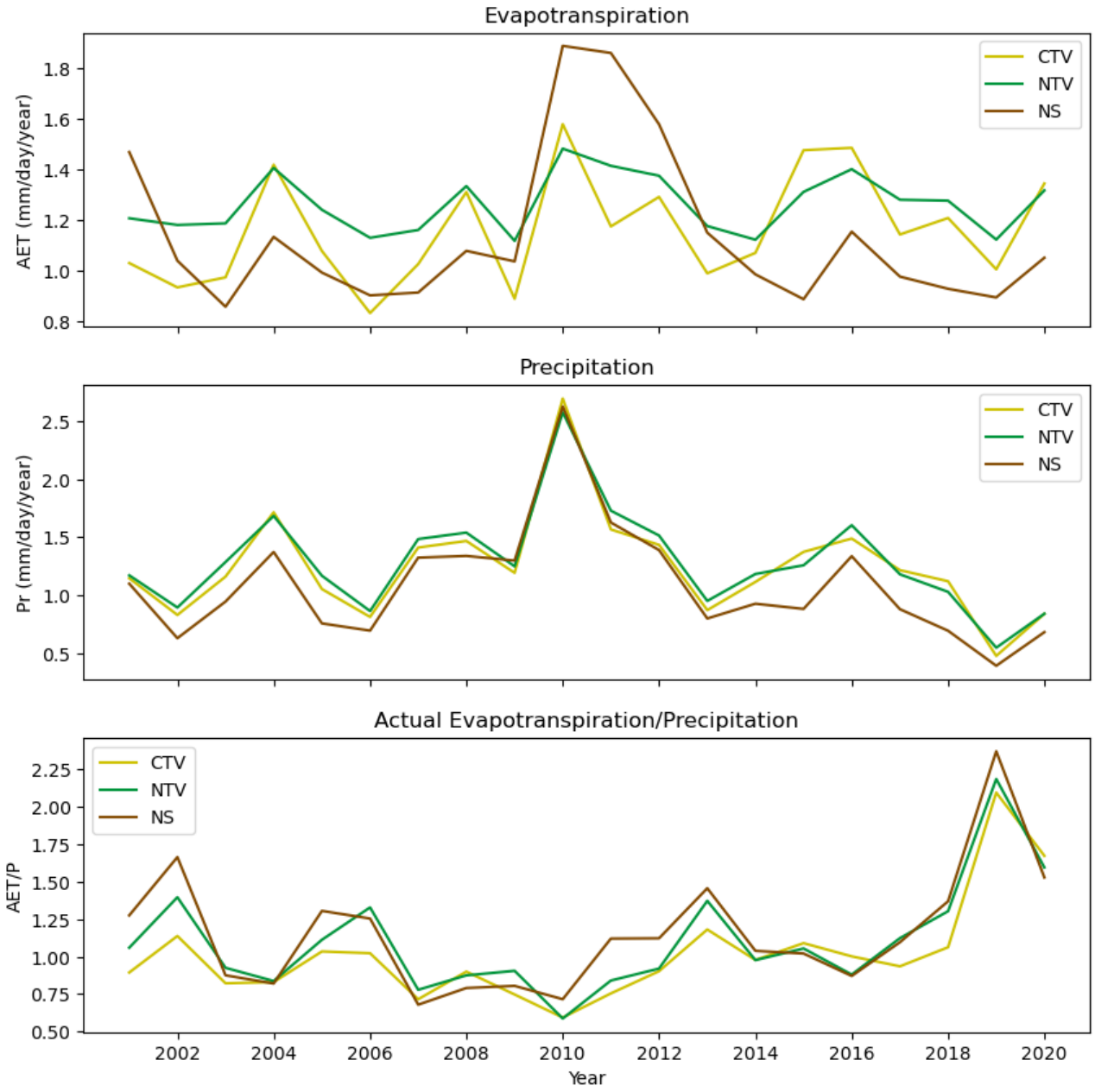

Test Results for AET\P
Comparing CTV,NTV and NS
F-value: 0.747, P-value: 0.478
==========
Comparing CTV and NTV
t-value: -0.768, p-value: 0.447
Comparing CTV and NS
t-value: -1.198, p-value: 0.238
Comparing NTV and NS
t-value: -0.469, p-value: 0.642

Test Results for AET
Comparing CTV,NTV and NS
F-value: 1.633, P-value: 0.204
==========
Comparing CTV and NTV
t-value: -1.810, p-value: 0.078
Comparing CTV and NS
t-value: 0.285, p-value: 0.777
Comparing NTV and NS
t-value: 1.664, p-value: 0.104

Figure B.5: Continued

GOULBURN-BROKEN

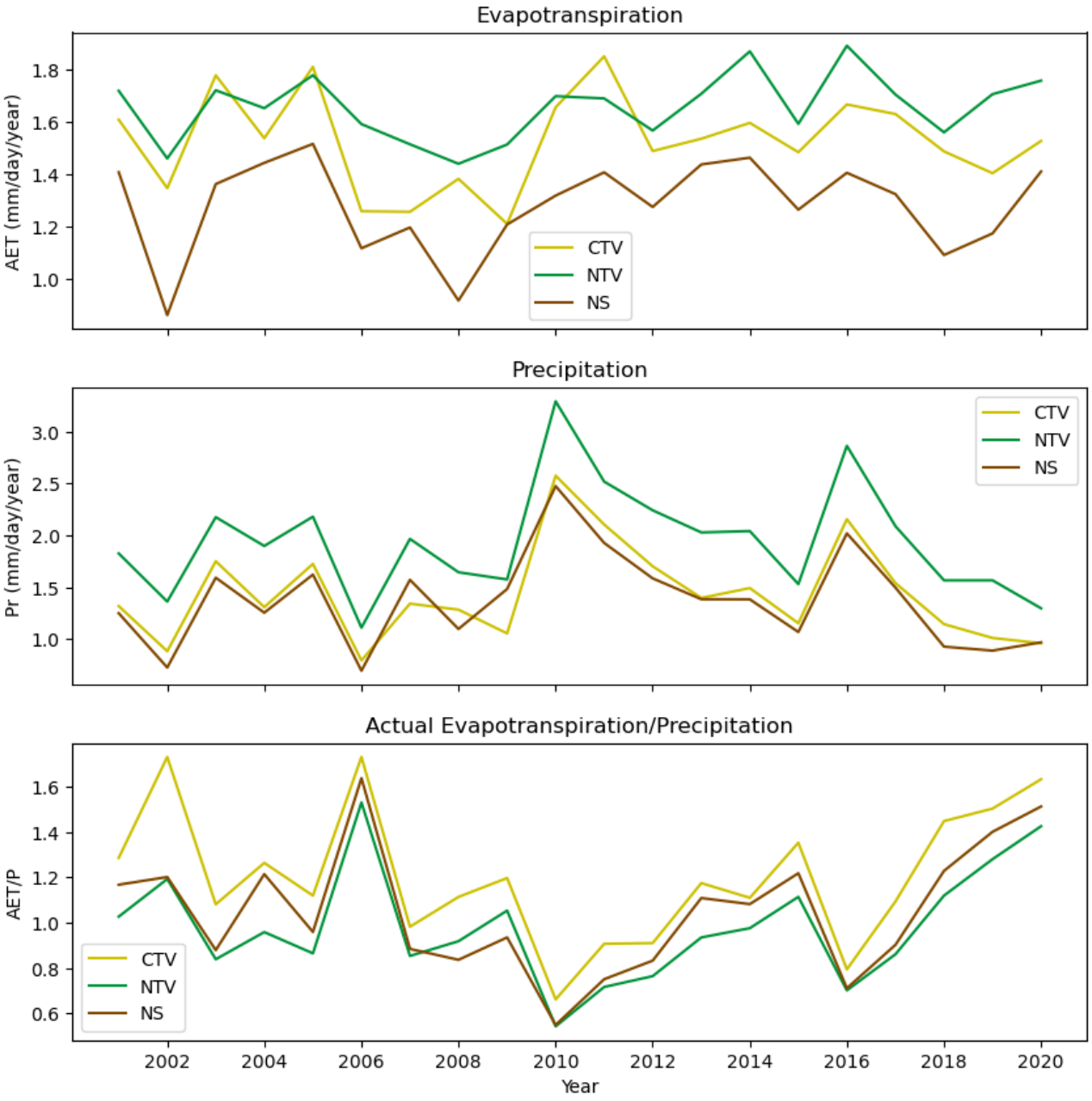

Test Results for AET\P
Comparing CTV,NTV and NS
F-value: 3.441, P-value: 0.039
==========
Comparing CTV and NTV
t-value: 2.577, p-value: 0.014
Comparing CTV and NS
t-value: 1.701, p-value: 0.097
Comparing NTV and NS
t-value: -0.810, p-value: 0.423

Test Results for AET
Comparing CTV,NTV and NS
F-value: 27.265, P-value: 0.000
==========
Comparing CTV and NTV
t-value: -2.661, p-value: 0.011
Comparing CTV and NS
t-value: 4.313, p-value: 0.000
Comparing NTV and NS
t-value: 7.723, p-value: 0.000

Figure B.5: Continued

GWYDIR

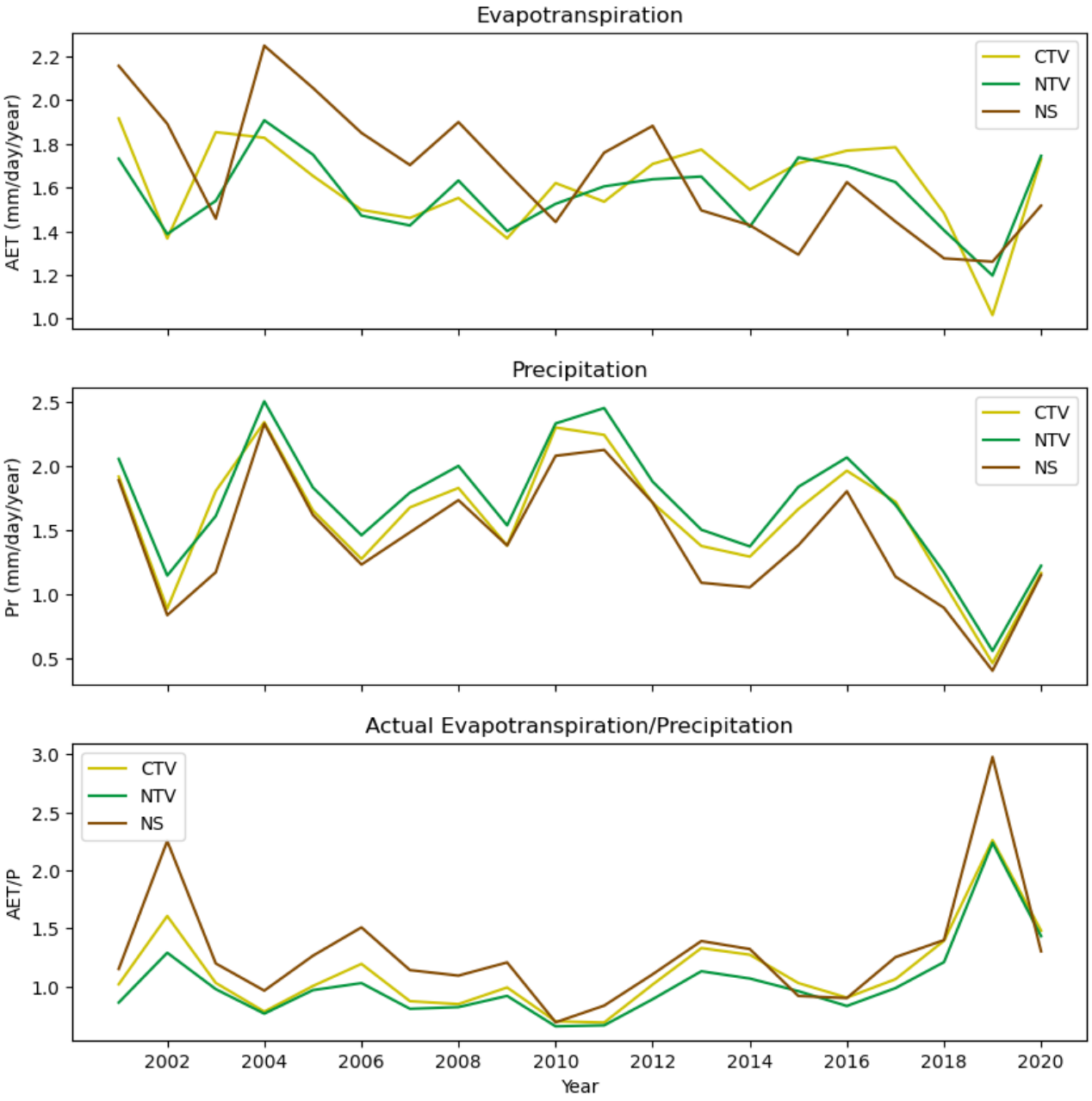

Test Results for AET\P
Comparing CTV,NTV and NS
F-value: 2.150, P-value: 0.126
==========
Comparing CTV and NTV
t-value: 0.881, p-value: 0.384
Comparing CTV and NS
t-value: -1.205, p-value: 0.236
Comparing NTV and NS
t-value: -1.947, p-value: 0.059

Test Results for AET
Comparing CTV,NTV and NS
F-value: 0.824, P-value: 0.444
==========
Comparing CTV and NTV
t-value: 0.596, p-value: 0.555
Comparing CTV and NS
t-value: -0.702, p-value: 0.487
Comparing NTV and NS
t-value: -1.225, p-value: 0.228

Figure B.5: Continued

KIEWA

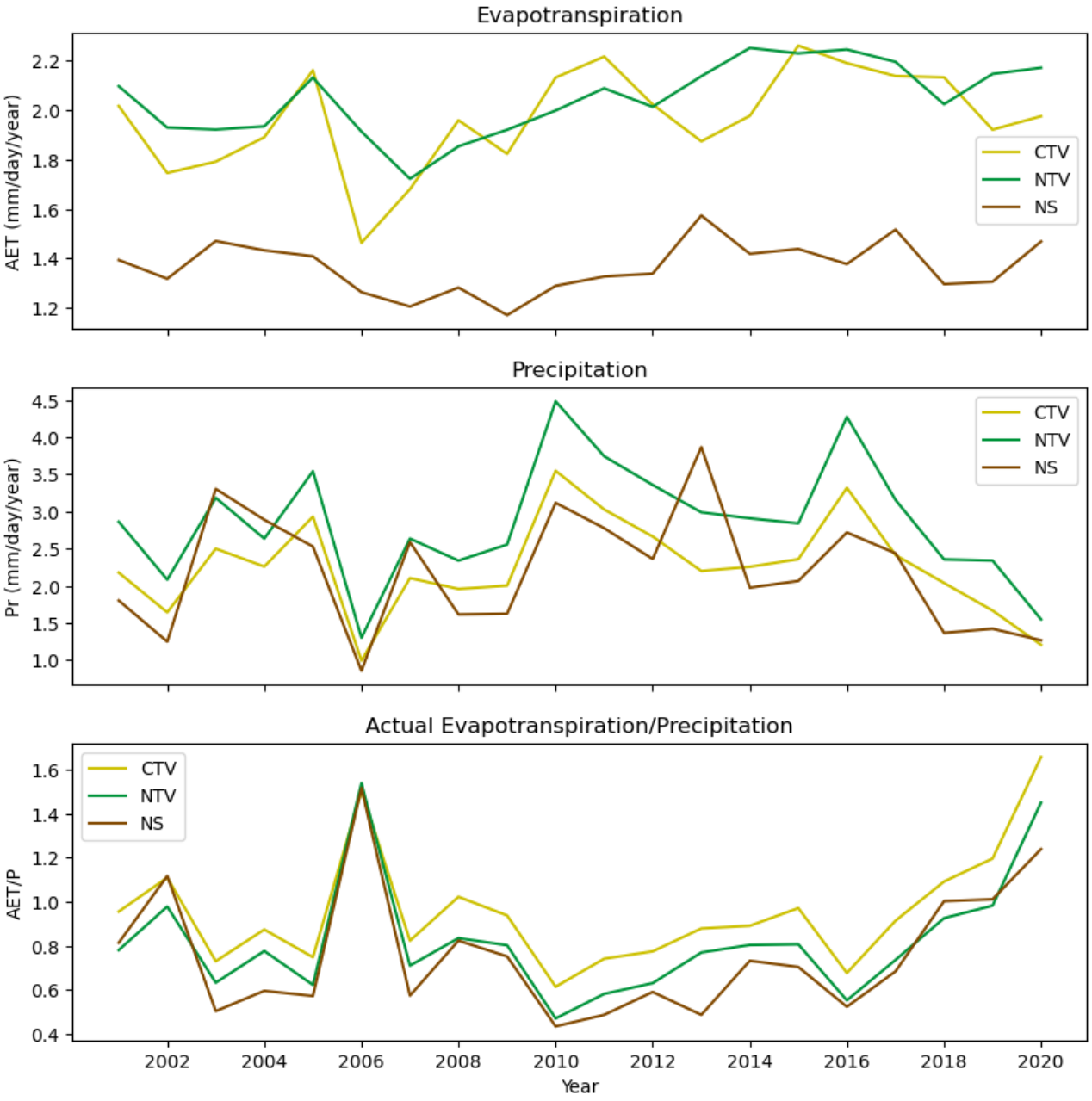

Test Results for AET\P
Comparing CTV,NTV and NS
F-value: 2.752, P-value: 0.072
==========
Comparing CTV and NTV
t-value: 1.628, p-value: 0.112
Comparing CTV and NS
t-value: 2.272, p-value: 0.029
Comparing NTV and NS
t-value: 0.696, p-value: 0.490

Test Results for AET
Comparing CTV,NTV and NS
F-value: 114.453, P-value: 0.000
==========
Comparing CTV and NTV
t-value: -1.392, p-value: 0.172
Comparing CTV and NS
t-value: 11.880, p-value: 0.000
Comparing NTV and NS
t-value: 17.044, p-value: 0.000

Figure B.5: Continued

LACHLAN

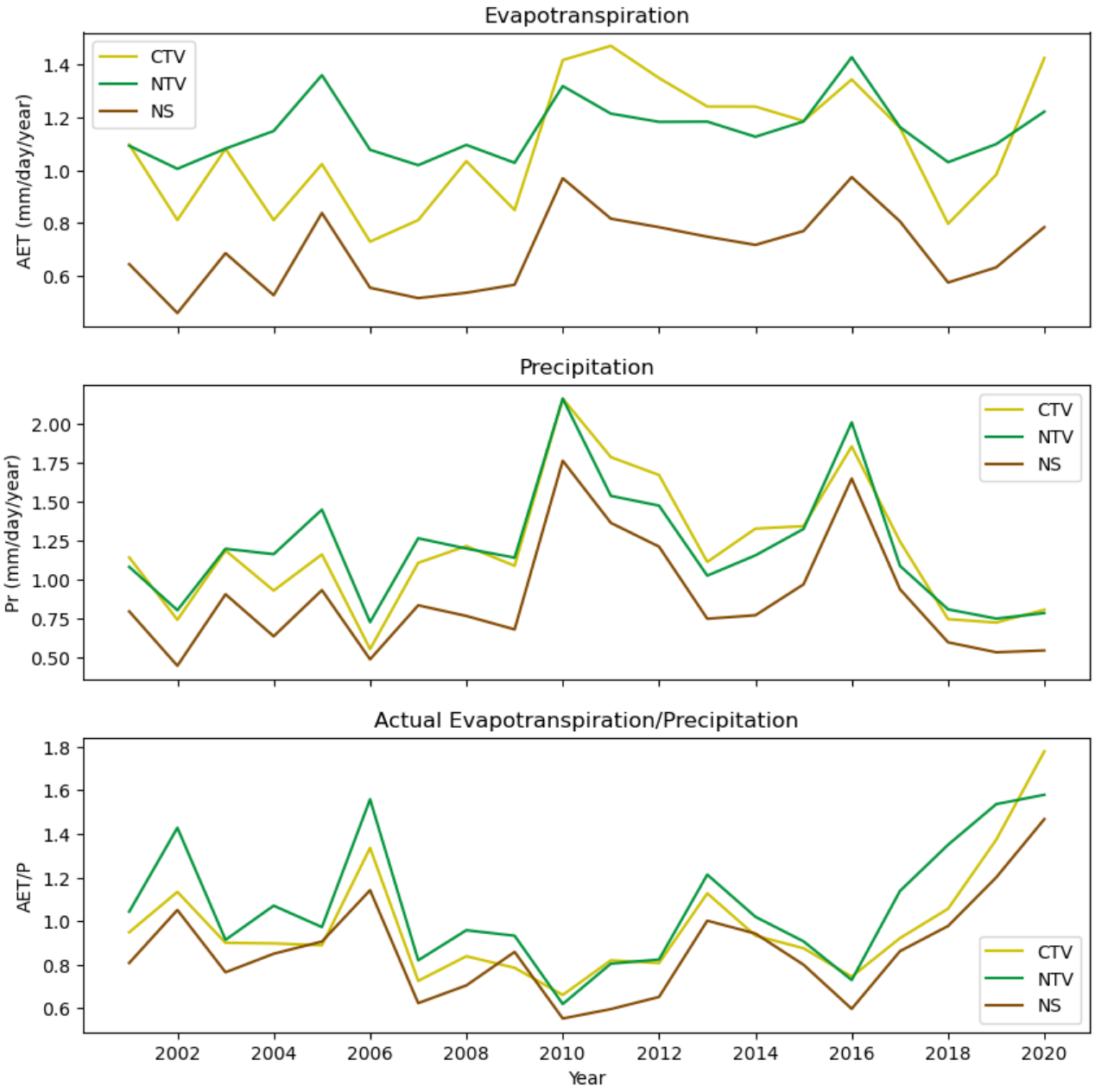

Test Results for AET\P
Comparing CTV,NTV and NS
F-value: 3.006, P-value: 0.057
==========
Comparing CTV and NTV
t-value: -1.067, p-value: 0.293
Comparing CTV and NS
t-value: 1.393, p-value: 0.172
Comparing NTV and NS
t-value: 2.468, p-value: 0.018

Test Results for AET
Comparing CTV,NTV and NS
F-value: 40.227, P-value: 0.000
==========
Comparing CTV and NTV
t-value: -1.013, p-value: 0.318
Comparing CTV and NS
t-value: 6.321, p-value: 0.000
Comparing NTV and NS
t-value: 10.876, p-value: 0.000

Figure B.5: Continued

LODDON-AVOCA

Test Results for AET\P
Comparing CTV,NTV and NS
F-value: 0.703, P-value: 0.499
==========
Comparing CTV and NTV
t-value: -0.751, p-value: 0.458
Comparing CTV and NS
t-value: -1.148, p-value: 0.258
Comparing NTV and NS
t-value: -0.482, p-value: 0.633

Test Results for AET
Comparing CTV,NTV and NS
F-value: 15.716, P-value: 0.000
==========
Comparing CTV and NTV
t-value: -4.618, p-value: 0.000
Comparing CTV and NS
t-value: 0.946, p-value: 0.350
Comparing NTV and NS
t-value: 5.565, p-value: 0.000

Figure B.5: Continued

LOWER_DARLING

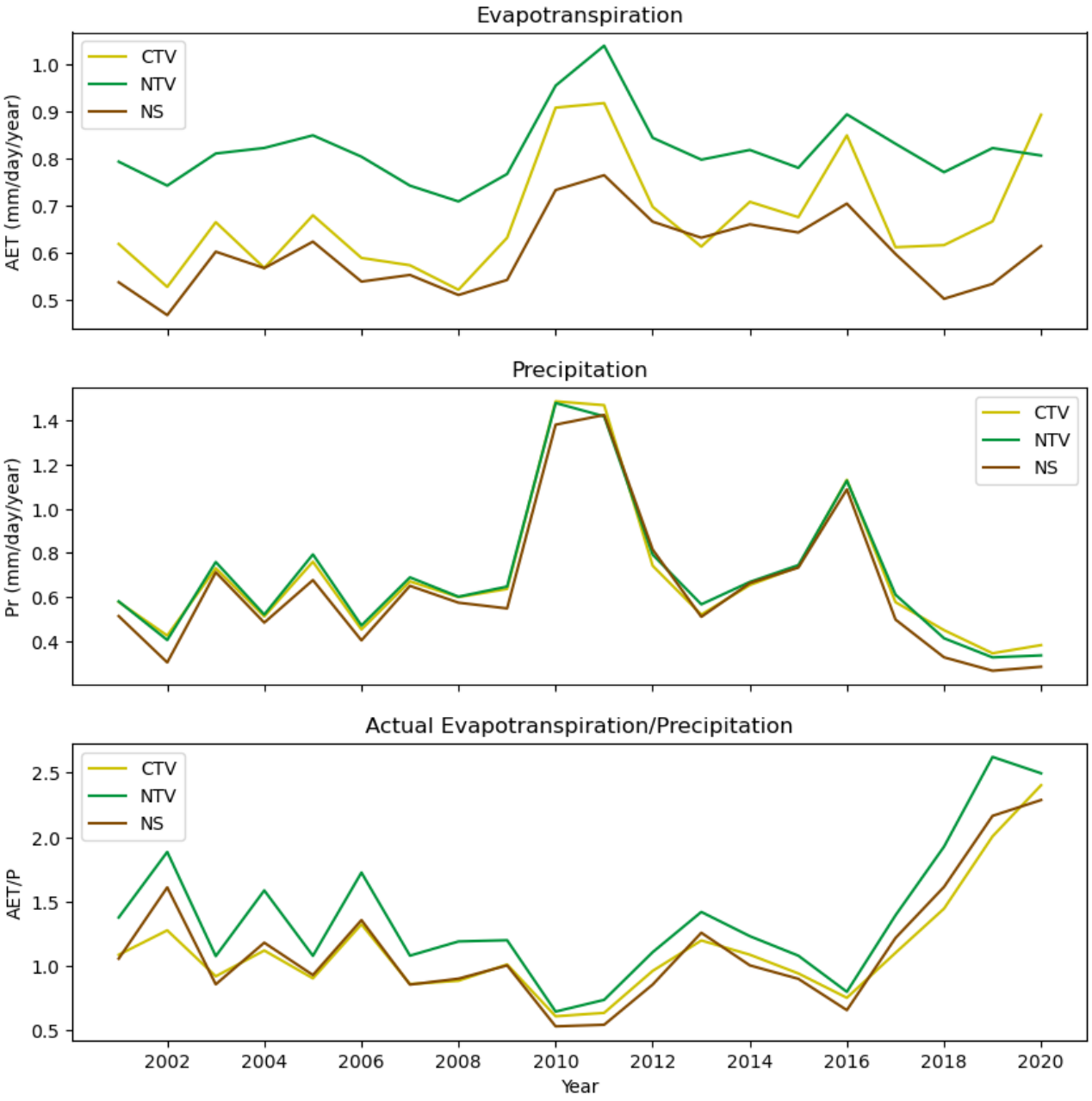

Test Results for AET\P
Comparing CTV,NTV and NS
F-value: 1.812, P-value: 0.173
==========
Comparing CTV and NTV
t-value: -1.681, p-value: 0.101
Comparing CTV and NS
t-value: -0.089, p-value: 0.929
Comparing NTV and NS
t-value: 1.531, p-value: 0.134

Test Results for AET
Comparing CTV,NTV and NS
F-value: 27.901, P-value: 0.000
==========
Comparing CTV and NTV
t-value: -4.479, p-value: 0.000
Comparing CTV and NS
t-value: 2.355, p-value: 0.024
Comparing NTV and NS
t-value: 9.008, p-value: 0.000

Figure B.5: Continued

LOWER_MURRAY

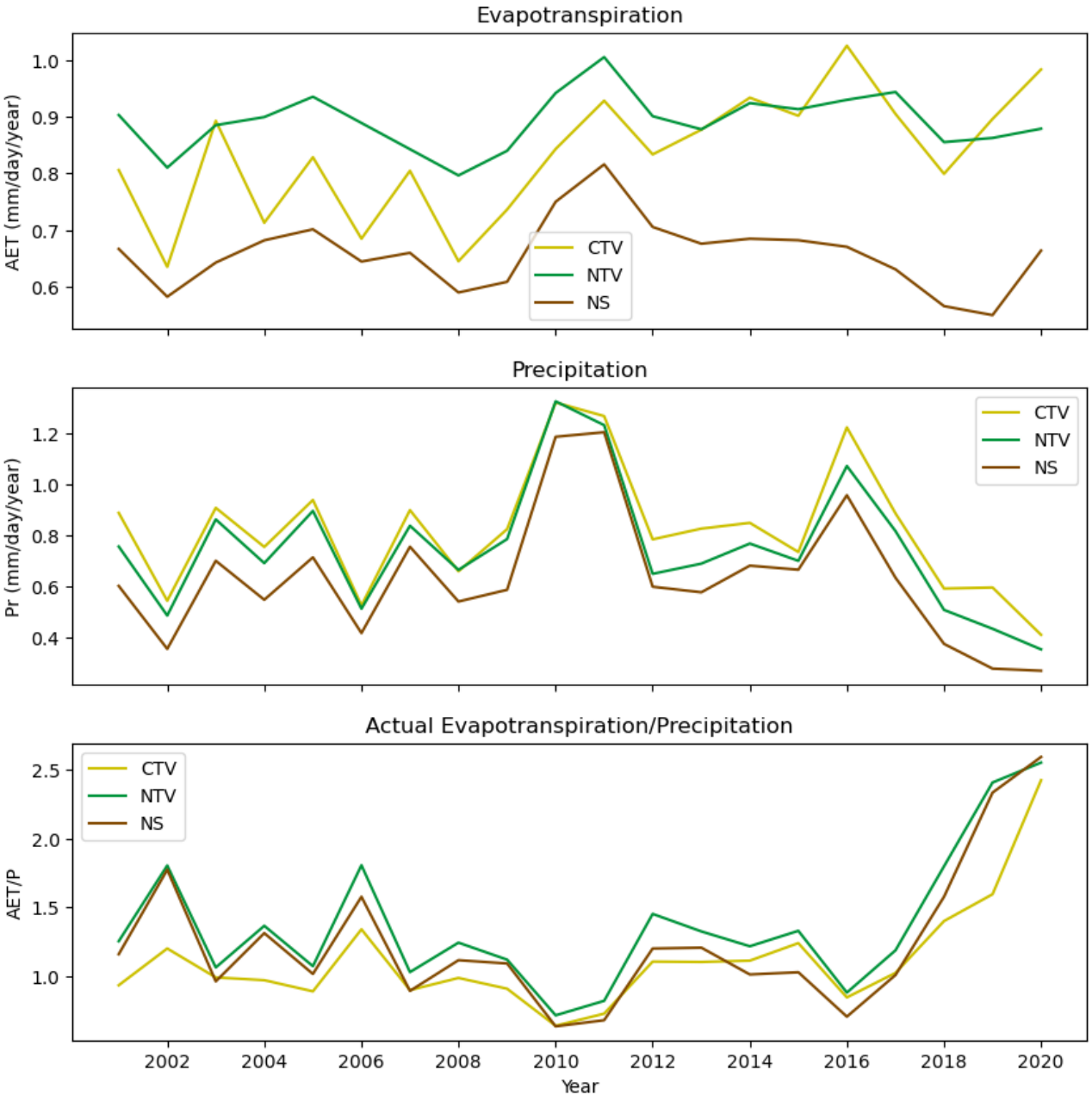

Test Results for AET\P
Comparing CTV,NTV and NS
F-value: 1.523, P-value: 0.227
==========
Comparing CTV and NTV
t-value: -1.849, p-value: 0.072
Comparing CTV and NS
t-value: -0.892, p-value: 0.378
Comparing NTV and NS
t-value: 0.813, p-value: 0.421

Test Results for AET
Comparing CTV,NTV and NS
F-value: 49.057, P-value: 0.000
==========
Comparing CTV and NTV
t-value: -2.188, p-value: 0.035
Comparing CTV and NS
t-value: 6.276, p-value: 0.000
Comparing NTV and NS
t-value: 13.073, p-value: 0.000

Figure B.5: Continued

MACQUARIE-CASTLEREAGH

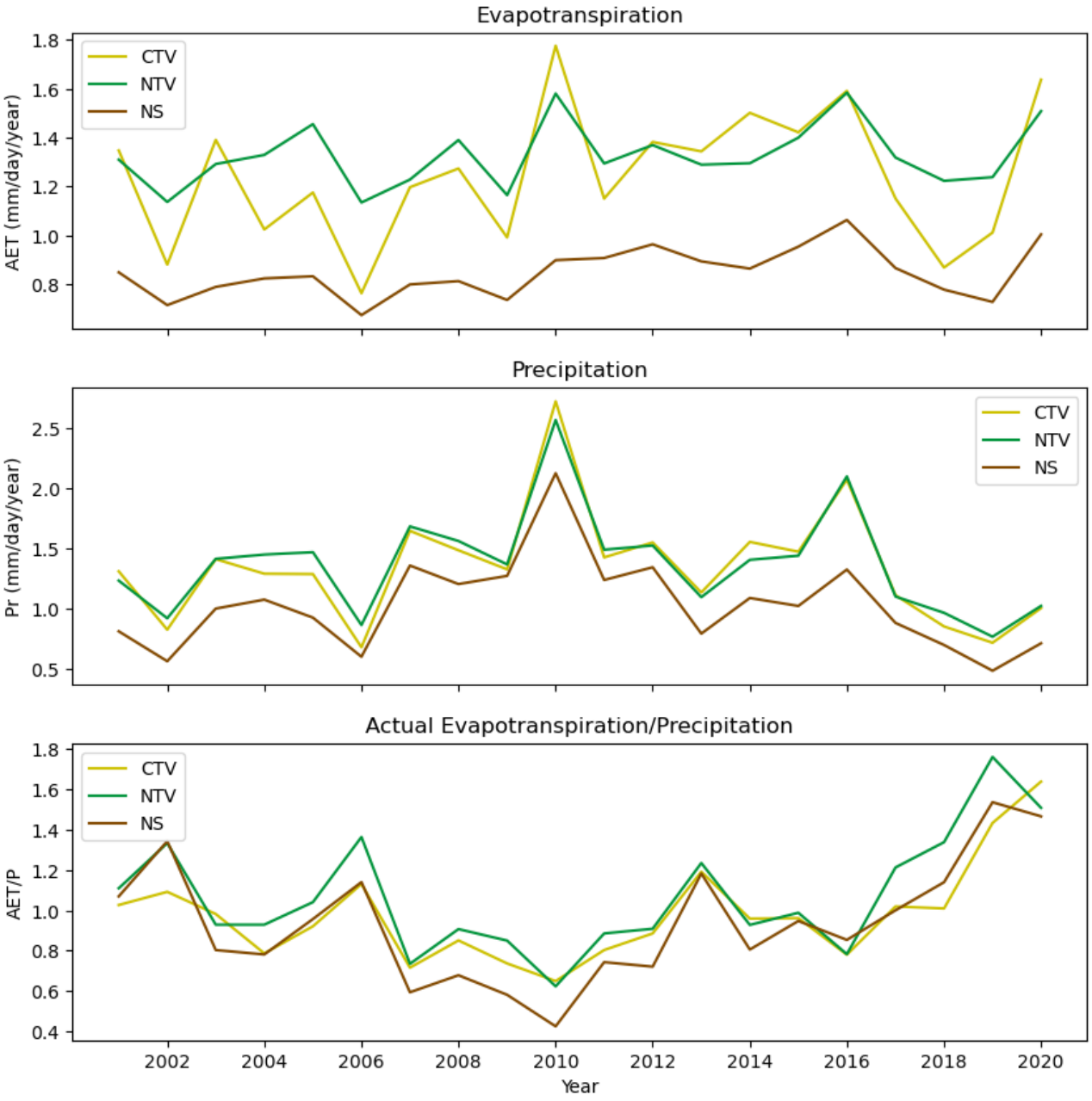

Test Results for AET\P
Comparing CTV,NTV and NS
F-value: 1.165, P-value: 0.319
==========
Comparing CTV and NTV
t-value: -1.076, p-value: 0.289
Comparing CTV and NS
t-value: 0.470, p-value: 0.641
Comparing NTV and NS
t-value: 1.409, p-value: 0.167

Test Results for AET
Comparing CTV,NTV and NS
F-value: 38.823, P-value: 0.000
==========
Comparing CTV and NTV
t-value: -1.229, p-value: 0.227
Comparing CTV and NS
t-value: 6.101, p-value: 0.000
Comparing NTV and NS
t-value: 13.020, p-value: 0.000

Figure B.5: Continued

MID_MURRAY

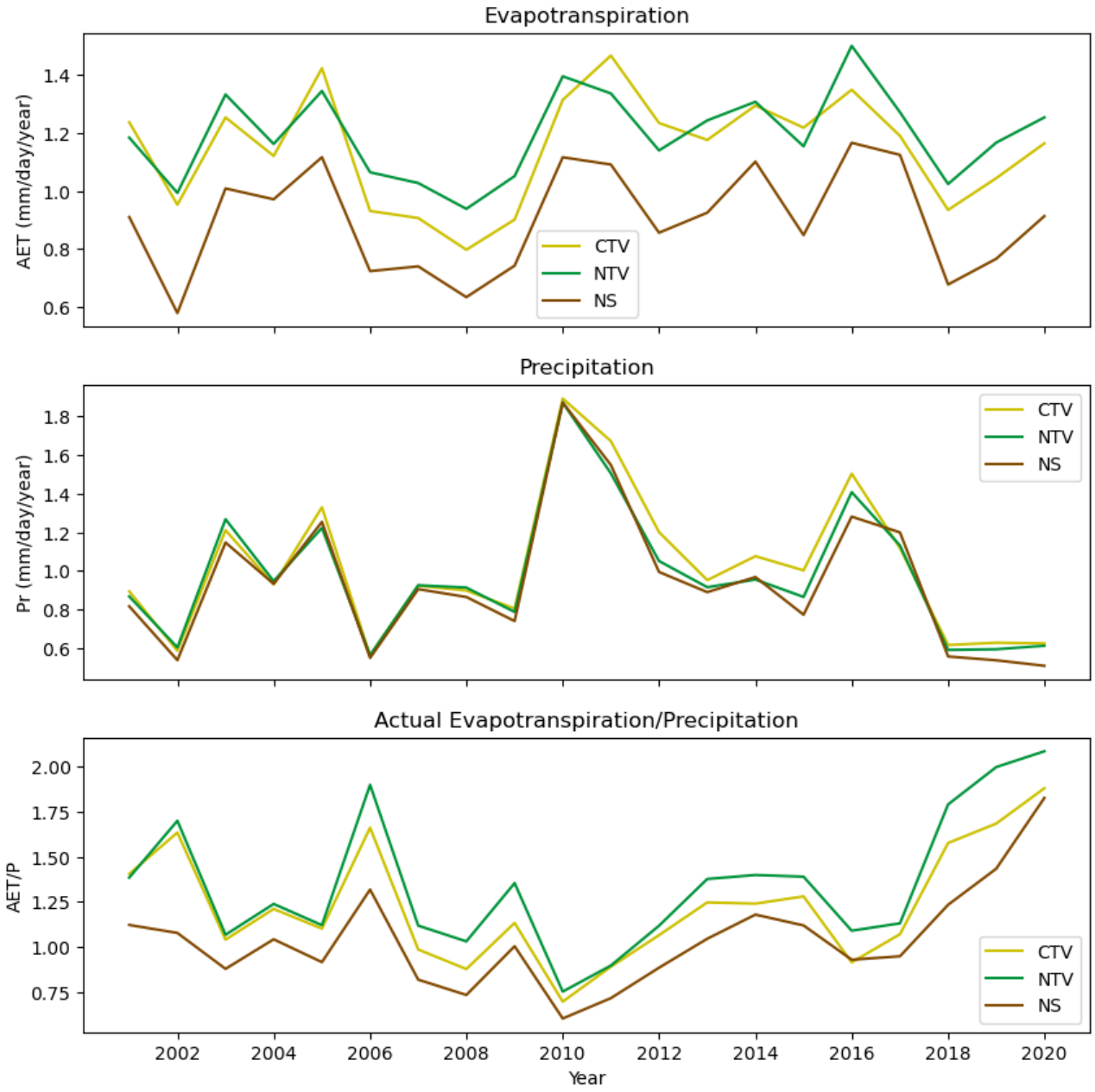

Test Results for AET\P
Comparing CTV,NTV and NS
F-value: 4.517, P-value: 0.015
==========
Comparing CTV and NTV
t-value: -1.071, p-value: 0.291
Comparing CTV and NS
t-value: 1.997, p-value: 0.053
Comparing NTV and NS
t-value: 2.954, p-value: 0.005

Test Results for AET
Comparing CTV,NTV and NS
F-value: 16.160, P-value: 0.000
==========
Comparing CTV and NTV
t-value: -0.907, p-value: 0.370
Comparing CTV and NS
t-value: 4.152, p-value: 0.000
Comparing NTV and NS
t-value: 5.555, p-value: 0.000

Figure B.5: Continued

MITTA_MITTA

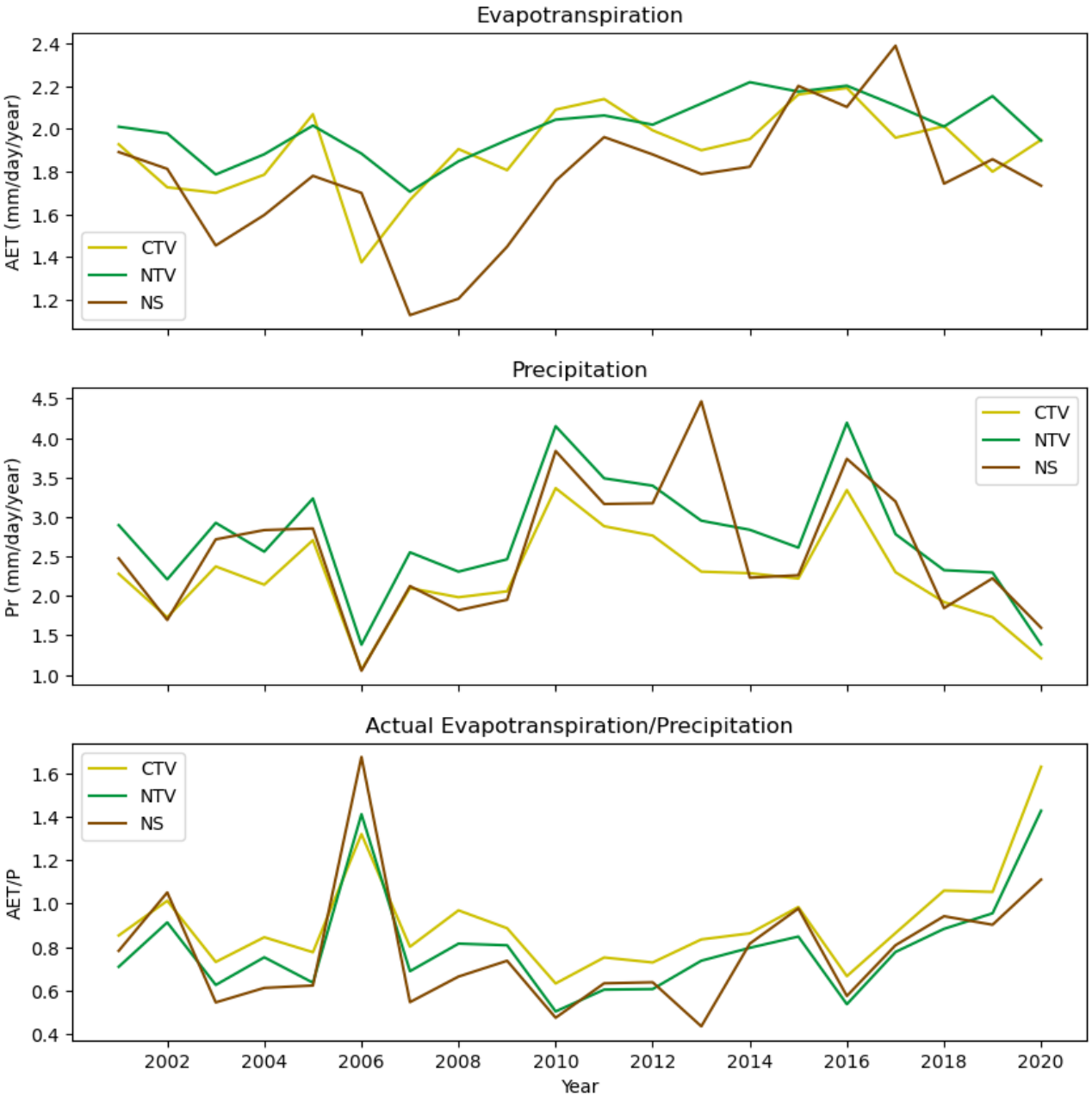

Test Results for AET\P
Comparing CTV,NTV and NS
F-value: 1.618, P-value: 0.207
==========
Comparing CTV and NTV
t-value: 1.479, p-value: 0.147
Comparing CTV and NS
t-value: 1.654, p-value: 0.106
Comparing NTV and NS
t-value: 0.292, p-value: 0.772

Test Results for AET
Comparing CTV,NTV and NS
F-value: 6.016, P-value: 0.004
==========
Comparing CTV and NTV
t-value: -1.864, p-value: 0.070
Comparing CTV and NS
t-value: 1.773, p-value: 0.084
Comparing NTV and NS
t-value: 3.277, p-value: 0.002

Figure B.5: Continued

MOONIE

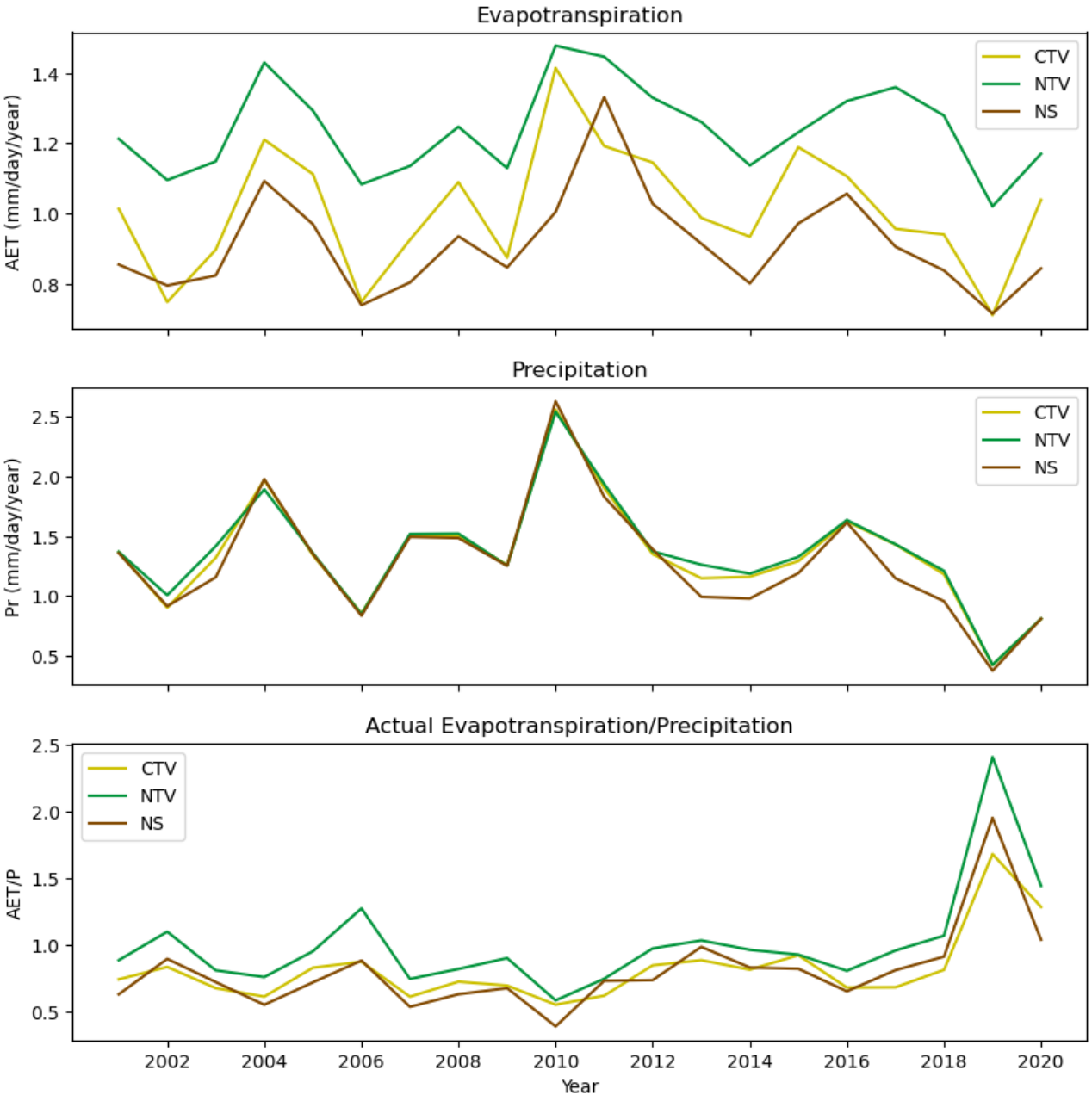

Test Results for AET\P
Comparing CTV,NTV and NS
F-value: 2.475, P-value: 0.093
==========
Comparing CTV and NTV
t-value: -1.831, p-value: 0.075
Comparing CTV and NS
t-value: 0.155, p-value: 0.878
Comparing NTV and NS
t-value: 1.835, p-value: 0.074

Test Results for AET
Comparing CTV,NTV and NS
F-value: 24.793, P-value: 0.000
==========
Comparing CTV and NTV
t-value: -4.690, p-value: 0.000
Comparing CTV and NS
t-value: 1.933, p-value: 0.061
Comparing NTV and NS
t-value: 7.609, p-value: 0.000

Figure B.5: Continued

MURRUMBIDGEE

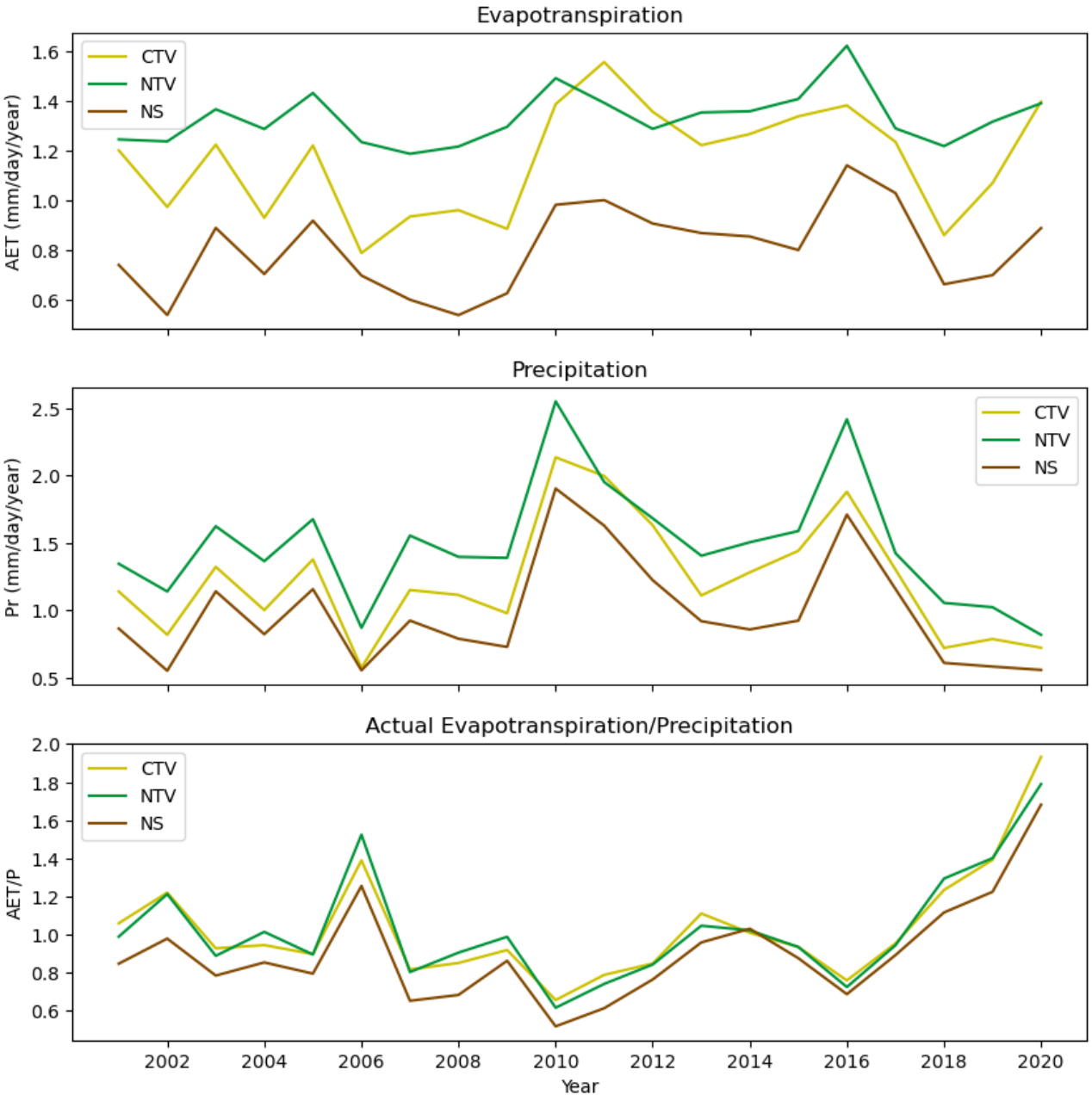

Test Results for AET\P
Comparing CTV,NTV and NS
F-value: 1.351, P-value: 0.267
==========
Comparing CTV and NTV
t-value: 0.038, p-value: 0.970
Comparing CTV and NS
t-value: 1.458, p-value: 0.153
Comparing NTV and NS
t-value: 1.427, p-value: 0.162

Test Results for AET
Comparing CTV,NTV and NS
F-value: 49.318, P-value: 0.000
==========
Comparing CTV and NTV
t-value: -3.168, p-value: 0.003
Comparing CTV and NS
t-value: 5.739, p-value: 0.000
Comparing NTV and NS
t-value: 11.744, p-value: 0.000

Figure B.5: Continued

NAMOI

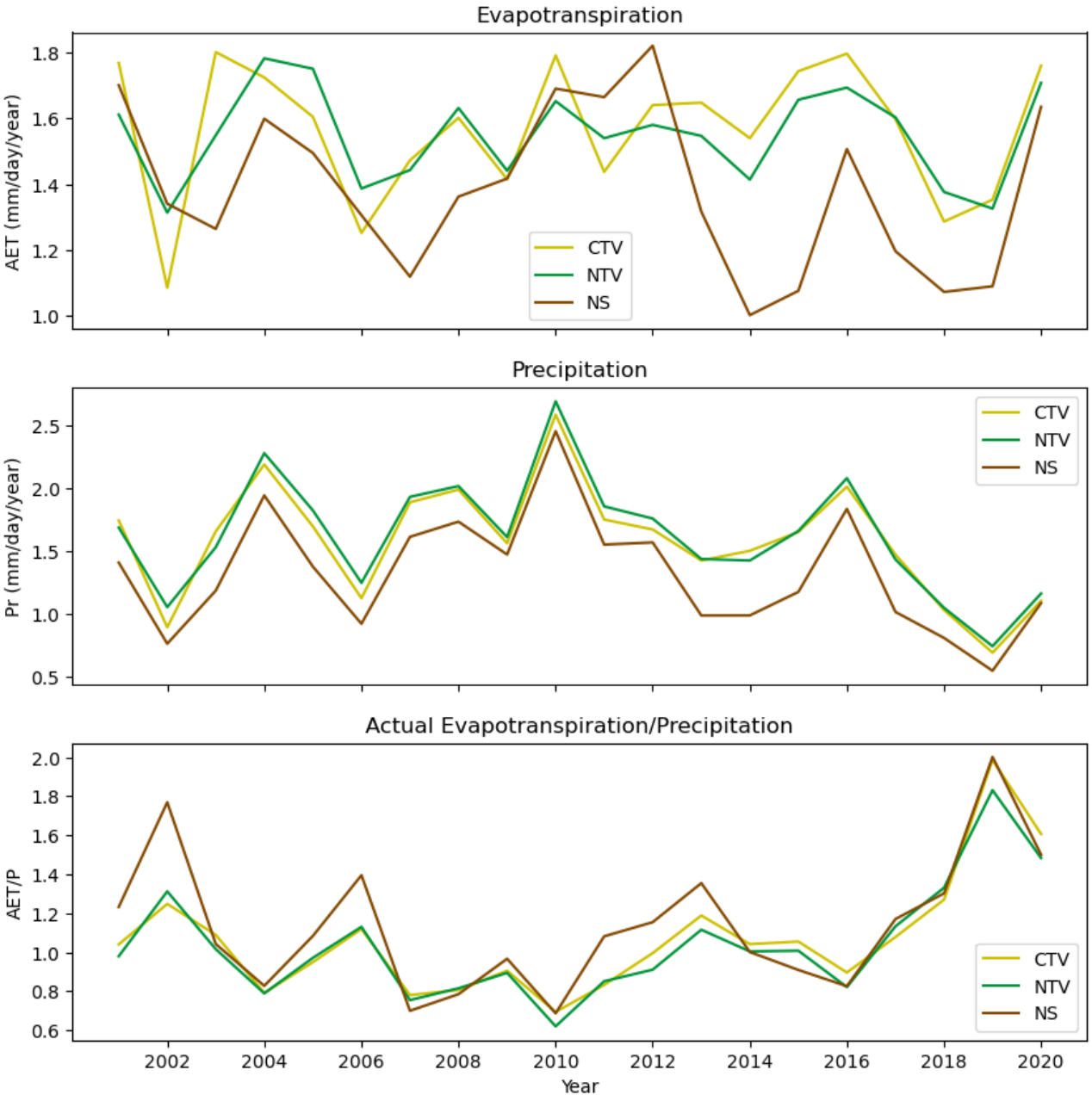

Test Results for AET\P
Comparing CTV,NTV and NS
F-value: 0.558, P-value: 0.576
==========
Comparing CTV and NTV
t-value: 0.326, p-value: 0.746
Comparing CTV and NS
t-value: -0.692, p-value: 0.493
Comparing NTV and NS
t-value: -1.014, p-value: 0.317

Test Results for AET
Comparing CTV,NTV and NS
F-value: 4.944, P-value: 0.010
==========
Comparing CTV and NTV
t-value: 0.279, p-value: 0.782
Comparing CTV and NS
t-value: 2.530, p-value: 0.016
Comparing NTV and NS
t-value: 2.617, p-value: 0.013

Figure B.5: Continued

OVENS

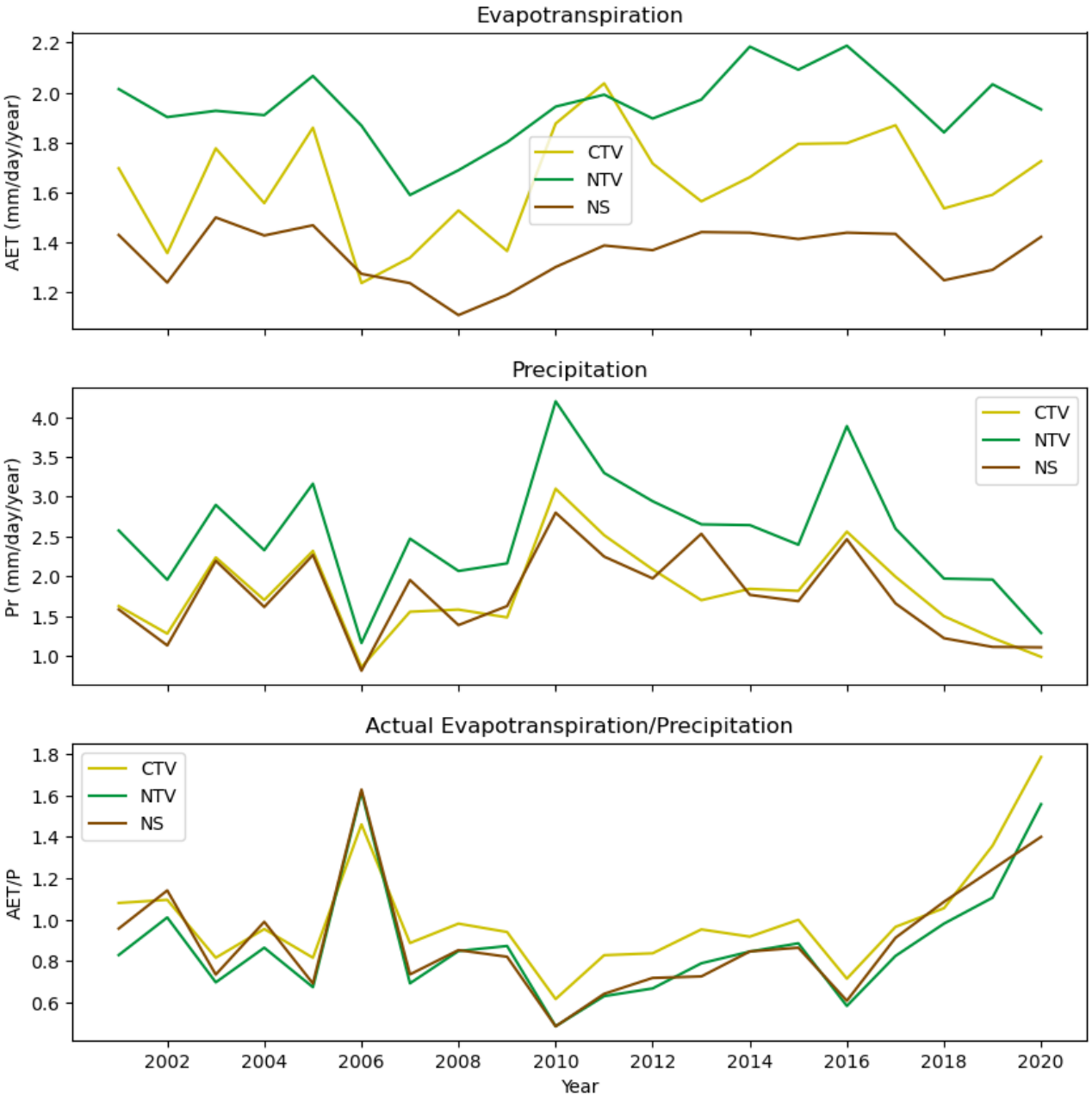

Test Results for AET\P
Comparing CTV,NTV and NS
F-value: 1.189, P-value: 0.312
==========
Comparing CTV and NTV
t-value: 1.483, p-value: 0.146
Comparing CTV and NS
t-value: 1.141, p-value: 0.261
Comparing NTV and NS
t-value: -0.345, p-value: 0.732

Test Results for AET
Comparing CTV,NTV and NS
F-value: 67.282, P-value: 0.000
==========
Comparing CTV and NTV
t-value: -5.204, p-value: 0.000
Comparing CTV and NS
t-value: 5.497, p-value: 0.000
Comparing NTV and NS
t-value: 14.486, p-value: 0.000

Figure B.5: Continued

PAROO

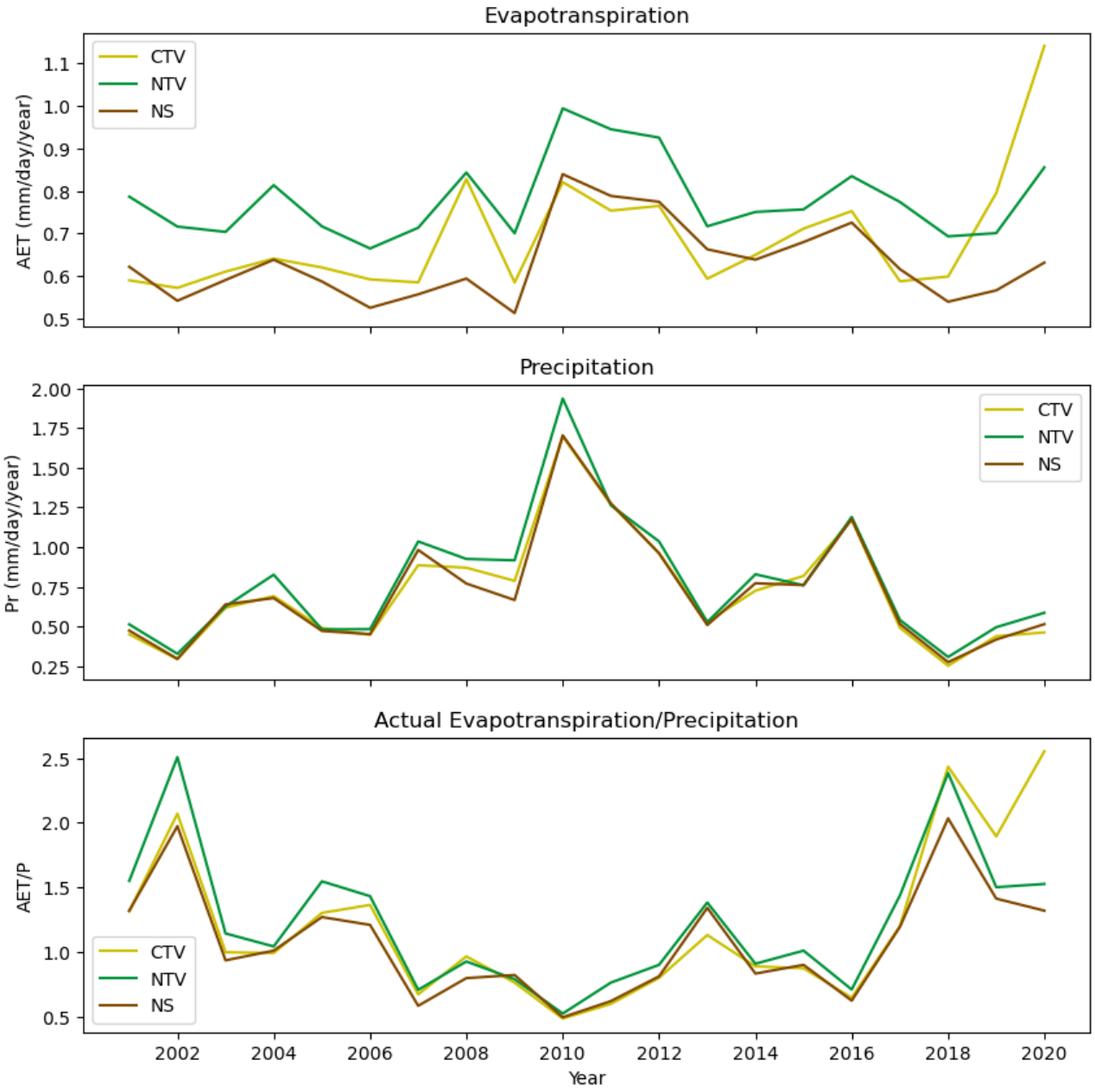

Test Results for AET\P
Comparing CTV,NTV and NS
F-value: 0.511, P-value: 0.603
==========
Comparing CTV and NTV
t-value: -0.209, p-value: 0.836
Comparing CTV and NS
t-value: 0.745, p-value: 0.461
Comparing NTV and NS
t-value: 1.053, p-value: 0.299

Test Results for AET
Comparing CTV,NTV and NS
F-value: 9.333, P-value: 0.000
==========
Comparing CTV and NTV
t-value: -2.430, p-value: 0.020
Comparing CTV and NS
t-value: 1.568, p-value: 0.125
Comparing NTV and NS
t-value: 5.103, p-value: 0.000

Figure B.5: Continued

UPPER_MURRAY

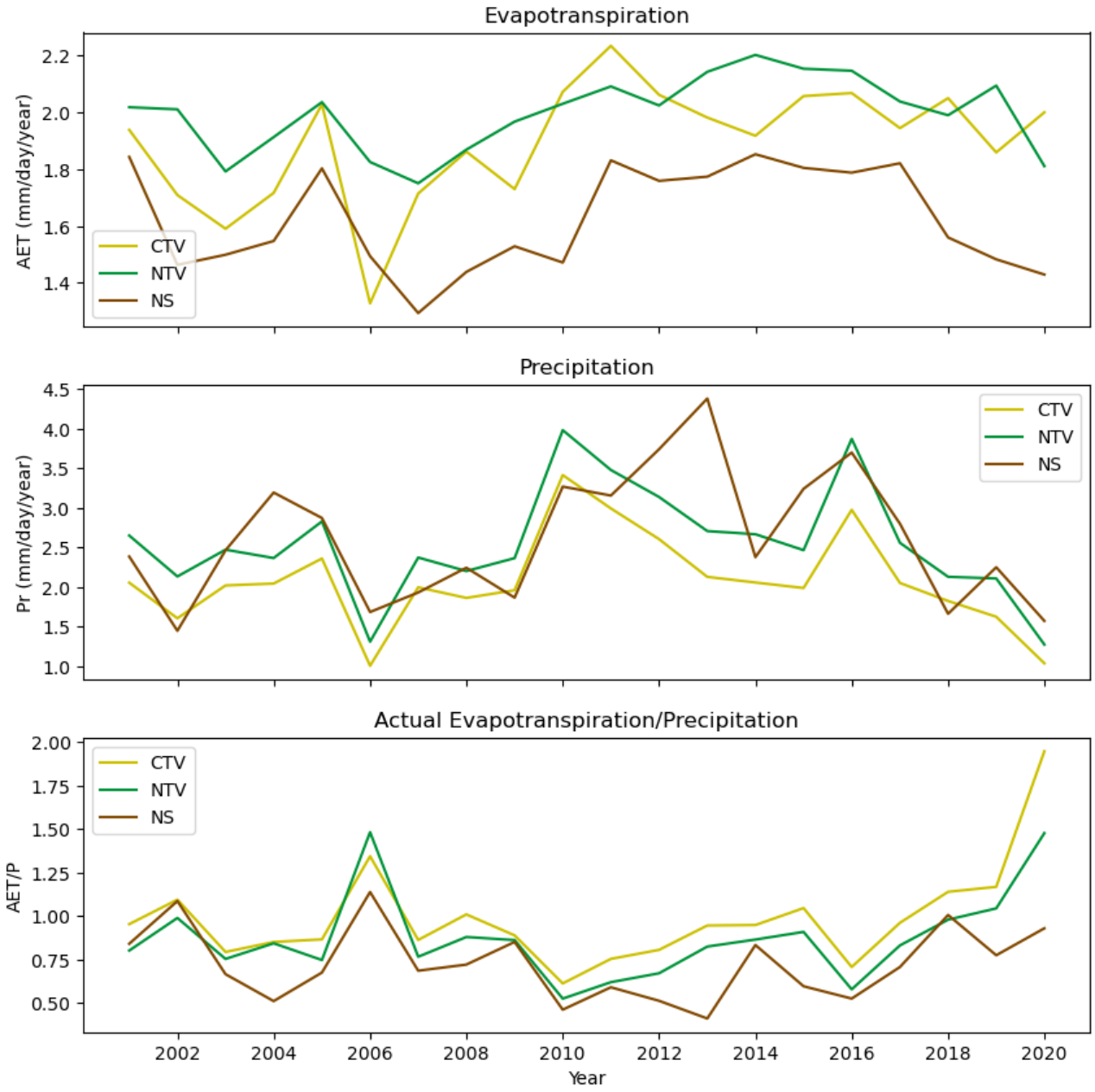

Test Results for AET\P
Comparing CTV,NTV and NS
F-value: 5.497, P-value: 0.007
==========
Comparing CTV and NTV
t-value: 1.338, p-value: 0.189
Comparing CTV and NS
t-value: 3.301, p-value: 0.002
Comparing NTV and NS
t-value: 2.035, p-value: 0.049

Test Results for AET
Comparing CTV,NTV and NS
F-value: 23.527, P-value: 0.000
==========
Comparing CTV and NTV
t-value: -1.844, p-value: 0.073
Comparing CTV and NS
t-value: 4.347, p-value: 0.000
Comparing NTV and NS
t-value: 7.454, p-value: 0.000

Figure B.5: Continued

WARREGO

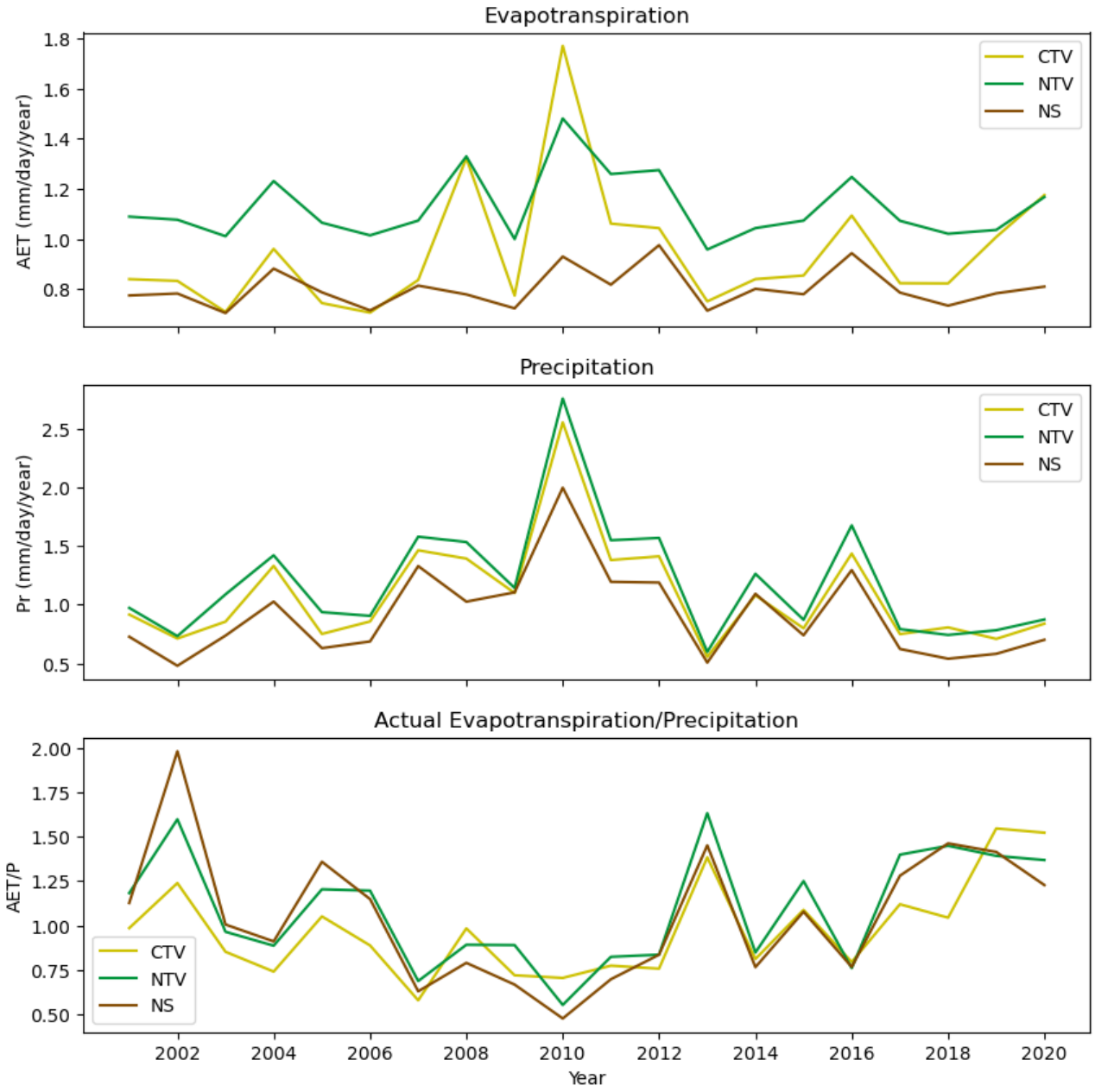

Test Results for AET\P
Comparing CTV,NTV and NS
F-value: 0.619, P-value: 0.542
==========
Comparing CTV and NTV
t-value: -1.191, p-value: 0.241
Comparing CTV and NS
t-value: -0.723, p-value: 0.474
Comparing NTV and NS
t-value: 0.340, p-value: 0.736

Test Results for AET
Comparing CTV,NTV and NS
F-value: 17.813, P-value: 0.000
==========
Comparing CTV and NTV
t-value: -2.759, p-value: 0.009
Comparing CTV and NS
t-value: 2.468, p-value: 0.018
Comparing NTV and NS
t-value: 9.344, p-value: 0.000

Figure B.5: Continued

WIMMERA

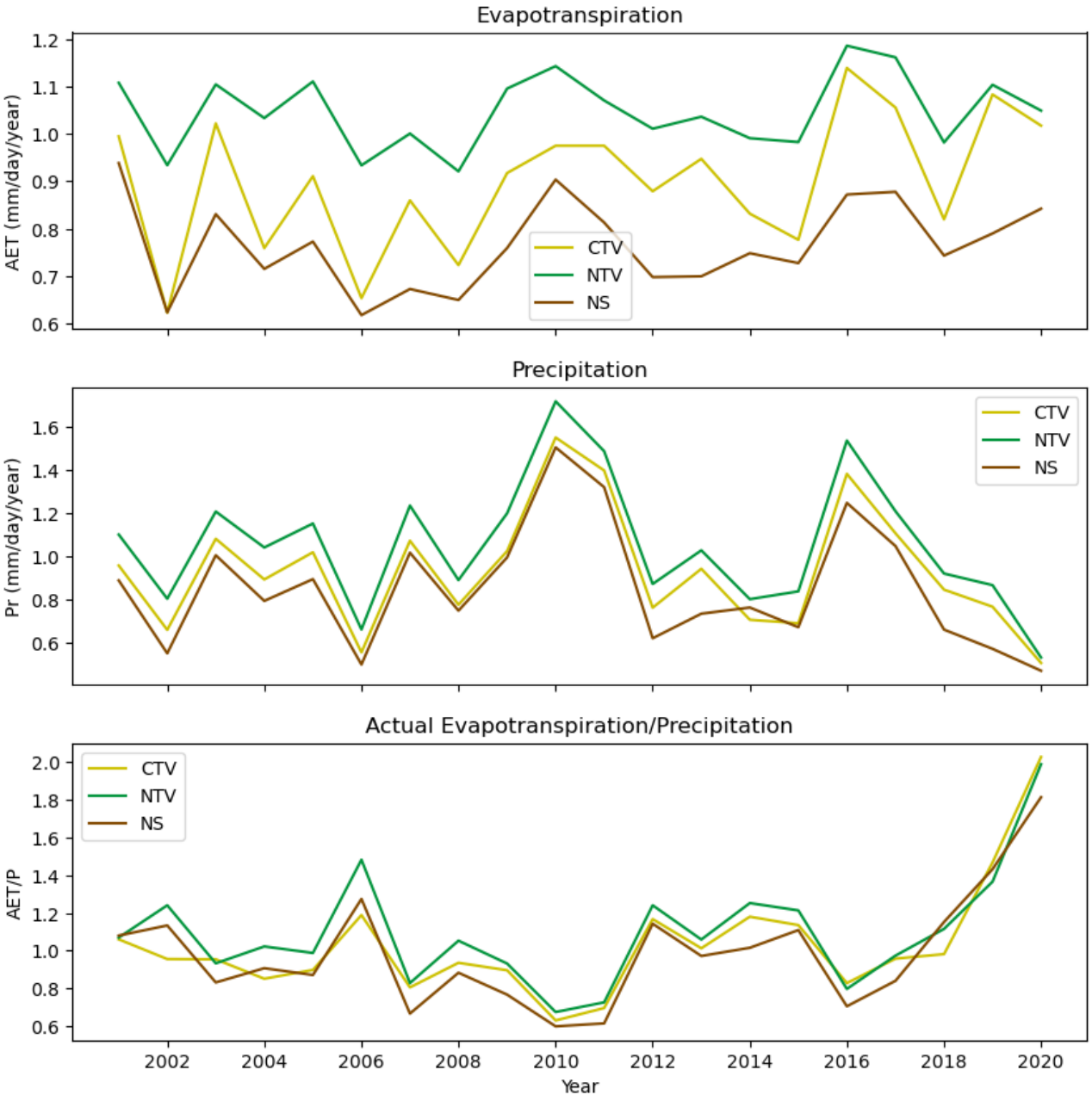

Test Results for AET\P
Comparing CTV,NTV and NS
F-value: 0.663, P-value: 0.519
==========
Comparing CTV and NTV
t-value: -0.703, p-value: 0.487
Comparing CTV and NS
t-value: 0.435, p-value: 0.666
Comparing NTV and NS
t-value: 1.148, p-value: 0.258

Test Results for AET
Comparing CTV,NTV and NS
F-value: 34.506, P-value: 0.000
==========
Comparing CTV and NTV
t-value: -4.131, p-value: 0.000
Comparing CTV and NS
t-value: 3.515, p-value: 0.001
Comparing NTV and NS
t-value: 10.443, p-value: 0.000

Figure B.5: Continued

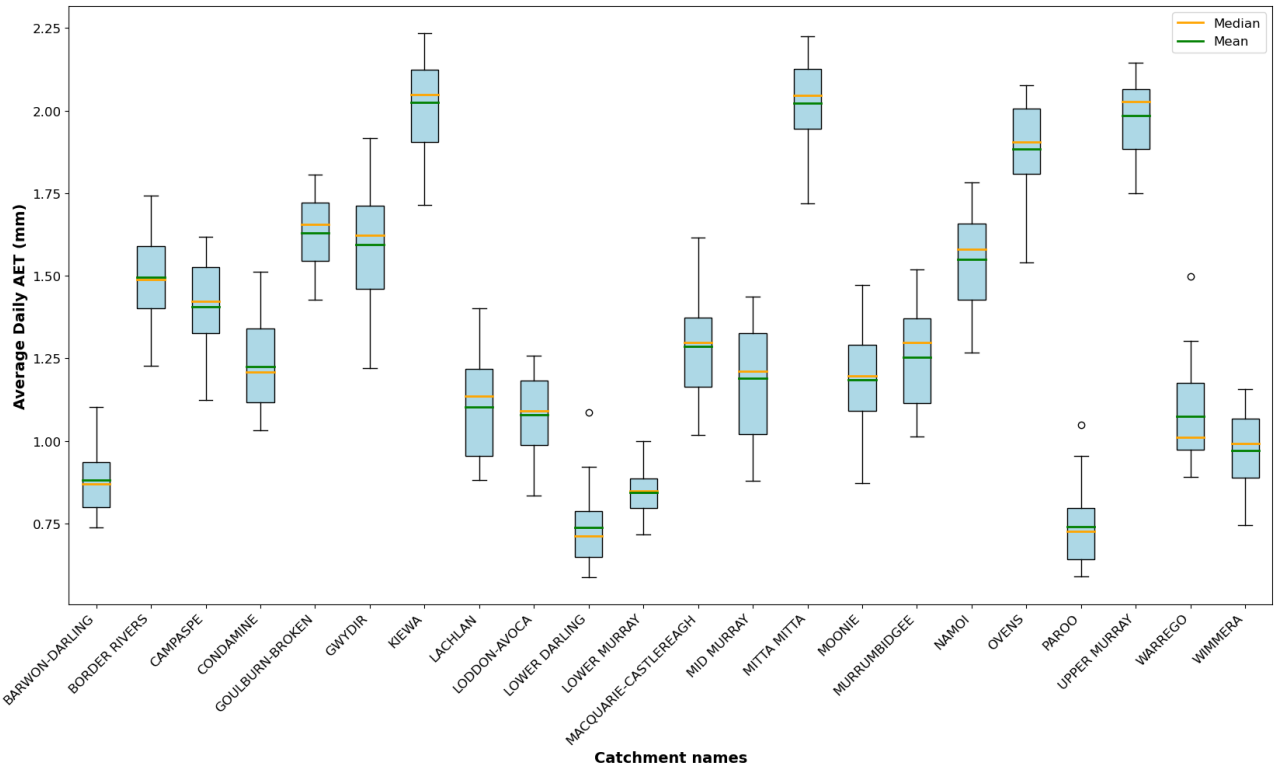

Figure B.6: Annual AET distribution across various MDB catchments during the 20-year period. Each boxplot displays the interquartile range, indicating the middle 50% of the data, with the central line representing the median AET. The 'whiskers' extend to the furthest points that are not considered outliers, and any data point outside of this range is represented as an open dot, which signifies a year with unusually high or low AET.

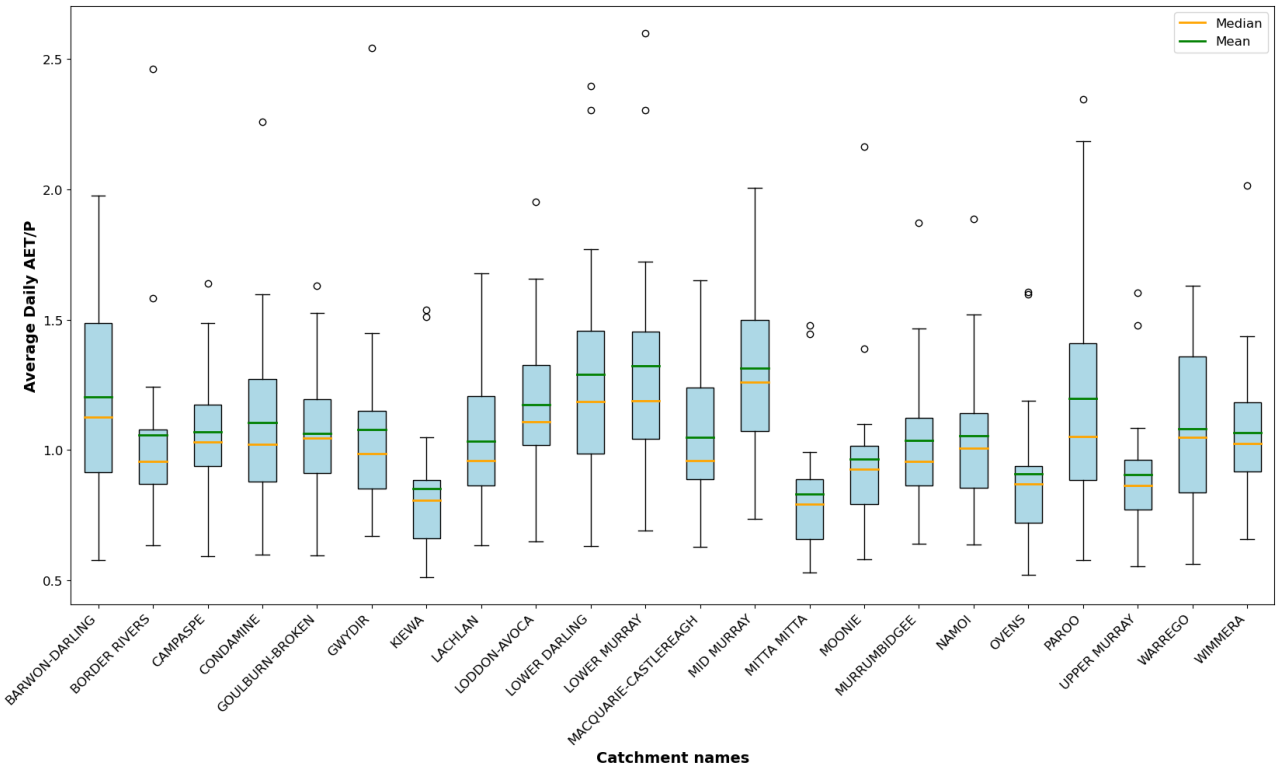

Figure B.7: Distribution of annual AET/P across various MDB catchments during the 20-year period. Each boxplot displays the interquartile range, indicating the middle 50% of the data, with the central line representing the median AET/P. The 'whiskers' extend to the furthest points that are not considered outliers, and any data point outside of this range is represented as an open dot, which signifies a year with unusually high or low AET\P.

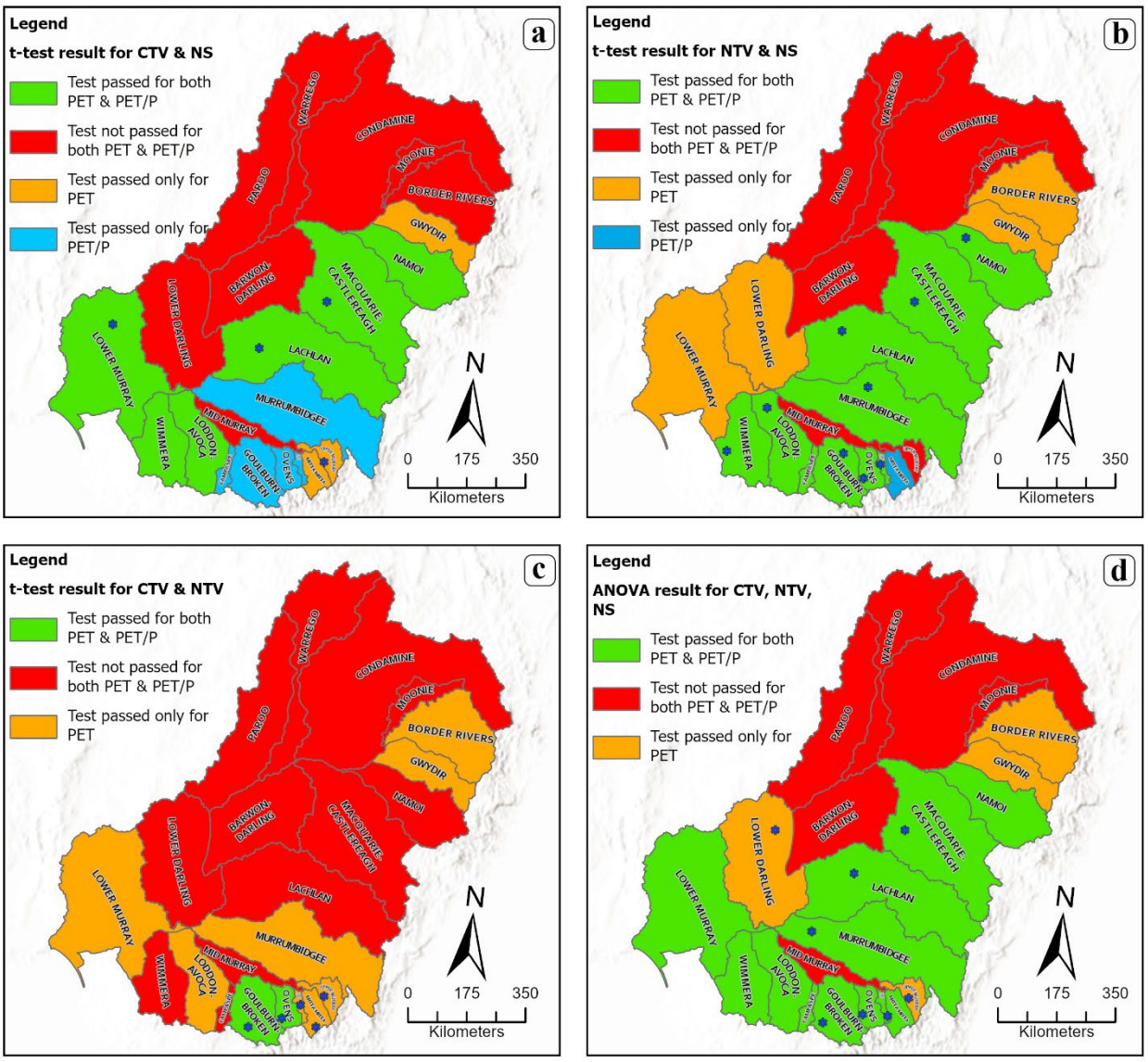

Figure B.8: The result of ANOVA and t-test for MODIS PET between (a) CTV (Cultivated Terrestrial Vegetation) and NS (Natural Bare Surface); (b) NTV (Natural Terrestrial Vegetation) and NS; (c) CTV and NTV; and (d) CTV, NTV and NS. (* indicates the catchments with significant difference in precipitation among given land covers)